VOLUME 49, NUMBER 7

July, 1961

published monthly by The Institute of Radio Engineers, Inc.

Proceedings of the IRE®

contents

COVER

Radioactive krypton was used to obtain this radiograph showing the presence of the inert gas in the sputtered deposit on the cathode of an ion pump. The ion pump is one of a number of the modern advances in high-vacuum techniques which are reviewed on page 1136.

published monthly by The Institute of Radio Engineers, Inc.

Proceedings of the IRE®

continued

PROCEEDINGS OF THE IRE, published monthly by The Institute of Radio Engineers, Inc., at 1 East 79 Street, New York 21, N. Y. Manuscripts should be submitted in triplicate to the Editorial Department. Correspondence column items should not exceed four double-spaced pages (illustrations count as one-half page each). Responsibility for contents of papers published rests upon the authors, and not the IRE or its members. All republication rights, including translations, are reserved by the IRE and granted only on request. Abstracting is permitted with mention of source.

Thirty days advance notice is required for change of address. Price per copy: members of the Institute of Radio Engineers, one additional copy $1.25; non-members $2.25. Yearly subscription price: to members $9.00, one additional subscription $13.50; to non-members in United States, Canada, and U. S. Possessions $18.00; to non-members in foreign countries $19.00. Second-class postage paid at Menasha, Wisconsin, under the act of March 3, 1879. Acceptance for mailing at a special rate of postage is provided for in the act of February 28, 1925, embodied in Paragraph 4, Section 412. P. L. and R., authorized October 26, 1927. Printed in U.S.A.

July, 1961
Vol. 49 No. 7

Proceedings of the IRE

Poles and Zeros

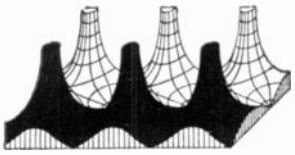

ECPD and IRE. The Board of Directors of IRE, at its meeting held in Phoenix, Ariz., on April 28, 1961, accepted the invitation extended by the Engineers' Council for Professional Development to become a participating body of that organization. Membership in ECPD is the culmination of the decision of the IRE Board, at its meeting in Houston, in April, 1957, to seek admission to ECPD.

Editor Fink, in Poles and Zeros, July, 1957, noted that, "This was by far the most far-reaching step taken at Houston." Editor Ryder reported in October, 1958, that at the time of the Board decision in 1957, "The ECPD charter was not then well adapted to expansion of membership, and so admission has been delayed while the legal amenities were being met." W. L. Everitt, President of ECPD (IRE President, 1945), reporting to ECPD (1959–1960) noted that the members of ECPD had given unanimous approval to a plan for additional member bodies. He further stated in his report, "I sincerely hope that prompt action can be taken so that the applications of IAeS, IRE, and NSPE can be approved. I feel that we need them even more than they need to join us and, if ECPD is to maintain its present position as a true unity organization in the field of engineering education, it must include other important engineering societies with major interest in this field."

IRE, with approximately 90,000 members, should add immense strength to the program and activities of ECPD. To accomplish this aim IRE members must be ready to lend their talents and time to the furtherance of the objectives of ECPD. This effort requires an understanding of the aims and objectives of ECPD on the part of IRE members. It appears appropriate to set forth on this page a few statements concerning ECPD.

The ECPD charter states: "The exclusive purpose of ECPD shall be to advance and promote scientific and engineering education with a view to the promotion of the public welfare through the development of better educated engineers." It further states: "The purpose of ECPD shall be carried out by a program of guidance to high school students, the formulation of criteria for colleges of engineering, the assistance of such colleges in planning and carrying out their educational program, cooperation with the State licensing agencies to maintain high educational standards, and the promotion of the intellectual development of the young engineer."

The work of ECPD is largely placed in the hands of its Education and Accreditation Committee and its standing committees comprising the Guidance Committee, Student Development Committee, Committee on Development of Young Engineers, Recognition Committee, Ethics Committee, and Information Committee. A brief statement of the responsibility of each of these committees is given below.

The Guidance Committee is charged with the responsibility of developing and reviewing, "methods for guiding young men who seek entrance to the engineering schools so that those who enter will have the high quality, aptitude, and capacity required for embarking upon an engineering career." The Student Development Committee coordinates all other relations between schools, societies, and industry to promote the intellectual development of students except those assumed by the Education and Accreditation Committee. This latter committee undertakes the task of developing "criteria for colleges of engineering which will insure to their graduates a sound educational foundation for the practice of engineering."

The Committee on the Development of Young Engineers develops "and administers plans for the further development of young engineers." The Recognition Committee is assigned the task of developing "methods whereby those engineers who have met suitable standards of competence and attainment may receive corresponding recognition . . ." The Ethics Committee administers "those activities related to the promulgation, adoption, and revision of the Canons of Ethics for Engineers," and the Information Committee is responsible for ECPD publications. For those readers who desire complete information about ECPD in all its phases a copy of the latest Annual Report may be obtained, for one dollar, from ECPD, 29 West 39th Street, New York 18, N. Y.

The brochure "Electronics-Career for the Future" (see Poles and Zeros, September, 1960), produced by the Cedar Rapids Section, is a direct contribution of IRE to the activities which are the responsibility of the Guidance Committee of ECPD. There is every reason to believe that IRE as a full-fledged member of ECPD will contribute in additional substantial manner to the long range objectives of ECPD.

President Berkner has been authorized by the Board of Directors to appoint IRE's representatives to ECPD and to allocate the necessary funds. IRE's membership in ECPD should not only strengthen ECPD but, also, further the advancement of engineering education and the professional objectives of IRE.

International Standardization. At its meeting in November, 1960, the Board of Directors approved a resolution in which IRE agreed to establish, with EIA, a Joint Standards Advisory Committee to work with the U. S. National Committee of the IEC to decide upon representation at and participation in international meetings of IEC. The resolution has now been implemented, and a jointly financed Secretariat has been created. The Committee consists of F. R. Lack as Chairman, Chester Page, M. W. Baldwin, Jr., and W. P. Boothroyd representing IRE, and J. Whitney, H. B. Fancher, and L. Podolsky representing EIA. IRE has taken an added step in its ever growing contribution to international matters.

—F.H., Jr.

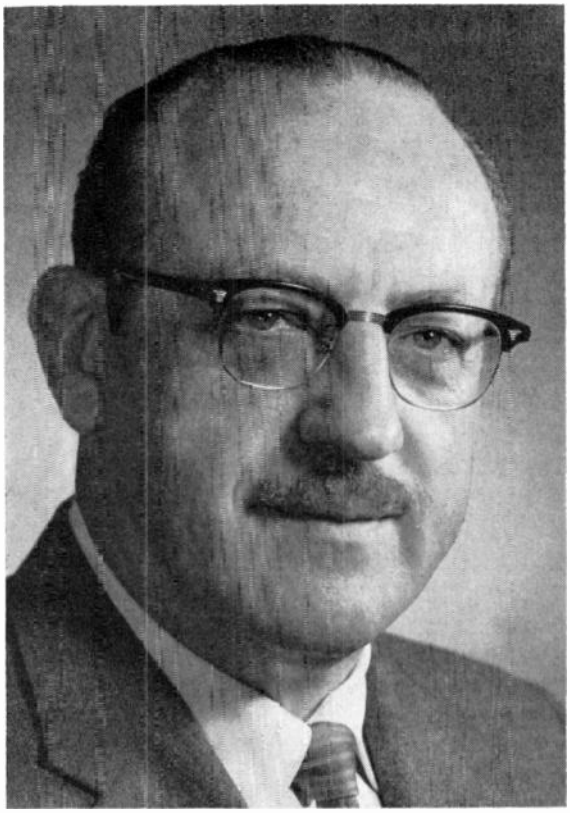

L. C. Van Atta

Director, 1961–1963

Lester C. Van Atta (M'42–SM'43–F'52) was born in Portland, Ore., in 1905. He received the B.A. degree in physics from Reed College, Portland, in 1927, and the Ph.D. degree from Washington University, St. Louis, Mo., in 1931. From 1931–1932 he was with Princeton University, Princeton, N. J., in the Physics Department; from 1932–1940 he was with the Massachusetts Institute of Technology, Cambridge, also in the Physics Department; and from 1940–1945 he headed the Antenna Group of the MIT Radiation Laboratory. He headed the Antenna Research Branch at the Naval Research Laboratory from 1945–1950, and since that time he has been with the Hughes Aircraft Company, Culver City, Calif. He has held the following positions with the company: Head of the Microwave Laboratory, Associate Director of the Research Laboratories, and, most recently, Director of Technical Information and Education. He is presently on professional leave from Hughes as Special Assistant for Arms Control to Dr. H. F. Cook in the Office of the Secretary of Defense.

He has been active in military research and development since 1940, at the MIT Radiation Laboratory, the Naval Research Laboratory, and at Hughes Aircraft Company. In addition, he has served on the Research and Development Board, as Chairman of the Panel on Antennas and Propagation (1946–1949). More recently, he participated in a series of WSEG studies of continental air defense (1956–1958), in a series of PISGAH and other research and development conferences for the Army (1957–1959), in two ARGUS studies at Lawrence Radiation Laboratory (1958–1959), and on the Gaither Committee (1959).

At Hughes Aircraft Company he has directed systems studies such as the Hemispherical Scan System for the Navy and the ICBM Passive Defense System for the Air Force—systems based on electronic beam scanning techniques.

His technical fields of specialization have included high resistors, electron scattering in gases, high voltage and high vacuum engineering, production and scattering of hard X rays, nuclear reactions by bombardment, microwave antennas, microwave components and systems.

He has published over thirty journal articles and many technical reports on physics and microwave electronics subjects. He holds some fifteen patents, with others pending, primarily on microwave antennas and systems.

Dr. Van Atta is a Fellow of the American Physical Society and has been active in the Research Society of America and the International Scientific Radio Union, especially Commission VI. He has been very active in the IRE, having served as Chairman of the Antenna and Waveguide Technical Committee, the Professional Group on Antennas and Propagation, the Los Angeles Section, and the 1960 Winter Convention on Military Electronics, as well as Vice Chairman of the Professional Groups Committee. In addition he is a member of the American Association for the Advancement of Science, the American Association of Physics Teachers and the American Geophysical Union.

Scanning the Issue

The Interplay of Electronics and Vacuum Technology (Lafferty and Vanderslice, p. 1136)—The subject of vacuums usually brings to mind electron tube developments of the past. The performance of many of the early tubes was seriously limited by an inability to obtain a high vacuum. Subsequent improvements in vacuum techniques contributed greatly to the progress of the electron tube art. The subject is by no means one that belongs to the past, however. Gas ionization still plays a significant role in the operation of a number of modern electron devices. The advent of the space age has opened up other fields of interest. Ultra-high vacuums are now required to simulate on earth the conditions which electronic equipment will encounter in space. Special measuring instruments have been developed for rocket and satellite studies of the upper atmosphere and for hot-plasma experiments related to fusion. Particularly noteworthy is the important progress now being made in the fabrication of a wide variety of novel electronic components by vacuum deposited thin films, a process which requires a carefully controlled ultra-high vacuum. The excellent review and tutorial discussion of modern ultra-high vacuum techniques and systems presented here is most timely, not only because the subject is of great current importance in many areas of electronics but also because electronic components are playing a vital role in the development of modern vacuum technology.

New Concepts in Thermoelectric Device Design (Clingman, p. 1155)—A subtle brand of alchemy has arisen in the last decade by which materials may be tailored to a substantial degree to have certain desired properties. The proficiency with which this art is now practiced is having a revolutionary effect on electronics. Many new and improved materials are rapidly becoming available to the electronics engineer, not the least important of which are those which exhibit thermoelectric properties. As a consequence, thermoelectric devices are more than a reality; they are now becoming practical. Substantial numbers of engineers are becoming interested in methods of designing these devices. The operation of a thermoelectric device depends on a rather complex interrelationship between its thermal and electrical circuits. It is customary, therefore, to make simplifying assumptions in carrying forward the design analysis. The specific approach to be taken, however, usually depends on the device application and which of such factors as power, weight, efficiency, or cost is most important. The author has found that when efficiency or coefficient of performance is a major objective, an irreversible thermodynamic analysis of the system can be very useful. The result provides a valuable tool for preliminary analysis of a proposed design of a thermoelectric device.

IRE Standards on Piezoelectric Crystals: Measurements of Piezoelectric Ceramics, 1961 (p. 1161)—The key word in the foregoing title is "ceramics." While the IRE has issued three standards in the last decade dealing with piezoelectric crystals in general, none have dealt specifically with piezoelectric ceramics. This latter category covers a group of polycrystalline ferroelectric substances, of which ceramic barium titanate is a familiar example, which can be given lasting polar properties, including pyroelectric and piezoelectric effects, by subjecting them to high electric fields for a short time. These "poled" ferroelectric ceramics have become an increasingly important component in electromechanical devices along with piezoelectric crystals and magnetostrictive materials. The definitions, relations, and measurement methods developed in earlier IRE standards for piezoelectric crystals in general have now been adapted in this standard to ferroelectric ceramics.

The Field-Effect Tetrode (Stone, Jr., and Warner, Jr., p. 1170)—A new four-terminal semiconductor device has been developed which provides two current channels which are physically independent from each other but which electrically interact with one another. The device might be likened to a field-effect transistor in which the gate is replaced by a second channel so that each channel acts as a gate for the other. It is this mutual interaction between the two channels that gives the device its interesting properties. In addition to its possibilities as an amplifier, the field-effect tetrode has applications as a gyrator, isolator, and an electronically variable resistor. The development of this device marks a significant step forward in the realm of field-effect devices and will be of general interest to those concerned with microelectronics as well as particular interest to semiconductor device fabricators.

An Experimental Study of Bistatic Scattering from Some Small Absorber-Coated, Metal Shapes (Garbacz and Moffatt, p. 1184)—There is of course a great deal of interest today in the reflective properties of targets and the effect of coating them with absorbent materials. It is a subject that concerns investigators in several fields, including electromagnetic experimenters, radar designers, and electronic countermeasures engineers. The experimental results reported in this paper add significantly to the available data on the reflection or scattering from ideal geometrical objects, such as spheres, cylinders and cones, which are of a size to be resonant at X band. The results, presented in the form of an atlas of curves, show that coating these objects with an absorber will reduce the energy that is back-scattered but will increase the energy that is forward-scattered.

IRE Standards on Video Techniques: Definitions of Terms Relating to Television, 1961 (p. 1193)—This document brings up to date the IRE standard definitions of over two score terms common to the television field. Those who are interested in the standard definitions of terms in other fields as well are reminded that all IRE definitions published through 1959 are contained in the "IRE Dictionary of Electronics Terms and Symbols," which is available from IRE headquarters.

The Elimination of Intersymbol Interference by Input Signal Shaping (Gerst and Diamond, p. 1195)—Intersymbol interference can arise in a binary system because a pulse, upon passing through the system, generates a tail which may interfere with the following binary digit, especially if the latter is supposed to be a "zero." This type of interference can be eliminated by increasing the spacing between digits at a cost of slowing down the transmission rate. Another approach is to design the system to reduce the tail. This paper considers still another approach, namely, that of shaping the input signal to reduce the tail on the output pulse. In fact, it is shown that using a properly shaped continuous wave, instead of pulses, at the input can result in output pulses with no tail at all. The results will be of considerable interest to those engaged in computer and pulse communications systems. In addition, in solving the problem the author develops certain properties of Laplace transforms that should hold considerable appeal to network theorists.

The Interplay of Electronics and Vacuum Technology*

J. M. LAFFERTY†, FELLOW, IRE, AND T. A. VANDERSLICE†

Summary—**Historically, vacuum technology has played an important part in the development of electron tubes. The operating characteristics of many early devices were dependent on the degree of vacuum obtained. The Roentgen X-ray tube and the Braun cathode-ray tube are examples of these. Improvement in vacuum technology made possible the development of many truly high-vacuum devices in which performance is independent of the inclosed gas pressure. Many modern electronic components no longer operate in a vacuum but are dependent on vacuum technology in their fabrication. These include microminiature circuit elements, cryotrons, photoconductor-electroluminescent devices and ferromagnetic memory systems—all dependent on vacuum evaporated films. Electronic components have also played an important part in the development of modern vacuum technology. These include thermistor gauges, electronic ionization gauges, ion pumps and electronic leak-detection equipment. This paper is devoted to a review of modern ultra-high vacuum systems and the electronic components used in them.**

Introduction

HISTORICALLY, vacuum technology has played an important part in the development of electron tubes. The quality and life of these devices have been dependent on the ability to produce and maintain a high vacuum in them. In many of the early tubes, it was impossible to obtain a high vacuum. This led to the development of tubes which were, in many cases, dependent on some gas being present for their successful operation. The presence of gas in the tube placed a serious limitation on the voltage which could be applied without complete breakdown. An example of this is the cold-cathode X-ray tube. The characteristics of the early Roentgen "gas" X-ray tube depended markedly on the gas pressure in the tube. The electron stream in these tubes was produced by a low-pressure gas discharge. The current, applied voltage, and gas pressure were all interdependent. It was not uncommon in those days for a radiologist to use a series of tubes at different gas pressures to produce X rays of various energies or voltages. It was not until the highly evacuated Coolidge tube, with a hot tungsten filament to supply the electrons, was developed that the current could be adjusted independently of the applied voltage. The controllable features of the Coolidge tube have greatly facilitated research and engineering applications of X rays, particularly where precise control is required.

Another tube in which the degree of evacuation has played an important part in its performance is the cathode-ray tube. In the early Braun cathode-ray tube the electrons were liberated and concentrated by means of a gas discharge. The gas present in these early tubes was not dense enough to cause serious scattering of the electrons in the beam, but some of the gas molecules lying in the path of the beam were ionized and formed a positive ion core in the beam. The converging electric field produced by the positive core produced a definite concentrating action on the electron beam. The strength of this focusing action is dependent on the rate of ionization, which in turn depends upon the nature and pressure of the gas and the electron-beam voltage and density. Gas focusing cathode-ray tubes were by necessity slow-speed devices because of the long transit times for the ions. The attainment of a higher degree of vacuum in the cathode-ray tube made possible the development of the modern oxide-coated cathode electron gun by Zworykin in 1933. However, even today, the vacuum technology as practiced in modern cathode-ray television picture-tube processing has not progressed to the point where gas ionization effects are completely absent. Positive ions formed in the beam strike the cathode and limit its life by sputtering. This has been corrected to a large extent by the ion-trap gun. Before the aluminized backing was added to the television picture tube, difficulty was frequently encountered with ion-spot burn of the phosphor in the center of the face plate. This was caused by bombardment of the phosphor by high-velocity negative ions formed by electron attachment.

Electron-beam spread due to space charge is reduced in many modern microwave beam-type tubes by a positive ion core. In many devices this effect is enhanced by adding ion-trap electrodes at the ends of the beam to retain the ions and prevent their draining into the cathode or electron-accelerating region of the device.

Many of our modern electronic components no longer depend on a discharge in vacuum; nevertheless, vacuum technology plays an important part in their manufacture or processing. One of the most important processes is vacuum evaporation of materials for microminiature circuit elements. This involves the evaporation of thin films for passive circuit elements such as resistors and capacitors as well as superconducting films for cryotrons in logic and memory circuits. Vacuum evaporated ferromagnetic films are used in computer memory systems. Several electro-optical elements involving photoconductor-electroluminescent combinations are made by vacuum deposited films. Lack of reproducibility and uniformity in these devices are frequently associated with poor vacuum conditions. In order to maintain uniformity in some of these components which are particularly sensitive to impurities, it is necessary to carry out the evaporation process under ultra-high vacuum conditions at pressures of 10^{-10} mm Hg or better.

* Received by the IRE, February 2, 1961; revised manuscript received, April 17, 1961. The material presented in this paper has been abstracted principally from the revised edition of the late S. Dushman's book, "Scientific Foundations of Vacuum Technique" to be published by John Wiley and Sons, Inc.

† General Electric Research Lab., Schenectady, N. Y.

The testing of electronic components under conditions simulating free space will probably require pressures as low as 10^{-16} mm Hg.

It is interesting to note that, while vacuum technology has historically played an important part in the development of electronic components and will continue to do so in the future, electronic components are playing a role of increasing importance in the development of modern vacuum technology. The modern vacuum system uses semiconducting thermistor gauges for measuring relatively high pressures, electronic ionization gauges for measuring low pressures, and ion pumps for producing low pressures. Leaks are detected in vacuum systems and various other devices by electronic leak detectors using mass spectrometers, scintillation counters, Geiger-Müller tubes, and negative-ion detectors with their associated electronic circuitry.

This paper is devoted to a review of modern ultra-high vacuum systems and the electronic components used in them.

Low Pressure Manometers

Low gas pressures are measured by many different types of gauges. They may be classified, according to the basic principles involved, as follows: 1) Manometers which use mercury or some very nonvolatile liquid. The familiar U-tube manometer, and the well-known McLeod gauge are examples of these. 2) Mechanical manometers which depend on the measurement of the mechanical deformation suffered by a thin wall or diaphragm under pressure. Gauges of this type include the Bourdon spiral and aneroid barometer. 3) Viscosity manometers which depend on the viscous drag in a gas or involve the transfer of momentum by a gas. In the decrement type of viscosity gauge, a surface is set in oscillation and the rate of decrease of amplitude of oscillation is taken as a measure of the pressure. In the rotating disk or molecular gauge, a surface is set in continuous rotation and the amount of twist imparted to an adjacent surface is used to measure the pressure. The molecules striking the moving surface acquire a momentum in the direction of motion which they tend in turn to impart to the other surface. 4) Radiometer-type manometers, which depend on a mechanical force exerted between two surfaces maintained at different temperatures in a gas at low pressure. Instruments of this type are the Crookes radiometer and the Knudsen gauge. In these devices the molecules striking the hotter surface rebound with a higher average kinetic energy than those that strike the colder surface. Consequently, a momentum is imparted to the hot surface which tends to make it move. 5) Heat-conductivity-type manometers, which involve the effect of pressure on the rate of heat transfer. Gauges of this type are the thermocouple gauge, the Pirani resistance gauge and the thermistor gauge. These gauges all depend on the loss of heat from a surface by conduction through the gas at pressures where the distance between the hot and cold surfaces is less than the mean free path. 6) Ionization gauges which depend on the collection and measurement of ions formed by collisions between the gas molecules and high-velocity electrons or other energetic particles.

Fig. 1 shows the approximate operating range of pressure of the gauges just described. Major advances have been made in electronic methods of measuring pressure rather than in mechanical methods. The operating pressure range for ionization gauges has been extended in both directions from about 1 to 10^{-13} mm Hg. As low-pressure measurements have taken on more sophistication there has been a trend towards the use of partial-pressure gauges (mass spectrometers) for the identification of individual gaseous components. These mass spectrometers have taken on a variety of forms from the older magnetic-deflection types with secondary emission multipliers to increase the sensitivity and sweep rate to the more modern time-of-flight instruments and ion-resonance devices using RF fields and strong-focusing quadrupole lenses.

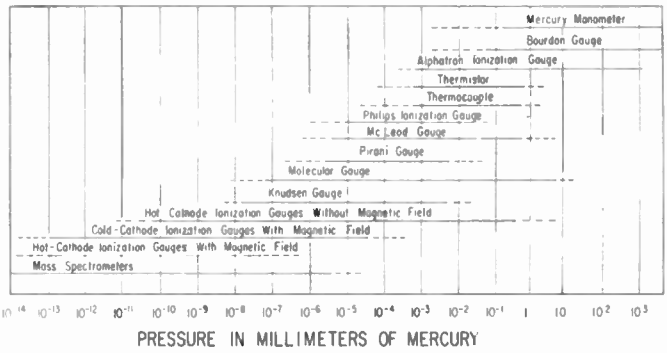

Fig. 1—Chart showing operating pressure ranges for different types of gauges.

Triode Gauges

The ionization gauge, in the form of a simple triode tube structure, is one of the oldest [1], [2] and still most widely used devices for measuring gas pressure under high-vacuum conditions. In this gauge, electrons from a thermionic cathode are accelerated through a positive grid structure. If the accelerating voltage is greater than the ionizing potential of the gas, there is a finite probability that the electrons will ionize the gas molecules on colliding with them. For a given geometry and constant grid voltage, the number of positive ions formed will be proportional to the gas pressure, provided the pressure is so low that any one electron does not make more than one ionizing collision during its flight. The number of positive ions produced is also proportional to the electron emission, provided space charge effects are negligible and do not alter the potential distribution in the gauge. A constant fraction of the ions produced is collected by an electrode which usually surrounds the grid and is negative with respect to the cathode. A measure of the resulting ion current gives an indication of the gas pressure. Let I_p denote the positive-ion current

to the ion collector, I_e the electron-emission current to the grid or anode, and P the gas pressure in the ionization gauge at some standard temperature. Then under the operating conditions discussed above

$$I_p = SI_eP \quad \text{or} \quad P = \frac{1}{S}\frac{I_p}{I_e}, \tag{1}$$

where the proportionality constant S is called the sensitivity of the gauge. If I_p and I_e are measured in the same units, S has the dimensions of reciprocal pressure. Obviously the sensitivity will depend on the nature of the gas present and the electrode geometry and voltages.

It is not uncommon for a triode ionization gauge, such as the VG-1A, shown in Fig. 2, for example, to have a sensitivity of $S = 20$/mm Hg for nitrogen. At a pressure of 10^{-6} mm Hg, substitution in (1) shows that only one ion is produced by every 50,000 electrons that travel from the cathode to the anode. The factors which affect the low-pressure limit of the triode gauge are discussed in the next section on gauges for ultra-high vacuums.

The upper pressure limit for most triode ionization gauges is about a micron. At higher pressures the ion current saturates, leveling off at a constant value independent of pressure. This is due to several effects. At high pressures the mean free path of the electrons between collisions with the gas molecules becomes comparable with the path length normally traveled by the electrons in going from the filament to the grid. Under these conditions the energy lost by the electrons in nonionizing inelastic collisions becomes important. The velocity of the electrons is reduced resulting in lower ionizing efficiencies during the latter part of their flight. The *effective* ionization potential [3] expressed in electron volts or average energy lost by the electrons per ionizing collision may well be equal to nearly half their initial kinetic energy of 150 ev.

The low-energy secondary electrons produced by ionizing collisions in a triode ionization gauge are, in most cases, not effective in producing further ionization. However, these electrons will be collected by the anode and measured with electrons emitted by the filament. If the total electron current to the grid is held constant during the operation of the gauge, as is often the case, the apparent gauge sensitivity will start to drop when these secondary electrons become comparable with the number of electrons emitted by the filament. It can be seen, by substituting numerical values in (1), that for the VG-1A with a sensitivity of $S = 20$/mm Hg, the ion current, and hence, the secondary electron current would just be equal to the electron-emission current at a pressure of 5×10^{-2} mm Hg, if the gauge could retain its sensitivity at this pressure. Actually, when the pressure becomes greater than a few microns, positive-ion space charge builds up around the cathode and an arc-like discharge is established. Under these conditions a characteristic glow may be observed in the gauge. The ion collector becomes a probe immersed in a plasma and collects the random ion current arriving at the sheath surrounding it. This current is no longer dependent on the pressure and cathode emission current in the usual way.

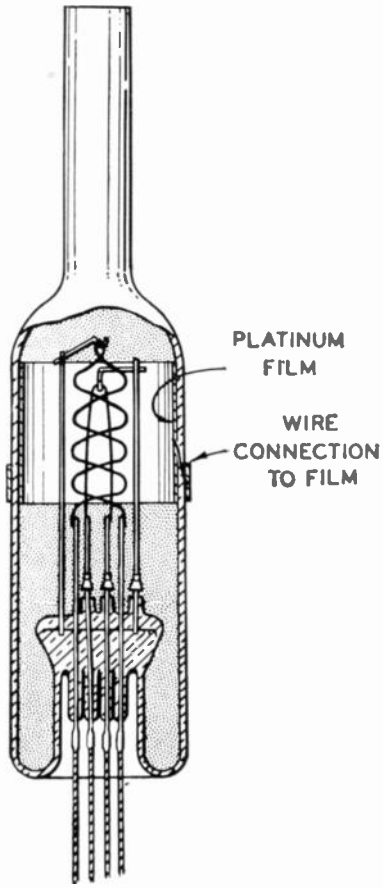

Fig. 2—The VG-1A triode ionization gauge. This popular high-vacuum gauge is outgassed by passing current through the grid and filament and by torching the envelope. The ion collector is a metallic film deposited on the wall of the envelope (Morse and Bowie).

Another factor that leads to nonlinearity in an ionization gauge at high pressures is a decrease in the ion collection efficiency. At high pressures the ions may be scattered to other electrodes before reaching the collector. This results in a smaller fraction of the total ions produced being collected by the ion collector.

Schulz and Phelps [4] have designed a high-pressure ionization gauge that takes these factors into account. Their gauge, the Westinghouse WX4145, shown in Fig. 3, operates in the approximate pressure range of 10^{-5} to 1 mm Hg. It has been used for measuring the pressure of chemically active gases as well as rare gases. The gauge consists of a 5-mil thoriated iridium filament located halfway between two parallel plates of molybdenum $\frac{3}{8} \times \frac{1}{2}$ inch spaced $\frac{1}{8}$ inch apart. The electrons emitted by the filament pass across the 60-mil gap directly to the anode plate without oscillatory motion.

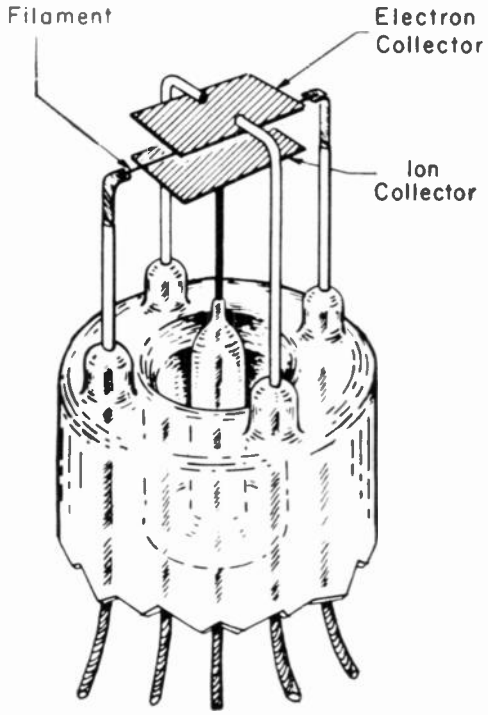

Fig. 3—High-pressure triode ionization gauge (Schulz and Phelps).

This gives the electrons a short path length independent of pressure with little chance of making more than one collision in passing from the filament to the anode. The short path length and the low anode voltage (60 v) give the gauge a sensitivity of only 0.6/mm Hg for nitrogen. This limits the secondary electrons produced by ionizing collisions to less than 10 per cent of the electron-emission current, even at pressures of 0.15 mm Hg. To insure efficient ion collection, the ion-collector electrode is made large compared to the filament, and its potential is adjusted to −60 v to assure parallel plane equipotential surfaces between the electrodes.

Philips Ionization Gauge

Many of the difficulties associated with chemically active gases reacting with the filament in the hot-cathode ionization gauges have been overcome by the Philips ionization manometer developed by Penning [5]. In this gauge, electrons are ejected from a cold cathode of zirconium, thorium, or other active surface by bombardment with positive ions which have been accelerated by passage through the cathode fall of potential. These secondary electrons are deflected by means of a magnetic field so that they travel in long helical paths before reaching the anode. The total length of path traveled by the electrons in going from the cathode to the anode is many hundreds of times the direct distance between the two electrodes. As a result, the ionization produced per electron at any given pressure is considerably greater than would be obtained in the absence of a magnetic field. The magnitude of the total discharge current, which is the sum of the positive-ion current to the cathode and the electron current from the same electrode, is used as a measure of the pressure of gas present.

Fig. 4 shows the construction of the gauge. The manometer tube M contains a ring-shaped anode R located between the cathode plates P. The magnetic field (about 370 oersteds) is applied by means of the permanent magnet H. A microammeter (to measure the current) and 1 megohm resistance are connected in series with the manometer across a dc source of about 2000 v.

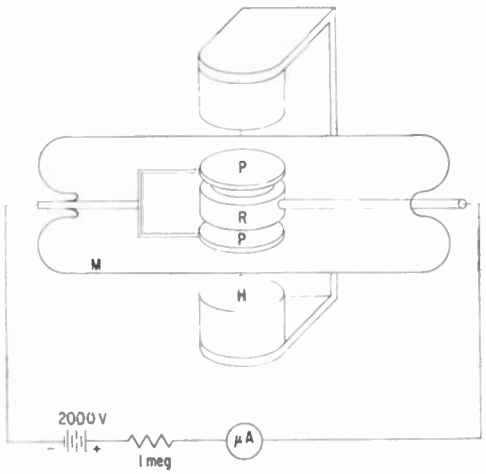

Fig. 4—Philips cold-cathode ionization gauge (Penning).

The Penning gauge does not have the accuracy of the hot-cathode triode gauge. Unstable oscillations generally occur in the glow discharge, and cause unpredictable jumps in the calibration curve. These discontinuities appear to be present in all gauges of this type, and may be as high as 10 per cent. In a later version of the gauge, Penning and Nienhauis [6] have improved the stability by replacing the ring anode with a cylinder.

Penning gauges operate over a pressure range of about 10^{-2} to 10^{-5} mm Hg. At lower pressures it becomes difficult to initiate the discharge, and in some cases it may fail completely to strike. The discharge in the Penning gauge removes gas from the sytem by processes that are discussed in a later section on ion pumps. This causes the gauge to act as a pump and disturbs the pressure distribution in the system. The rate at which gas is pumped by these cold-cathode discharge gauges is from 10 to 100 times greater than that of a hot-cathode triode gauge. For this reason they should be provided with a large tubulation with adequate conductance to prevent a pressure drop between the gauge and the vacuum system. Notwithstanding these disadvantages, the Penning gauge has found wide applications because of its simplicity and ruggedness.

Radioactive Ionization Gauges

A novel type of cold-cathode gauge was developed by Downing and Mellen [7] in the laboratories of the NRC Equipment Corporation of Newton, Mass.; it was designated the "Alphatron," to indicate that the ionization is produced by alpha particles. Fig. 5 shows a schematic diagram of the ionization chambers and electrical circuit. A dc potential of 108 v is applied between the ionization chambers and the ion collectors. The very small ionization current, produced by the alpha particles from the radium sources, is greatly amplified so that it can be read on a standard type of microammeter. The dc voltage, as well as the power for operating the amplifier, is obtained from the regular ac 60-cycle, 110-volt supply. The radium sources are so constructed that a small quantity of radium in equilibrium with its disintegration products, radon, radium A, radium B, and so forth, radiates alpha particles at a constant rate. Since radon, the first distintegration product of radium, is a gas, the source must be sealed in a plaque to prevent the loss of radon gas so that the succeeding products may be held in the source and their alpha activity utilized.

By using two ionization chambers, the Model 530 Alphatron gauge is made to operate with a linear response for air from 10^{-3} to 10^{3} mm Hg. The large chamber has a volume of 51 cc and with a radium source of 100 microcuries has a sensitivity for air of about 10^{-10} a/mm Hg. In the three high-pressure ranges from 10 to 1000 mm Hg the small ionization chamber is used in order to keep ionization current loss down due to volume recombination. The small chamber has a volume of 0.2 cc, and with a radium source of 1.5 microcuries has a sensitivity for air of about 1.5×10^{-13} a/mm Hg.

The sensitivity of the Alphatron depends on the kind of gas being measured. Conversion factors for the more common gases which are to be applied to the output current meter are given in Fig. 6. Due to recombination, the readings for gases heavier than air are not linear in the pressure range of 100 to 1000 mm Hg.

One obvious advantage of this gauge is that there is no filament to burn out and no possibility of chemical reaction between the gas and the cathode. It will also measure higher pressures than the triode ionization gauges. On the other hand, there are certain precautions (discussed very fully in the operating instructions) which have to be carefully attended to in using the gauge, in order to avoid any possible physiological effects arising from the radium emanation.

Spencer and Boggess [8] and their colleagues at the University of Michigan have also developed a radioactive ionization gauge using tritium for the radioactive source.

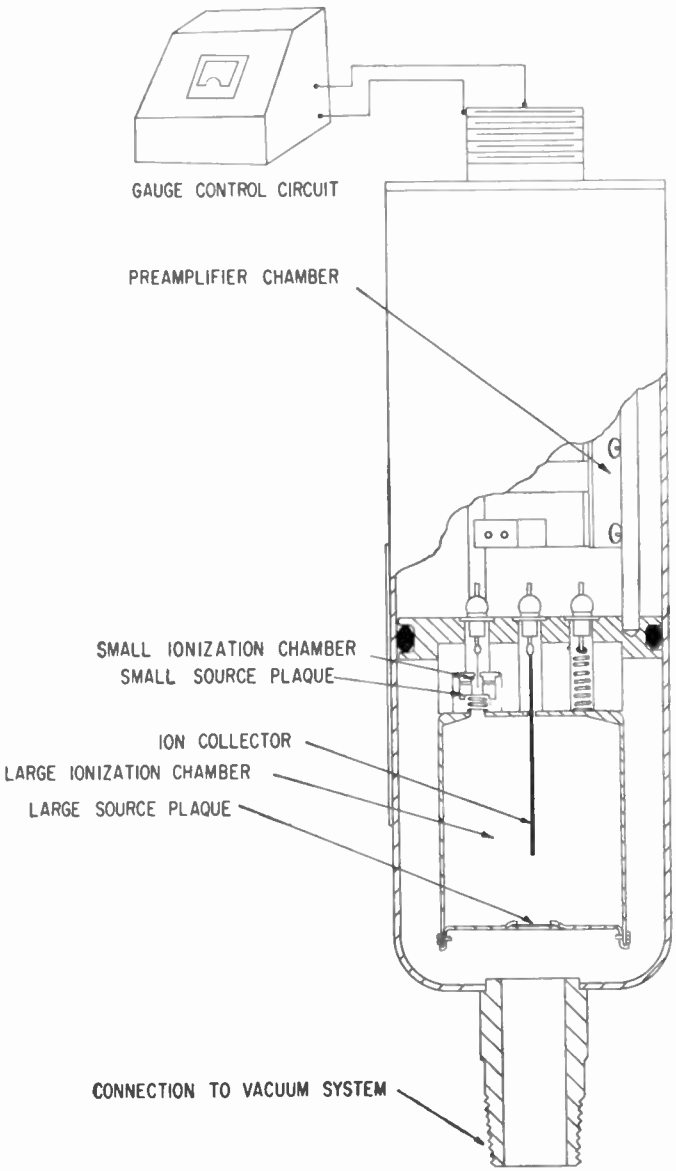

Fig. 5—Schematic sketch of the Alphatron ionization gauge which uses a radioactive source (Downing and Mellen).

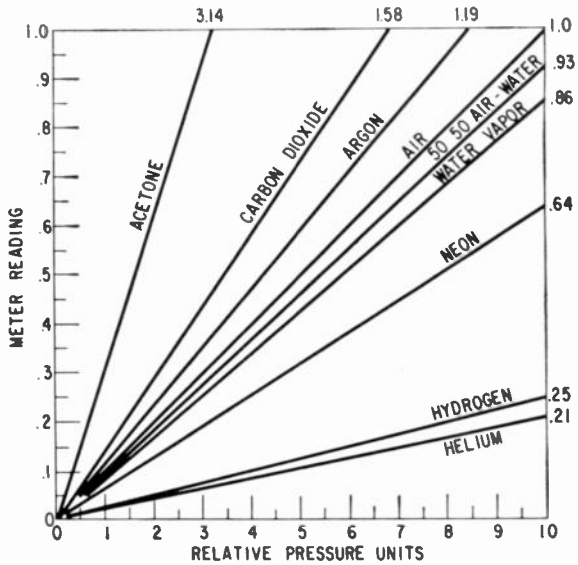

Fig. 6—Relative response of the Alphatron gauge to various gases.

Gauges for Ultra-High Vacuums

The conventional ionization gauge used prior to 1948 was not capable of measuring pressures below about 10^{-8} mm Hg. However, Nottingham and Apker had observed, in attempting to evacuate electronic devices to extremely low pressures, that thermionic and photoelectric emission characteristics indicated pressures much lower than 10^{-8} mm Hg. In 1947, Nottingham [9] presented evidence of a residual current to the ion collector which is completely independent of the pressure. This current is caused by photoelectrons ejected from the ion collector by soft X rays produced by 150-volt electrons striking the grid. Since the photoelectrons *emitted* from the ion collector cannot be distinguished on the current meter from the positive ions *incident* on the collector, there must exist a lower limit to the collector current, with decrease in pressure, which corresponds to pure photoelectric emission. For conventional gauges at normal operating voltages this X-ray photocurrent is about 2×10^{-7} times the anode current. Thus for a gauge with a sensitivity of $S=20$/mm Hg, the ion current to the collector would just be equal to the photoelectric current at a pressure of 10^{-8} mm Hg.

Bayard-Alpert Gauge

A consideration of these problems led Bayard and Alpert [10] in 1950 to develop the inverted ionization gauge shown in Fig. 7. The filament is placed outside the cylindrical grid, and the ion collector, consisting of a very fine wire, is suspended within the grid. The usual potentials are applied to the electrodes, +150 v on the grid and −45 v on the ion collector. Electrons from the filament are accelerated into the grid cylinder where they make ionizing collisions. A large fraction of the ions thus formed inside the grid are collected by the center wire. With this arrangement, the ion collector intercepts only a small fraction of the X rays produced at the grid. The small surface area of the collector wire presents a solid angle to the X rays from the grid that is several hundred times smaller than that for the conventional cylindrical collector.

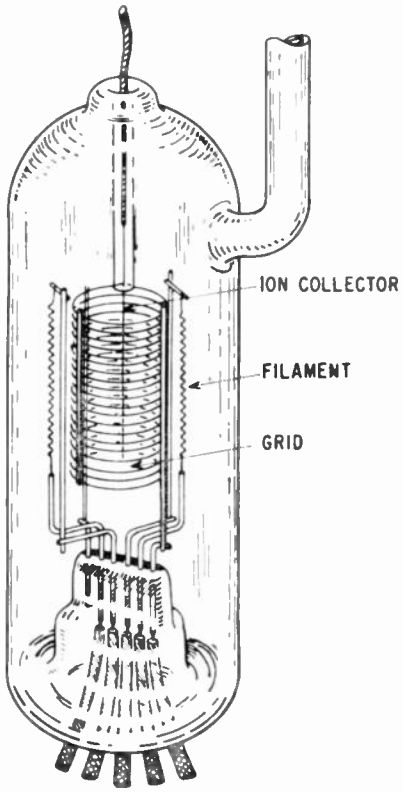

Fig. 7—The inverted triode ionization gauge (Bayard and Alpert).

A unique feature of the Bayard-Alpert gauge is the logarithmic potential distribution in the ionizing region between the cylindrical grid and coaxial ion collector. Since the potential inside the grid is nearly uniform, except in the immediate vicinity of the collector wire, the electrons travel within most of the grid volume with an efficient ionizing energy of nearly 150 ev. This is a distinct advantage over the conventional gauge, where the potential fall approximates a linear distribution between the grid and ion collector. In this case the electrons are decelerated to energies inefficient for ionization over a sizable portion of the volume between the grid and ion collector.

The almost uniform energy of the electrons in the ionizing space of the Bayard-Alpert gauge has allowed Nottingham to identify residual gases by measuring the appearance potential for ionization.

The second filament in the Bayard-Alpert gauge is electrically separated from the first, and not only serves as a spare, but may be used in connection with the flash-filament technique of estimating low gas pressure developed by Apker [11].

The glass sleeve around the ion collector lead prevents X rays from striking the large diameter lead-in wire, and provides a long leakage path between the collector and wall of the gauge which may become charged or electrically conducting from metallic deposits.

Nottingham [12] and Alpert [13] have suggested modifications of the Bayard-Alpert gauge to improve its sensitivity. The cylindrical grid is closed at top and bottom and a second grid, acting as a screen grid, is installed around all the electrodes. The purpose of closing the cylindrical grid is to prevent ions from escaping to the negatively-charged glass wall. At low pressures the ions may oscillate about the collector wire many times before being collected. Since the ions are likely to have velocity components parallel to the collector wire, they may escape through the ends of the grid before being collected unless the grid is closed. The screen grid shields the gauge from the wall charges. Operation of the screen grid at a negative potential causes the electrons to oscillate several times through the positive grid before being collected. This increases their average path length and gives the gauge a higher sensitivity. In some cases the screen grid is made by coating the glass envelope with a conducting film that is connected to an external lead. These improvements have increased the sensitivity by factors of two or three.

Nottingham [14] reported finding that at normal calibrating pressures the ion collector in the modified Bayard-Alpert gauge did not collect a constant fraction of the ions generated inside the grid. He found that for nitrogen at a pressure of 2.4×10^{-3} mm Hg the gauge may be in error by as much as a factor of 2 at emission currents of 100 μa and a factor of 6 at 1 ma. Correct readings are obtained at 10 μa and less. He observed similar effects to a smaller degree in the Bayard-Alpert gauge of type WL-5966. As the gas pressure is reduced the maximum permissible electron current increases inversely with the square root of the pressure. Nottingham suggests that this effect may be due to positive-ion space charge in the vicinity of the ion-collector wire.

The Bayard-Alpert gauge, in the form of the Westinghouse WL-5966, has a sensitivity of $S=12$/mm Hg for nitrogen and has a linear calibration curve over the pressure range of 10^{-9} to 10^{-4} mm Hg. The helium sensitivity is a factor of ten lower. Because of its simplicity of construction, ease of outgassing, and dual filaments, this gauge has found wide acceptance and use by workers in all phases of the high-vacuum field.

Cold-Cathode Inverted Magnetron Gauge

The Penning type of cold-cathode discharge gauge would appear to have certain advantages over the hot-cathode triode ionization gauges for measurement of ultra-high vacuums. There is no limitation on pressure measurements due to X-ray photoemission, since the number of electrons that strike the anode and produce the X rays decreases with the pressure. The vapor pressure of a hot tungsten filament also presents no limitations on the low-pressure limit. However, there are certain inherent disadvantages in the operation of a Penning gauge at pressures below 10^{-6} mm Hg. In most gauges the discharge fails to strike below these pressures. The application of higher voltages to start and maintain the discharge leads to field emission from the ion-collector electrode which cannot be distinguished from ion current by the external measuring circuit. This field-emission current establishes a lower-pressure limit for the operation of the Penning gauge analogous to the X-ray limit for the Bayard-Alpert gauge. To circumvent these difficulties Hobson and Redhead [15] designed an ionization gauge employing a cold-cathode discharge in crossed electric and magnetic fields. Their gauge, shown in Fig. 8, has the structure of an inverted magnetron with an auxiliary cathode. This geometry provides efficient electron trapping in the discharge region, and the auxiliary cathode provides the initial field emission for starting and allows the positive-ion current to be measured independently of the field-emission current. The auxiliary cathode also acts as an electrostatic shield for the ion collector. The two short tubular shields, which project 2 mm into the ion collector from the auxiliary cathode, protect the end plates of the ion collector from the high electric fields and provide the field emission which initiates the discharge.

The gauge operates with an applied magnetic field of 2060 oersteds and a potential of six kv on the anode. Under these conditions the relationship between ion collector current and pressure is given by

$$i_p = cP^n, \tag{2}$$

where i_p is the collector current in amperes, P is the pressure in mm Hg, c is a constant between 1 and 10, and n lies between 1.10 and 1.4 for various gauges. According to Hobson and Redhead, the value of n is essentially independent of the anode voltage, and approaches unity as the magnetic field is increased. The dimensions of the gauge have little effect on the value of n. In the theory of the Townsend discharge applied to the inverted magnetron gauge, Redhead [16] has pointed out that this nonlinear relationship between the ion current and pressure exists because the striking voltage is a slowly varying function of the pressure.

Unlike the triode gauges, the sensitivity ratio of the inverted magnetron gauge for various gases is a function of pressure. The sensitivity ratio for helium to air decreases with pressure and is also a function of the anode voltage.

Oscillations were observed in the inverted magnetron gauge under most operating conditions. Discontinuous jumps in the mode of oscillation from one frequency to another give only small discontinuities in the current-pressure characteristics.

The time lag between the application of anode voltage to the gauge and the initiation of the discharge becomes

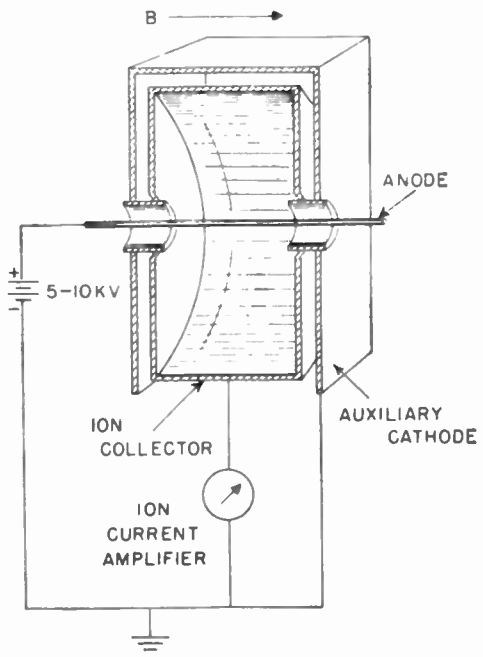

Fig. 8—The cold-cathode inverted magnetron ionization gauge (Hobson and Redhead).

appreciable and variable at pressures below 10^{-8} mm Hg. At pressures near 10^{-12} mm Hg the time lag was as long as ten minutes; however, it is reported that no gauges failed to strike.

A commercial version of this gauge, type 2205-02, is now manufactured by the NRC Equipment Corporation of Newton, Mass. The commercial gauge operates over a pressure range from 10^{-4} to 10^{-12} mm Hg with a sensitivity of 4.5 a/mm Hg for air at 6000 v with a magnetic field strength of 1000 oersteds.

Hot-Cathode Magnetron Ionization Gauge

In order to extend the low-pressure limit of the conventional hot-cathode ionization gauge it is necessary, at a given emission current, to increase the ratio of the ion current to the X-ray photocurrent. As previously explained, this was accomplished in the Bayard-Alpert gauge by reducing the X-ray photocurrent without substantial loss of gauge sensitivity. This ratio may also be increased by increasing the sensitivity of the ionization gauge. It is evident that if the gauge is modified in such a way that the electrons travel in longer paths before they are collected by the positive grid or anode, the probability of their colliding with and ionizing a gas molecule will be greatly enhanced and the sensitivity of the gauge will be improved with no increase in X-ray photoemission. Lafferty [17] has applied this principle in developing a hot-cathode magnetron ionization gauge for ultra-high vacuum use. In this arrangement, shown in Fig. 9, a cylindrical magnetron is operated with a magnetic field greater than cutoff. Two end plates maintained at a negative potential relative to the cathode prevent the escape of electrons. One or both of these plates may be used to collect the positive-ion current generated in the magnetron. Electrons emitted by the tungsten-filament spiral around the axial magnetic field in the region between the negative end plates. If the magnetic field is sufficiently high, most of the electrons fail to reach the anode. Some of the electrons make many orbits around the cathode before being collected. The electron density is therefore increased by the presence of the magnetic field and the probability of ionizing the gas is considerably increased. This is illustrated in Fig. 10, where the ion current to one end plate and the electron current to the anode are plotted as a function of magnetic field for a magnetron gauge with an anode

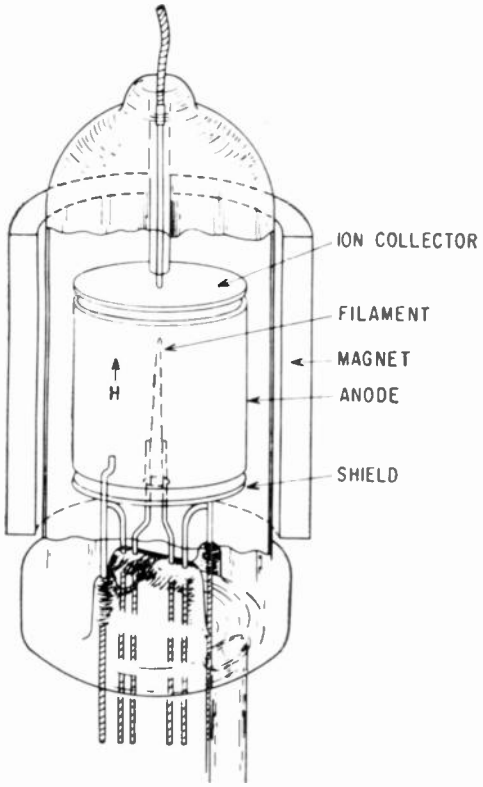

Fig. 9—The hot-cathode magnetron ionization gauge (Lafferty).

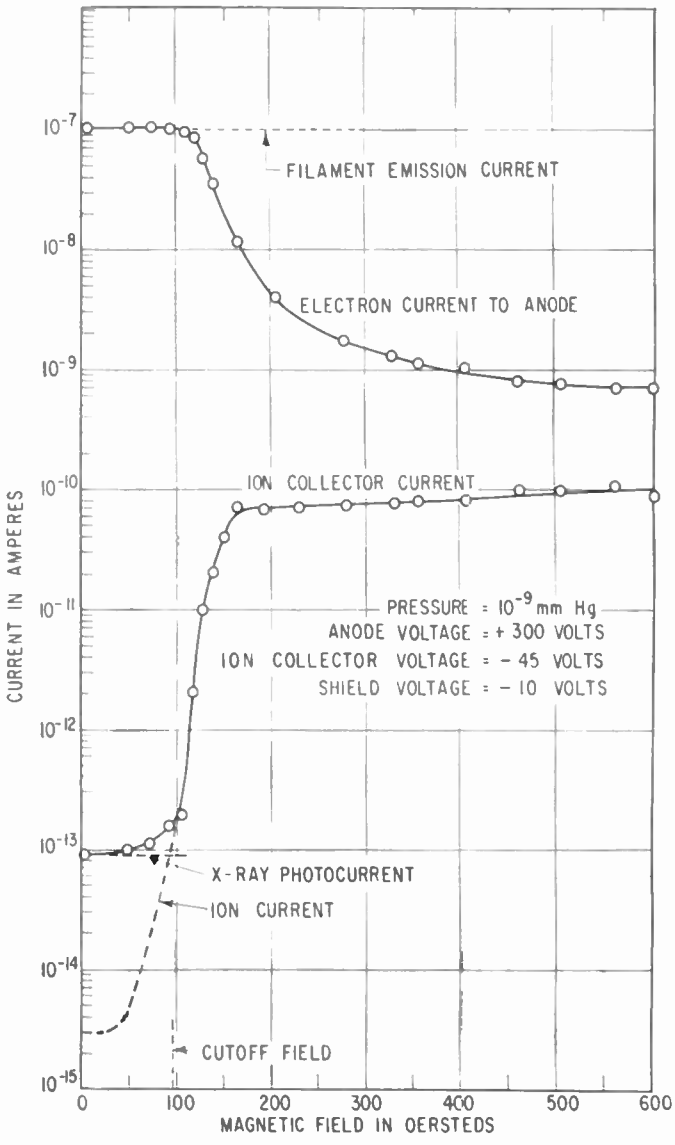

Fig. 10—Ion-collector current and anode electron current as a function of magnetic field for the hot-cathode magnetron gauge.

15/16 inch in diameter and $1\frac{1}{8}$ inches long. The 8-mil hairpin tungsten filament is $\frac{3}{4}$ inch long, separated 40 mils at the base. The filament temperature is adjusted to give an emission current of 10^{-7} a with zero magnetic field. Under these conditions the ion-collector current is nearly 10^{-13} a at a pressure of 10^{-9} mm Hg. However, from measurements made in the 10^{-6} mm Hg pressure range, the sensitivity of the gauge is known to be 30/mm Hg. Thus the true ion current at a pressure of 10^{-9} mm Hg would be only 3×10^{-15} a, as shown by the dotted line in Fig. 10. The actual current measured in the ion-collector circuit is 30 times this value and is essentially all photocurrent produced by X rays from the 300-volt electrons striking the anode. From this it would appear that on the average one photoelectron is emitted by the ion collector for every million electrons striking the anode. As the magnetic field is increased and the electrons begin to miss the anode, their path length is increased. This is indicated by a sharp rise in the ion current and a drop in the electron current collected by the anode. At a magnetic field strength of 250 oersteds, the ion current is enhanced 25,000 times over what it would be without the field, and the electron current collected drops to 1/50 of its former value. The ratio of ion current to X-ray photocurrent is thus increased 1.25×10^{6} times by application of the magnetic field. Since the cutoff current to the anode remains constant independent of pressure at these low pressures, the ion current to the collector would just equal the X-ray photocurrent at a pressure of 2.4×10^{-14} mm Hg. Thus, pressures at least this low could be measured. In practice, the ability to read low pressure is limited by the sensitivity of the external circuit used to measure the ion current.

Hot-cathode magnetron gauges have been shown to have extremely high sensitivities when operated in the ma electron-emission range at pressures of the order of 10^{-5} mm Hg [18]. However, they have always been subject to excessive pumping action and unstable operation frequently associated with oscillations. Lafferty has found that these conditions may be avoided by operating the magnetron gauge at very low electron-emission levels.

Partial-Pressure Gauges

While the ionization gauges give a measure of the total residual pressure of the gases in a vacuum system, there are times when it would be highly desirable to know what these residual gases are. In the hot-plasma experiments related to fusion, it is important to know the purity of the gases involved since the presence of ions of large mass compared to the hydrogen isotopes tend to cool the plasma. Recent interest in determining the neutral and ionic components of the upper atmosphere and beyond has stimulated the design of special equipment for this purpose. Successful rocket and satellite flights have already been made with the Bennett radio-frequency type of mass spectrometer. Many more such devices are sure to follow for space investigations.

Omegatron

The omegatron, originally developed by Sommer, Thomas, and Hipple [19] for measuring atomic constants, has been used by Alpert and Buritz [20] as a mass spectrometer for measuring the partial pressures of the various gases in an ultra-high vacuum system. A simplified version of the omegatron capable of high-temperature outgassing as developed by Alpert and Buritz is shown in Fig. 11.

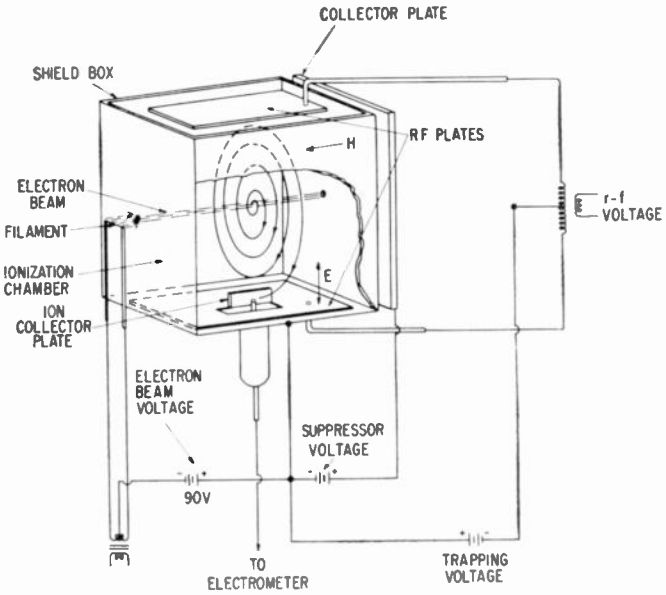

Fig. 11—Schematic diagram of a simplified version of the omegatron (Sommer, Thomas, and Hipple) developed by Alpert and Buritz.

The operation of the omegatron is similar to that of the cyclotron. Electrons emitted from the hot filament are accelerated through a 1/16-inch-diameter aperture to form a 4-μa beam at 90 v. This beam, which produces ions in the ionization chamber, emerges through a second aperture and is collected by a collector plate biased positively with respect to the shield to suppress secondary emission. The parallel magnetic field H has a strong collimating action on the electron beam. The shield box forms a 2-cm cube. The RF plates, which form the top and bottom of the ionization chamber, are connected to a source of RF voltage (about one or two volts). These plates produce an RF field E across the ionization chamber perpendicular to the magnetic field. Ions formed by electrons colliding with the gas molecules within the electron beam are caused to spiral around the magnetic lines of force by their own thermal and dissociation energies. The radii of these spirals are very small and few ions would normally escape from the electron beam due to their own initial energy. However, the applied weak electric RF field causes the ions to be accelerated in Archimedes-like spiral orbits of increasing size provided the frequency of the applied RF voltage is the same as the cyclotron frequency of the ions. A trapping voltage that is positive with respect to the RF

plates is applied to the shield box to produce an electric field which retards the loss of ions in the axial direction of the magnetic field. This gives the RF field an opportunity to act on the ions over a greater number of cycles. The spiral orbits terminate on a 1/16-inch-square ion-collector plate. The ion current to this electrode, detected by a vibrating-reed electrometer, is a measure of the abundance of the gas with a cyclotron frequency equal to applied frequency.

Alpert and Buritz report that an omegatron of this design has a sensitivity of $S = 10$/mm Hg which is comparable to that of an ionization gauge. With a magnetic field intensity of 2100 oersteds the RF oscillator must be swept from 3.2 Mc to 81 kc to cover a mass range from 1 to 40. There is some discrepancy between the observed and calculated frequency for a given mass, presumably due to lack of uniformity of the RF field. However, the instrument has adequate resolution up to at least mass 40.

An analysis of the ion motion in the omegatron has been made by Sommer, Thomas, and Hipple [21] assuming a uniform sinusoidal varying RF field normal to a constant magnetic field. The results of their study may be summarized as follows:

Cyclotron or resonant frequency:

$$f = 1.54 \frac{H}{M} \text{ kc.}$$

Number of revolutions made by ions before reaching collector at resonance:

$$n = 3.06 \cdot 10^{-5} \frac{R_0 H^2}{E_0 M}.$$

Time for ions to reach collector at resonance:

$$t = 0.02 \frac{R_0 H}{E_0} \mu\text{sec.}$$

Length of spiral path for ions at resonance:

$$L = 9.6 \cdot 10^{-5} \frac{R_0^2 H^2}{E_0 M} \text{ cm.}$$

Final energy of resonant ions at collector:

$$V = 4.8 \cdot 10^{-5} \frac{R_0^2 H^2}{M} \text{ ev.}$$

Maximum radius attained by nonresonant ions differing in mass by the amount ΔM from the resonant ions of mass M:

$$r_m = \frac{2}{\pi n} \frac{M}{\Delta M} R_0 \text{ cm.}$$

Resolution (defined as midpeak frequency per width of resonant peak, theory assumes parallel-sided peaks):

$$\frac{M}{\Delta M} = 4.8 \cdot 10^{-5} \frac{R_0 H^2}{E_0 M},$$

where

E_0 = peak value of sinusoidal RF field in v/cm,
M = mass of ion in atomic mass units,
R_0 = distance from electron beam to ion collector in cm, and
H = magnetic field intensity in oersteds.

If these equations are applied to the Alpert and Buritz omegatron it is found that if one assumes $E_0 = 1$ v/cm, $R_0 = 1$ cm and $H = 2100$ oersteds, then for helium the required radio frequency for resonance is 810 kc. At resonance the helium ions will spiral around 34 times traveling about one meter in 42 μsec before being collected. The helium ions will gain 53 ev of energy from the RF field. At the resonance frequency for helium, the molecular ions of hydrogen travel less than 0.4 mm away from the electron beam. The resolution is nearly 53.

The resolution of an omegatron may be improved by operating at low RF voltages. However, under these conditions the ion-path length becomes large and the device must be operated at low pressures to prevent scattering. Further effects of varying the operating parameters on the performance of the omegatron are discussed by Edwards [22].

Magnetic-Deflection Mass Spectrometers

Mass spectrometers of the magnetic-deflection type have also been used in measuring the residual gases in ultra-high vacuum systems. Reynolds [23] has described a high-sensitivity mass spectrometer for noble gas analysis. A nine-stage electron multiplier with magnesium-silver dynodes is used to give a gain in the range of 10^3 to 10^6 electrons per ion. This increase in sensitivity permitted Reynolds to measure partial gas pressures of the order of 10^{-12} mm Hg. A total pressure of 5×10^{-10} mm Hg was achieved during operation of the spectrometer after rigorous bakeouts.

A small, portable, magnetic-deflection-type mass spectrometer with a secondary emission electron multiplier has also been developed by Davis and Vanderslice [24] for studying residual gases at ultra-high vacuums and for making transient pressure studies. This device is shown in Fig. 12. Because of its small size, it has the advantage that it can be sealed directly to the tube or system being investigated and is easily transportable. The spectrometer may be baked out at 450°C and operated at ultra-high vacuums when properly processed.

The design consists of a 90° sector-5-cm radius of curvature magnetic analyzer which will resolve adjacent mass peaks up to about mass 140. A Nier-type ion source is used and the ion detector is a ten-stage DuMont 6467 electrostatically focused electron multiplier

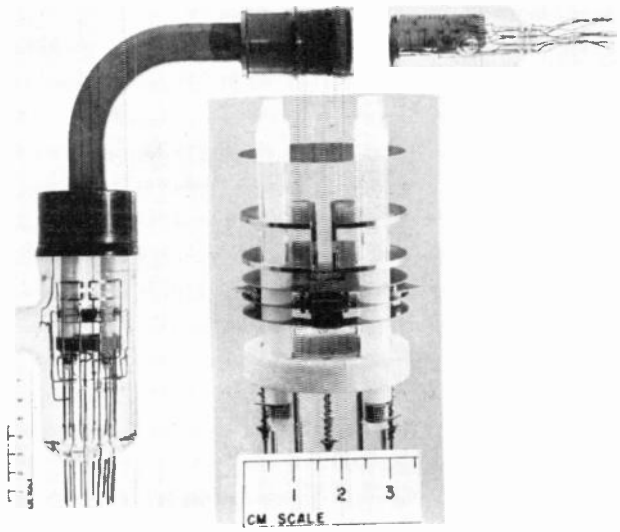

Fig. 12—A small portable mass spectrometer with secondary emission multiplier for the study of transient pressure phenomena at ultra-high vacuums (Davis and Vanderslice).

with a gain of one to ten million. The sensitivity of this spectrometer is in the range of 0.02 to 0.2/mm Hg without the multiplier. Assuming that the lowest current which can be conveniently measured is 10^{-14} a, this spectrometer, without the multiplier, could be used to detect partial pressures of about 10^{-10} mm Hg. With the multiplier, the output current is increased by a factor of 10^6 to 10^7, but because of the multiplier dark current, a gain in sensitivity of only 10^3 can be realized at room temperature. Under normal conditions a dark current of 10^{-10} a was obtained. With a multiplier gain of 10^7 this corresponds to an equivalent ion current of 10^{-17} a. This is equal to the signal current that would be produced by a partial pressure of 10^{-13} mm Hg. Cooling the multiplier in liquid nitrogen or counting individual ion pulses reduces the dark current by a factor of 100, making pressures of the order of 10^{-15} mm Hg measurable.

An additional advantage of the multiplier is that it raises the signal level to a point where a low output load resistance may be used to give a short response time. This makes it possible to scan the mass range and display the spectrum on an oscilloscope. Several ion species may thus be observed almost simultaneously during a transient pressure or composition phenomenon. The saw-tooth voltage which is available on a Tektronix 545 scope and automatically synchronized with the display makes an excellent source of sweep voltage. Fig. 13 shows an example of an oscilloscope display for the isotope spectrum of CO^+ obtained after bakeout at a pressure of 6×10^{-8} mm Hg. The mass peaks 28, 29, and 30 correspond to $C_{12}O_{16}^+$, $C_{13}O_{16}^+$, and $C_{12}O_{18}^+$ respectively. These peaks occur in the ratio 100:1:0.2. This spectrum was taken at a sweep speed of 3 msec per unit mass. Sweep rates as high as 1.5 μsec per unit mass have been used successfully. At the higher sweep rates the familiar well-defined mass peaks degenerate into groupings of pulses due to the collection of individual ions.

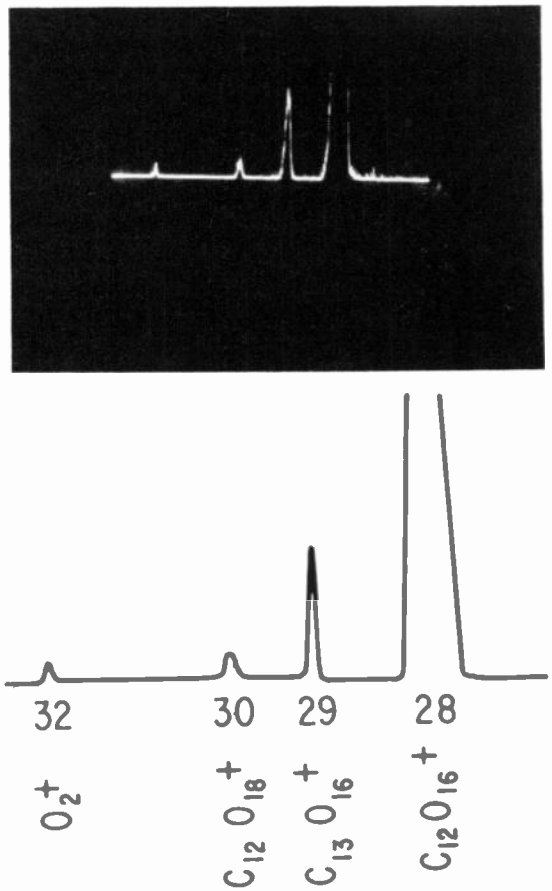

Fig. 13—Oscillogram of CO^+ isotopes taken at 6×10^{-8} mm Hg with a sweep speed of 3 msec/unit mass with the spectrometer shown in Fig. 12.

Vacuum Systems

For any operating vacuum system there will be established a stationary pressure P_e, which corresponds to the equilibrium between the flux of gas into the system and rate of exhaust. This rate of flow of gas Q into the system may arise from desorption from the walls of the system, back diffusion from the pumps, or atmospheric gas permeation of the walls. For a system of volume V and pumping speed S, the rate of reduction of pressure is given by

$$\frac{dP}{dt} = -\frac{S}{V}P + \frac{Q}{V}. \tag{3}$$

For the simple case in which S and Q are constants, independent of pressure, the solution of this equation is

$$P = \frac{Q}{S} + \left(P_0 - \frac{Q}{S}\right)e^{-t/(V/S)}, \tag{4}$$

where V/S is now the pumping-time constant or characteristic pumping time of the system, *i.e.*, the time required to pump the system down to 0.368 of its initial pressure P_0. The equilibrium pressure finally attained in the system will be

$$P_e = \frac{Q}{S}. \tag{5}$$

Obviously, then, to achieve ultra-high vacuum it is necessary that the rate of gas leakage into the system divided by the pumping speed of the system be small.

In order to keep the influx of gas low, it is necessary to keep back diffusion from pumps at a minimum by using effective traps with low-backstreaming pumps.

Desorption from walls of the system is a major source of gas, and this is generally decreased by baking the system to temperatures up to 500°C or by immersing the system in a refrigerant such as liquid helium [25]. The required high-temperature bakeout makes the use of stopcocks, glass taper fittings, wax, etc., impractical.

The leak rate of gas through the walls of the system must be small. Alpert and Buritz [26] have shown that the ultimate limit to the achievement of very low pressures in glass systems is fixed by the diffusion of atmospheric helium through the walls of the system. They measured this rate for borosilicate glass as approximately 10^{-15} mm l/sec/cm². A one-liter system with a surface area of 1000 cm² would require a pumping speed of only 0.01 l/sec to maintain a pressure of 10^{-10} mm Hg. Norton [27] has made measurements of the permeation rate of helium through various glasses and the results are shown in Fig. 14. The rate for borosilicate glass is in substantial agreement with the value given by Alpert and Buritz.

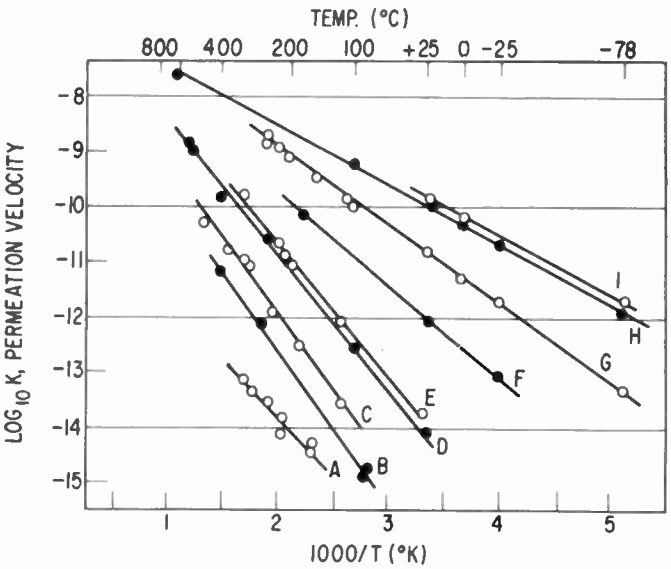

Fig. 14—The log of the permeation velocity K of helium plotted against the reciprocal of the absolute temperature T for various glasses. K is in units of cm³ gas (NTP/sec/cm² area/mm thickness/cm Hg gas-pressure difference). Curve A) Lead borate glass. B) X-ray shield glass. C) Combustion tubing Corning No. 1720. D) Soda-lime glass Corning No. 0080. E) Phosphate glass. F) Borosilicate glass Kimball No. 650. G) Chemical Pyrex-brand glass No. 7740. H) Fused silica. I) Vycor-brand glass.

As the graph shows, the permeation of atmospheric helium can be decreased by a selection of the glass used in the vacuum system. Corning 1720, for example, has a permeation rate 10^{-5} lower than ordinary borosilicate glass (Corning 7740). Since the diffusion rate of helium is much lower through crystalline materials than through glass, it is expected that an all ceramic-metal system would have a low permeation rate for helium and that the ultimate pressure would only be limited by the outgassing of the metal and ceramic.

Another limit to the achievement of low pressures is the finite vapor pressure of the tungsten filament in the ionization gauge. At 2300°K, for example [28], the vapor pressure is 10^{-12} mm Hg. This limits the temperature to which a tungsten filament may be heated in an ultra-high vacuum ionization gauge. However, lanthanum boride [29] produces 10 ma emission at 1000°K and the vapor pressure is about 10^{-4} lower than tungsten at the same electron-emission current density.

In the past few years, a variety of components specifically designed for ultra-high vacuum systems have become available. A discussion of these follows.

Pumps for Ultra-High Vacuum

Diffusion Pumps

The operation of a diffusion pump depends on the effusion of gas molecules from the region being evacuated into the directed vapor stream of the pump [30]. Some of the directed momentum of the vapor molecules is imparted to the gas molecules in the system thus creating a pressure gradient causing the gas to flow through the pump. This process is independent of pressure once the pressure had been lowered by a backing pump to a value at which molecular flow or effusion can occur and the pumping speed will rise to a plateau value and remain there for all lower pressures. The rate of gas evolution from the pump itself becomes significant at lower pressures and eventually exceeds the measured rate of introduction of gases into the pump from the vacuum system. Eventually, then, the net pumping speed of the diffusion pump falls to zero due to the gas evolution and backstreaming of the pump fluid from the pump itself.

Hagstrum [31] and Becker and Hartman [32] at the Bell Telephone Laboratories have used mercury-diffusion pumps with liquid-nitrogen-cooled traps to attain ultra-high vacuum. Recent experiments by Venema and Bandringa [33] have demonstrated that a properly designed mercury pump and a series of traps will attain a vacuum of at least 10^{-12} mm Hg. Vanderslice has achieved a pressure of 3×10^{-12} mm Hg at room temperature using the techniques of the above authors.

Oil diffusion pumps have very high pumping speeds, but until recently it was felt that their pressure limit was in the vicinity of 10^{-7} mm Hg. Even with a high pumping speed, the ultimate pressure is limited by the high value of backstreaming. Alpert [34] has shown that at some pressure between 10^{-7} and 10^{-8} mm Hg the conventional oil diffusion pump becomes a source of contamination for a "clean" vacuum system. The oil pumps were at first used to evacuate the systems down to 10^{-7} mm Hg and after the system was closed off from the oil pumps, the pumping action of the ionization gauge was

used to pump to lower pressures. Alpert [35] subsequently designed a copper-foil trap, shown in Fig. 15, that would prevent the backstreaming of oil vapor but would not seriously restrict the conductance and pumping speed of the system. With the gettering action of the copper-eliminating backstreaming, the oil pump evacuated the system to pressures below 10^{-10} mm Hg. The copper-foil trap was effective even at room temperature and for periods of several months. The trap was reactivated by baking with the rest of the system. The exact mechanism whereby the trap adsorbs backstreaming oil vapor at room temperature is not fully understood, but with proper traps an oil diffusion pump may be used in ultra-high vacuum experiments.

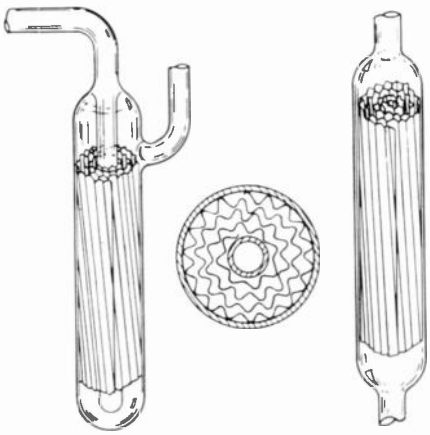

Fig. 15—Copper-foil trap (Alpert).

The recent work of Biondi [36] utilizing nonrefrigerated molecular sieve traps has had, and will continue to have, a profound impact on the use of oil pumps for ultra-high vacuum experiments. With these traps it is now possible to achieve ultra-high vacuum with oil pumps without the use of refrigerants for reasonably long times. The most popular materials at the moment are zeolite and alumina with some advantages being claimed for alumina. Harris [37] has demonstrated that the activity of oxide cathodes may be maintained for a period of several days, and perhaps longer with the use of alumina traps. A comparative test without alumina and with conventional cold trapping showed that a similar oxide cathode lost much of its activity in a comparable time.

Ion Pumps

The ionization gauge itself may be used for pumping, once the pressure has been brought to a low value. The pumping speed of ionization gauges is low, of the order of hundredths of liters per second, but with a low influx of gas Q the speed is sufficient for a well-baked-out system. Alpert [38] has demonstrated that a Bayard-Alpert gauge with titanium continually evaporated to the wall has a pumping speed of at least 20 liters/sec at low pressures.

The most important development in the last few years has been the advent of commercially available ion pumps with relatively high pumping speeds down to at least 10^{-9} mm Hg. Hall [39] reports a pressure of 10^{-11} mm Hg using a baked-metal system and an ion pump.

The cold-cathode ion pump is basically a variation of a Penning ionization gauge consisting of a ring anode and two cathode plates in a magnetic field as shown in Fig. 4. The anode is operated at high-positive potential with respect to the cathode. Electrons emitted by the cold cathode are forced into a spiral path by the presence of a strong magnetic field. The increased electron path results in a high probability for collision and ionization between electrons and gas molecules. The positive ions then bombard the cathode and sputter metal from the cathode. The sputtered metal deposits in various regions of the tube forming stable compounds with the chemically active gas molecules. Chemically inert gas atoms such as argon are also pumped, but by a different mechanism. In an ion pump much of the inert gas is initially found in the sputtered deposit on the cathode. Fig. 16 shows a radiograph of the cathode of a commercial two-electrode pump in which radioactive krypton 85 has been pumped. The pump was disassembled and the cathode placed in contact with a photographic film showing that the krypton was chiefly located in the sputtered deposit on the cathode.

If the ion current density on an electrode surface is uniform, the clean-up of inert gas on that surface is zero after a short period of time. Initially a small number of ions will be imbedded in the surface, but as soon as sputtering occurs, imbedded gas is released. A condition is soon reached in which the net clean-up rate is zero since the rate at which ions are driven into the newly exposed surface is just equal to the rate of release of gas from the surface by sputtering. If an ion current density gradient exists on the electrode surface, there will be a build-up of sputtered metal in areas of low current density and consequently gas clean-up will occur. The Penning-type discharge in a two-electrode pump is somewhat unstable during operation, producing changes in the distribution of the ion current density at the cathode surface. This results in the resputtering of previously sputtered metal on the cathode, and consequently in the release of gas previously cleaned up. This is frequently referred to as the ion pump memory effect. This effect is reported to be minimized by grooving the cathode [40].

Inert gases are also cleaned up at the anode to some extent [40], [41]. The gas is found in the metal which has been sputtered from the cathode. There is the question how the gas sticks to the anode since unexcited inert gas atoms are not adsorbed on the electrode surfaces for long enough times at room temperature to be covered by sputtered metal and the ions normally do not have sufficient kinetic energy to reach the anode. There are several plausible explanations for this: 1) neutral inert gas atoms are excited by the discharge stick

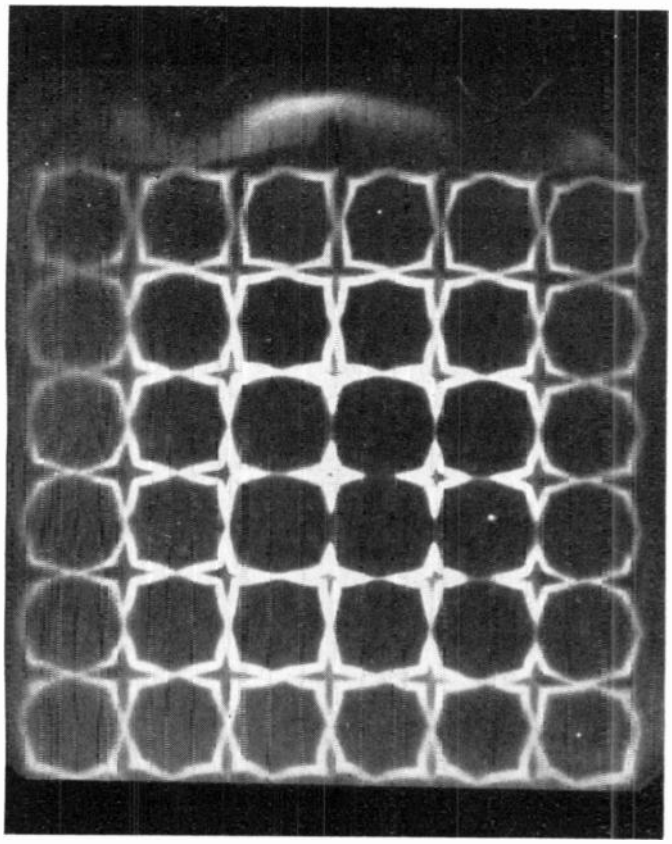

Fig. 16—Radiograph showing the location of radioactive krypton 85 in the sputtered deposit on the cathode of an ion pump.

to the anode and are covered by sputtered metal from the cathode; 2) high-velocity neutral atoms produced by charge exchange are driven into the anode and then covered by sputtered metal from the cathode; 3) the gas ions gain sufficient kinetic energy to reach the anode through oscillations in the discharge; and 4) the gas is swept out of the space between the electrodes by the high flux of the metal vapor. The first two explanations appear more likely. Although the anode mechanism is less efficient than coverage of ions at the cathode, the clean-up is permanent because resputtering of material from the anode cannot occur.

Three-electrode ion pumps have been studied in this laboratory [41] and elsewhere [42]. In the arrangement shown in Fig. 17, the third electrode is placed in a favorable position to receive sputtered metal from the cathode. The voltage applied to this electrode is intermediate between the cathode and anode so that the inert gas ions are driven into it with sufficient energy to be embedded but not sufficient to cause appreciable sputtering. Thus gas cleaned up by this electrode is permanent.

Ion pumps offer great promise of replacing many conventional diffusion pumps. Their principal advantages are that the system is never exposed to contamination from diffusion-pump fluids and no refrigerants are necessary. One of their present disadvantages is the difficulty of pumping large quantities of organic vapors of high molecular weight such as benzene and toluene at pressures above 10^{-5} mm Hg. Another disadvantage is their inability continually to pump large amounts of gas at high pressure because of excessive cathode heating and sputtering.

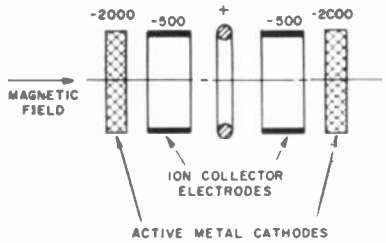

Fig. 17—Three-electrode ion pump.

Cryogenic Pumps

Immersion of the whole or part of a vacuum system in liquid air or immersion of a trap containing charcoal in liquid air was a convenient way of producing low pressures in the days before the advent of diffusion pumps. In recent years with the need for large systems for space simulation and routine experiments at ultra-high vacuum, cryogenic pumping is again becoming popular. At liquid-helium temperatures, only helium and hydrogen have appreciable vapor presseses. All other gases condense out on the surface of the cooled container. The sticking probability for most gases approaches unity as the temperature is lowered, and the total pressure can be reduced to the ultra-high vacuum range in the absence of hydrogen or helium. If hydrogen or helium are present in quantities greater than monolayer amounts, they can be removed by other means such as ion pumping. The speed of a cryogenic pump is determined by the area of the cold surface and the conductance of the connecting tubing.

For the efficient design of a cryogenic pump, it is necessary to reduce the radiation incident on the trap from the walls of the vessel. The helium trap is normally jacketed by liquid nitrogen.

Cryogenic pumping shows much promise for large specialized system applications such as space-simulation chambers. The General Electric Missile and Space Vehicle Department in Philadelphia, Pa., is constructing a gigantic space simulator using low-temperature gaseous helium-cooled walls as pumps.

Ultra-High Vacuum Components

Since mercury cutoffs, standard stopcocks, and rubber gaskets are not bakeable, their use in ultra-high vacuum systems is prohibited. Stopcock grease, mercury or other fluids used in cutoffs tend to contain large amounts of occluded gas. This has led to the development of a new line of hardware components for ultra-high vacuum systems.

Vacuum Tubes

Alpert [35] has developed a tube (Fig. 18) which can withstand bakeout at ~450°C and has a sufficiently large conductance for ultra-high vacuum systems. Since then there have been many improvements in this general type of tube [43]. A popular commercially available tube is made by the Granville-Phillips Corporation of Pullman, Wash., and is shown in Fig. 19. This particular tube has a conductance variable from one liter/sec to less than 10^{-14} liter/sec.

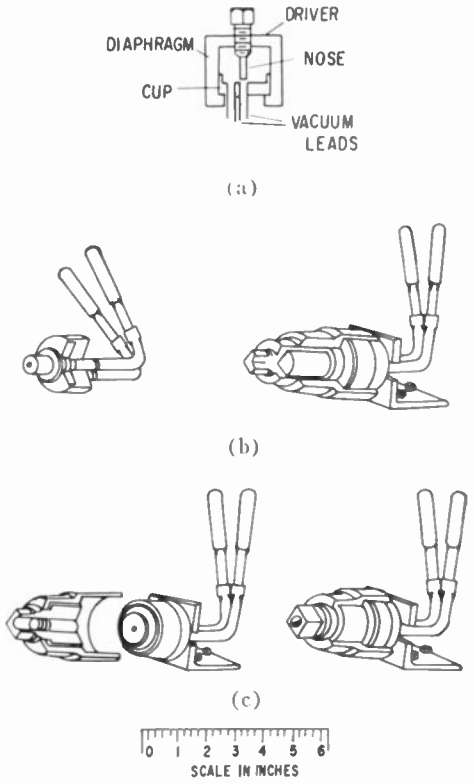

Fig. 18—Ultra-high vacuum bakeable metal valve (Alpert). (a) Schematic diagram. (b) Tube with differential screw-driving mechanism. (c) Tube with simple screw-driving mechanism.

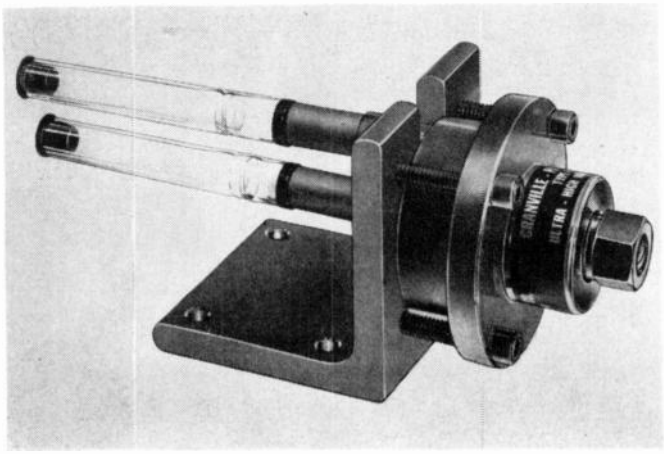

Fig. 19—Granville-Phillips tube.

Molten-metal tubes are becoming more popular [44]. The advantage of this type of tube over ordinary mercury cutoffs is that the metal is a solid at room temperature having a low vapor pressure. The metal is raised into the seal-off position while the tube is hot and then is allowed to solidify by cooling and this completes the seal. They lack some of the convenience of other types of tubes, but have the advantage of simplicity.

Demountable Seals

The convenience of a demountable seal is often desired even in an ultra-high vacuum device. The usual device consists of a metal gasket crushed between two flanges [35], [45]. The gasket metal is selected for its ductility as well as its low vapor pressure at bakeout temperatures. Pattee [46] described a demountable joint which was used in a field-emission apparatus. The seal (Fig. 20) consists of a knife edge which seats in an annealed copper gasket. The knife edge is machined on heavy wall stainless-steel tubing. It has a 0.005-inch radius at the tip and a 45° wedge angle. Adjustment is permitted by deformation of the copper by the clamping screws.

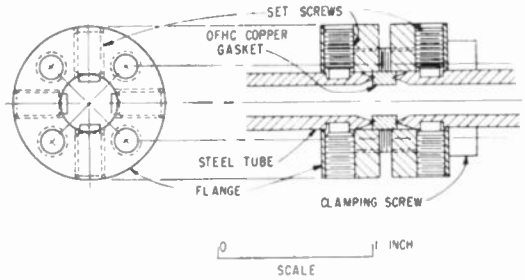

Fig. 20—Demountable vacuum seal (Pattee).

Modern Vacuum Systems

A major requirement of an ultra-high vacuum system is that the system be capable of being baked at high temperatures. This is most conveniently done by having a furnace placed around the entire vacuum system. There are many possible arrangements and one which has been found convenient in this laboratory is shown in Fig. 21. Two walls of the oven are fixed permanently in place. These can be made of insulated stainless-steel or asbestos board. The vacuum components, such as tubes, are attached directly to the surface with flexible glass bellows or long glass U bends inserted between each fixed point. Lightweight insulated aluminum modular ovens are placed over the system during bakeout and the temperature is controlled by any convenient pyrometer. Only a number of the heating units (Calrods) is controlled by the pyrometer and the others are controlled manually. If it is desired to bring the system quickly to temperature, the manually-controlled Cal-

rods are turned on. When the bakeout temperature is approached, these heating units are turned off and the automatically-controlled Calrods maintain the temperature in the vicinity of the desired value. The automatically-controlled heating units do not have enough power to heat the oven more than 50°C above the desired temperature. In this manner, if the controller fails to function, there is less danger of melting the glassware. In practice, however, the automatically-controlled heaters are used to bring the furnace to temperature in a few hours.

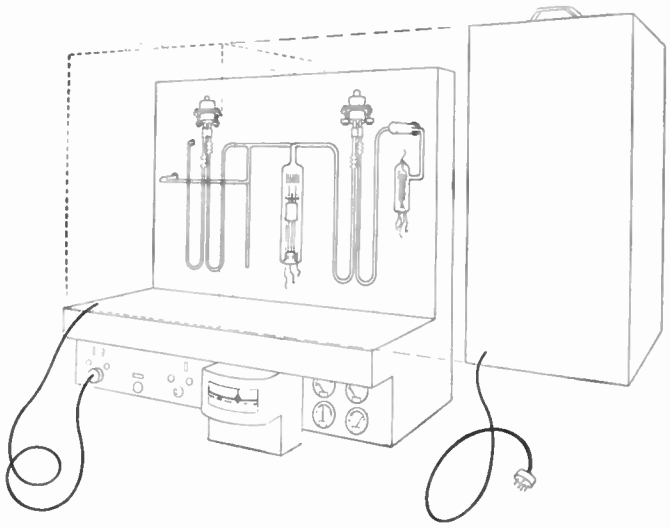

Fig. 21—Typical laboratory ultra-high vacuum system.

The procedure is much the same whether mercury, oil or ion pumps are used. The system is first pumped to $\sim 10^{-6}$ mm Hg and a cursory check for leaks is made. The ovens are usually placed over the system and the automatic controller is set to the desired temperature. The entire system, including the traps, back to the pumps is baked at 425°C. After four or five hours at 425°C, the furnace on the trap closest to the pump is shut off. With mercury pumps, the trap is cooled by a Dewar filled with liquid nitrogen. When alumina traps are used in conjunction with oil diffusion pumps, the trap is simply allowed to cool to room temperature. With ion pumps no trap is needed. A common procedure is to use two ion pumps in sequence, one of which is baked out and the other is used to pump the system during bakeout. When mercury or oil pumps are used the system is kept hot for approximately four hours after the traps have cooled before allowing to cool slowly to room temperature. The ovens are removed and the pressure of the system is checked with an ionization gauge, and a check is made for small leaks. The detection of leaks is quite simple in the pressure range below 10^{-8} mm Hg. Acetone and carbon tetrachloride, for example, applied to a small leak cause the positive-ion current reading on the ionization gauge to increase suddenly, or they clog the leak temporarily and cause the current to decrease. Helium and hydrogen can also be used with success. Measurement of the rate of rise of pressure also will detect a leak, and by shutting off various sections of the system, the leak can be isolated. Final pin-pointing is usually done with the ionization gauge. If no leaks are found, the metal parts are outgassed at high temperatures by electron bombardment or by RF heating. In some cases a second bakeout is done after the outgassing and pressures of 10^{-10} mm Hg are routinely obtained.

Leak Detectors

To the experimenter interested in using vacuum systems, one of the greatest problems is leaks. Leaks may occur from a variety of causes, and the increasing complexity of tube design has multiplied the number of these causes to a great extent. The time-honored method of detecting leaks in glass systems by means of a Tesla spark coil has become obsolete with all-metal vacuum systems. Leak detectors involving a change in thermionic emission caused by an adsorbed layer of gas on the filament of a diode or ionization gauge have been used successfully as described in the previous section. The present trend in leak detection is towards the sensitive high-speed helium mass spectrometer. The development of a new leak detecting process using radioactive gas has made it possible to detect leaks in sealed systems or devices without destruction or opening to air. Some of the leak detectors of current interest are described below.

Mass Spectrometers

A very sensitive method for the detection of leaks, and one which also gives an indication in a minimum of time, was developed by Jacobs and Zuhr [47]. It involves the use of a mass spectrometer with helium [48], and the principle by which it operates may be described briefly as follows: When a beam of positive ions, accelerated by a potential V, is passed through a magnetic field of strength H, the ions are sorted out according to their values of e/m, where m is the mass of the ion and e the charge. The radius of curvature R of the path of any given type of singly-charged ion is determined by

$$R = 143.9 \frac{\sqrt{MV}}{H}, \qquad (6)$$

where R is expressed in centimeters, V in volts, H in oersteds, and M is the molar mass of the ion in grams.

For example, for $R = 4.0$ cm and $H = 1500$ oersteds, the values of V for helium ($M = 4.003$) and nitrogen ($M = 14.008$, since N^+ is formed), are found to be 434 and 124 v, respectively. Thus, for a given value of the radius of curvature, the ions reaching a collector may be differentiated by varying the value of V, and the mag-

nitude of the ion current at any given voltage setting will depend on the concentration of the ions in the beam, that is, on the rate at which the corresponding molecules leak into the spectrometer.

For the detection of leaks, helium has been chosen as testing gas for the following reasons:

1. Because of the low value of M, the rate of diffusion through a leak is greater than that of any other gas except hydrogen.
2. Helium occurs in the atmosphere to the extent of only one part in 200,000 parts of air.
3. There is little possibility that an ion due to any other gas will give an indication that can be mistaken for helium.

The application of the mass spectrometer to the detection of leaks has been described in two papers, one by Worcester and Doughty [49] and the other by Thomas, Williams, and Hipple [50].

A modern version of the helium mass spectrometer leak detector is shown in Fig. 22. This instrument is capable of detecting leaks as small as 10^{-10} cc of air per sec in evacuated enclosures. Such a leak is so small that more than 5000 years would be required for one cubic inch of air at atmospheric pressure to pass through the opening. For pressurized enclosures leaks down to 10^{-6} cc per sec can be located. In this spectrometer the helium ions are deflected through 90° by the magnetic field. The current generated by collection of the helium ions is amplified and used to indicate a leak on the leak-rate meter and on an audible alarm. The components to be leak checked are connected to a manifold which is first exhausted by the mechanical roughing pump, and when the pressure, as indicated, for instance, by a thermocouple gauge connected to the test manifold is sufficiently low the throttle valve to the spectrometer tube is opened. A fine jet of helium is passed over suspected parts in each of the tubes, and the presence of a leak is indicated on the leak-rate meter.

Fig. 22—Mass-spectrometer leak detector (General Electric, M-60).

Fast leak testing is made possible with this spectrometer by the incorporation of an automatic balance circuit. This circuit allows the leak detector to respond only to a rapid increase in helium signal such as obtained when a jet of helium passes near a leak. When large systems are being tested, large leaks are sometimes encountered with the jet of helium which cause the mass-spectrometer vacuum system to become partially saturated with helium. Normally, the operator would have to wait a considerable time before the helium has been pumped out of the system to a point where leak testing can be resumed. However, with the automatic balance circuit the helium background is balanced out and a leak signal is given only when the operator passes the jet of helium near a leak.

Radiflow Method

A new method of leak testing hermetically-sealed components nondestructively by utilizing a radioactive gas has been described by Cassen and Burnham [51]. Leakage rates in the order of 10^{-12} cc per sec can be measured under favorable conditions by this process called "radiflo." Equipment for this leak detection system is manufactured by the Analytical and Control Division of Consolidated Electrodynamics Corporation, Pasadena, Calif. The basic principle involves the detection of radioactive krypton 85 which has been allowed to diffuse into the leaky components. Krypton 85 has a half-life of 10.3 years. Over 99 per cent of the disintegrations involve the emission of beta rays with a maximum energy of 0.67 Mev, while only 0.7 per cent of the disintegrations give 0.54-mev gamma rays. The gamma emitting disintegrations are used to detect the leaks since the gamma rays will pass readily through most materials. Detection of the beta rays may be used under some circumstances to determine the presence of occluded krypton on the surface of the components under test. The testing procedure is as follows: The components to be tested are placed in an activating tank which is then sealed. Air in the tank is evacuated down to approximately 2 mm Hg and diluted krypton 85 is pumped into the tank under pressure up to 7 atmospheres. The radioactive gas diffuses into existing leaks in the components. After a prescribed "soaking" period, which may be from several minutes to a few hundred hours, the krypton is pumped out of the activating tank and returned to storage for reuse. If the leaks follow Poiseuille's Law, the quantity of krypton diffusing into leaky components will increase with the square of the pressure and linearly with time. Thus a suitable combination of krypton pressure and "soaking" time may be selected to give the desired sensitivity. Next, an air wash is circulated over the components to remove any residual krypton from the external surfaces. The com-

ponents are then removed from the activating tank. Those with leaks will retain some radioactive atoms which emit gamma radiation. This radiation is detected by a scintillation counter and the intensity is determined by a ratemeter. When this radiation intensity is related to the conditions of the activation process, the leak rate may be determined.

Some components may have absorptive surfaces such as organic coatings, gaskets, or insulation which will retain krypton 85 for various lengths of time after the pressure is released. The gamma radiation emitted by this absorbed gas could make the components appear as leakers when, in fact, they are not. A routine check of rejected parts with a thin-window Geiger-Müller counter tube for beta ray activity reveals surface contaminations.

Halogen-Ion Detector

Quite different in principle from all the other methods of leak detection described above is that involved in the positive-ion detector for halogen compounds which has been described by White and Hickey [52].

Some of the earliest investigators in the field of thermionic emission, such as O. W. Richardson, had observed that platinum, even in air at a temperature of a red heat, emits positive ions, and that the rate of ion emission increases with temperatures according to a relation similar to that observed for electron emission from incandescent cathodes. This positive-ion emission is probably due mostly to the presence in the anode of salts of the alkali metals, although this may not be the correct interpretation of the mechanism of operation of the device described below.

It was observed by C. W. Rice of the General Electric Company that this emission, at any given anode temperature, of positive ions in air is increased very markedly when vapors of compounds containing a halogen strike the electrode surface. This observation forms the basis of the detector developed and described by White and Hickey.

A diagrammatic sketch of the device and simple circuit used for its operation are shown in Fig. 23. The detector consists of a platinum cylinder P which is heated by an insulated platinum filament F, the low voltage required for this purpose being supplied by the transformer T. A metal cylinder C, concentric with P, is connected through a microammeter (μA) to the negative end of a dc source of voltage (50–500 v) while P is connected through the midpoint of the secondary of T to the positive end of the voltage source.

In using the device for detection of leaks, air or any other suitable gas containing a halogen vapor is introduced into the system at a positive pressure. This positive pressure forces the air containing the halogen out through the leak where it may be picked up by the device and is indicated by the meter in the detector circuit. Or the detector may be sealed on the vacuum system in series with the pump (preferably between the rough and the fine pumps). Air containing a halogen vapor is forced under pressure through a very small jet and directed at any suspected spot in the system and then is picked up by the detector.

In using the detector, the temperature of the anode should be between 850°C and 950°C. At lower temperatures, the positive-ion emission is too small, and at higher temperatures the emission becomes unstable. Typical halogen compounds which are fairly volatile at room temperatures and therefore applicable in using the positive-ion detector are "Freon," carbon tetrachloride, and chloroform.

A convenient form of the halogen-leak detector is shown in Fig. 24. The unit contains a power supply, amplifier, sensing element and an air pump. The detector probe is connected to the contro. unit through a flexible cable. Air drawn in at the probe passes through

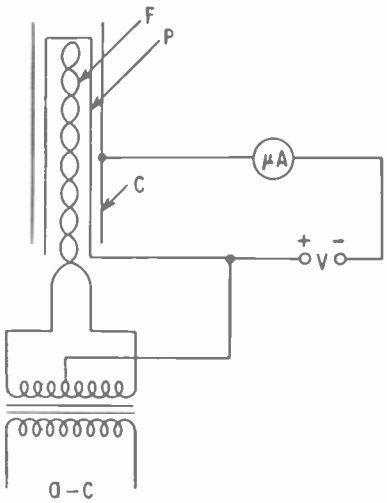

Fig. 23—Schematic diagram of the thermionic detector and circuit used for detection of halogen compounds (White and Hickey).

Fig. 24—Gun-type halogen leak detector (General Electric, H-2).

the sensing element and is exhausted through the pump. When the probe is moved so as to pass near a leak, the sudden increase of halogen gas mixing with the air going into the probe will cause an increase in the detector ion emission. This current is amplified and measured on the leak-rate meter. The detector may be used to locate leaks down to 5×10^{-5} cc/sec in an atmosphere with contamination up to 1000 parts of halogen gas per million parts of air.

The halogen-leak detector has a special advantage in that no helium is required. This has given this method preference in instances where scarcity of helium has been a problem [53].

Bibliography

[1] O. E. Buckley, "An ionization manometer," *Proc. Natl. Acad. Sci. U. S.*, vol. 2, pp. 683–685; 1916.
[2] S. Dushman and C. G. Found, "Studies with the ionization gauge," *Phys. Rev.*, vol. 17, pp. 7–19; January, 1921.
[3] J. D. Cobine, "Gaseous Conductors," Dover Publications, Inc., New York, N. Y., p. 81; 1958.
[4] G. J. Schulz and A. V. Phelps, "Ionization gauges for measuring pressures up to the millimeter range," *Rev. Sci. Instr.*, vol. 28, pp. 1051–154; December, 1957.
[5] F. M. Penning, "Ein Neues Manometer für Niedrige Gasdrucke, Insbesondere Zwischen 10^{-3} und 10^{-5} mm," *Physica*, vol. 4, pp. 71–75; February, 1937.
[6] ——, and K. Nienhuis, "Construction and applications of a new design of the Philips vacuum gauge," *Philips Tech. Rev.*, vol. 11, pp. 116–122; October, 1949.
[7] J. R. Downing and G. Mellen, "A sensitive vacuum gauge with linear response," *Rev. Sci. Instr.*, vol. 17, pp. 218–223, June, 1946; also G. L. Mellen, "Radium-type vacuum gage," *Electronics*, vol. 19, pp. 142–146, April, 1946.
[8] N. W. Spencer and R. L. Boggess, "A radioactive ionization gage pressure measurement system," *J. Am. Rocket Soc.*, vol. 29, pp. 68–71; January, 1959.
[9] W. B. Nottingham, "Comments on Vacuum Gauges," presented at the 7th Annual Conf. on Phys. Electronics, Mass. Inst. Tech., Cambridge; March, 1947.
[10] R. T. Bayard and D. Alpert, "Extension of the low pressure range of the ionization gauge," *Rev. Sci. Instr.*, vol. 21, pp. 571–572; June, 1950.
[11] L. Apker, "Surface phenomena useful in vacuum technique," *Ind. Engrg. Chem.*, vol. 40, pp. 846–847; May, 1948.
[12] W. B. Nottingham, "Design and Properties of the Modified Bayard-Alpert Gauge," in "Vacuum Symposium Transactions," Committee on Vacuum Techniques, Inc., Boston, Mass.; pp. 76–80; 1954.
[13] D. Alpert, "New developments in the production and measurement of ultra high vacuum," *J. Appl. Phys.*, vol. 24, pp. 860–876; July, 1953.
[14] W. B. Nottingham, "A Detailed Examination of the Principles of Ion Gauge Calibration," presented at the Am. Vacuum Soc. Symp., Cleveland, Ohio; October, 1960.
[15] J. P. Hobson and P. A. Redhead, "Operation of an inverted magnetron gauge in the pressure range 10^{-3} to 10^{-12} mm Hg," *Can. J. Phys.*, vol. 36, pp. 271–288; March, 1958.
[16] P. A. Redhead, "The Townsend discharge in a coaxial diode with axial magnetic field," *Can. J. Phys.*, vol. 36, pp. 255–270; March, 1958.
[17] J. M. Lafferty, "Hot-cathode magnetron ionization gauge for the measurement of ultrahigh vacua," *J. Appl. Phys.*, vol. 32, pp. 424–434; March, 1961; U. S. Patent No. 2,884,550; October 17, 1957.
[18] G. K. T. Conn and H. N. Daglish, "A thermionic ionization gauge of high sensitivity employing a magnetic field," *J. Sci. Instr.*, vol. 31, pp. 412–416; November, 1954.
[19] H. Sommer, *et al.*, "The measurement of e/M by cyclotron resonance," *Phys. Rev.*, vol. 82, pp. 697–702; June, 1951.
[20] D. Alpert and R. S. Buritz, "Ultra-high vacuum. II. Limiting factors on the attainment of very low pressure," *J. Appl. Phys.*, vol. 25, pp. 202–209; February, 1954.
[21] H. Sommer, *et al.*, "The measurement of e/M by cyclotron resonance," *Phys. Rev.*, vol. 82, pp. 697–702; June, 1951.
[22] A. G. Edwards, "Some properties of a simple omegatron-type mass spectrometer," *Brit. J. Appl. Phys.*, vol. 6, pp. 44–48; February, 1955.
[23] J. H. Reynolds, "High sensitivity mass spectrometer for Noble gas analysis," *Rev. Sci. Instr.*, vol. 27, pp. 928–934; November, 1956.
[24] W. D. Davis and T. A. Vanderslice, "A Sensitive, High-Speed Mass Spectrometer for Ultrahigh Vacuum Work," presented at the Am. Vacuum Soc. Symp., Cleveland, Ohio; October, 1960.
[25] P. A. Redhead and E. V. Kornelsen, "High vacuum techniques," *Vakuum-Tech.*, in press.
[26] D. Alpert and R. S. Buritz, "Ultra-high vacuum. II. Limiting factors on the attainment of very low pressure," *J. Appl. Phys.*, vol. 25, pp. 202–209; February, 1954.
[27] F. J. Norton, "Helium diffusion through glass," *J. Am. Ceram. Soc.*, vol. 36, pp. 90–96; March, 1953.
[28] D. Alpert and R. S. Buritz, "Ultra-high vacuum. II. Limiting factors on the attainment of very low pressure," *J. Appl. Phys.*, vol. 25, pp. 202–209; February, 1954.
[29] J. M. Lafferty, "Boride cathodes," *J. Appl. Phys.*, vol. 22, pp. 299–309; March, 1951.
[30] G. W. Sears, "Ultimate vacua of diffusion pumps," *Rev. Sci. Instr.*, vol. 20, pp. 458–459; June, 1949.
[31] H. D. Hagstrum, "Electron ejection from Mo by He^+, He^{++}, and He_2^+," *Phys. Rev.*, vol. 89, pp. 244–255; January, 1953.
[32] J. A. Becker and C. D. Hartman, "Field emission microscope and flash filament techniques for the study of structure and adsorption on metal surfaces," *J. Phys. Chem.*, vol. 57, pp. 153–159; February, 1953.
[33] A. Venema and M. Bandringa, "The production and measurement of ultra-high vacua," *Phillips Tech. Rev.*, vol. 20, pp. 145–157; December, 1958.
[34] D. Alpert, "New developments in the production and measurement of ultra high vacuum," *J. Appl. Phys.*, vol. 24, pp. 860–876; July, 1953.
[35] ——, "Vacuum valve for the handling of very pure gases," *Rev. Sci. Instr.*, vol. 22, pp. 536–537; July, 1951.
[36] M. A. Biondi, "High-speed nonrefrigerated isolation traps for ultra-high vacuum systems," *Rev. Sci. Instr.*, vol. 30, pp. 831–832; September, 1959.
[37] L. A. Harris, "Trapping with alumina in vacuum systems and its effect on cathode activity," *Rev. Sci. Instr.*, vol. 31, pp. 903–904; August, 1960.
[38] D. Alpert, "Recent advances in ultra-high vacuum technology," *Vacuum*, vol. 9, pp. 89–96; May, 1959.
[39] L. D. Hall, "Ionic vacuum pumps," *Science*, vol. 128, pp. 279–285; August, 1958.
[40] R. L. Jepsen, *et al.*, "Stabilized Air Pumping with Diode Type Getter-Ion Pumps," presented at the Am. Vacuum Soc. Symp., Cleveland, Ohio; October, 1960.
[41] K. B. Blodgett and T. A. Vanderslice, "Mechanism of Argon Cleanup in a Gas Discharge," presented at Gaseous Electronics Conf., New York, N. Y.; October, 1958.
[42] W. M. Brubaker, "A Method for Greatly Enhancing the Pumping Action of a Penning Discharge," 6th Natl. Symp. on Vacuum Tech., pp. 302–306; October, 1959.
[43] D. Alpert, "Production and measurement of ultrahigh vacuum," in "Handbuch der Physik," vol. 12, Springer Verlag, Berlin, Germany; 1958.
[44] For example, see N. N. Axelrod, "Ultrahigh-vacuum valve," *Rev. Sci. Instr.*, vol. 30, pp. 944–945; October, 1959.
[45] H. Hintenberger, "Erfahrungen mit Metallfolien als Hochvakuumdichtungen," *Z. Naturforsch.*, vol. 6a, pp. 459–462; 1959.
[46] H. H. Pattee, "A demountable ultra-high vacuum joint," *Rev. Sci. Instr.*, vol. 25, pp. 1132–1133; November, 1954.
[47] R. B. Jacobs and H. F. Zuhr, "New developments in vacuum engineering," *J. Appl. Phys.*, vol. 18, pp. 34–48; January, 1947.
[48] A. O. Nier, *et al.*, "Mass spectrometer for leak detection," *J. Appl. Phys.*, vol. 18, pp. 30–33; January, 1947.
[49] W. G. Worcester and E. G. Doughty, "High vacuum leak testing with the mass spectrometer," *Trans. Am. Inst. Elect. Engrs.*, vol. 65, pp. 946–955; December, 1946.
[50] H. A. Thomas, *et al.*, "A mass spectrometer type of leak detector," *Rev. Sci. Instr.*, vol. 17, pp. 368–372, October, 1946; also "Detecting vacuum leaks electronically," *Westinghouse Engr.*, vol. 6, pp. 108–110, July, 1946.
[51] B. Cassen and D. Burnham, "A method of leak testing hermetically sealed components utilizing radioactive gas," *Intern. J. Appl. Radiation and Isotopes*, vol. 9, pp. 54–59; December, 1960.
[52] W. C. White and J. S. Hickey, "Electronics simulates sense of smell," *Electronics*, vol. 21, pp. 100–102; March, 1948.
[53] A. Weber, "Lecksucher nach dem Halogenverfahren für Hochvakuumröhren," *Glas- u. Hochvakuum-Tech.*, vol. 2, pp. 259–262; September, 1953.

New Concepts in Thermoelectric Device Design*

W. H. CLINGMAN†

Summary—**When optimizing thermoelectric device design for a given set of materials and technology, the system of equations used will be different for various device applications. Whenever efficiency or coefficient of performance is important in the application, an irreversible thermodynamic analysis of the design problem is useful. In this analysis, the effects of the thermal and electrical circuit on entropy production within the device are considered. The design problem is analyzed by comparing the relative contribution of various parts of the system to the total entropy production. This irreversible thermodynamic approach is illustrated with examples concerning several different design questions. Often qualitative conclusions can be drawn more readily than with other methods.**

Introduction

THE ultimate objectives of industrial thermoelectric research are to increase the coefficient of performance or efficiency and to reduce the cost of Peltier coolers and thermoelectric generators. Increasing the power-to-weight ratio is also significant in some applications. Toward these objectives, new materials with a higher figure of merit or lower cost are being sought and new methods of fabrication developed. The area of research analyzed in this paper, however, is the optimum design of the thermoelectric system itself, using available materials and technology.

A thermoelectric system consists, in general, of both a thermal circuit and an electrical circuit. This is illustrated for a single thermocouple generator in Fig. 1. Usually there are three parts to the system: two junctions, the thermocouple legs, and the thermal resistances, B_H and B_C, between the couple and the heat source and sink. In the legs and junctions, the heat and electrical current flow through the same material. Interconversion of thermal and electrical energy occurs within this material. Heat is added or removed from the thermal circuit by the Peltier effect at the junctions and by Joule and Thomson heating in the legs. These sources of heat current will affect the heat flow through B_H and B_C. Thus, for fixed source and sink temperatures, the junction temperatures will depend on the magnitude of the thermoelectric effects. Alternatively, however, the temperatures of the hot and cold junctions will determine the open-circuit voltage of the couple and the Peltier coefficients. There is a complex interaction between the thermal and electrical circuits involving even that part of the thermal circuit which carries no electrical current.

The equations describing the behavior of the system contain the material properties: thermoelectric power (α), resistivity (ρ), and the thermal conductivity (k).

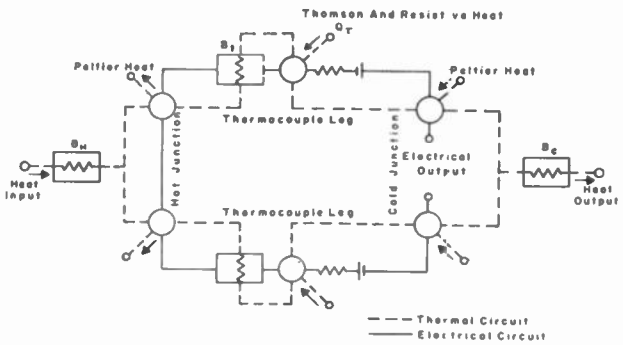

Fig. 1—Thermal and electrical circuits.

Each is a function of temperature, and a digital computer is required for an exact solution. Where B_H and B_C are zero, computer calculations of efficiency and coefficient of performance have been made.[1] Calculations were recently extended to thermocouple legs containing several different materials.[2] Using such calculations or suitable approximations, one can choose device dimensions, within the constraints of a particular application, to maximize efficiency or coefficient of performance.

The nature of the design and the equations to be solved, however, depend upon the particular application. Even the relative importance of various parts of the thermal circuit will depend on the quantity to be optimized. For example, in optimizing the efficiency of a generator, the thermocouple legs are chosen sufficiently long that B_H and B_C are negligible with respect to B_L, the thermal resistance of the legs. The electrical contact resistance of the junctions must be negligible also, with respect to the electrical resistance of the legs. Assuming that the device design is chosen to satisfy these conditons, B_C, B_H, and contact resistance may be set equal to zero in the general equations describing the behavior of the system.

To optimize power output per unit weight of thermoelectric material used, however, the situation is quite different.[3] A new set of approximations will apply in simplifying the general equations, and the design equations used in maximizing efficiency will no longer be applicable. When the thermocouple legs in a maximum

* Received by the IRE, February 28, 1961. Reprinted from the 1961 IRE International Convention Record, pt. 6.
† Central Res. Labs., Texas Instruments, Inc., Dallas Tex.

[1] B. Sherman, R. R. Heikes, and R. W. Ure, Jr., "Calculation of efficiency of thermoelectric devices," *J. Appl. Phys.*, vol. 31, pp. 1–16; January, 1960.
[2] R. G. Moore, Jr., "Exact Computer Solution of Segmented Thermoelectric Devices," presented at Symp. on Thermoelectric Energy Conversion, Dallas, Tex.; January 8–13, 1961.
[3] B. R. West, "A Method for Designing a Thermoelectric Generator Based on the Thermal Characteristics of the Device," presented at Symp. on Thermoelectric Energy Conversion, Dallas, Tex.; January 8–13, 1961.

efficiency design are shortened, the internal resistance of the generator decreases; the open-circuit voltage remains the same; and the power output increases. Shortening the legs, however, is equivalent to reducing B_t, and a point will be reached where B_H and B_C are no longer negligible compared with B_t. The open-circuit voltage will then drop because of temperature changes at the hot and cold junctions. Also, as the legs are shortened, the internal resistance will approach a constant value equal to the contact resistance of the junctions. Thus, the power output will pass through a maximum (Fig. 2). With lead telluride generators, this maximum power output occurs at a design point where both electrical contact resistance and B_C and B_H are significant.[3] In fact, when there is an upper temperature limit for operation of the cold junction (*e.g.*, as required for stability of a soldered contact), the optimum design can be determined by considering only B_t and B_C.[3] To a first approximation, the optimum thermocouple leg length will be independent of the electrical properties of the material.

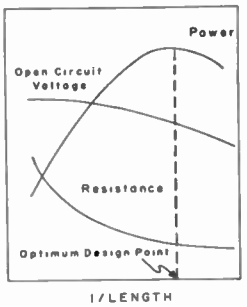

Fig. 2—Designing for maximum power per unit material weight.

Thus, in some design problems the objectives are unrelated to efficiency or coefficient of performance. Whenever these quantities are important, however, an irreversible thermodynamic analysis of the system can be useful. This approach is developed below and illustrated with examples for particular cases.

Irreversible Thermodynamic Analysis

Interpretation of the thermal and electrical circuit interaction shown in Fig. 1 can be simplified by a new description of the system based on irreversible thermodynamic concepts. The thermoelectric generator or cooler can be considered as a basic heat engine shown in Fig. 3. The engine is characterized by specifying the operating temperatures, T_H and T_C; the heat flows in and out of the device, Q_H and Q_C; and the power output, P. In the case of heat pumps, P is the power input. As a result of heat flow, the entropy of the heat source decreases at the rate Q_H/T_H. Similarly, the entropy of the heat sink increases at the rate Q_C/T_C. The thermoelectric system operates in a steady-state condition; therefore, its entropy remains constant with time. The difference between Q_H/T_H and Q_C/T_C is the total rate of entropy production Σ due to irreversible processes in the thermoelectric system.

$$\Sigma = \frac{Q_C}{T_C} - \frac{Q_H}{T_H} . \tag{1}$$

Minimizing Σ is equivalent to optimizing efficiency or coefficient of performance. Various design problems can be treated by first dividing the system into parts and analyzing the entropy production in each part. The design of the parts is then chosen to minimize entropy production. Whenever efficiency or coefficient of performance is important for a particular application, this type of analysis can be used. The method is simpler than considering the details of the thermal and electrical circuits. Several otherwise unrelated design problems can be analyzed in terms of the same concepts. The basic ideas of the irreversible thermodynamic theory will be developed and illustrated with specific examples. The results are of two types, those allowing a choice between different designs, and those giving a guide to materials development.

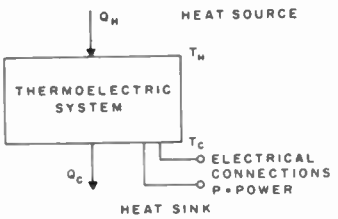

Fig. 3—Basic heat engine.

First, efficiency and coefficient of performance will be related to total entropy production. The efficiency η is defined as

$$\eta = \frac{P}{Q_H} . \tag{2}$$

Also, since energy is conserved,

$$P = Q_H - Q_C. \tag{3}$$

Eliminating Q_H and Q_C from (1)–(3) gives

$$\eta = \left(\frac{T_H - T_C}{T_H}\right) \cdot \frac{1}{1 + T_C \Sigma / P} . \tag{4}$$

The coefficient of performance ϕ of a heat pump is defined as

$$\phi = \frac{Q_C}{P} . \tag{5}$$

where the direction of the heat flows is now reversed. The coefficient of performance is given in terms of the entropy production as follows:

$$\phi = \frac{T_C}{T_H - T_C} \cdot [1 - T_H \Sigma / P]. \tag{6}$$

Eqs. (4) and (6) are the desired results relating device performance to the ratio (Σ/P). In the heat pump, it is necessary that $\Sigma < P/T_H$ for the coefficient of performance to be greater than zero. Thus, the entropy production must be below a certain maximum value before the device will work as a cooler.

Let us now consider the application of these equations to thermoelectric generators with segmented legs, *i.e.*, thermocouple legs containing several different materials. Here, each of the materials may be used over its optimum temperature range for maximum figure of merit Z where $Z = \alpha^2/\rho k$. Sometimes efficiency may be increased by adding a material to the hot side of the thermocouple and operating the new thermocouple over a higher temperature range. This is illustrated in Fig. 4, where material B is added to the thermocouple composed of material A. Material B then operates over the temperature range from T_H to T_1, and material A from T_1 to T_C. The corresponding heat-flow diagrams are shown below the thermocouples. One might expect a higher efficiency of the combined thermocouple [Fig. 4(d)] because of an increase in Carnot efficiency from

$$\left(\frac{T_1 - T_C}{T_1}\right) \text{ to } \left(\frac{T_H - T_C}{T_C}\right).$$

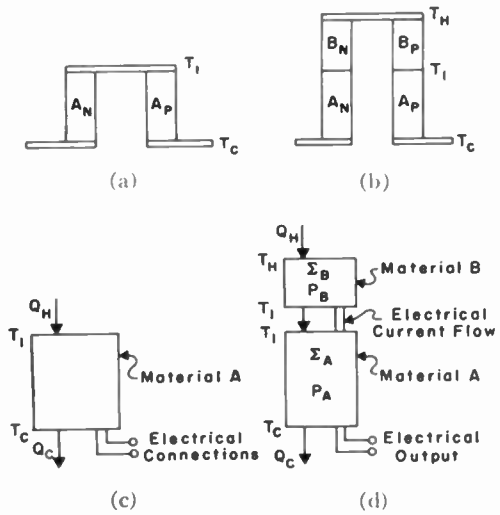

Fig. 4—Adding segments to generator.

If the entropy production in material B is sufficiently high, however, the combined thermocouple efficiency may actually be lower than that of the couple using only material A. The efficiency of the combined couple may be written

$$\eta = \eta_c \cdot \frac{1}{1 + T_C(\Sigma/P)}, \tag{7}$$

where

$$\eta_c = \frac{T_H - T_C}{T_C} = \text{Carnot efficiency.}$$

The entropy and power production in materials A and B are additive. Thus,

$$(\Sigma/P) = \frac{P_A(\Sigma_A/P_A) + P_B(\Sigma_B/P_B)}{P_A + P_B}. \tag{8}$$

The entropy-to-power production ratio for the combined generator is an average of this ratio for each material, with the fraction of the power produced by each material as the weighting factor. Let η^A and η^B equal the efficiencies of generators composed only of part A or B of the combined couple, with the same current as in the combined couple.

$$\eta^A = \frac{T_1 - T_C}{T_1} \cdot \frac{1}{1 + T_C(\Sigma_A/P_A)} = \eta_c{}^A \cdot \frac{1}{1 + T_C(\Sigma_A/P_A)}. \tag{9}$$

$$\eta^B = \frac{T_H - T_1}{T_H} \cdot \frac{1}{1 + T_1(\Sigma_B/P_B)} = \eta_c{}^B \cdot \frac{1}{1 + T_1(\Sigma_B/P_B)}. \tag{10}$$

For

$$\frac{\eta}{\eta_c} \geq \frac{\eta^A}{\eta_c{}^A},$$

it is necessary and sufficient that $(\Sigma_B/P_B) \leq (\Sigma_A/P_A)$. This relation gives the upper limit to the entropy production in part B so that the fraction of the Carnot efficiency is the same in the combined generator as in the original thermocouple.

A more quantitative relation between the efficiencies, η, η^A, and η^B can be obtained from (8) by expressing the entropy-to-power production ratios in terms of these efficiencies. The result is as follows:

$$\frac{P}{T_C}\left[\frac{\eta_c}{\eta} - 1\right] = \frac{P_A}{T_C}\left[\frac{\eta_c{}^A}{\eta^A} - 1\right] + \frac{P_B}{T_1}\left[\frac{\eta_c{}^B}{\eta^B} - 1\right] = \Sigma. \tag{11}$$

This equation merely states that the total entropy production is the sum of the entropy production in materials A and B.

We will now consider a second application of these concepts. In the combination shown in Fig. 5, a pure thermal resistance is inserted between the thermoelectric generator and the heat sink. The heat transfer coefficient h_C of the thermal resistance is defined as

$$h_C = \frac{Q_C}{A(T_1 - T_C)}, \tag{12}$$

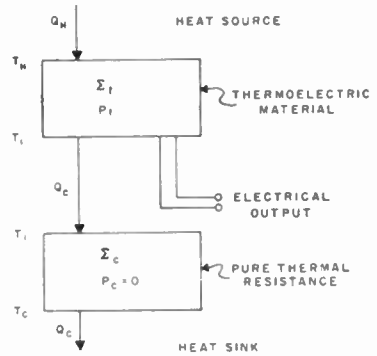

Fig. 5—Analysis of thermal resistance for a generator.

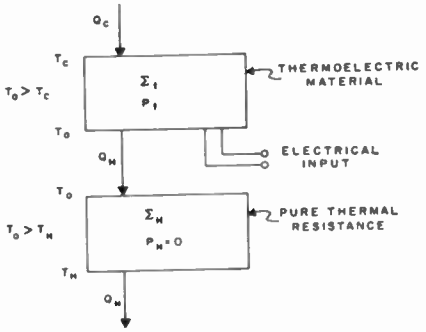

Fig. 6—Analysis of thermal resistance for a heat pump.

where A is the heat transfer area. The question to be analyzed is the condition on h_C for the thermal resistance to have a negligible effect on efficiency. The total entropy production is again divided in two parts, that produced in the thermoelectric material and that produced in the thermal resistance.

$$\eta = \frac{T_H - T_C}{T_H} \cdot \frac{1}{1 + T_C[\Sigma_t + \Sigma_C]/P_t} \cdot \tag{13}$$

The above requirement on h_C can be expressed as

$$\Sigma_C \ll \Sigma_t. \tag{14}$$

When (14) is satisfied, $T_1 \approx T_C$, and Σ_t is given as

$$\Sigma_t \approx \frac{P_t}{T_C}\left[\frac{\eta_c}{\eta} - 1\right]. \tag{15}$$

In addition,

$$\Sigma_C = Q_C\left[\frac{1}{T_C} - \frac{1}{T_1}\right] \approx \frac{Q_C^2}{Ah_C} \cdot \frac{1}{T_C^2}$$

$$Q_C = P_t\left(\frac{1}{\eta} - 1\right). \tag{16}$$

$$\therefore\ h_C \gg \frac{P_t}{AT_C}\left[\frac{1}{\eta} - 1\right]^2 \Big/ \left[\frac{\eta_c}{\eta} - 1\right]. \tag{17}$$

To assess the order of magnitude of the right-hand side of (17) assume that $P_t/A = 1$ watt/cm²; $\eta = 0.05$; $T_C = 300°K$; and $T_H = 500°K$. Then (17) becomes $h_C \gg 0.17$ watt/cm²-°C. The heat transfer coefficient of metal-insulator contacts is of the order of 0.5 watt/cm²-°C or less. Thus, in the example, electrical insulation at the cold end of the generator will lower efficiency somewhat.

A similar analysis can be made for adding thermal resistance to the hot end of a heat pump. A heat-flow diagram for this case is given in Fig. 6. Coefficient of performance is given by

$$\phi = \frac{T_C}{T_H - T_C}[1 - T_H(\Sigma_t + \Sigma_H)/P_t]. \tag{18}$$

The requirement for a negligible effect of thermal resistance on coefficient of performance is now given by

$$T_H \frac{\Sigma_H}{P_t} \ll 1 - T_H \frac{\Sigma_t}{P_t} \cdot \tag{19}$$

Evaluting Σ_t and Σ_H as before gives

$$h_H \gg \frac{Q_C}{AT_H}\left(\frac{1}{\phi} + 1\right)^2 \phi_c, \tag{20}$$

where

$$h_H = \frac{Q_H}{A(T_C - T_H)}$$

= heat transfer coefficient of thermal resistance,

and

$$\phi_c = \frac{T_C}{T_H - T_C} = \text{Carnot maximum for coefficient of performance.}$$

If the heat pump is operated close to the maximum possible temperature difference, ϕ is small, and h_H must be large to avoid having a significant effect on performance. Assume that with $T_H = 300°K$, the maximum temperature difference for the couple is 70°K. Eq. (20) will be evaluated for the following operating conditions: $T_H = 300°K$; $T_C = 240°K$; $Q_C/A = 1$ watt/cm². Under these conditions and at the current for maximum heat pumping, $\phi = 0.0571$ and $\phi_c = 4.0$. Eq. (20) becomes

$$h_H \gg 4.6 \text{ watts/cm}^2 - \text{deg}. \tag{21}$$

It would be impossible to satisfy this equation from a practical standpoint, and electrical insulation at the hot junction would have a very significant effect on thermocouple performance.

In the examples given, the system was divided in two parts, and the contribution of each part to the total entropy production was analyzed. It is also possible to subdivide the system into a large number of parts by isothermal surfaces through the device. One can then consider the local entropy production ($\sigma\Delta T$) and power production ($p\Delta T$) in the material between two isothermal surfaces differing by a small temperature increment, ΔT (Fig. 7). In general, σ and p are functions of

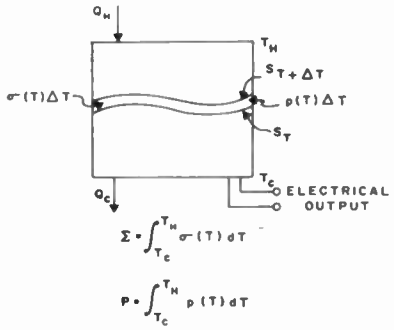

Fig. 7—Local entropy and power production.

temperature throughout the system. This approach is advantageous because the local entropy and power productions at temperature T can be simply expressed in terms of the thermal and electrical currents crossing the isothermal surface S_T and the thermoelectric properties of the material at T. If at each temperature there are only two thermoelectric materials, N and P types, then σ and p are given by the following:[4]

$$\sigma(T) = \frac{1}{T^2}(Q_P + Q_N) + \frac{I^2}{T}\left[\frac{(\rho k)_P}{Q_P} + \frac{(\rho k)_N}{Q_N}\right] \qquad (22)$$

$$p(T) = I(\alpha_P - \alpha_N) - I^2\left[\frac{(\rho k)_P}{Q_P} + \frac{(\rho k)_N}{Q_N}\right], \qquad (23)$$

where I is electrical current, and Q_P and Q_N are the heat flows in the P and N type material, respectively. For generators, $I>0$; for coolers, $I<0$. The first term in the expression for σ is due to irreversible heat conduction and the second term to irreversible Joule heating. The expression for power production contains a term related to the Seebeck voltage and a second term to correct for the I^2R loss. In the case of coolers the convention is made that $p(T)<0$.

Eq. (4) for efficiency now becomes

$$\eta = \frac{T_H - T_C}{T_H} \cdot \frac{1}{1 + T_C \int_{T_C}^{T_H} p(T)[\sigma/p]dT \Big/ \int_{T_C}^{T_H} p(T)dT} \cdot \qquad (24)$$

The total entropy-to-power production ratio, Σ/P, is an average over the ratios, $\sigma(T)/p(T)$, corresponding to each temperature in the system. The function $p(T)$ is the weighting factor in the average. The efficiency depends not only on the local entropy-to-power production ratios, but also on the weighting factors $p(T)$ at each temperature.

[4] W. H. Clingman, "Entropy Production and Optimum Device Design," presented at Symp. on Thermoelectric Energy Conversion, Dallas, Tex.; January 8–13, 1961.

By a more detailed irreversible thermodynamic analysis of the system it is possible to relate the efficiency to the ratios, $\sigma(T)/p(T)$, only.[4] The expressions for efficiency and coefficient of performance then become

$$\eta = 1 - \exp\left[-\int_{T_C}^{T_H} \frac{\xi(T)}{T}\,dT\right]$$

$$\phi = 1 \Big/ \left\{\exp\left[-\int_{T_C}^{T_H} \frac{\xi(T)}{T}\,dT\right] - 1\right\}, \qquad (25)$$

where

$$\xi(T) = \frac{1}{1 + T\sigma(T)/p(T)} \cdot$$

With these equations, optimum device design can be considered from the standpoint of minimizing $\sigma(T)/p(T)$ at each temperature in the system. When (22) and (23) are substituted in the expression for $\xi(T)$, one obtains the following:

$$\xi(T) = \frac{I(\alpha_P - \alpha_N) - I^2[(\rho k)_P\, Q_P + (\rho k)_N\, Q_N]}{I(\alpha_P - \alpha_N) + 1/T[Q_P + Q_N]} \cdot \qquad (26)$$

For generators, $\xi(T)<1$; and for coolers, $\xi(T)>1$. For any given values of the material parameters and current, there will be optimum heat fluxes, Q_N° and Q_P°, for each leg. These optimum heat fluxes will maximize ξ for generators and minimize ξ for coolers. The optimum ratio in either case is given by

$$\frac{Q_P^\circ}{Q_N^\circ} = \frac{(\rho k)_P^{1/2}}{(\rho k)_N^{1/2}} \cdot \qquad (27)$$

In theory, this optimum ratio could be achieved by adjusting the ratio of the areas of the two legs and by transferring heat from one leg to the other at intermediate temperatures. If it is assumed that $Q_P/Q_N = (\rho k)_P^{1/2}/(\rho k)_N^{1/2}$, (26) can be simplified to

$$\xi(T) = [1 - (1/ZT)(1/c)]/[1 + c], \qquad (28)$$

where

$$Z = \frac{(\alpha_P - \alpha_N)^2}{[(\rho k)_P^{1/2} + (\rho k)_N^{1/2}]^2}$$

= the device figure of merit evaluated from material properties at the temperature T,

and

$$c = \frac{Q_P + Q_N}{I(\alpha_P - \alpha_N)T} = \text{a dimensionless heat flux.}$$

In general, both Z and c are functions of temperature. The figure of merit Z depends only on the thermoelectric materials used, while c depends on both the materials and the device design.

In Fig. 8, $\xi(T)$ is shown as a function of c for three values of ZT. The curves for negative values of c correspond to cooler performance and those for positive c,

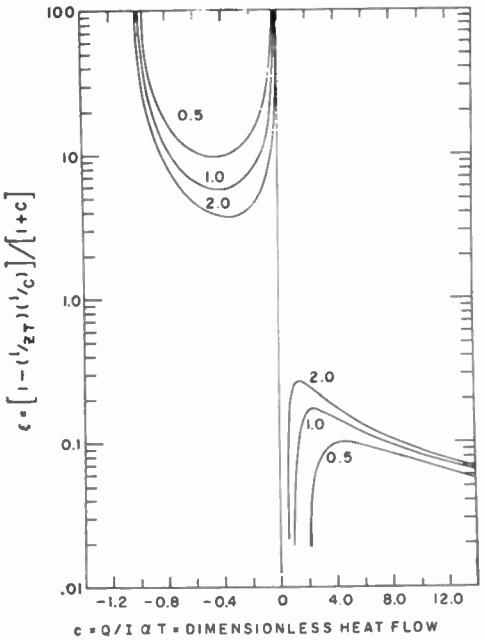

Fig. 8—Variation of ξ with dimensionless heat flow.

to generators. To illustrate the interpretation of these curves, consider a generator for which ZT has the constant value of 0.5 over its entire operating range. For optimum efficiency, the device should operate at a constant value of c equal to 4.5. For two reasons, however, c will increase as one moves from the hot to the cold junction: 1) (Q_P+Q_N) increases due to Joule heating in the legs and 2) temperature appears in the denominator of c. Two methods may be used to keep c constant. First, the device design can be changed from a single stage to several stages between the heat source and sink.[5] In this case, changing the current adjusts c toward its optimum value between each stage. Second, if the Thomson effect absorbs heat and is of sufficient magnitude, it can counter-balance the Joule heating and keep c from increasing with decreasing temperature. Every thermoelectric material has an optimum value for its Thomson coefficient at a given temperature, and this optimum value depends on the other material properties at this temperature.[4]

The advantage gained by these techniques can be judged from the curves in Fig. 8. The wider the range in c for a device, the greater the deviations from the optimum value of ξ. For example, in a lead telluride generator (n-type doped with 0.03 per cent PbI_2 and p-type doped with 0.3 per cent Na) operating between 425°K and 825°K at the maximum efficiency current, $c(T_H)=4.3$ and $c(T_C)=9.5$. The average value of ZT over this temperature range is 0.48. The value of ξ varies from 0.10 to 0.076. The efficiency is 6.07 per cent, and the efficiency with ξ constant at 0.10 is 6.68 per cent. In this case, operation is over the slowly varying part of the ξ-c curve and there is little advantage in staging. However, the range of c increases as the temperature range is extended and several materials are used in a single generator leg. In this case, staging will be a greater advantage.

Approximate calculations of efficiency or coefficient of performance are made by analyzing a device composed of fictitious material. The parameters of this material are chosen as close as possible to those of the real material. The approximate calculation may be interpreted in terms of the functions $\xi(T)$ and $c(T)$. Let the approximate values of the two quantities be denoted by $\xi'(T)$ and $c'(T)$. If a generator is operating over the slowly varying part of the ξ-c curve, errors in the figure of merit and c' will cause only small errors in ξ'. Also there will be some temperatures at which ξ' is too high and some where it is too low, resulting in error cancellation when evaluating the efficiency (25). Approximate generator efficiency calculations are in excellent agreement with exact computer calculations.[1,2]

In some parts of the ξ-c curve, ξ varies rapidly with c. This is particularly true when $|c|$ is close to zero. When heat pumps operate close to their maximum temperature difference, c will approach zero at the hot end of the device. In this case, small errors in c' will make large errors in ξ'. For this reason the relative importance of the Thomson effect on the value of ξ will be greater, and staging will be more significant than for most generators. By staging, the absolute value of the entropy-to-power production ratio is decreased, allowing a greater temperature difference to be maintained between the junctions.

Conclusions

The exact interaction between the thermal and electrical circuits in a thermoelectric device is quite complex. In design analysis simplifying assumptions are normally made, and these will depend on the particular device application. Thus, the actual system of design equations used will vary with the application. In some cases efficiency and coefficient of performance will be unrelated to design objectives. Whenever these quantities are important, however, an irreversible thermodynamic analysis of the system is useful.

In all examples of this approach, the design problem was analyzed by determining the relative contribution of various parts of the device to the total entropy production. This approach often has the advantage of simpler equations, allowing qualitative conclusions to be drawn more readily. In addition, several different design questions can be analyzed in terms of the same concepts.

Acknowledgment

The author appreciates many helpful discussions with R. G. Moore, M. Norwood, and B. R. West of the Central Research Laboratories, Texas Instruments Inc.

[5] T. C. Harmon, "Multiple stage thermoelectric generation of power," *J. Appl. Phys.* vol. 29, pp. 1471–1473; October, 1958.

IRE Standards on Piezoelectric Crystals: Measurements of Piezoelectric Ceramics, 1961*

61 IRE 14.S1

COMMITTEE PERSONNEL

Subcommittee on Piezoelectric Ceramics

1958–1960

H. JAFFE, *Chairman* 1958–1960

D. Berlincourt T. Kinsley T. M. Lambert D. Schwartz

Piezoelectric and Ferroelectric Crystals Committee

1958–1960

E. A. GERBER, *Chairman* 1958–1960
I. E. FAIR, *Vice Chairman* 1958–1960

J. R. Anderson
J. H. Armstrong
H. G. Baerwald
R. Bechmann
W. G. Cady
W. A. Edson
S. L. Ehrlich
W. D. George
R. L. Harvey
H. Jaffe
E. D. Kennedy
T. M. Lambert
W. P. Mason
C. F. Pulvari
P. L. Smith
R. A. Sykes
K. S. Van Dyke

Standards Committee

1960

C. H. PAGE, *Chairman*
J. G. KREER, JR., *Vice Chairman*
H. R. MIMNO, *Vice Chairman*
L. G. CUMMING, *Vice Chairman*

J. H. Armstrong
J. Avins
G. S. Axelby
M. W. Baldwin, Jr.
W. R. Bennett
J. G. Brainerd
A. G. Clavier
S. Doba, Jr.
R. D. Elbourn
G. A. Espersen
R. J. Farber
D. G. Fink
G. L. Fredendall
E. A. Gerber
A. B. Glenn
V. M. Graham
R. A. Hackbusch
R. T. Haviland
A. G. Jensen
R. W. Johnston
I. Kerney
E. R. Kretzmer
S. J. Mason
W. Mason
E. E. Maxwell
R. L. McFarlan
P. Mertz
H. I. Metz
E. Mittelmann
L. H. Montgomery, Jr.
S. M. Morrison
G. A. Morton
R. C. Moyer
J. H. Mulligan, Jr.
A. A. Oliner
M. L. Phillips
R. L. Pritchard
P. A. Redhead
C. M. Ryerson
G. A. Schupp, Jr.
R. Serrell
R. F. Shea
W. A. Shipman
H. R. Terhune
E. Weber
J. W. Wentworth
W. T. Wintringham

Measurements Coordinator

J. G. KREER, JR.

* Approved by the IRE Standards Committee, May 12, 1960. Reprints of this Standard 61 IRE 14.S1 may be purchased while available from the Institute of Radio Engineers, 1 East 79th Street, New York, N. Y., at $0.70 per copy. A 20 per cent discount will be allowed for 100 or more copies mailed to one address.

1. Classification of Phenomena

Certain polycrystalline ferroelectric substances, of which ceramic barium titanate ($BaTiO_3$) is the prototype, can be given lasting polar properties, including pyroelectric and piezoelectric effects, by treatment with high electric fields for a short time. The term "to pole" is recommended for this treatment.

Poled ferroelectric ceramics have become an important component in electromechanical devices along with piezoelectric crystals and magnetostrictive materials. The purpose of this standard is to adapt the definitions, relations and measurement methods developed for piezoelectric crystals in general [1]–[3] to ferroelectric ceramics. The higher symmetry of these ceramics leads to simpler relations than for most piezoelectric crystals. The high coupling constants, low mechanical quality factor Q, and noticeable dielectric loss factor of the ferroelectrics, on the other hand, limit the applicability of some approximation formulas of the 1957 and 1958 Standards. Piezoelectric ceramics are sometimes also referred to as "electrostrictive." The choice of designation depends on the degree of penetration into the basic mechanisms involved, but the formalism of piezoelectricity is applicable within the limits stated in the following sections.

1.1 Symmetry Relations

Poled ferroelectric ceramics in their normal operating range show substantially linear relations between stress and strain components on the one hand and electric field and displacement components on the other, just as do piezoelectric crystals, and are called piezoelectric ceramics for this reason. However, with ferroelectric crystals and poled ceramics these relationships are linear only over limited ranges of the input signal. In addition, mechanical and dielectric loss factors are functions of mechanical strain and electric field, respectively.

The symmetry elements of poled ferroelectric ceramics are an axis of rotation of infinite order in the direction of polarization and the infinite set of all planes parallel to that axis as reflection planes. This axis, chosen as the Z axis, is polar. Any direction perpendicular to the Z axis may be chosen as X axis. The set of independent elastic, piezoelectric, and dielectric constants[1] different from zero for this symmetry are

$$s_{11},\ s_{33},\ s_{55},\ s_{12},\ s_{13};\ d_{31},\ d_{33},\ d_{15};\ \epsilon_{11},\ \epsilon_{33}.$$

Additional coefficients are given by the symmetry relations

$$s_{22} = s_{11};\ s_{23} = s_{13};\ s_{44} = s_{55};\ s_{66} = 2(s_{11} - s_{12});$$

$$d_{32} = d_{31},\ d_{24} = d_{15};\ \epsilon_{22} = \epsilon_{11}.$$

This is the same set as for the dihexagonal polar crystal class ($6\text{ mm} = C_{6v}$).

1.2 Electrostrictive Effects

Before poling, the ferroelectric ceramic material is isotropic and shows no piezoelectric effect. For small applied signals ordinary electrostrictive effects are present; there is a strain proportional to the square of the applied electric field and a change in permittivity proportional to an applied mechanical stress. For high electric fields hysteresis effects are pronounced, and it is not possible to derive electromechanical behavior from electrostrictive coefficients relating strain to field strength. Total strain is, however, found approximately proportional to the square of the total electric displacement. Linear terms are thus obtained in a relation between an applied small signal electric displacement and the change in strain caused by this signal. If vectorial superposition of remanent and signal displacement is assumed, and dependence of dielectric and electrostrictive coefficients on magnitude of displacement is disregarded, the following relations between piezoelectric and electrostrictive coefficients result:[2]

$$\begin{aligned} d_{31}/\epsilon_{33}^T &= g_{31} = 2q_{31}D_0, \\ d_{33}/\epsilon_{33}^T &= g_{33} = 2q_{33}D_0, \\ d_{15}/\epsilon_{11}^T &= g_{15} = 2(q_{33} - q_{31})D_0, \\ d_p/\epsilon_{33}^T &= g_p = 4q_{31}D_0, \\ d_h/\epsilon_{33}^T &= g_h = 2D_0(q_{33} + 2q_{31}). \end{aligned} \tag{1}$$

Measurements indicate the assumptions upon which these relations depend are valid in rough approximation. Refined relations have been derived [4], [5].

1.3 Ferroelectric Crystals and Ceramics

Ferroelectric single crystals in general have lower symmetry than the poled ceramic form of the same substance. For this reason measurement methods described in this Standard do not in all cases apply to ferroelectric single crystals. The 1958 Standards on Piezoelectric Crystals describe measurement methods for the most general symmetry conditions, and are, therefore, applicable to ferroelectric single crystals or poled ceramics. In both ferroelectric crystals and ceramics, however, the relations between stress and strain components on the one hand and electric field and displacement on the other are linear only over limited ranges of the input signal; higher signals cause domain reversals resulting in gross deviation from linearity.

[1] See Table II at end of Standards for identification of symbols.

[2] All equations in the present Standard are written in rationalized form.

The most widely used piezoelectric ceramic is barium titanate ($BaTiO_3$). Frequently, barium is replaced in part by lead or calcium. Other ceramic systems showing strong piezoelectric effects are lead metaniobate ($PbNb_2O_6$), solid solutions of lead titanate ($PbTiO_3$) with lead zirconate ($PbZrO_3$), and sodium niobate ($NaNbO_3$) with partial replacement of sodium by potassium, lead, or cadmium.

2. Measurement Methods

Methods developed for measurement of dielectric, elastic and piezoelectric constants of crystals are generally applicable to poled ferroelectric ceramics, but the particular properties of the latter make some special methods advantageous. High values of permittivity usually allow one to disregard stray capacitances, and the relatively high internal mechanical damping (low Q) of the material permits the use of relatively crude specimen holders. High values of piezoelectric coupling generally require the use of complete rather than approximate formulas relating $(f_p - f_s)$ with coupling factors.

The properties of ceramics are functions of the preparation process, and are subject to systematic and statistical fluctuations within a given batch. These fluctuations may be caused by inhomogeneous chemical composition, mechanical differences in the forming process, varying shrinkage and chemical modification during firing, and by varying response to the poling treatment. Nevertheless, measured coefficients of ceramics of definite composition and high density (95 per cent or more of crystal density) converge to values which vary no more than 5 per cent for elastic, 10 per cent for piezoelectric, and 20 per cent for dielectric constants. Proper statistical sampling is necessary to obtain representative constants for a given material. To obtain a complete set of constants for a composition, one must either measure each constant on a large number of samples, or make experiments giving ratios of constants, since such ratios are much less variable than the individual constants. Compliances s_{11}^E and s_{12}^E, for instance, may be determined from the resonance frequencies of two contour-extensional modes of a square plate. Compliance s_{11}^E may also be determined from the resonance frequency of a slim transversely poled bar, and s_{55}^D can be calculated from f_p of overtones of the thickness shear mode of the same bar with electrodes applied to another pair of faces. This establishes ratios s_{12}^E/s_{11}^E and s_{55}^D/s_{11}^E, and thus s_{12}^E/s_{55}^D. An outline of a measurement scheme for determining all the piezoelectric, dielectric, and elastic constants in this manner is shown in Table I. Resonance methods of measurement are preferred, and one procedure is described in detail in the next section. Static and quasi-static methods are then described, and finally measurements and terms in the nonlinear or high-signal range are discussed.

TABLE I

Measurement Scheme for Piezoelectric Ceramics

Constants	Specimen and Orientation	Measurement Scheme, or Calculation Method
s_{11}^E, k_{31}, d_{31}	Bar plated on faces perpendicular to Z.	Resonance measurements of the length extensional mode.
s_{11}^D	Bar plated on faces perpendicular to Z.	From above, using $s_{11}^D=(1-k_{31}^2)s_{11}^E$.
ϵ_{33}^T	Bar plated on faces perpendicular to Z.	Measurement of low-frequency capacitance.
s_{55}^D	Bar poled along Z, but with plating on faces perpendicular to X.	Overtones of thickness shear mode of the same bar as above, but with signal field along X.
ϵ_{11}^T	Bar poled along Z, but with plating on faces perpendicular to X.	Measurement of low-frequency capacitance.
ϵ_{11}^S	Bar poled along Z, but with plating on faces perpendicular to X.	Measurement of high-frequency (clamped) capacitance.
k_{15}	Bar poled along Z, but with plating on faces perpendicular to X.	$k_{15}^2=1-\epsilon_{11}^S/\epsilon_{11}^T$.
s_{55}^E	Bar poled along Z, but with plating on faces perpendicular to X.	$s_{55}^E=s_{55}^D/(1-k_{15}^2)$.
s_{11}^E, s_{12}^E	Square plate with faces perpendicular to Z.	Fundamental resonance frequencies of the two contour-extensional modes of a square plate.
s_{12}^D	Square plate with faces perpendicular to Z.	$s_{12}^D=s_{12}^E-k_{31}^2s_{11}^E$.
s_{33}^D, d_{33}, k_{33}	Bar plated on faces perpendicular to Z, and with length along Z.	Resonance measurements of length extensional mode.
s_{33}^E	Bar plated on faces perpendicular to Z, and with length along Z.	$s_{33}^E=s_{33}^D/(1-k_{33}^2)$.
s_{11}^E, k_p, d_{31}	Disk with faces perpendicular to Z.	Resonance measurements of planar extensional mode.
k_t	Disk with faces perpendicular to Z.	Resonance measurements of thickness extensional mode.
d_h	Disk with faces perpendicular to Z.	Measurement of response to hydrostatic pressure.
d_{33}	Disk with faces perpendicular to Z.	$d_{33}=d_h-2d_{31}$.
ϵ_{33}^D	Disk with faces perpendicular to Z.	Overtones f_p of thickness extensional mode.
s_{13}^D	Calculation.	Calculated from ϵ_{33}^D, s_{12}^D, s_{11}^D, and s_{33}^D.
s_{13}^E	Calculation.	$s_{13}^E=s_{13}^D+d_{31}d_{33}/\epsilon_{33}^T$.
ϵ_{33}^S	Calculation.	$\epsilon_{33}^S=\epsilon_{33}^T\left[1-\dfrac{k_p^2+k_{33}^2+2Ak_pk_{33}}{1-A^2}\right]$, where
	or	$A=\dfrac{\sqrt{2}\,s_{13}^E}{\sqrt{s_{33}^E(s_{11}^E+s_{12}^E)}}$
	Plate with faces perpendicular to Z.	Measurement of high-frequency (clamped) capacitance.

Note: s_{12}, s_{13}, and d_{31} are generally negative. k_p is taken to be positive when d_{31} is negative.

TABLE II

LIST OF SYMBOLS*

Symbol	Meaning	MKS Unit	Reference or Equation
c, c'	Aging coefficients.		(21), (22)
c_{33}	Elastic stiffness constant.	newton/meter^2	[1]
C_0	Shunt capacitance of sample.	farad	[2]
C_1	Series capacitance of sample.	farad	[2]
d	Diameter.	meter	
d_{31}, d_{32}, d_{33} d_{15}, d_{24}	Piezoelectric strain constants.	meter/volt = coulomb/newton	[1]
d_p	Planar piezoelectric strain constants.	meter/volt = coulomb/newton	[3]
d_h	Hydrostatic piezoelectric strain constants.	meter/volt = coulomb/newton	[3]
D (superscript)	At constant electric displacement.		[1]
D_1, D_3	Electric displacement components.	coulomb/meter^2	
D_0	Remanent or bias displacement.	coulomb/meter^2	[6]
D (Section 3.1)	Dissipation factor.		
E (superscript)	At constant electric field.		[1]
E, E_1, E_3	Electric field and its components.	volt/meter	
f	Frequency.	cycles/second	
f_a	Antiresonance frequency.	cycles/second	[2]
f_r	Resonance frequency.	cycles/second	[2]
f_n	Frequency at maximum impedance.	cycles/second	[2]
f_m	Frequency at minimum impedance.	cycles/second	[2]
f_p	Parallel resonance frequency.	cycles/second	[2]
f_s	Motional (series) resonance frequency.	cycles/second	[2]
Δf	$f_p - f_s$.	cycles/second	[2]
g_{31}, g_{33}, g_{15}	Piezoelectric "voltage" constants.	volt meter/newton = meter^2/coulomb	[1]
g_p, g_h	Piezoelectric "voltage" constants.	volt meter/newton = meter^2/coulomb	
h_{33}	Piezoelectric "stiffness" constant.	volt/meter = newton/coulomb	[1]
H	Dissipated power/unit volume.	watt/meter^3	
i	Order of overtone.		
k_{31}	Transverse coupling factor.		[3]
k_{33}	Longitudinal coupling factor.		(8)
k_{15}	Shear coupling factor.		(9)
k_t	Thickness coupling factor.		(13)
k_p	Planar coupling factor.		[3]
l	Length.	meter	
M	Oscillator figure of merit.		[2]
P	Electric polarization.	coulomb/meter^2	
q_{31}, q_{33}	Electrostrictive constants.	(meter^2/coulomb)^2	[4]
Q	Mechanical quality factor.		[2]
R_1	Series resistance of sample.	ohm	[2]
R_T	Terminating resistance.	ohm	Fig. 1
s_{11}, s_{22}, s_{33} s_{13}, s_{23} s_{44}, s_{55}, s_{66}	Elastic compliance constants.	meter^2/newton	[1]
S (superscript)	At constant strain.		[1]
S_1, S_3	Strain components.		[1]
t (except Sec. 4 and 5)	Thickness.	meter	
t (Sec. 4 and 5)	Time.	second	
T (superscript)	At constant stress.		[1]
T_1, T_3	Stress components.	newton/meter^2	[1]
y	Any time-variable material constant.		
w	Width.	meter	
$\|Z\|$ min	Minimum impedance of sample.	ohm	
ϵ	Permittivity.		†
ϵ_{11}, ϵ_{22}, ϵ_{33}	Permittivity components.	farad/meter	
η_1	Root of a Bessel equation.		(5)
ρ	Density.	kilogram/meter^3	
σ	Cross contraction (Poisson) ratio.		(5)

* For further explanations, see the references indicated in the last column.

† It is customary to list relative dielectric constants K_1, K_3 obtained from ϵ_{11}, ϵ_{33} by division by the permittivity of free space $\epsilon_0 = 8.85 \times 10^{-12}$ farad/meter.

2.1 Resonance Method

2.1.1 General: The resonance method in general is covered in the IRE Standards on Piezoelectric Crystals, 1958 [3]. Procedures are described in the Standards on Piezoelectric Crystals, 1957 [2], and in the literature [6]–[8]. The transmission method is used for determination of f_m, the frequency at minimum impedance of the sample. In addition to this measurement, the present Standard also specifies the measurement of the frequency at maximum impedance f_n. A simplification of the transmission network in the 1957 Standard (Fig. 4) may be used in view of the range of parameters found in the ceramics. This simplified circuit is shown in Fig. 1. The signal generator should have an output impedance lower than the minimum impedance of the test specimen. The terminating resistance (R_T) should also be lower than the minimum impedance of the test specimen. In determining the frequency of maximum impedance a higher terminating resistance may be used. The frequency at maximum impedance can be determined accurately only if the harmonic content of the signal generator is relatively low. The effective shunt or

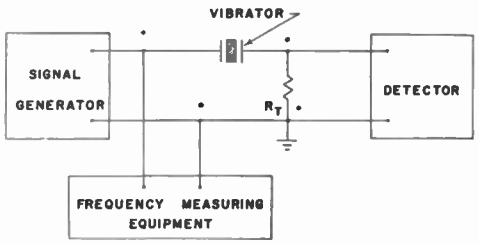

Fig. 1—Transmission network for determination of f_m and f_n of piezoelectric ceramic vibrator.

fringing capacitance across the test specimen should be very low compared to the capacitance of the test specimen. This is generally no problem with high-dielectric-constant ceramics, except in the determination of the longitudinal coupling factor k_{33} for elongated cylinders. In this case it is advisable to use double shielding, whereby the effective shunt capacitance is placed across the signal generator so that current through this shunt capacitance does not pass through the series resistance. The shunt capacitance affects the determination of the frequency at maximum impedance f_n, but not the frequency at minimum impedance f_m, and its effect is such that the apparent maximum-impedance frequency is lowered. The shielding should, therefore, be adjusted for the highest maximum-impedance frequency.

2.1.2 Applicable Approximation: The equations which follow contain the parallel resonance frequency f_p and the series resonance frequency f_s. Another characteristic pair for a resonance range are the frequencies of zero reactance, f_a (antiresonance) and f_r (resonance). The frequency differences are in the order

$$(f_n - f_m) > (f_p - f_s) > (f_a - f_r).$$

With piezoelectric ceramics of high coupling factor and reasonably high mechanical and dielectric quality factors, these three frequency differences are nearly equal. In the presence of high mechanical losses, however, $(f_n - f_m)$ cannot be used directly in calculating coupling factors, and a closer approximation for $(f_p - f_s)$ in terms of the measured frequency difference $(f_n - f_m)$ must be used as follows:

$$\Delta f = (f_p - f_s) \sim \frac{f_n - f_m}{\sqrt{1 + \frac{4}{M^2}}}. \tag{2}$$

where the figure of merit M is given by

$$M = \frac{1}{2\pi f_s R_1 C_0} \approx \frac{1}{2\pi f_m (C_0 + C_1)\,|Z|_{\min}}. \tag{3}$$

Measurements indicate that the assumptions on which these relations depend are valid in rough approximation. The sum $(C_0 + C_1)$ is the static capacitance which may be measured at a frequency well below the fundamental resonance, for instance at 1 kc.

The error made in $(f_p - f_s)$ by use of the approximate equations (2) and (3) is less than 1 per cent if $M^2(f_p - f_s)/f_s > 100$.

2.1.3 Measurements on Disks in Radial Vibration: One of the fundamental measurements for piezoelectric ceramics is that of determining the planar coupling factor k_p. The term "planar" is used because the stress is two-dimensional (plane) isotropic. The planar coupling factor is related to the conventional piezoelectric and elastic constants by

$$k_p^2 = \frac{2d_{31}^2}{\epsilon_{33}^T(s_{11}^E + s_{12}^E)} = \left(\frac{2}{1 - \sigma^E}\right) k_{31}^2. \tag{4}$$

The cross contraction or Poisson's ratio σ^E is the ratio $-s_{12}^E/s_{11}^E$, and k_{31} is termed the transverse coupling factor. Poisson's ratio lies between 0.28 and 0.32 for barium titanate, modified barium titanate, and lead titanate zirconate ceramics. For any piezoelectric ceramic, its value can be accurately determined from resonances of square plates as shown in the Standard on Piezoelectric Crystals, 1958 [3], Section 2.7.2.

The planar coupling factor is obtained from the fundamental mode f_p and f_s of a thin disc with faces perpendicular to the Z axis as follows [9]:

$$\frac{k_p^2}{1 - k_p^2} = \frac{(1-\sigma^E)J_1[\eta_1(1+\Delta f/f_s)] - \eta_1(1+\Delta f/f_s)J_0[\eta_1(1+\Delta f/f_s)]}{(1+\sigma^E)J_1[\eta_1(1+\Delta f/f_s)]}, \tag{5}$$

where

J_0 = Bessel function of first kind and zero order,

J_1 = Bessel function of first kind and first order,

η_1 = lowest positive root of $(1+\sigma^E)J_1(\eta) = \eta J_0(\eta)$. (For $\sigma^E = 0.31$, $\eta_1 = 2.05$).

This relationship is plotted in Fig. 2, where k_n is shown as a function of $\Delta f/f_s$. The curve is drawn for $\sigma^E = 0.31$, but the deviation for σ^E between 0.27 and 0.35 is too small to show on the graph.

Eq. (5) was derived for an infinitely thin disk. For disks of finite thickness, the value for k_p obtained from (5) is higher than the true k_p of the material. For typical ceramics, the error is less than 1 per cent for a thickness to diameter ratio t/d smaller than 0.1. Rayleigh-type corrections may be made [10], and characteristic corrections are shown in Fig. 3. Even though corrections up to 10 per cent are shown, it is recommended that corrections over 3 per cent be considered only approximate. It may be readily inferred from Fig. 3 that the correction increases rapidly with increasing t/d, and that it is higher for compositions with low piezoelectric coupling and high $|d_{33}/d_{31}|$.

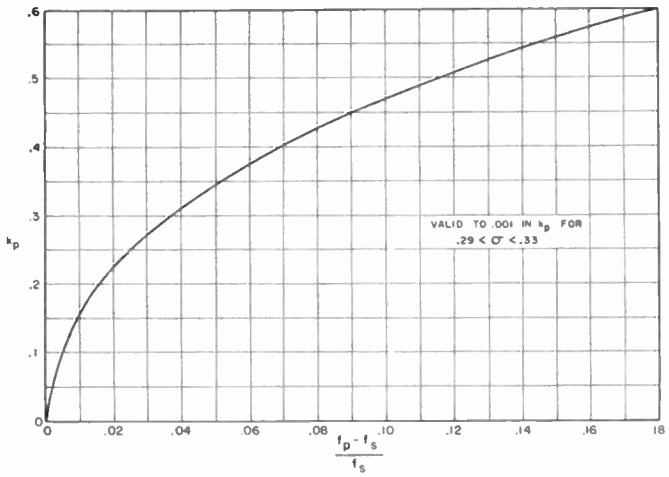

Fig. 2—Planar coupling factor of thin disk.

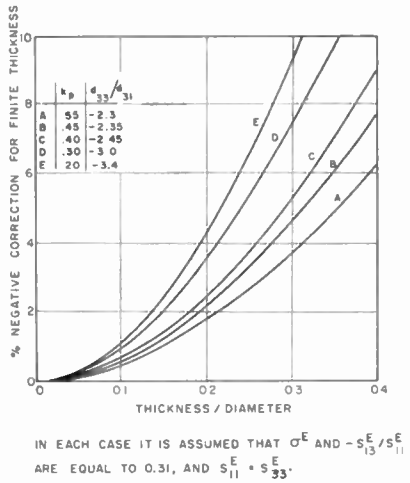

Fig. 3—Rayleigh correction for disk of finite thickness (applied to ordinate of Fig. 2 to obtain true k_p).

From the measured planar coupling factor, free dielectric constant, fundamental planar resonance frequency, and the density of a disk, the piezoelectric constants d_{31} and g_{31} may be calculated, as follows:

$$k_{31}^2 = \left(\frac{1 - \sigma^E}{2}\right) k_p^2,$$

$$\frac{1}{s_{11}^E} = \frac{\pi^2 d^2 f_s^2 (1 - \sigma^{E^2})\rho}{\eta_1^2},$$

$$d_{31} = k_{31}\sqrt{\epsilon_{33}^T s_{11}^E},$$

and

$$g_{31} = d_{31}/\epsilon_{33}^T. \tag{6}$$

2.1.4 Measurements on Bars and Thin Cylinders: The transverse coupling factor k_{31} may be determined according to (7) directly from the fundamental f_p and f_s of bars with thickness along the poling axis:

$$\frac{k_{31}^2}{1 - k_{31}^2} = \frac{\pi}{2}\frac{f_p}{f_s}\tan\left(\frac{\pi}{2}\frac{\Delta f}{f_s}\right). \tag{7}$$

The bars should have $(l/t)^2$ and $(l/w)^2$ both greater than 10. Combination of (7) with the first of (6) gives Poisson's ratio σ^E, provided that the bar and disk are in the same condition of polarization.

The longitudinal coupling factor k_{33} may be determined from the fundamental f_p and f_s of thin cylinders or bars electroded at the ends. This is generally most conveniently done with square or circular cross section, and the length should be at least two and one-half times the largest lateral dimension. The following relations then hold:

$$k_{33}^2 = \frac{\pi}{2}\frac{f_s}{f_p}\tan\frac{\pi}{2}\frac{\Delta f}{f_p},$$

$$\frac{1}{s_{33}^D} = 4\rho f_p^2 l^2,$$

$$s_{33}^E = s_{33}^D/(1 - k_{33}^2),$$

$$d_{33} = k_{33}\sqrt{\epsilon_{33}^T s_{33}^E},$$

and

$$g_{33} = d_{33}/\epsilon_{33}^T. \tag{8}$$

2.1.5 Measurements Relating to Shear Modes: The shear piezoelectric coupling factor k_{15} is preferably determined from dielectric measurements. A bar of square or rectangular cross section with length approximately twice the largest lateral dimension is poled along the length. Then another pair of faces is electroded. The shear deformation then occurs in the plane containing both the poling and signal fields. The free permittivity ϵ_{11}^T is obtained by a measurement of the capacitance at a frequency well below the fundamental resonance, which is determined by the dimension along the direction of the signal field. The clamped permittivity ϵ_{11}^S is determined by measurement of the capacitance at a frequency above any pronounced overtone of the thickness shear mode. The coupling factor is determined from the relation

$$\epsilon_{11}^S = (1 - k_{15}^2)\epsilon_{11}^T, \tag{9}$$

where

$$k_{15}^2 = \frac{d_{15}^2}{\epsilon_{11}^T s_{55}^E}.$$

Many ferroelectric ceramics have slowly decreasing capacitance with increasing frequency. The capacitance should therefore be measured over a frequency range below the fundamental resonance and above any pronounced overtones. Each curve may then be extrapolated to the resonance frequency.

The elastic compliance s_{55}^D may be determined from the successive parallel resonance frequencies f_{p_i} at a series of overtones of the thickness shear mode divided by the respective integers according to (10):

$$\frac{1}{s_{55}^D} = 4\rho(f_{p_i}t/i)^2; \qquad i = 1, 3, 5, \cdots. \tag{10}$$

Third, fifth, and seventh overtones should in this case deviate from a harmonic sequence by less than about 1 per cent, and may be averaged. The piezoelectric strain constants g_{15} and d_{15} are then given by

$$s_{55}^E = s_{55}^D/(1 - k_{15}^2),$$
$$d_{15} = k_{15}\sqrt{\epsilon_{11}^T s_{55}^E}, \tag{11}$$

and

$$g_{15} = d_{15}/\epsilon_{11}^T.$$

2.1.6 Measurements on Plates in Thickness Vibration: The elastic stiffness c_{33}^D may be determined by measurement of f_{p_i} at overtones of the thickness extensional mode of a thin plate with faces perpendicular to the Z axis:

$$c_{33}^D = 4\rho(f_{p_i}t/i)^2. \tag{12}$$

A measurement of the laterally-clamped thickness coupling factor k_t is not recommended in general, since the fundamental thickness extensional resonance of thin plates is not always free from unwanted resonances. The coupling factor k_t is directly related to the piezoelectric stress constant h_{33} rather than the strain constant d_{33}. For a very thin plate with infinite lateral dimensions, the square of the coupling factor is

$$k_t^2 = \frac{\pi}{2}\frac{f_s}{f_p}\tan\left(\frac{\pi}{2}\frac{\Delta f}{f_p}\right), \tag{13}$$

where

$$k_t^2 = h_{33}^2\epsilon_{33}^S/c_{33}^D.$$

Corrections for finite lateral dimensions have been not calculated, but they may be fairly high, since finite dimensions require a set of boundary conditions at the extreme edges.

The elastic stiffness c_{33}^E is given by

$$c_{33}^E = c_{33}^D(1 - k_t^2). \tag{14}$$

The clamped permittivity ϵ_{33}^S may be obtained from measurement of the capacitance of a thin plate in a frequency range above the fundamental thickness resonance and all pronounced overtones, and extrapolation to the operating frequency. In view of the substantial frequency dependence of ϵ_{33}^S in the megacycle range, a calculation from ϵ_{33}^T and piezoelectric data is preferred (see Table I).

2.1.7 Measurement of Q: The mechanical quality factor[3] Q is obtained from determination of the minimum impedance $|Z_m|$ at the fundamental resonance. This measurement may be accomplished by substitution of a variable resistance for the test specimen and adjustment for a current equal to the current through the specimen at f_m. For this measurement it is important that the specimen be held only at nodal points, although this is not nearly so critical as for high-Q crystals such as quartz. Q is given by the relation

$$\frac{1}{Q} = 2\pi f_s|Z_m|(C_0 + C_1)\left(\frac{f_p^2 - f_s^2}{f_p^2}\right)$$
$$\sim 4\pi\Delta f|Z_m|(C_0 + C_1). \tag{15}$$

The approximate expression leads to an error in Q of about 6.5 per cent for $\Delta f/f_s = 0.05$, 13 per cent for $\Delta f/f_s = 0.10$, and 23 per cent for $\Delta f/f_s = 0.20$. In each case the approximate expression gives a value which is too low.

Q is not independent of configuration or mode of vibration. It is generally lower for shear than for dilatational modes.

2.2 Static and Quasi-Static Methods

Piezoelectric strain constants may be measured under static or quasi-static conditions with reasonable accuracy, although the precision is inferior to that obtained with the resonance method. Both quasi-static and static piezoelectric measurements are described in the literature [6]. The relations used are

$$d_{31} = \left(\frac{\partial D_3}{\partial T_1}\right)_E = \left(\frac{\partial S_1}{\partial E_3}\right)_T,$$

and

$$d_{33} = \left(\frac{\partial D_3}{\partial T_3}\right)_E = \left(\frac{\partial S_3}{\partial E_3}\right)_T. \tag{16}$$

The high values of the strain constants d_{31} and d_{33} and good insulation resistance of typical piezoelectric ceramics at room temperature make direct measurement of response to static stress convenient. A recommended procedure is shock-free lifting of a previously applied weight from the specimen. The generated charge flows into a low-loss capacitor, whose capacitance is at least 10 and preferably 100 times that of the specimen. Voltage is measured by a tube electrometer; it is typically in the 0.1- to 10-volt range. Total generated charge is then calculated as the product of observed voltage and the sum of shunt capacitance and static specimen capacitance.

[3] The symbol Q in this and the preceding Standards on Piezoelectric Crystals always designates the mechanical quality factor (ratio of strain in-phase to strain out-of-phase with stress), which becomes observable electrically through the piezoelectric effect. The dielectric Q factor found in the capacitor literature is the reciprocal of the dissipation factor introduced in (19).

The hydrostatic response can be measured at 10 to 100 cps as described in the literature [6]. The hydrostatic strain constant d_h is related to d_{33} and d_{31} as follows:

$$d_h = 2d_{31} + d_{33}. \tag{17}$$

This provides a convenient means for routine measurement of both d_{33} and d_{31} on the same test specimen. The latter may be determined from resonance measurements on a thin disk, and the former may be calculated using d_{31} and d_h and (17). This involves combining measurements at widely differing frequencies. Experience with $BaTiO_3$ has not shown any frequency dependence of piezoelectric low-signal coefficients over a very wide range, at least from 100 cps to 100 kc [11].

3. Response to Large Signals

As previously noted, piezoelectric ceramics and ferroelectric crystals show linear relations between components of stress and strain on the one hand and electric field and displacement on the other only over limited ranges of the input signal. The limit of linear behavior is related to the coercive force and varies widely with ceramic composition.

3.1 Condition of Electric Drive

A direct measurement of mechanical strain as a function of driving electric field may be obtained on an oscilloscope using a displacement meter [6] or strain gauges. Of even greater practical importance for designers of piezoelectric ceramic transducers are dielectric losses resulting from dielectric hysteresis. This is due to the fact that in itself nonlinearity of the strain-field relationship results only in harmonic distortion of the acoustic power output, whereas a sharp increase in dielectric losses at high field amplitudes results in lowered acoustic efficiency and increased generation of internal heat which may lead to depoling.

For transducer applications the desired effect is mechanical strain; internal heat generation is the undesired effect. For quasi-static conditions, the strain is given by

$$S_3 = d_{33}E_3$$

or

$$S_1 = d_{31}E_3. \tag{18}$$

The power lost to internal heat is given by

$$H = 2\pi f \epsilon D E^2. \tag{19}$$

It is necessary to measure both the permittivity ϵ and the dissipation factor D as functions of applied field E, since both are field-dependent. It is suggested that the performance of ferroelectric ceramics under high electric drive be specified by a plot of internally generated heat per cycle as a function of strain amplitude. The internally generated heat per unit volume per cycle is given by $2\pi\epsilon DE^2$, and the strain is given by (18). The nonlinearity of the strain-field relationship may be disregarded. With ceramic barium titanate, for instance, the strain-field relationship is linear up to fields of 6000 to 8000 volts/cm; at this field level the dielectric dissipation factor has already increased from less than 0.01 to over 0.10.

Measurements of permittivity and dissipation factor as function of electric driving field should be made with the specimen immersed in a stirred oil bath. Otherwise, the generation of internal heat leads to a temperature rise dependent upon the configuration of the test specimen.

Dependence of mechanical losses on strain amplitude may be obtained from the series resonance resistance R_1 of an unloaded vibrator, or from the temperature rise of such a vibrator. Mechanical as well as dielectric losses in the piezoelectric transducer material detract from the efficiency of a loaded transducer. If all other factors are known this may allow a determination of the mechanical loss factor. In the case of well-loaded acoustic transducers it has been assumed that internal dielectric losses are considerably greater than internal mechanical losses.

High ac electric fields depolarize poled ferroelectric ceramics. The degree of depolarization is a function of the applied ac field and temperature. For typical barium titanate, at room temperature, depolarization may become noticeable at 400 volts/mm rms and be substantially complete at 800 volts/mm rms. The depolarization test should be made in an oil bath so that the temperature may be controlled . Test specimens should be subjected to progressively higher electric driving fields, with the relative frequency separation $(f_p - f_s)/f_s$ measured after each exposure. The frequency of the electric driving field should be such that internal heating is not too great; 60 cps is convenient.

3.2 Condition of Mechanical Drive

For some applications the nonlinear response to high mechanical stress is utilized. In the linear range the charge density and field caused by an axial stress T_3 are

$$D_3 = d_{33}T_3$$

and

$$E_3 = g_{33}T_3. \tag{20}$$

The generated electric charge density increases more than proportionally to applied stress over a pressure range, typically 20 to 100 million newton/meter^2 for $BaTiO_3$, and then approaches a saturation value equal to the total electric polarization of the poled ceramic, about 8 micro coulomb/cm^2 for barium titanate. After

stressing near to saturation, the electric polarization is not recovered upon release of the stress.

Test specimens for study of these effects should have the largest lateral dimension not more than twice the length to avoid lateral constraint. The stress should be applied as nearly perpendicular to the specimen faces as possible, using a mechanical or hydraulic press. The released charges should be collected on a large capacitance connected in parallel with the test specimen.

It has been shown that for a given ceramic composition the total ferroelectric charge of a specimen is approximately proportional to its piezoelectric coupling coefficient. Once a relationship between, for instance, k_p and total ferroelectric charge has been established for a ceramic composition, it is necessary to measure only k_p for other specimens of the same composition in order to determine suitability for an application utilizing the total ferroelectric charge.

The open-circuit field remains a nearly linear function of stress to far higher stress levels than does the electric displacement, and no permanent loss of polarization occurs. For measurements of open-circuit voltage a very-high-impedance electrometer must be used.

4. Pyroelectric Effects

The magnitude of ferroelectric polarization is temperature dependent. Over a range of temperature below the Curie point and excluding other phase transitions the temperature variation of this ferroelectric polarization is reversible and may be defined by a pyroelectric coefficient $(\partial P/\partial\theta)_T$. As noted, the measurement is normally at constant stress, and hence includes both the primary and secondary effects [12].

A convenient measurement of the integrated pyroelectric effect can be made by suddenly immersing the test specimen in heated oil and collecting the electric charges on a capacitance connected in parallel. This method is, however, satisfactory only so long as the time constant of the test specimen and parallel capacitance is high enough so that only negligible decay occurs during the time required for domain realignment and the relief of thermal stresses. A low-impedance circuit method is, therefore, recommended. A fairly sensitive galvanometer is connected across the test specimen, which is slowly heated. Both pyroelectric current and specimen temperature are recorded as function of time. The ratio of current per unit area to $\partial\theta/\partial t$ gives directly the pyroelectric coefficient. An integration of the current-time curve over specific temperature intervals is recommended to obtain the electric moment as a function of temperature.

5. Aging

The parameters of ferroelectric ceramics change with time after major disturbances, such as temporary heating to high temperature for electroding, or the poling process. These changes are in the direction of decreasing dielectric and piezoelectric constants and mechanical compliance, and, hence, increase in frequency constant. The aging rate may be expressed in the form

$$\frac{1}{y(1)}\frac{dy}{dt} = ct^{-1}, \tag{21}$$

where y is the parameter under consideration, $y(1)$ is its value at unit time (such as one day) after the disturbance, and c is a coefficient characteristic of the material and parameter involved. With c independent of time, (21) can be integrated to

$$\frac{y - y(1)}{y(1)} = c \ln t = c' \log_{10} t. \tag{22}$$

The latter relation is the basis for specifying "aging per decade" with typical values of c' for resonance frequency constants in the range of 0.05 per cent to 1.5 per cent, and for piezoelectric coupling factors and dielectric constants in the range from -0.5 per cent to -5 per cent. Even higher negative aging rates are found for the dissipation factor, and higher positive rates for Q.

The coefficient c in (21) itself varies slowly with time, usually in a decreasing sense of its absolute value, and therefore (22) is only an approximation. For a typical barium titanate ceramic, the frequency constant was found to increase by 0.54 per cent from 1 day to 10 days after poling, by 0.51 per cent from 10 days to 100 days, and by 0.42 per cent from 100 days to 1000 days. The decade or decades to be used for specifying c' should therefore be stated.

References

[1] "IRE standards on piezoelectric crystals, 1949," Proc. IRE, vol. 37, pp. 1378–1395; December, 1949.
[2] "IRE standards on piezoelectric crystals—the piezoelectric vibrator: definitions and methods of measurement, 1957," Proc. IRE, vol. 45, pp. 353–358; March, 1957.
[3] "IRE standards on piezoelectric crystals: determination of the elastic, piezoelectric, and dielectric constants—the electromechanical coupling factor, 1958," Proc. IRE, vol. 46, pp. 764–778; April, 1958.
[4] W. P. Mason, "Piezoelectric Crystals and Their Application to Ultrasonics," D. Van Nostrand and Co., Inc., New York, N. Y., pp. 296–304; 1950.
[5] H. G. Baerwald; "Thermodynamic theory of ferroelectric Ceramics," *Phys. Rev.*, vol. 105, pp. 480–486; January, 1957.
[6] W. P. Mason and H. Jaffe, "Methods for measuring piezoelectric, elastic, and dielectric coefficients of crystals and ceramics," Proc. IRE, vol. 42, pp. 921–930; June, 1954.
[7] W. P. Mason, *op. cit.*, pp. 61–68 and 289–296.
[8] E. A. Gerber and L. F. Koerner, "Methods of measurement of the parameters of piezoelectric vibrators," Proc. IRE, vol. 46, pp. 1731–1737; October, 1958.
[9] W. P. Mason, "Electrostrictive effect in barium titanate ceramics," *Phys. Rev.*, vol. 74, pp. 1134–1147; November, 1948.
[10] H. G. Baerwald, "Electrical Admittance of a Circular Ferroelectric Disc." Tech. Rept. No. 3, Office of Nav. Res., Contract No. Nonr 1055(00), January, 1955; U. S. Dept. of Commerce, Office of Tech. Services, PB119233.
[11] D. Berlincourt, "Recent developments in ferroelectric ceramics," IRE Trans. on Ultrasonic Engineering, vol. UE-4, pp. 53–65; August, 1956.
[12] W. G. Cady, "Piezoelectricity," McGraw-Hill Book Co., New York, N. Y., pp. 40 and 699; 1946.

The Field-Effect Tetrode*

H. A. STONE, JR.†, SENIOR MEMBER, IRE, AND R. M. WARNER, JR.‡, SENIOR MEMBER, IRE

Summary—The new device described here consists basically of a thin *N* region adjacent to a comparably thin *P* region. Two contacts are made to the *N* side and two to the *P* side so that currents can be passed through each thin region parallel to the single junction of the device. The two currents do not mix because reverse bias is maintained on the junction. A current in either side affects the resistance of the other side, and hence the current in the other side, through the medium of the depletion layer; this mutual interaction of currents gives the device its unique properties. The field-effect tetrode has applications as a gyrator and isolator. In a two-terminal connection it exhibits voltage-controlled negative resistance. Also, it can be applied as a truly linear, yet electronically variable, resistor. Equations are developed for its behavior in these applications and experimental results are discussed. In the models to date, the thin regions were shaped by rather tedious mechanical and chemical procedures. Epitaxial film techniques may be well adapted to its fabrication in the future.

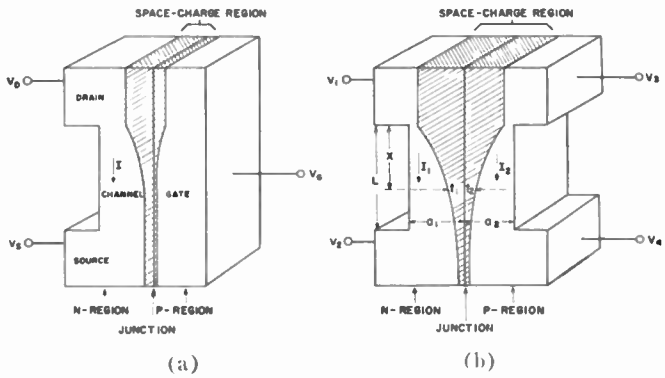

Fig. 1—Field-effect devices. (a) Field-effect transistor. (b) Field-effect tetrode.

I. INTRODUCTION

THE field-effect tetrode[1] embodies the principles of field effect in a new type of semiconductor device. The structure consists of two independently terminated conducting channels so disposed that the conductance of each is modulated along its length by the voltage conditions in the other. Conceptually, the field-effect tetrode may be likened to a field-effect transistor[2] in which the gate is replaced by a second channel and each of the channels acts as a gate for the other.

The geometry is shown schematically and is compared to a field-effect transistor in Fig. 1. Voltages may be applied to all of the four terminals, and subject only to the restriction that reverse bias should obtain, these voltages may be mutually independent. The pattern of depletion-layer penetration and the resulting conductances of the two channels are uniquely determined by the voltage differences $V_1 - V_3$ and $V_2 - V_4$ appearing across the junction at the two ends of the channels, and are independent of the voltage drop along the channels $V_1 - V_2$ and $V_3 - V_4$.

In addition to its implications as an amplifier, the field-effect tetrode can be adapted to a variety of other circuit functions. These include impedance inversion, undistorted large-signal modulation and, in a two-terminal configuration, voltage-controlled negative resistance.

Units have been made at Bell Laboratories from silicon crystals with diffused junctions, the required geometry being achieved by grinding and etching. Measurements on models have confirmed some of the predicted device behavior.

II. CURRENT-VOLTAGE EQUATIONS

Associated with a field-effect transistor is the "pinch-off" voltage.[2] This is the voltage which, if applied as a reverse bias across the junction, would cause the depletion layer to extend completely across the channel. A field-effect tetrode may be considered to have two pinch-off voltages since there are two channels and the voltages required for the depletion layer to traverse them need not be the same. The following derivation of the current-voltage equation is undertaken for the case where they are exactly equal.

General equations, where no restrictions are put on the pinch-off voltages, are developed in Appendix II. These equations have a transcendental term and cannot be solved explicitly. However, approximate solutions are derived for the case where the pinch-off voltages are nearly equal. For most practical applications it is likely that interest will center around devices whose pinch-off voltages are not widely different.

A number of simplifying approximations will be made in developing the current-voltage equations. Among them is the assumption that the impurities in each region are uniformly distributed. In a diffused structure this is, of course, not so; and while this leads to differences in detail, it does not basically alter the behavior described by the equation.

A one-dimensional model is used, assuming that the potential at any point along the channel is independent of its location with respect to the depletion layer and the surface.

* Received by the IRE, January 30, 1961.
† Component Dev., Bell Telephone Labs., Inc., Murray Hill, N. J.
‡ Motorola Semiconductor Products Div., Motorola, Inc., Phoenix, Ariz. Formerly with Bell Telephone Labs. Inc., Murray Hill, N. J.
[1] H. A. Stone, Jr. "The field-effect tetrode," 1959 IRE NATIONAL CONVENTION RECORD, pt. 3, pp. 3–8.
[2] W. Shockley, "A unipolar 'field-effect' transistor," PROC. IRE, vol. 40, pp. 1365–1376; November, 1952.

Another assumption is that there are no abrupt changes in the depletion-layer thickness along the channel. This condition is probably not seriously violated except when the bias voltages are close to the pinch-off values. The built-in voltage has been ignored in the analysis. It can be accommodated after the fact by suitably adjusting the numbers used for the bias voltages. It is assumed that the donors and acceptors are completely ionized and that the depletion layer has a sharp boundary. Finally, no attempt has been made to take into account limiting velocities in high fields, and this also may lead to some discrepancy as the pinch-off voltage is approached.

A. Symmetrical Case

Consider the structure symbolized in Fig. 1. Let the applied voltages at the terminals be V_1, V_2, V_3, V_4 as shown. The restrictions on these voltages are:

1) V_1 positive with respect to V_3, and V_2 positive with respect to V_4, so that all parts of the junction will be reverse biased.
2) $V_1 - V_3 \leq W_p$ and $V_2 - V_4 \leq W_p$, where W_p is the potential difference across the junction which will cause at least one side to pinch-off.

The thicknesses of the depletion layers are shown in Appendix I to be given by

$$t_1^2 = \frac{2\kappa\epsilon_0}{q} \frac{P}{N(P+N)} (v_1 - v_2) \tag{1}$$

$$t_2^2 = \frac{2\kappa\epsilon_0}{q} \frac{N}{P(P+N)} (v_1 - v_2), \tag{2}$$

where v_1 and v_2 are the potentials in the N and P channels, respectively, at some value of x; N is the net donor density in channel 1 and P is the net acceptor density in channel 2. The pinch-off voltage in the N channel W_{1p} is defined as the value of $v_1 - v_2$ for which $t_1 = a_1$.

$$W_{1P} = \frac{qNa_1^2(P+N)}{2\kappa\epsilon_0 P}. \tag{3}$$

Similarly, the pinch-off voltage in the P channel is defined by

$$W_{2P} = \frac{qPa_2^2(P+N)}{2\kappa\epsilon_0 N}. \tag{4}$$

In the symmetrical case,

$$W_{1P} = W_{2P} = W_P \tag{5}$$

and

$$a_1 N = a_2 P = \sqrt{\frac{2\kappa\epsilon_0}{q}} \sqrt{\frac{PN}{P+N}} W_P^{1/2}. \tag{6}$$

Also, at any point along the channels,

$$t_1 N = t_2 P = \sqrt{\frac{2\kappa\epsilon_0}{q}} \sqrt{\frac{PN}{P+N}} (v_1 - v_2)^{1/2} \tag{7}$$

and

$$\frac{t_1}{a_1} = \frac{t_2}{a_2} = \frac{(v_1 - v_2)^{1/2}}{(W_P)^{1/2}}. \tag{8}$$

At any point x along the channels, the resistances of the elements of length are

$$dR_1 = \frac{dx}{q\mu_1 NZ(a_1 - t_1)} = \frac{dx}{G_1 L\left(1 - \frac{t_1}{a_1}\right)} \tag{9}$$

and

$$dR_2 = \frac{dx}{q\mu_2 PZ(a_2 - t_2)} = \frac{dx}{G_2 L\left(1 - \frac{t_2}{a_2}\right)}, \tag{10}$$

where μ_1 and μ_2 are the N and P carrier mobilities, respectively, L is the channel length, Z is the width (into the paper) of the channel and G_1 and G_2 are the initial conductances of the respective channels.

The currents in the channels are

$$I_1 = -\frac{dv_1}{dR_1} = -G_1 L\left(1 - \frac{t_1}{a_1}\right)\frac{dv_1}{dx} \tag{11}$$

and

$$I_2 = -\frac{dv_2}{dR_2} = -G_2 L\left(1 - \frac{t_2}{a_2}\right)\frac{dv_2}{dx}. \tag{12}$$

In the symmetrical case, from (8)

$$I_1 dx = -G_1 L\left[1 - \frac{(v_1 - v_2)^{1/2}}{(W_P)^{1/2}}\right] dv_1 \tag{13}$$

$$I_2 dx = -G_2 L\left[1 - \frac{(v_1 - v_2)^{1/2}}{(W_P)^{1/2}}\right] dv_2. \tag{14}$$

These equations can be solved simultaneously for the two currents. For the first solution, (13) is divided by (14)

$$\frac{I_1}{G_1} dv_2 = \frac{I_2}{G_2} dv_1$$

and integrated

$$\frac{I_1}{G_1}\int_{V_3}^{V_4} dv_2 = \frac{I_2}{G_2}\int_{V_1}^{V_2} dv_1$$

$$\frac{I_1}{G_1}(V_3 - V_4) = \frac{I_2}{G_2}(V_1 - V_2). \tag{15}$$

For the second solution,

$$dv_1 - dv_2 = d(v_1 - v_2) = -\frac{\frac{I_1}{G_1} - \frac{I_2}{G_2}}{L\left[1 - \frac{(v_1 - v_2)^{1/2}}{(W_P)^{1/2}}\right]} dx.$$

Integrating

$$\int_{V_1-V_3}^{V_2-V_4} \left[1 - \frac{(v_1 - v_2)^{1/2}}{(W_P)^{1/2}}\right] d(v_1 - v_2) = -\frac{\frac{I_1}{G_1} - \frac{I_2}{G_2}}{L} \int_0^L dx$$

$$\frac{I_1}{G_1} - \frac{I_2}{G_2} = [(V_1 - V_3) - (V_2 - V_4)] - \frac{2}{3W_P^{1/2}}[(V_1 - V_3)^{3/2} - (V_2 - V_4)^{3/2}]. \quad (16)$$

From (15) and (16), the current equations are found to be

$$I_1 = G_1(V_1 - V_2) \cdot \left[1 - \frac{2}{3W_P^{1/2}} \frac{(V_1 - V_3)^{3/2} - (V_2 - V_4)^{3/2}}{(V_1 - V_3) - (V_2 - V_4)}\right] \quad (17)$$

$$I_2 = G_2(V_3 - V_4) \cdot \left[1 - \frac{2}{3W_P^{1/2}} \frac{(V_1 - V_3)^{3/2} - (V_2 - V_4)^{3/2}}{(V_1 - V_3) - (V_2 - V_4)}\right]. \quad (18)$$

It will be noted that the first term in each equation is simply Ohm's law for that channel, and the second term describes the modulation of conductance in terms of the voltage differences $V_1 - V_3$ and $V_2 - V_4$ appearing across the two ends of the device.

B. Comparison with Field-Effect Transistor

It can be shown that the field-effect transistor[2] is a limiting case of the field-effect tetrode. It is apparent that if no current flows in one of the channels, that channel will behave as a field-effect transistor gate. If, in Fig. 1, we let

$$V_3 = V_4 \equiv V_G$$

$$V_1 \equiv V_D$$

and

$$V_2 \equiv V_S,$$

(17) will reduce to

$$I_1 = J(V_D - V_G) - J(V_S - V_G), \quad (19)$$

where the function $J(\lambda)$ is defined by

$$J(\lambda) = G_1\lambda\left\{1 - \frac{2\lambda^{1/2}}{3W_P^{1/2}}\right\}. \quad (20)$$

These are the equations for a field-effect transistor.

Strictly speaking, (17) applies only to symmetrical structures. However, (20) can also be derived from (90), Appendix II, in a similar manner and without any restriction on the symmetry of the unit.

The field-effect tetrode bears a superficial resemblance to a pair of complementary field-effect transistors connected back to back. It is of interest to explore whether the behavior of two field-effect transistors, interconnected as shown in Fig. 2, would be equivalent to that of the tetrode. In order that the equations we derive can be compared directly to (17) and (18) for the tetrode, we will restrict ourselves to the case where both units have the same value of pinch-off voltage.

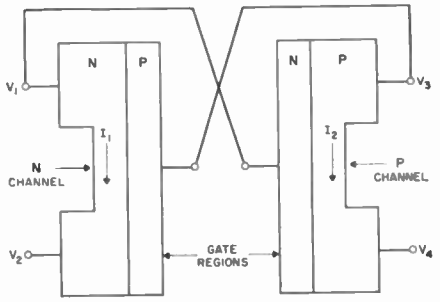

Fig. 2—Complementary field-effect transistors in back-to-back configuration.

Consider first the unit on the left with the P-type gate and N-type channel. Noting that V_1 corresponds to the drain and V_2 to the source, (19) becomes

$$I_1 = J_1(V_1 - V_3) - J_1(V_2 - V_3), \quad (21)$$

where J_1 is defined as in (20). Similarly, in the unit on the right, with the N-type gate and P-type channel, the current can be shown to be

$$I_2 = J_2(V_3 - V_1) - J_2(V_4 - V_1), \quad (22)$$

where

$$J_2 = G_2\lambda\left\{1 - \frac{2\lambda^{1/2}}{3W_P^{1/2}}\right\}. \quad (23)$$

To facilitate comparison with (17) and (18), (21) and (22) can be written in a similar form. They become

$$I_1 = G_1(V_1 - V_2) \cdot \left[1 - \frac{2}{3W_P^{1/2}} \frac{(V_1 - V_3)^{3/2} - (V_2 - V_3)^{3/2}}{(V_1 - V_3) - (V_2 - V_3)}\right] \quad (24)$$

$$I_2 = G_2(V_3 - V_4) \cdot \left[1 - \frac{2}{3W_P^{1/2}} \frac{(V_1 - V_3)^{3/2} - (V_1 - V_4)^{3/2}}{(V_1 - V_3) - (V_1 - V_4)}\right]. \quad (25)$$

We note that the currents in each channel of the tetrode are a function of all four applied voltages, whereas each of the currents in the two field-effect transistors depends on three applied voltages only. There is a symmetry in the tetrode (indicated by the fact that the expressions in brackets are identical) which is lacking in the field-effect transistor. The importance of this factor becomes evident in the discussion of the electronically variable resistor, whose performance cannot be duplicated with field-effect transistors

The other applications discussed in this paper could be effected with complementary field-effect transistors; only the quantitative considerations would be different.

III. Voltage-Controlled Negative Resistance

If terminals 2 and 3 of the field-effect tetrode [Fig. 1(b)] are interconnected, the characteristics measured between terminals 1 and 4 are of some interest. In the following analysis, we will set terminal 4 at reference zero and examine the current as a function of the voltage applied at terminal 1. For the symmetrical case, (17) and (18) reduce to

$$I_1 \equiv I = G_1(V_1 - V_2) \cdot \left[1 - \frac{2}{3W_P^{1/2}} \frac{(V_1 - V_2)^{3/2} - V_2^{3/2}}{(V_1 - V_2) - V_2}\right] \quad (26)$$

$$I_2 = I = G_2V_2\left[1 - \frac{2}{3W_P^{1/2}} \frac{(V_1 - V_2)^{3/2} - V_2^{3/2}}{(V_1 - V_2) - V_2}\right]. \quad (27)$$

We can solve these equations, eliminating V_2 and expressing the current as a function of V_1. One way to proceed is to divide (26) by (27) and establish that

$$V_2 = \frac{G_1}{G_1 + G_2} V_1. \quad (28)$$

Noting from (6) that a_1N and a_2P are equal, it follows that

$$\frac{G_1}{G_2} = \frac{\mu_1}{\mu_2} \equiv b. \quad (29)$$

From (28) and (29),

$$V_2 = \frac{b}{b + 1} V_1 \quad (30)$$

and

$$(V_1 - V_2) = \frac{1}{b + 1} V_1. \quad (31)$$

Inserting these values in (26), we obtain

$$I = \frac{G_1}{b + 1} V_1 \left\{1 - \frac{2}{3}\left(\frac{V_1}{W_P}\right)^{1/2} \frac{b^{3/2} - 1}{(b + 1)^{1/2}(b - 1)}\right\}. \quad (32)$$

It is to be noted that pinch-off does not occur when V_1 equals W_P, but rather when the voltage across the junction, $(V_1 - V_2)$ or V_2, first reaches that value. In a real semiconductor $\mu_1 > \mu_2$ and $b > 1$. Eqs. (30) and (31) show that in a symmetrical unit V_2 is always greater than $V_1 - V_2$; thus pinch-off occurs when V_2 reaches the value W_P. The corresponding value of applied voltage V_P is

$$V_P = \frac{b + 1}{b} W_P. \quad (33)$$

We can rewrite (32) in terms of the applied voltage which will produce pinch-off:

$$I = \frac{1}{b} G_1W_P\left(\frac{V_1}{V_P}\right) \cdot \left\{1 - \frac{2}{3}\left(\frac{V_1}{V_P}\right)^{1/2} \frac{b + b^{1/2} + 1}{b + b^{1/2}}\right\}. \quad (34)$$

At pinch-off the current becomes

$$I_P = \frac{1}{b} G_1W_P\left\{1 - \frac{2}{3} \frac{b + b^{1/2} + 1}{b + b^{1/2}}\right\}. \quad (35)$$

We can now normalize (34) in terms of the pinch-off current:

$$\frac{I}{I_P} = \frac{1 - \frac{2}{3} \frac{b + b^{1/2} + 1}{b + b^{1/2}}\left(\frac{V_1}{V_P}\right)^{1/2}}{1 - \frac{2}{3} \frac{b + b^{1/2} + 1}{b + b^{1/2}}}\left(\frac{V_1}{V_P}\right). \quad (36)$$

For silicon, assuming $b = 3.0$, (36) becomes

$$\frac{I}{I_P} = 5.25\left(\frac{V_1}{V_P}\right) - 4.25\left(\frac{V_1}{V_P}\right)^{3/2}. \quad (37)$$

This equation is plotted in Fig. 3, and Fig. 4 shows a photograph of the V-I characteristic of a laboratory unit.

The type of negative resistance displayed by the field-effect tetrode bears a resemblance to that of the Esaki[3] diode. However, there are two important differences: first, the impedance levels of the field-effect tetrode are very much higher, from several hundred to several thousand ohms; second, the tetrode is limited in speed by the time constant associated with the junction capacitance and channel resistance.

[3] L. Esaki, "New phenomenon in narrow germanium P-N junctions," *Phys. Rev.*, vol. 109; pp. 603-604; January 15, 1958.

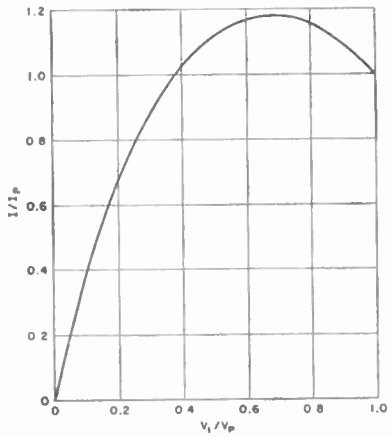

Fig. 3—*V-I* characteristic of field-effect tetrode in negative resistance configuration.

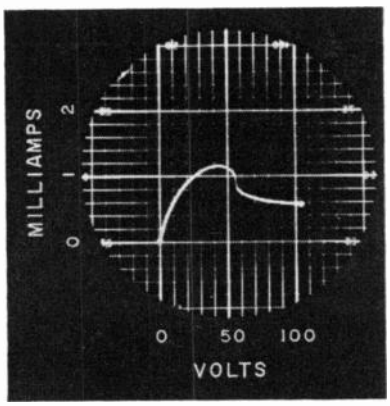

Fig. 4—Voltage-controlled negative resistance in laboratory model of field-effect tetrode.

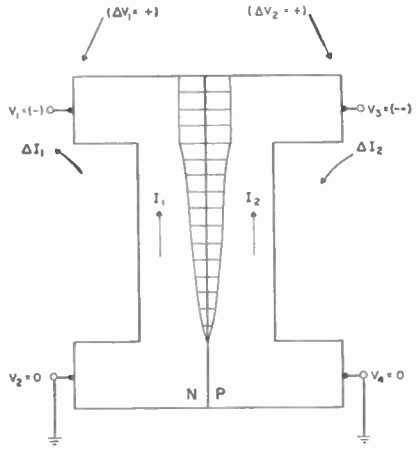

Fig. 5—Bias arrangement for admittances of opposite sign.

IV. Gyrator

A. *Basic Nonreciprocal Properties*

The field-effect tetrode, treated as a four-terminal network for the case of small ac signals, exhibits nonreciprocity in all except a special class of bias conditions which are discussed in Section V; that is, under most bias conditions its transfer admittances are unequal. Within well-defined bias ranges its transfer admittances can be made unequal in magnitude though the same in sign, while in other well-defined ranges these admittances can be made to have opposite signs. It is in this last situation that the tetrode exhibits gyrator properties and is capable of inverting impedances. Most of the present discussion is directed toward that end.

Fig. 5 shows one of the simple cases in which the tetrode displays transfer admittances of opposite sign. Negative voltages are applied to terminals 1 and 3, but terminal 3 is made more negative to reverse bias the junction. Terminals 2 and 4 are both at ac and dc ground potential, while terminals 1 and 3 carry the signal voltages.

Several restrictions must be placed on signal and bias voltages. For quasi-linear operation, the magnitude of the signal voltage must be small compared to the dc voltage across the junction. This also automatically insures that the junction will never be forward biased. In addition, we will for present purposes rule out operation beyond pinch-off, because fundamental analysis of the device in that range has not yet been done.

Fig. 5 also gives an illustration of the fact that transfer admittances are opposite in sign for these bias conditions. When a positive increment ΔV_1 is placed on V_1, with V_3 held constant, reverse bias on the junction increases, the depletion layer expands, the resistance of channel 2 increases, and the current I_2 decreases—a change which can be represented by an *inward*-flowing incremental current ΔI_2. Applying a positive increment ΔV_3 to V_3, with V_1 held constant, causes the depletion layer to contract, and I_1 increases. This can be represented by an *outward*-flowing ΔI_1 on the left side.

If terminals 1 and 3 are both made positive, the currents and current increments change sign, but it is still true that a positive voltage increment leads to an inward current increment for one direction of transfer and to an outward current increment for the other direction.

However, by making terminal 1 positive and terminal 3 negative with respect to the common terminals, it can be seen by going through an argument similar to the one given above that the transfer admittances take on the same sign.

The dependence of the sign of the ratio of the transfer admittances, y_{12}/y_{21}, on bias is summarized graphically in Fig. 6. Here V_1 and V_3 are plotted against each other. The scales are normalized in terms of the pinch-off voltage W_p. Two lines are plotted, the lower corresponding to zero bias across the junction, $V_1 - V_3 = 0$, and the upper corresponding to the pinched-off condition, $V_1 - V_3 = W_p$. Hence, for a vanishingly small signal voltage, all bias combinations lying within the diagonal band are permissible. Limits at the ends of the region are fixed by dissipation considerations. The example given in Fig. 5 falls, of course, in the third quadrant.

For present purposes, discussion will be confined to the case of two independent dc biases and a common ground, as illustrated in Figs. 5 and 6; the principles are adequately demonstrated in this way, and all of the exploratory measurements to date have been made with this arrangement. Other possible biasing arrangements are taken up in Section V.

B. Admittance Analysis

As shown in Section II-A, (17) and (18), the current in each channel of a "symmetrical" tetrode can be expressed as a function of the dc voltages at the four terminals. These equations are based on a purely resistive model of the tetrode. The special case of Fig. 5 introduces the simplification that $V_2 = V_4 = 0$. Hence from these equations we can write,

$$I_1 = G_1 V_1 \left(1 - \frac{2}{3}\sqrt{\frac{V_1 - V_3}{W_P}}\right) \tag{38}$$

$$I_2 = G_2 V_3 \left(1 - \frac{2}{3}\sqrt{\frac{V_1 - V_3}{W_P}}\right). \tag{39}$$

From these equations the small-signal admittances, all real, can be calculated directly:

$$y_{11} = \frac{\partial I_1}{\partial V_1} = G_1\left[1 - \frac{3V_1 - 2V_3}{3\sqrt{W_P(V_1 - V_3)}}\right] \tag{40}$$

$$y_{22} = \frac{\partial I_2}{\partial V_2} = G_1\frac{\mu_2}{\mu_1}\left[1 - \frac{2V_1 - 3V_3}{3\sqrt{W_P(V_1 - V_3)}}\right] \tag{41}$$

$$y_{12} = \frac{\partial I_1}{\partial V_2} = G_1\frac{V_1}{3\sqrt{W_P(V_1 - V_3)}} \tag{42}$$

$$y_{21} = \frac{\partial I_2}{\partial V_1} = -G_1\frac{\mu_2}{\mu_1}\frac{V_3}{3\sqrt{W_P(V_1 - V_3)}}. \tag{43}$$

It is of interest to compare the tetrode and an ideal gyrator in a straightforward way. An ideal gyrator is usually defined as a four-terminal element whose self-admittances, y_{11} and y_{22}, are zero and whose transfer admittances, y_{12} and y_{21}, are equal in magnitude and opposite in sign.[4] In the case where V_1 and V_3 are both negative, as shown in Fig. 5, it can be seen from (42) and (43) that the transfer admittances of the tetrode are indeed opposite in sign and will be equal in magnitude provided

$$\frac{\mu_2}{\mu_1} = \frac{V_1}{V_3}. \tag{44}$$

In Fig. 7 the dotted line in the first and third quadrants indicates this condition graphically for the case $\mu_2/\mu_1 = \frac{1}{3}$. Note that equal and opposite transfer admittances occur within the permissible bias range only in the third quadrant. They cannot be achieved by using positive biases on terminals 1 and 3.

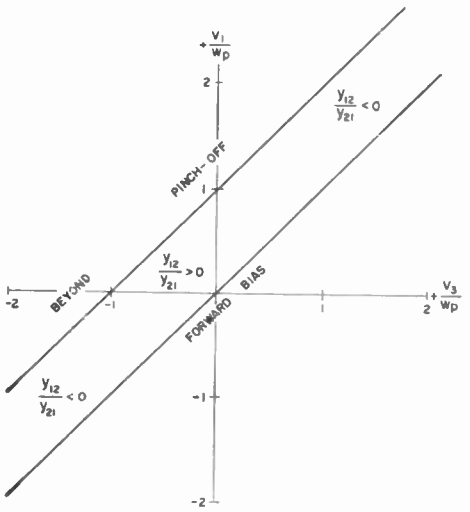

Fig. 6—Permissible range of bias voltages.

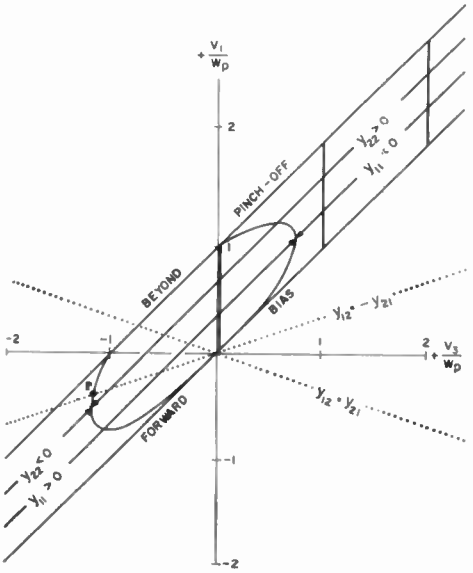

Fig. 7—Relationship between bias voltages and admittances.

Now consider the self-admittances: It is implicit in (40) that the minimum value of y_{11}, using negative biases, is obtained by letting $V_1 \to 0$ and $V_3 \to W_P$, which gives

$$y_{11} = \tfrac{1}{3}G_1. \tag{45}$$

Hence y_{11} remains positive and finite for permissible biases in the third quadrant. Additional insight can be gained here by means of a qualitative argument based on Fig. 5: a positive increment on V_1 decreases the end-to-end voltage on channel 1 and simultaneously increases its resistance; the reverse is true for a negative increment. Thus, the resistance and "driving voltage" changes are additive as far as channel current is concerned, so the self-admittance of channel 1 cannot vanish for these bias conditions.

[4] B. D. H. Tellegen, "The gyrator, a new electric network element," *Philips Res. Repts.*, vol. 3, pp. 80–101; April, 1948.

In channel 2, however, a positive increment on V_3 decreases the driving voltage but also decreases the channel resistance. It turns out that the two effects can be balanced to give zero change in I_2 and hence a zero value of y_{22}. Fig. 7 shows the locus of third-quadrant biases for which this is true.

Thus, by biasing at the point P in Fig. 7 ($V_1 = -18W_P/49$, $V_3 = -54W_P/49$), it is possible to have the transfer admittances equal and opposite, and to have one of the self-admittances, y_{22}, equal to zero. The other self-admittance has not vanished, however. Specifically, $y_{11} = (4/7)G_1$. This operating point has not proved to be the most advantageous one for practical impedance inversion, but it does illustrate the comparison of the field-effect tetrode with an ideal gyrator.

C. Inductor Analysis

A gyrator is capable of inverting an admittance. It can, for example, change the admittance of an ideal capacitor

$$y = j\omega C \tag{46}$$

into an ideal inductive admittance

$$y = \frac{y_t^2}{j\omega C}, \tag{47}$$

where y_t is the common magnitude of the ideal gyrator's transfer admittances. Hence for such an inductor,

$$L = \frac{C}{y_t^2}. \tag{48}$$

Because of the practical interest attaching to a miniature solid-state inductor, all experimental work to date on the gyrator aspect of the tetrode has been directed toward the inversion of capacitive admittances. We shall analyze this case and then give a specific numerical prediction based on this analysis for the behavior of the resulting inductor.

The input admittance at port 1 of a two-port network which is terminated on port 2 by an admittance y_{load} is

$$y_{in1} = y_{11} - \frac{y_{12}y_{21}}{y_{22} + y_{load}}. \tag{49}$$

For the situation where the load is at port 1, the input admittance similarly is

$$y_{in2} = y_{22} - \frac{y_{12}y_{21}}{y_{11} + y_{load}}. \tag{50}$$

Now let the two-port network be the field-effect tetrode, and let the load be a capacitor. The admittance of a capacitor having a leakage conductance G and a parasitic series resistance R_s can be written

$$y_c = \frac{G + G^2R_s + \omega^2C^2R_s + j\omega C}{1 + 2GR_s + G^2R_s^2 + \omega^2C^2R_s^2}. \tag{51}$$

This expression can be substituted into (49) and (50), and bulky expressions for effective Q and effective inductance can be obtained for each of the two configurations. These expressions are simplified, however, by considering the load to be a mica or other high-quality capacitor having a negligible series resistance.

For the leakage conductance of a mica capacitor in the range 10^2 to 10^7 cps we can write

$$G < \frac{\omega C}{10^3}. \tag{52}$$

This equation states that the Q of the capacitor is above 1000. The calculations are further simplified by assuming the Q to be equal to 1000 over the stated frequency range, for then

$$y_c = \omega C(10^{-3} + j). \tag{53}$$

To develop a specific example, let us select these first-quadrant biases:

$$V_1 = 0.75W_P$$
$$V_3 = 0.65W_P. \tag{54}$$

These values cause y_{11} in (49) to vanish. Making use of (53), it can be written

$$y_{in1} = -\frac{y_{12}y_{21}\left(y_{22} + \frac{\omega C}{10^3} - j\omega C\right)}{\left(y_{22} + \frac{\omega C}{10^3}\right)^2 + \omega^2C^2}. \tag{55}$$

Let us call this Case 1. For this case, the Q of the inductor is evidently

$$Q_1 = \frac{1}{10^{-3} + \frac{y_{22}}{\omega C}}, \tag{56}$$

and the inductance is

$$L_1 = -\frac{C}{y_{12}y_{21}}. \tag{57}$$

In a similar way we can write for Case 2, where the load admittance is on side 1,

$$y_{in2} = y_{22} - \frac{y_{12}y_{21}}{\omega C(10^{-3} + j)}. \tag{58}$$

Therefore,

$$Q_2 = \frac{1}{10^{-3} - \frac{\omega C y_{22}}{y_{12}y_{21}}}, \tag{59}$$

and

$$L_2 = -\frac{C}{y_{12}y_{21} - \frac{2y_{22}\omega C}{10^3} + \frac{y_{22}^2\omega^2C^2}{y_{12}y_{21}}}. \tag{60}$$

Eqs. (56), (57), (59), and (60) are plotted in Fig. 8. For purposes of this example, a value of 10^{-3} mho was chosen for G_1, the conductance of channel 1 with no voltage across the junction, and the value $\frac{1}{3}$ was taken for μ_2/μ_1. Thus it was possible to evaluate the admittances.

Fig. 8 shows Q and L vs frequency for three values of load capacitance. Multiple scales, labeled according to capacitance, are used for frequency and inductance. Evidently Case 1 is appropriate for high frequencies and Case 2 for low. It is implicit in (56) and (59) that the frequency for which the Q's are equal is given by

$$\omega = \frac{\sqrt{-y_{12}y_{21}}}{C}. \tag{61}$$

The value of Q at this frequency is given by

$$Q = \frac{\sqrt{-y_{12}y_{21}}}{y_{22}}, \tag{62}$$

and in this particular example its value is 0.86.

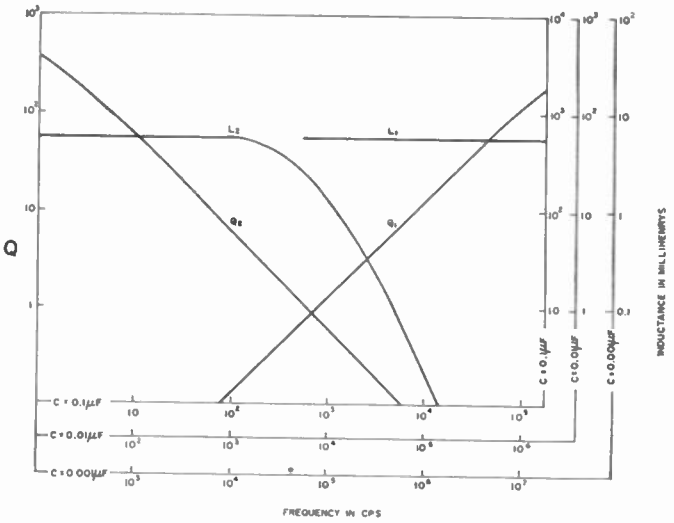

Fig. 8—Inductance and Q of field-effect gyrator with a capacitor load.

D. Experimental Results, Inductor

Because the self-admittance of a tetrode can be negative (Fig. 7), the bias arrangements must be made carefully to insure stable operation. This problem can be clarified by looking at tetrode input properties in terms of static current-voltage characteristics.

Let one of the independent biases be fixed, such as V_3 in Fig. 5, and then observe the dependence of I_1 on V_1. Let V_2 and V_4 be set equal to zero once more, but let V_1 and V_3 be made positive. Fig. 9 shows a family of I_1 vs V_1 characteristics, plotted from (38) for this case of first-quadrant bias. Note that voltage-controlled negative resistance (or "short-circuit-stable" negative resistance) is exhibited throughout the permissible bias range for all but one of the curves shown. The insert shows experimental confirmation of this behavior.[5]

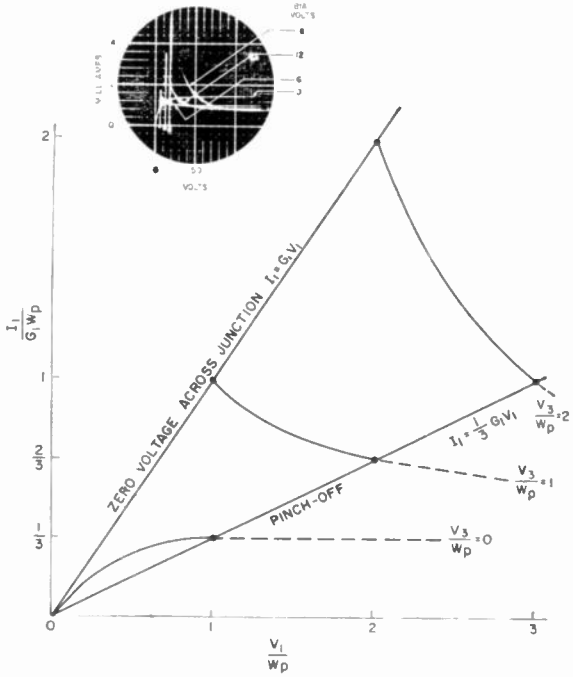

Fig. 9—Effect of biases on input characteristics.

The slope at any point of a curve in Fig. 9 is, of course, defined as y_{11} at that bias. The loci of bias points traversed in tracing out these curves are plotted as heavy lines in Fig. 7. Note that the lowest curve of Fig. 9, which shows positive slope, falls within the zone of Fig. 7 for which $y_{11}>0$, while the curves exhibiting negative slope fall outside it. The other self-admittance, y_{22}, is positive throughout the first quadrant.

A limited amount of experimental evidence indicates that negative input admittances will not occur at a given port if the channel on the opposite side is caused to pinch-off first by a thickness reduction through etching or some other means. For positive or first-quadrant biases where y_{11} is negative when W_{1P} is equal to or slightly less than W_{2P}, the experimental evidence suggests that y_{11} will be made positive by reducing W_{2P} to a value less than W_{1P}. A complementary statement applies to third-quadrant biases. Possibly this is related to the fact that the "current-limiter" characteristic of a given channel can be degraded by reducing the thickness of the opposite channel until it has a lower pinch-off voltage, because the pattern of available charges in the "gate" is altered by such a change in the thickness of the gate region.

[5] The nearly vertical regions in the trace are not significant, since here the junction is forward biased and as a result the current in channel 1 (I_1) and the current *to* terminal 1 are no longer the same. It is the latter current which is being recorded. It changes very rapidly with V_1 and can even be negative for small V_1 because V_3 then drives current backward through the V_1 supply.

Experimental results indicate an advantage insofar as Q is concerned in biasing to obtain negative self-admittance. The tetrode for which the following data are reported exhibited this property in the first quadrant, and our measurements are restricted to this condition. Furthermore, frequency limitations in our bridge and exploratory circuit confined us to Case 2, or low-frequency measurements. In this configuration, the port of negative or potentially negative self-admittance faces the capacitor. Hence, the bias supply on the side of the capacitative load is most critical from the point of view of stable operation. As is well known, stable operation in a voltage-controlled negative-resistance region requires a source resistance (or load resistance) R less than the magnitude of the negative resistance at the point in question. Fig. 10 shows that such a value of R is necessary to achieve a single intersection of the I-V characteristic by the load line. In the Case 2 configuration, R is in shunt with the capacitor, lowering the Q of the reactance which the tetrode is to invert.

In the experimental reconciliation of these conflicting requirements, large R for efficiency and small R for stability, low Q inductances were the result. The Q values were at most of the order of unity.

Study of Fig. 10 suggests that one could move the operating point to the right, thus avoiding the most steeply descending portion of the I_1V_1 characteristic and permitting a larger R. This amounts to increasing V_1-V_3. But another consideration imposes limitations here: Eq. (59) shows that Q_2 is favored by a large value of $y_{12}y_{21}/y_{22}$. From (41), (42) and (43),

$$\frac{y_{12}y_{21}}{y_{22}} = -\frac{G_1V_1V_3}{3\sqrt{W_P(V_1-V_3)}\left[3\sqrt{W_P(V_1-V_3)}-(2V_1-3V_3)\right]}. \tag{63}$$

Thus Q_2 is enhanced by small V_1-V_3. The transfer admittances (or transconductances) y_{12} and y_{21} are a maximum for zero voltage across the junction for the same reason that transconductance in a field-effect transistor is a maximum for zero gate bias. The rate of change of depletion-layer thickness with respect to voltage is greatest near zero voltage. Experimentally we were limited to values of V_1-V_3 less than 4 volts to have usably high transconductances.

Eq. (63) shows that G_1 should be increased to enhance $y_{12}y_{21}/y_{22}$ and, therefore, Q_2 for a given W_P and a given set of biases. This can be accomplished by increasing Z/L, which increases G_1 without affecting W_P. Therefore, the ideal tetrode for low frequency or Case 2 operation should be a "high-Z/L" device. Note in (56), however, that the high-frequency quality factor Q is favored by small y_{22}, and hence small G_1. Thus, our relatively low-conductance devices ($G_1=100$–500 μmho) might have performed better in Case 1 operation.

Four tetrodes were used in these experiments but only two gave measurable inductance. One did so with first-quadrant biasing and the other with third-quadrant biasing. The former gave the best results and some of these only are reported. It is unfortunate that the most symmetrical tetrodes were damaged in handling before this phase of the work.

All of the exploratory inductance measurements reported here were made with a Maxwell bridge having a superimposed dc feature which supplied one of the two tetrode biases. Results were obtained in terms of equivalent series inductance and resistance. The bridge, a rather elaborate one, exhibited good sensitivity down to Q values as low as 0.1.

Fig. 11 shows the circuit which, except for minor variations, was used for all of the following measurements. The transistor was used as a very high impedance or constant current source. It was shunted by a variable resistor in order to adjust to varying amounts of negative resistance in the I_1-V_1 characteristic and also to observe the effect on the inductor of changing capacitor Q.

Fig. 12(a) shows measured L_2 and Q_2 vs frequency for $C_L=1000$ $\mu\mu$f and $R=10^5$ ohms. For comparison, the Q of the capacitor combined with the shunting resistor is

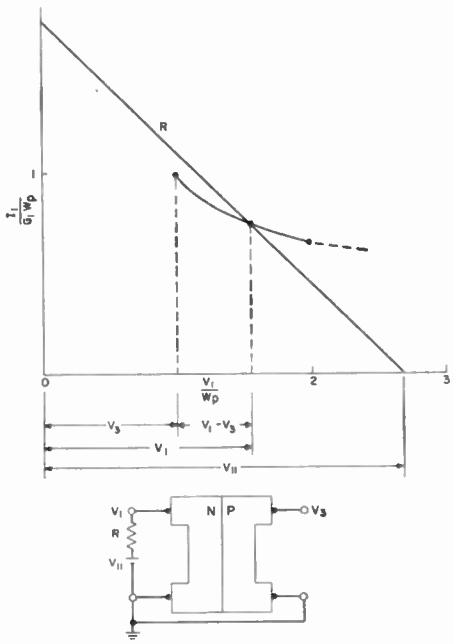

Fig. 10—Load line condition for field-effect tetrode terminated in resistance.

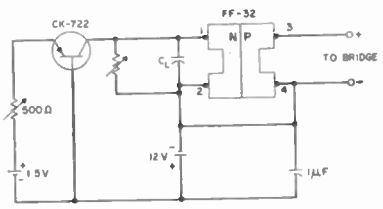

Fig. 11—Circuit used for impedance inversion with field-effect tetrodes.

also plotted. Evidently, this cuts down the Q of the inductor on the low-frequency side. Thus Q_2 peaks at about 12 kc. V_{ac} is the magnitude of the signal voltage applied to the bridge.

Similar data are plotted in Fig. 12(b) and 12(c) for $C_L = 3800$ $\mu\mu$f and for two values of R. Here Q_2 rises above unity but both peaks occur at lower frequencies.

Direct comparison with the simple theory is not possible because the two channels in this particular tetrode did not pinch-off simultaneously. But there is evident qualitative agreement between Figs. 8 and 12 with respect to the constant L_2 in the neighborhood of the Q_2 maximum, and the falling L_2 at higher frequencies.

The magnitude of inductor Q which has so far been obtained is much too low for practical application. However, the measurements have confirmed the expected nonreciprocity, and the analysis indicates that, with units having higher Z/L, improvements in Q may be expected.

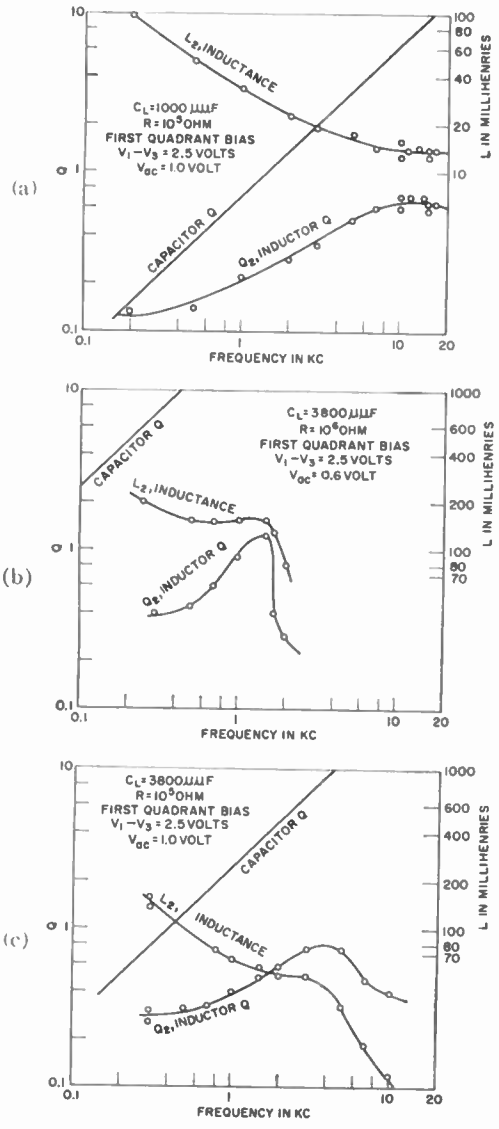

Fig. 12—Measured inductance and Q of field-effect tetrode terminated by (a) 1000 $\mu\mu$f, 10^5 ohms, (b) 3800 $\mu\mu$f, 10^6 ohms and (c) 3800 $\mu\mu$f, 10^5 ohms.

V. Isolator and Negative Impedance Inverter

When the field-effect tetrode is biased at a point on one of the axes in Fig. 7, and again assuming $V_2 = V_4 = 0$, one of the channels carries no current and hence there can be no output to a load on that side. Under such conditions the device is an "isolator," for it transmits signals in one direction but blocks signals in the other. Because the isolation so achieved can be made to face in either direction simply by choice of bias, the tetrode can be regarded as an isolation "switch." The field-effect transistor is, by comparison, a unidirectional isolator.

When biased at a point on the dotted line in the second quadrant of Fig. 7, a simultaneous pinch-off tetrode exhibits transfer admittances which have the same sign and are equal in magnitude. Thus it becomes a negative impedance inverter, and would, for example, convert a capacitative load into a negative inductance.

The situation depicted in Figs. 5 and 6 can be generalized by giving one of the common terminals a variable dc bias while holding it at ground with respect to ac. When a third dimension V_4/W_P is added to Fig. 6, the region of permissible bias expands into a rectangular prism and the condition $y_{12}/y_{21} > 0$ obtains within an inscribed tetrahedral volume of which the triangle in Fig. 6 is one face.

A common ac ground of diagonally opposite terminals yields a complementary situation. If terminals 2 and 3 are so connected, for example, the condition $y_{12}/y_{21} > 0$ holds in those regions of the prism of permissible biases lying outside the tetrahedron mentioned above. With this arrangement, the depletion layer is free to fluctuate at both ends, while in the situation shown in Fig. 5 it can vary only at one end. To this degree, at least, the two situations are not strictly complementary. The case of depletion-layer variations at both ends has not been treated exhaustively, but it may hold some interest because of its greater flexibility.

VI. Electronically Variable Resistor

The unique qualities of the field-effect tetrode in this application can be appreciated by first considering a field-effect triode[2] in the same application. If the triode is connected as shown in Fig. 13(a), it can indeed be used as an electronically variable resistor. Control voltage V_g alters the resistance of the channel. However, signal voltage applied to this resistor also modulates the depletion layer and hence the resistance of the channel. For quasi-linear operation, therefore, the signal voltage must be kept small compared to the pinch-off voltage of the device. Further, a frequency limitation exists because the junction capacitance shunts the signal to ground.

Fig. 13(b) illustrates the principle involved in using a field-effect tetrode as an electronically variable resistor. The bias voltage V_b establishes a uniform deple-

tion layer through the junction region. A capacitor C, whose reactance is small compared to channel resistance at the frequency of the signal voltage V_s, insures that the signal voltage will not appear to any significant degree across the junction. Therefore, signal voltage can exceed bias voltage, pinch-off voltage, and even junction breakdown voltage. Limits on signal are set by dissipation considerations. To an excellent approximation the full signal voltage is applied from end-to-end on the two channels in parallel, and signal currents flow in inverse ratio to the channel resistances.

Because signal modulation of the depletion layer is thus eliminated, the tetrode can be used as a variable resistor for very high-frequency signals.

Fig. 14 shows a practical circuit which includes a load resistance R_L. The resistor R_s has a value, small compared with the resistance of the junction, with which it is in series, but large enough for isolation purposes. In this circuit, V_b can be a dc bias, as before, or it can be a low-frequency ac voltage which modulates the signal from V_s. Thus the tetrode can function as a nondistorting modulator. In this case, the capacitors C must be chosen for small reactance at the frequency of V_s and large reactance at the frequency of V_b. They and the junction capacitance limit the bias frequency.

From such a modulator it is a short step to an amplifier wherein V_s is a "pump" source driving large amounts of power into R_L in the form of a signal which is modulated by the low power signal V_b.

For analysis of the configuration shown in Fig. 14, we observe the following voltages at the terminals of the device:

$$V_1 = V_b + V_s$$
$$V_2 = V_b + V_0$$
$$V_3 = V_s$$
$$V_4 = V_0.$$

Putting these values in (17) and (18), the total current is

$$I = I_1 + I_2 = (G_1 + G_2)(V_s - V_0)\left(1 - \sqrt{\frac{V_b}{W_P}}\right). \quad (64)$$

The effective resistance of the tetrode to the signal voltage is

$$R = \frac{V_s - V_0}{I} = \frac{1}{(G_1 + G_2)\left(1 - \sqrt{\frac{V_b}{W_P}}\right)}. \quad (65)$$

Normalized in terms of the resistance for zero bias, this becomes

$$\frac{R}{R_0} = \frac{1}{1 - \sqrt{\frac{V_b}{W_P}}}. \quad (66)$$

This characteristic is plotted in Fig. 15.

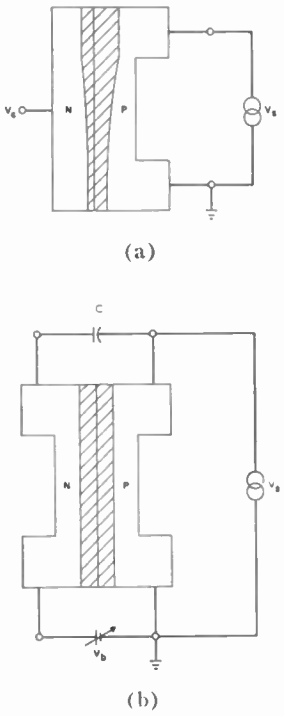

Fig. 13—Principle of (a) field-effect transistor and (b) field-effect tetrode as electronically variable resistor.

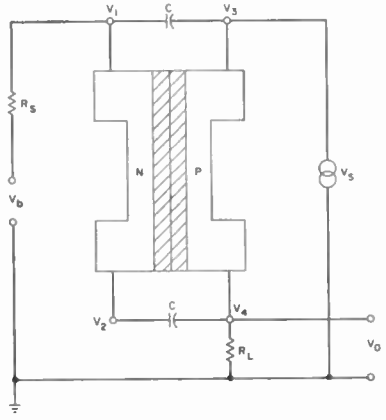

Fig. 14—Laboratory circuit for using field-effect tetrode as electronically variable resistor.

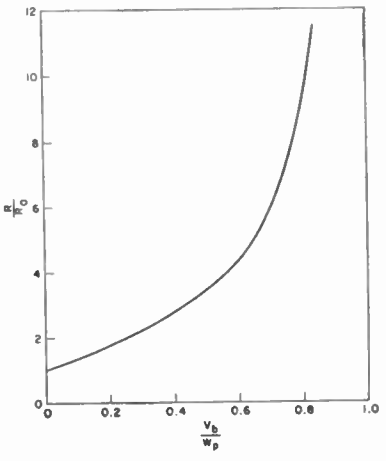

Fig. 15—Resistance vs bias for field-effect tetrode as electronically variable resistor.

Unsymmetrical tetrodes can also be used as electronically variable resistors. But if one of the channels has appreciable conductance when the other is pinched off, then the "tuning range" or maximum R/R_0 is limited. The models available when experiments were done on this mode of operation were quite unsymmetrical, and the range of controlled resistance variation was about 2.5 to 1.

VII. Structure and Fabrication

Fig. 16 shows the structure of the exploratory field-effect tetrode. A sectioned view is presented to show more clearly the relationship between the schematic structure considered above and the geometry of an actual device. A circular shape was chosen to achieve reasonable mechanical strength in spite of the thin web which constitutes the channel region. To make this web as thick as possible, high resistivity-starting material and a deep low-gradient junction were employed.

Steps in fabricating such a field-effect tetrode can be outlined as follows: Starting with a 0.020-inch slice of 100-ohm-cm P-type silicon, phosphorus is diffused into the surface to produce an N layer 0.004 inch thick. One side of the slice is lapped reducing the slice thickness to 0.008-inch, thus producing a slice with a junction at its median plane. A light boron diffusion is performed on the P side to cut down contact and spreading resistance in the final device. The slice is gold plated heavily on both sides, and disks 0.100 inch in diameter are cut out using an ultrasonic tool. Opposed circular trenches are then cut on the two sides of the disk using either another ultrasonic tool or a rotating tube (*i.e.*, by trepanning). An abrasive must be used in either case. The mean diameter of a trench is typically 0.060 inch and its L dimension (outside-minus-inside radius) is about 0.005 inch.

If sufficiently fine abrasives are used, it is possible to finish the surface of the trench without etching. Otherwise, light etching is necessary to remove damaged material. Etching can also be used, of course, to make fine reductions in channel thickness in order to adjust channel resistance. In practice, it has always been necessary thus far to make final adjustments in channel thickness on a cut-and-try basis, using electrical characteristics of the device as criteria. These final adjustments in channel thickness have been made successfully both by etching and by polishing alone, using the trepanning method. Final channel thicknesses are typically 0.0007 inch for the P side and 0.0003 inch for the N side.

In fabricating field-effect tetrodes it is often helpful to compare the channels by testing each one in turn as a current-limiter channel.[6] From (17) and (18) it can be shown that when simultaneous pinch-off has been achieved, the "pinch-off currents" of the two channels will stand in the ratio of the mobilities. This has been confirmed experimentally. However, a rather high degree of precision in channel shaping and placement is necessary to demonstrate this behavior. If a good current-limiter characteristic is achieved on side 1, and side 2 is subsequently cut a little too deeply, the characteristic of side 1 will be degraded, as mentioned in Section IV-D. Fortunately, unsymmetrical as well as symmetrical devices exhibit the unique tetrode properties, though in lesser degree.

Finally, leads are attached to the four isolated gold-plated regions of the disk and are welded to the header leads. Fig. 17 shows a completed tetrode. The leads in this case are 0.003-inch gold on the outer rim and 0.015-inch gold at the center, all attached by thermocompression bonding.

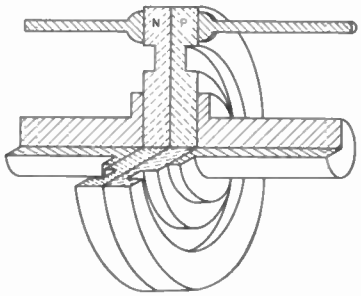

Fig. 16—Circular geometry of the field-effect tetrode.

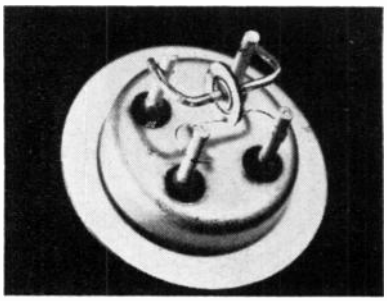

Fig. 17—Field-effect tetrode mounted on header.

Appendix I

The Space-Charge Depth on Either Side of Junction Formed by Uniformly but Unequally Doped Regions

Fig. 18 shows schematically a junction between an N region with uniform donor density N and a P region with uniform acceptor density P. A voltage V is applied across the junction and this gives rise to a space-charge layer of thickness t_1 in the N region and t_2 in the P region. We wish to find t_1 as a function of the impurity densities and the applied voltage.

In the N region, Poisson's equation is

$$\frac{d^2\Psi}{dx^2} = -\frac{qN}{\kappa\epsilon_0}. \tag{67}$$

[6] R. M. Warner, Jr., W. H. Jackson, E. I. Doucette, and H. A. Stone, Jr., "A semiconductor current limiter," Proc. IRE, vol. 47, pp. 44–56; January, 1959.

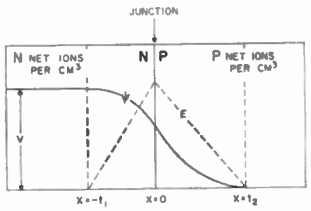

Fig. 18—Potential and field within uniformly but unequally doped regions in a semiconductor.

For the P side, it is

$$\frac{d^2\Psi}{dx^2} = -\frac{(-q)P}{K\epsilon_0}. \tag{68}$$

Integrating:

$$\frac{d\Psi}{dx} = -\frac{qN}{K\epsilon_0}(x + C_1) \tag{69}$$

$$\frac{d\Psi}{dx} = \frac{qP}{K\epsilon_0}(x + C_2). \tag{70}$$

When $x = -t_1$, that is, at the depletion-layer boundary in the N region, $d\Psi/dx = 0$. Therefore $C_1 = t_1$. Also, when $x = t_2$, $d\Psi/dx = 0$, so $C_2 = -t_2$.

Therefore,

$$\frac{d\Psi}{dx} = -\frac{qN}{K\epsilon_0}(x + t_1) \tag{71}$$

$$\frac{d\Psi}{dx} = \frac{qP}{K\epsilon_0}(x - t_2). \tag{72}$$

Both equations are valid when $x = 0$. Thus we can derive

$$\frac{t_1}{t_2} = \frac{P}{N}. \tag{73}$$

Integrating again:

$$\Psi = -\frac{qN}{K\epsilon_0}\left(\frac{x^2}{2} + t_1x + C_{11}\right) \tag{74}$$

$$\Psi = \frac{qP}{K\epsilon_0}\left(\frac{x^2}{2} - t_2x + C_{22}\right). \tag{75}$$

On the N side where $x = -t_1$, $\Psi = V$. Therefore,

$$C_{11} = \frac{K\epsilon_0 V}{qN} + \frac{t_1^2}{2}.$$

On the P side where $x = t_2$, $\Psi = 0$. Therefore,

$$C_{22} = \frac{t_2^2}{2}.$$

So (74) and (75) become

$$\Psi = V - \frac{qN}{K\epsilon_0}\left(\frac{x^2}{2} + t_1x + \frac{t_1^2}{2}\right) \tag{76}$$

$$\Psi = \frac{qP}{K\epsilon_0}\left(\frac{x^2}{2} - t_2x + \frac{t_2^2}{2}\right). \tag{77}$$

When $x = 0$, both equations are valid and

$$\Psi_0 = V - \frac{qNt_1^2}{2K\epsilon_0} = \frac{qPt_2^2}{2K\epsilon_0}. \tag{78}$$

But, from (71)

$$t_2 = \frac{N}{P}t_1.$$

So

$$t_1^2 = \frac{2K\epsilon_0}{q}\frac{N}{P}\frac{V}{N+P} \tag{79}$$

and

$$t_2^2 = \frac{2K\epsilon_0}{q}\frac{N}{P}\frac{V}{N+P}. \tag{80}$$

Substituting (79) in (78), the potential at the junction is seen to be

$$\Psi_0 = \frac{N}{N+P}V. \tag{81}$$

Appendix II

Unrestricted Current-Voltage Equations

Eqs. (17) and (18) are valid only if the pinch-off voltages in the two channels are exactly equal. In this appendix, current-voltage equations are derived without any restrictions on the relative magnitudes of the pinch-off voltages. Approximate solutions are then derived for the case where the pinch-off voltages are nearly equal. The simplifying assumptions outlined in Section II apply here also.

In view of (1)–(4), the differential equations (11) and (12) may be written

$$I_1 = -G_1L\left(1 - \sqrt{\frac{v_1 - v_2}{W_{1P}}}\right)\frac{dv_1}{dx} \tag{82}$$

$$I_2 = -G_2L\left(1 - \sqrt{\frac{v_1 - v_2}{W_{2P}}}\right)\frac{dv_2}{dx}. \tag{83}$$

or

$$\alpha_1 = (\mu - \beta_1)\frac{dv_1}{dx} \tag{84}$$

$$\alpha_2 = (\mu - \beta_2)\frac{dv_2}{dx}. \tag{85}$$

where

$$\alpha_i = \frac{I_i\beta_i}{G_iL} \tag{86}$$

$$\beta_i = \sqrt{W_{iP}} \tag{87}$$

$$\mu = \sqrt{v_1 - v_2}. \tag{88}$$

For the first solution,

$$(\alpha_1 - \alpha_2)\int_0^L dx = 2\int_{\sqrt{V_2 - V_4}}^{\sqrt{V_1 - V_3}} u^2 d\mu - \beta_1 \int_{V_3}^{V_2} dv_1 + \beta_2 \int_{V_3}^{V_1} dv_2 \tag{89}$$

$$(\alpha_1 - \alpha_2)L = \beta_1(V_1 - V_2) - \beta_2(V_3 - V_4) - \frac{2}{3}\left[(V_1 - V_3)^{3/2} - (V_2 - V_4)^{3/2}\right]. \tag{90}$$

The second solution is obtained from (84) and (85) as follows:

$$\frac{dv_1}{dx} - \frac{dv_2}{dx} = 2\mu\frac{d\mu}{dx} = \frac{\alpha_1}{\mu - \beta_1} - \frac{\alpha_2}{\mu - \beta_2} \tag{91}$$

$$(\alpha_1 - \alpha_2)dx = 2\frac{\mu^3 - (\beta_1 + \beta_2)\mu^2 + \beta_1\beta_2\mu}{\mu - \gamma}d\mu, \tag{92}$$

where

$$\gamma \equiv \frac{\alpha_1\beta_2 - \alpha_2\beta_1}{\alpha_1 - \alpha_2}. \tag{93}$$

Eq. (92) reduces to

$$(\alpha_1 - \alpha_2)dx = 2\left\{\mu^2 + \left[\gamma - (\beta_1 + \beta_2)\right]\mu + \left[(\gamma - \beta_1)(\gamma - \beta_2)\right] + \frac{\gamma(\gamma - \beta_1)(\gamma - \beta_2)}{\mu - \gamma}\right\}d\mu. \tag{94}$$

Integrating along the length of the channel

$$(\alpha_1 - \alpha_2)L = -\frac{2}{3}\left[(V_1 - V_3)^{3/2} - (V_2 - V_4)^{3/2}\right] - \left[\gamma - (\beta_1 + \beta_2)\right]\left[(V_1 - V_3) - (V_2 - V_4)\right] - 2\left[(\gamma - \beta_1)(\gamma - \beta_2)\right]\left[\sqrt{V_1 - V_2} - \sqrt{V_2 - V_4}\right] - 2\gamma\left[(\gamma - \beta_1)(\gamma - \beta_2)\right]\ln\frac{\sqrt{V_1 - V_3} - \gamma}{\sqrt{V_2 - V_4} - \gamma}. \tag{95}$$

The appearance of (95) can be improved by subtracting it from (90) and putting in the value for γ. It becomes

$$\frac{(\alpha_1 - \alpha_2)^2}{\beta_1 - \beta_2}\left[\frac{V_1 - V_2}{\alpha_1} - \frac{V_3 - V_4}{\alpha_2}\right] - 2(\alpha_1 - \alpha_2)\left[\sqrt{V_1 - V_3} - \sqrt{V_2 - V_4}\right] - 2(\alpha_1\beta_2 - \alpha_2\beta_1)\ln\frac{(\alpha_1 - \alpha_2)\sqrt{V_1 - V_3} - (\alpha_1\beta_2 - \alpha_2\beta_1)}{(\alpha_1 - \alpha_2)\sqrt{V_2 - V_4} - (\alpha_1\beta_2 - \alpha_2\beta_1)} = 0. \tag{96}$$

Eqs. (90) and (96) contain implicitly the solutions for α_1 and α_2 and thus for I_1 and I_2, in terms of the applied voltages. Because of the log term in (96), they are intractable except when restrictions are put on the pinch-off voltages.

If β_1 is nearly equal to β_2 (and if $\alpha_1 \neq \alpha_2$), the first term in (96) predominates and it becomes approximately

$$\frac{(\alpha_1 - \alpha_2)^2}{\beta_1 - \beta_2}\left[\frac{V_1 - V_2}{\alpha_1} - \frac{V_3 - V_4}{\alpha_2}\right] = 0 \tag{97}$$

$$\frac{V_1 - V_2}{\alpha_1} = \frac{V_3 - V_4}{\alpha_2}. \tag{98}$$

Solving (94) and (102) simultaneously

$$\alpha_1 = \frac{V_1 - V_2}{L}\left\{\frac{\beta_1(V_1 - V_2) - \beta_2(V_3 - V_4)}{(V_1 - V_2) - (V_3 - V_4)} - \frac{2}{3}\frac{(V_1 - V_3)^{3/2} - (V_2 - V_4)^{3/2}}{(V_1 - V_3) - (V_2 - V_4)}\right\}. \tag{99}$$

$$\alpha_2 = \frac{V_3 - V_4}{L}\left\{\frac{\beta_1(V_1 - V_2) - \beta_2(V_3 - V_4)}{(V_1 - V_2) - (V_3 - V_4)} - \frac{2}{3}\frac{(V_1 - V_3)^{3/2} - (V_2 - V_4)^{3/2}}{(V_1 - V_3) - (V_2 - V_4)}\right\} \tag{100}$$

or, from (86) and (87)

$$I_1 = G_1(V_1 - V_2)\left\{\frac{(V_1 - V_2) - \sqrt{\frac{W_{2P}}{W_{1P}}}(V_3 - V_4)}{(V_1 - V_2) - (V_3 - V_4)} - \frac{2}{3\sqrt{W_{1P}}}\frac{(V_1 - V_3)^{3/2} - (V_2 - V_4)^{3/2}}{(V_1 - V_3) - (V_2 - V_4)}\right\}. \tag{101}$$

$$I_2 = G_2(V_3 - V_4)\left\{\frac{\sqrt{\frac{W_{1P}}{W_{2P}}}(V_1 - V_2) - (V_3 - V_4)}{(V_1 - V_2) - (V_3 - V_4)} - \frac{2}{3\sqrt{W_{2P}}}\frac{(V_1 - V_3)^{3/2} - (V_2 - V_4)^{3/2}}{(V_1 - V_3) - (V_2 - V_4)}\right\}. \tag{102}$$

Since $W_{1P} \approx W_{2P}$, a further approximation can be made

$$I_1 = G_1(V_1 - V_2)\cdot\left\{1 - \frac{2}{3\sqrt{W_{1P}}}\frac{(V_1 - V_3)^{3/2} - (V_2 - V_4)^{3/2}}{(V_1 - V_3) - (V_2 - V_4)}\right\}. \tag{103}$$

$$I_2 = G_2(V_3 - V_4)\cdot\left\{1 - \frac{2}{3\sqrt{W_{2P}}}\frac{(V_1 - V_3)^{3/2} - (V_2 - V_4)^{3/2}}{(V_1 - V_3) - (V_2 - V_4)}\right\}. \tag{104}$$

Acknowledgment

The authors are indebted to E. F. O'Connell, Jr. for exploratory device fabrication, and to W. H. Jackson, J. M. Sipress, and W. J. Grubbs for assistance in the analysis.

An Experimental Study of Bistatic Scattering from Some Small, Absorber-Coated, Metal Shapes*

R. J. GARBACZ†, MEMBER, IRE, AND D. L. MOFFATT†, MEMBER, IRE

Summary—**Experimental data are presented on the bistatic scattering cross sections of some small metal bodies, uncoated and coated with a resonant, lossy layer. All of the targets—spheres, cylinders, and cones—are of a size to be in the resonant region at wavelengths of approximately 3 cm. All of the bodies indicate a similar trend—the coated bodies are effectively camouflaged in the back hemisphere, but not in the forward hemisphere. In the forward direction, the scattering cross sections of the coated bodies are at least as large as, or larger than, those of the uncoated bodies. The bistatic angles beyond which this enhancement is effective become smaller as the electrical size of the body decreases, *i.e.*, as frequency decreases.**

Introduction

THE purpose of this experimental study is to investigate the scattering characteristics of some simple shapes coated with a lossy, resonant material. Data are presented on the bistatic scattering cross sections of spheres, cylinders, and cones of the order of one to three wavelengths in circumference at X-band frequencies. In each case, scattering from the uncoated body and that from its coated counterpart are compared for both vertical and horizontal polarizations of the incident E field and scattered E field. (The term, "coated counterpart," will always mean the uncoated body simply coated by the constant thickness absorbing material.) The absorber used on all the bodies is a lossy, resonant type developed at the Naval Research Laboratory.[1] Fabrication techniques are given.[2] The permeability of this absorber is frequency-sensitive and so necessitates a change in composition with change in desired resonant (optimum absorption) frequency. For any given composition there is a critical layer thickness for resonance. Also, a given material which is resonant when coating a flat surface is generally not resonant at the same frequency when coating curved surfaces, which necessitates "custom fitting" the absorber to such curved surfaces if optimum performance is to be realized. The targets used for this report were borrowed from the Naval Research Laboratory and are the same ones discussed by Wright, *et al.*[1] They are coated with an absorber whose thickness and composition were determined by the Naval Research Laboratory for flat plate resonance at about $\lambda = 3.2$ cm, and whose relative constitutive constants are $\mu_2 \cong 1.5 + j1.5$ and $\epsilon_2 \cong 8 + j0.5$. The thickness of the coating is 0.077 inch. It should be evident from the above that the data presented here do not necessarily represent optimum performance of the absorber.

Results of the following tests will be found in this paper:

1) Scattering cross sections, for bistatic angles of 0° to 160°, of uncoated metal spheres 0.50 inch, 1.00 inch, and 1.587 inches in diameter, and their coated counterparts, were recorded at frequencies of 8.65 kMc, 9.375 kMc, and 10.00 kMc. In addition, uncoated metal spheres 0.25 inch, 0.40 inch, and 1.312 inches in diameter and their coated counterparts were recorded at 10.00 kMc. For each of these tests, vertical polarization of the E field was first transmitted and received, then horizontal polarization of the E field was transmitted and received. The receiver was separated from the transmitter by the bistatic angle β, measured in the horizontal plane.

2) Scattering cross sections, for bistatic angles of 0° to 160°, of uncoated metal rods 5 inches long and 0.155 inch, 0.200 inch, 0.310 inch, 0.400 inch, 0.470 inch, 0.620 inch, and 0.780 inch in diameter, and their coated counterparts (except that the ends were left uncoated), were recorded at 10.00 kMc. 180° azimuth patterns were taken at each bistatic angle by rotating the rods about a vertical axis normal to the longitudinal axes of the rods. Vertical polarization of the E field was first transmitted and received, then horizontal polarization of the E field was transmitted and received.

3) Scattering cross sections, for bistatic angles of 0° to 160°, of an uncoated metal right circular cone with a slant height of 2.86 inches and an apex angle of 38.5°[3] and its coated counterpart, were recorded at 9.375 kMc. Two sets of 180° azimuth patterns were taken, by rotating the cones about a vertical axis normal to and at 45° to the axis of symmetry of the cones. For each of these orientations, vertical polarization of the E field was first transmitted and received, then horizontal polarization of the E field was transmitted and received.

A brief description of the test equipment is included in the Appendix.

* Received by the IRE, November 7, 1960; revised manuscript received, April 3, 1961. This work was supported by Rome Air Dev. Ctr., Griffiss AFB, Rome, N. Y., under contract AF 30(602)-2042.

† Antenna Lab., Dept. of Elec. Engrg., The Ohio State University, Columbus, Ohio.

[1] R. W. Wright, W. H. Emerson, and D. H. Phillips, "Reflectivity of camouflaged small simple objects," *Proc. Second Annual RADC Internatl. RAM Symp.*, Rome Air Dev. Ctr., Griffiss AFB, Rome, N. Y., Secret, vol. 2, pp. 80–84, spheres; pp. 75–77, cylinders; pp. 78–80, cones; June, 1959.

[2] W. H. Emerson and M. V. McDowell, "Radar camouflage of warhead models," *Proc. Second Annual RADC Internatl. RAM Symp*, Rome Air Dev. Ctr., Griffiss AFB, Rome, N. Y., Secret, vol. 2, pp. 89–90; June, 1959.

[3] Wright, *et al.*, *op. cit.*, this is the cone designated "B," p. 78.

Experimental Results

A. Spheres

In order that there be no confusion about what data were taken, Fig. 1 sketches the geometry of the scattering patterns. The coordinate system used is the standard spherical one, with the E field of the incident wave directed in the x direction and propagating in the positive z direction. The H plane scattering patterns are those in which the scattered E field, which is polarized in the x direction, is detected by a receiver that moves in the y-z plane and is separated from the transmitter by a bistatic angle β. The E plane scattering patterns are those in which the scattered E field, which is polarized in the θ direction (θ is measured from the $+z$ axis as usual), is detected by a receiver that moves in the x-z plane and is separated from the transmitter by a bistatic angle β. In actual darkroom practice, the H plane patterns were taken with the transmitter and receiver polarizations, shown in Fig. 1, by moving the receiver in a horizontal (y-z) plane along a semicircular track built into the floor. Then, in order to record the E plane patterns and retain use of the track, the polarization of the incident E field was rotated 90° and the receiver antenna was rotated 90°. The targets were rotated by means of strings about a vertical axis, the azimuth or rotation angle being θ, and $\theta=0$ when the projection of the symmetry axis of the body onto a horizontal plane corresponded to the transmitter direction. The bistatic scattering cross sections of several sphere sizes at three frequencies are given in Figs. 2–4 (pp. 1186–1187). The broken lines represent the uncoated spheres, and the solid lines represent the coated spheres. On each polar plot, the left side gives data for vertical polarization of the transmitted and received E fields (called H-plane patterns), and the right side gives data for horizontal polarization of the transmitted and received E fields (called E-plane patterns). The radial coordinate represents the bistatic scattering cross section, σ, in db above or below one square wavelength and the angular coordinate represents the bistatic angle β.

Figs. 5–7 (p. 1188) are plots of the reduction or enhancement of the bistatic scattering cross sections due to the absorber coating.

Some remarks concerning the validity of the data should be made here. The scatter-measuring range used in these experiments was capable of "seeing" targets which were 26 db below a square wavelength within ±2 db. Returns below this level are correspondingly less accurate, and when they appear on the data they should be taken only as approximations. Thus, in some cases the backscatter ($\beta=0°$), which should be independent of incident polarization for spheres and which presents the lowest return levels to the measuring system, differs slightly for the two polarizations. This is a measure of the experimental accuracy at these levels. On the other hand, when the scattering cross sections are greater than 15 db below a square wavelength, the data are accurate within ±0.5 db. These limitations should be considered when looking at the echo enhancement and reduction curves. Fig. 8 is an example of the actual recorded data for a one-inch diameter sphere, uncoated and coated, at $f=8.65$ kMc, $\beta=40°$ and horizontal polarization. A record of the nulled background signal with no scatterer present is also given. The levels of the uncoated spheres were rarely in question, but those of the coated spheres were obtained by a visual averaging of the variations.

B. Cylinders

The bistatic scattering cross sections of seven 5-inch rods with uncoated diameters of 0.155 inch to 0.780 inch were measured at 10 kMc, coated and uncoated, for both polarizations. Fig. 9 shows typical azimuth patterns for the uncoated and coated bodies. Fig. 10 (p. 1189) is a plot of the scattering cross-section reduction or enhancement due to absorber coating for the broadside specular reflection; Fig. 11 gives the same information in a different manner. Note in these last figures that λ is a constant in the abscissa variable d/λ.

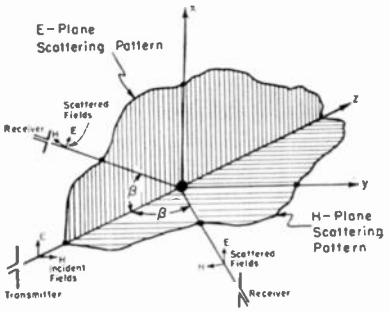

Fig. 1—The E-plane and H-plane scattering patterns, which lie, respectively, in the planes of the incident E vector and H vector. For convenience in the darkroom, instead of measuring the E-plane pattern in a plane normal to the floor as indicated in this diagram, the polarizations of the transmitter and receiver were rotated 90° and the E-plane pattern was measured in a plane parallel to the floor

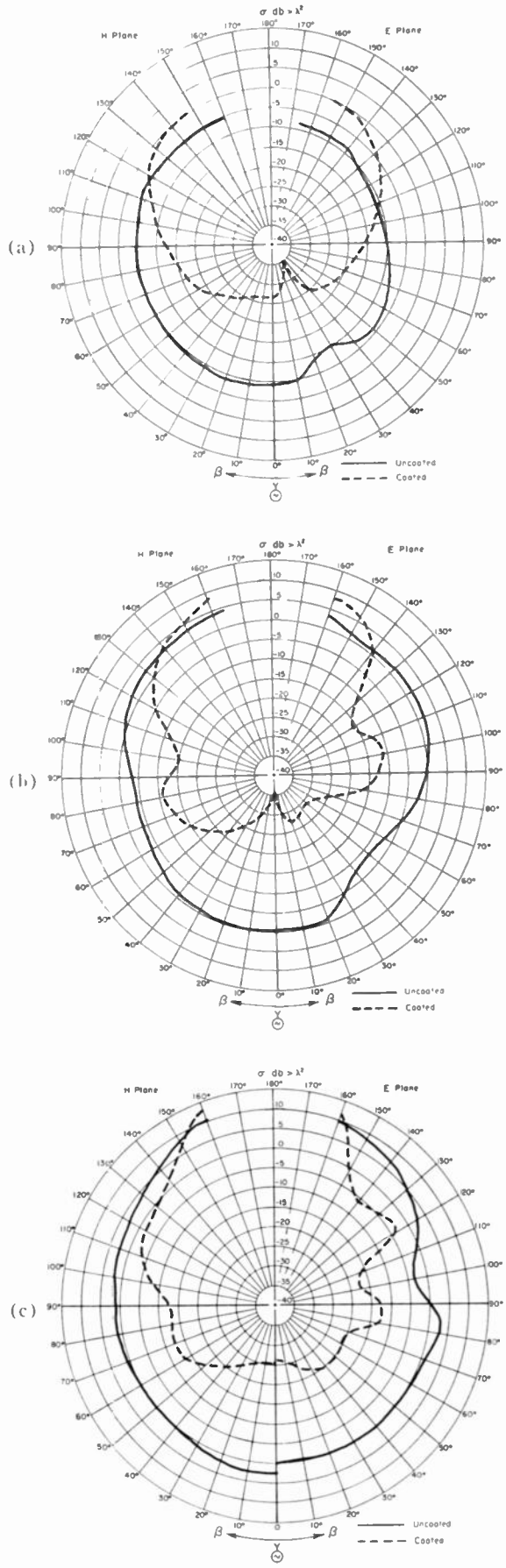

Fig. 2—Bistatic scattering cross sections of uncoated metal spheres and their coated counterparts, for vertical and horizontal polarizations of E field. $f=8.65$ kMc, $\lambda=3.47$ cm. The diameters refer to the metal core diameters. (a) 0.50-inch diameter. (b) 1.00-inch diameter. (c) 1.587-inch diameter.

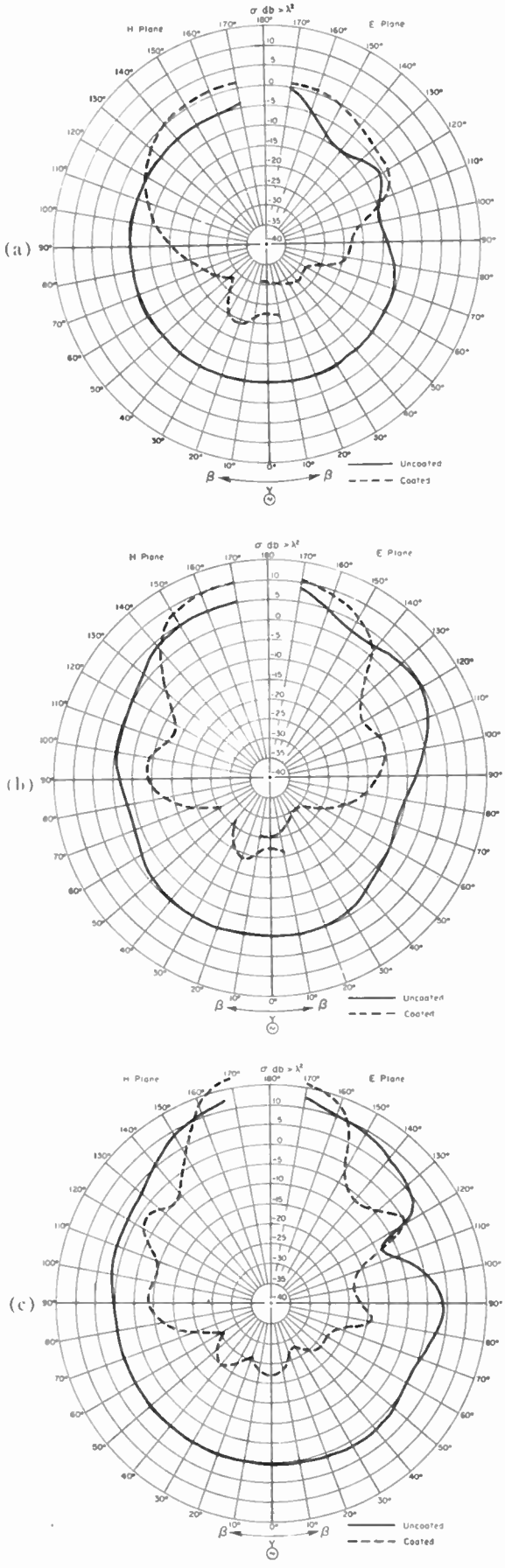

Fig. 3—Bistatic scattering cross sections of uncoated metal spheres and their coated counterparts, for vertical and horizontal polarizations of E field. $f=9.375$ kMc, $\lambda=3.2$ cm. The diameters refer to the metal core diameters. (a) 0.50-inch diameter. (b) 1.00-inch diameter. (c) 1.587-inch diameter.

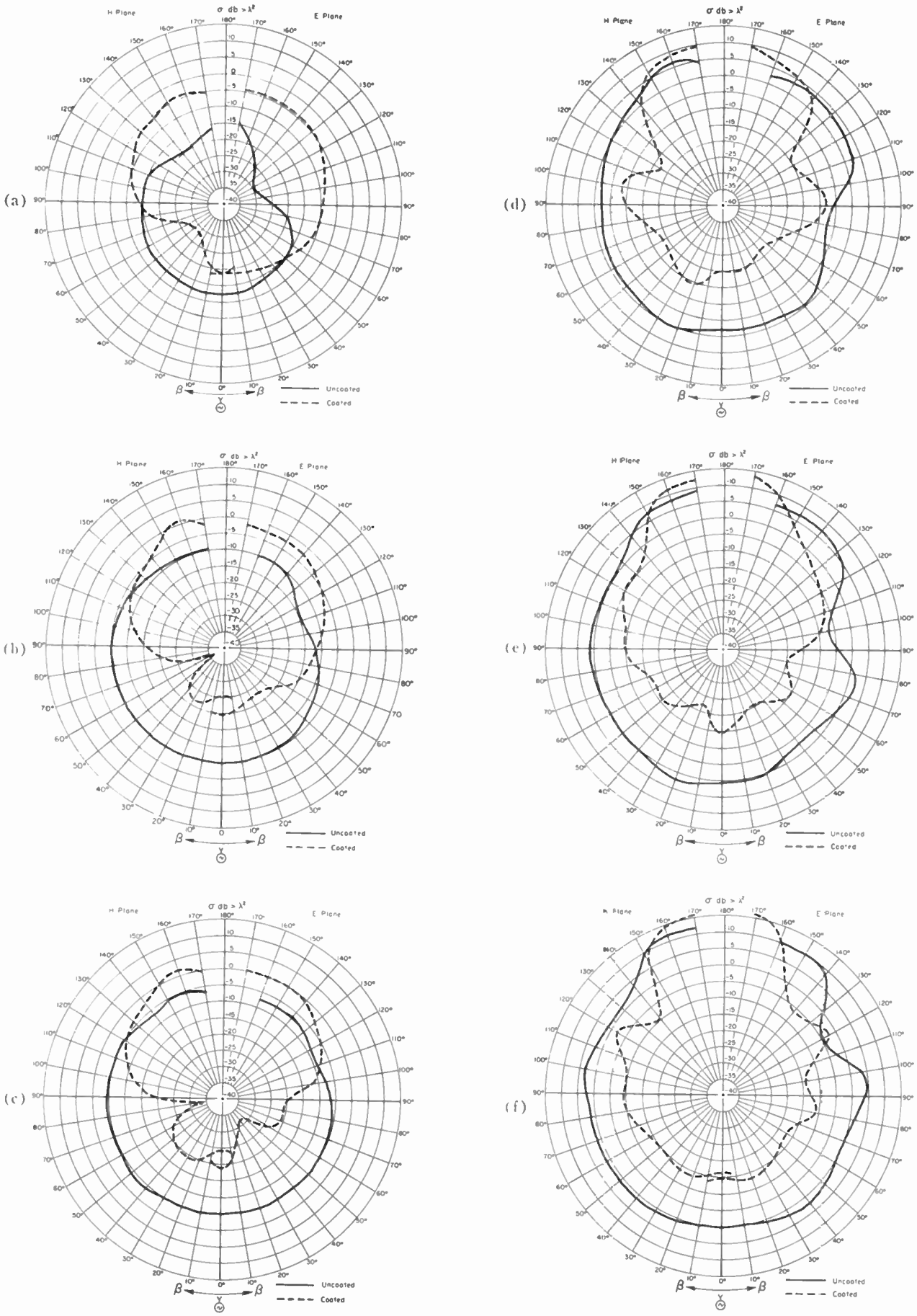

Fig. 4—Bistatic scattering cross sections of uncoated metal spheres and their coated counterparts, for vertical and horizontal polarizations of E field. $f = 10$ kMc, $\lambda = 3.0$ cm. The diameters refer to the metal core diameters. (a) 0.25-inch diameter. (b) 0.40-inch diameter. (c) 0.50-inch diameter. (d) 1.00-inch diameter. (e) 1.312-inch diameter. (f) 1.587-inch diameter.

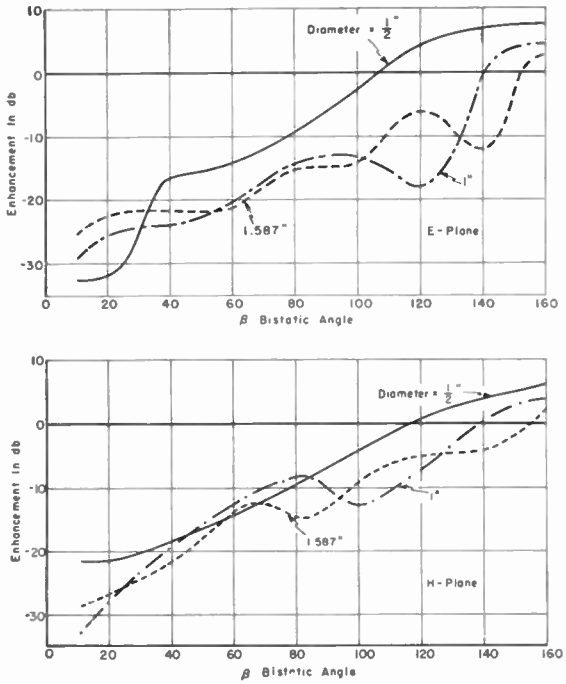

Fig. 5—Reduction or enhancement of the bistatic scattering cross sections of spheres due to absorber coating as a function of bistatic angle. $f = 8.65$ kMc, $\lambda = 3.47$ cm.

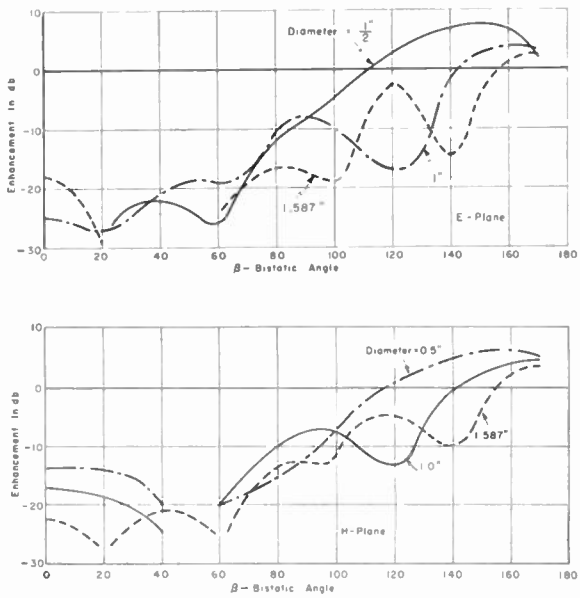

Fig. 6—Reduction or enhancement of the bistatic scattering cross sections of spheres due to absorber coating as a function of bistatic angle. $f = 9.375$ kMc, $\lambda = 3.2$ cm.

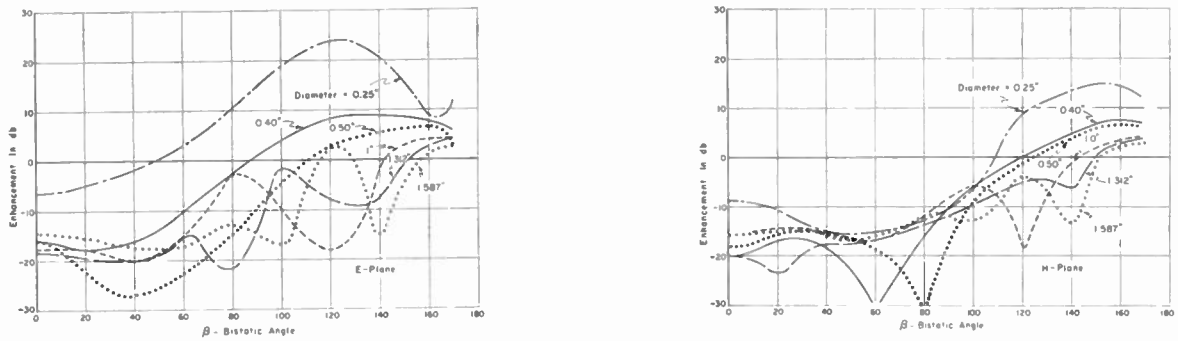

(a) (b)

Fig. 7—Reduction or enhancement of the bistatic scattering cross sections of spheres due to absorber coating as a function of bistatic angle. $f = 10$ kMc, $\lambda = 3.0$ cm.

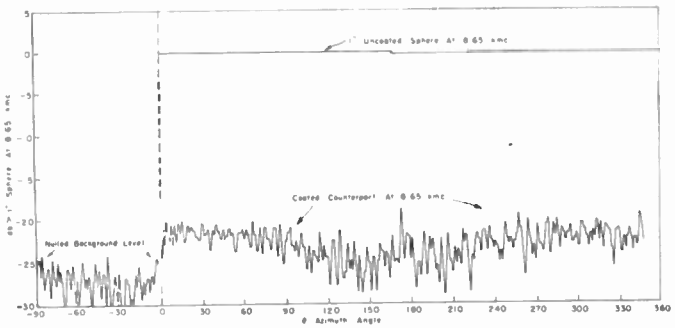

Fig. 8—An example of a data record for a 1.0-inch diameter uncoated sphere and its coated counterpart and nulled background level. $f = 8.65$ kMc, $\beta = 40°$, horizontal polarization.

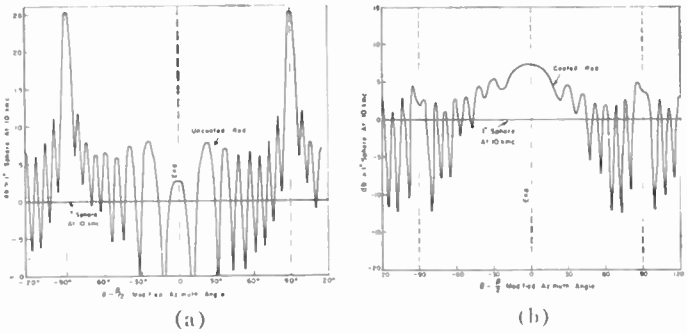

(a) (b)

Fig. 9—An example of a data record for an uncoated 0.400-inch diameter rod and its coated counterpart. $f = 10$ kMc, $\beta = 40°$ vertical polarization.

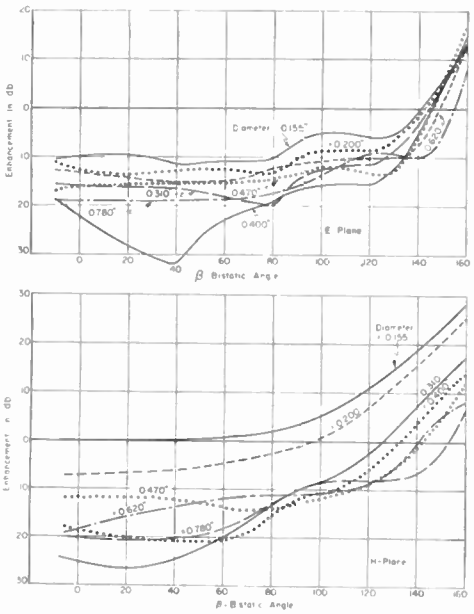

Fig. 10—Reduction or enhancement of the broadside specular reflection of rods due to absorber coating. Rod diameter is parameter. $f=10$ kMc, $\lambda=3$ cm.

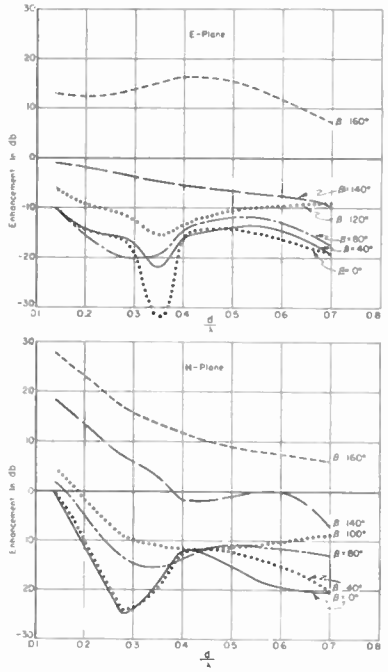

Fig. 11—Reduction or enhancement of the broadside specular reflection of rods due to absorber coating. Bistatic angle is parameter. $f=10$ kMc, $\lambda=3$ cm.

C. Cones

The bistatic scattering cross sections from a right circular cone with a slant height of 2.86 inches and an apex angle of 38.5°, and its coated counterpart, were recorded for both polarizations at 9.375 kMc. Two orientations were investigated, in which the body was rotated about a vertical axis with its axis of symmetry perpendicular to and at 45° to this vertical axis. For the interesting geometry of the cone, a more complete presentation of the data than just that of specular reflection is desirable, especially for comparison of the uncoated and coated cones. An array of azimuth patterns of scattering cross section, each for a different bistatic angle, is extremely cumbersome and cannot present an integrated picture of what is taking place. In this report the cone data are presented in the form of bistatic contour maps, in which equilevel contours of scattering cross section $\sigma(\theta, \beta)$ are plotted on rectangular coordinates of β, the bistatic angle, and $\theta-\beta/2$, the azimuth angle minus half the bistatic angle. Such maps are derived from the actual records, an example of which is shown in Fig. 12, by using discrete cross-section levels. Thus, some information is lost in the construction of the maps, but by choosing level increments and bistatic angle increments to suit the rates of change of σ with these variables, the important salient features can be shown accurately enough for the present comparison purposes.

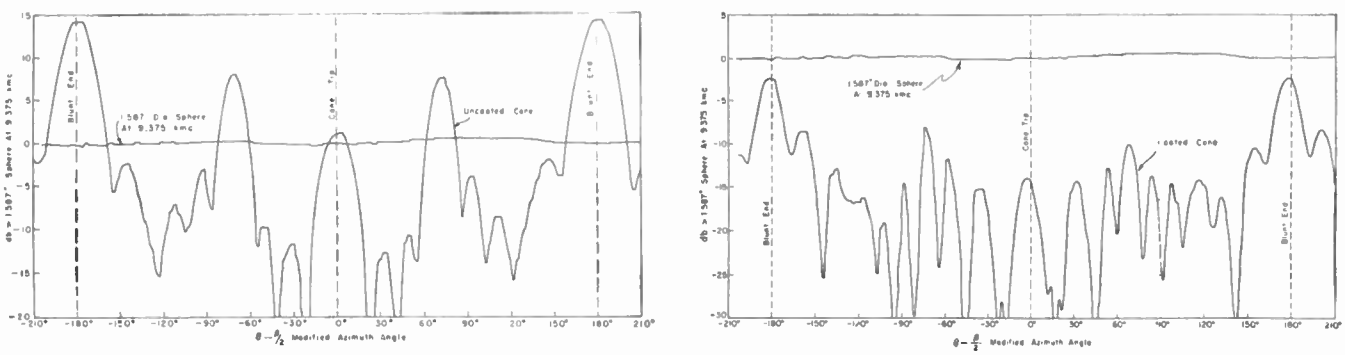

(a) (b)

Fig. 12—An example of a data record for an uncoated and coated cone. $f=9.375$ kMc, $\beta=40°$, vertical polarization.

Contour maps of the cones, rotated about a vertical axis with their axes of symmetry perpendicular to this axis of rotation, are shown in Figs. 13 and 14, uncoated and coated respectively for horizontal polarization of the transmitted and scattered E fields.

Corresponding maps for vertical polarization are shown in Figs. 15 and 16. Similar maps are drawn in Figs. 17–20 (opposite) for the cones rotated about a vertical axis with their axes of symmetry tilted 45° from this axis of rotation.

The effects of an absorber coating on the scattering from resonant-size cones are easily discernible from the bistatic contour maps shown in Figs. 13–20. However, since the contour mapping technique has not been used extensively in the literature, some of the more salient features of the maps will be pointed out.

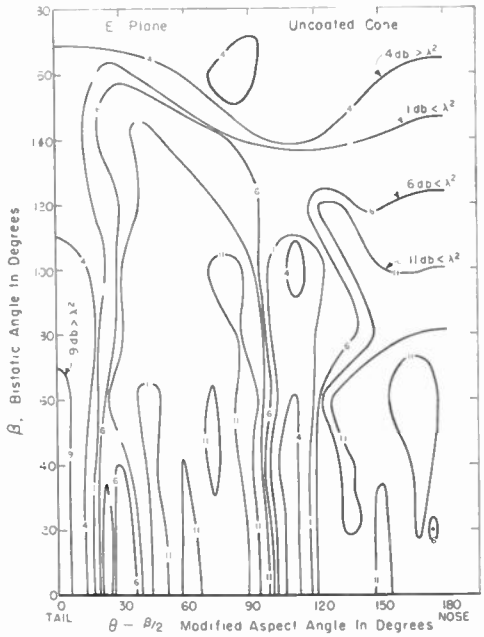

Fig. 13—Contour map for uncoated cone rotated with its longitudinal axis perpendicular to the vertical axis of rotation, horizontal polarization of E field, $f=9.375$ kMc, $\lambda=3.2$ cm.

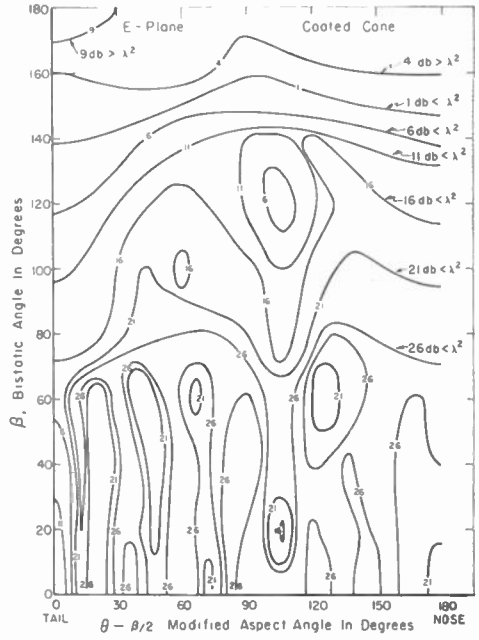

Fig. 14—Contour map for coated cone rotated with its longitudinal axis perpendicular to the vertical axis of rotation, horizontal polarization of E field, $f=9.375$ kMc, $\lambda=3.2$ cm.

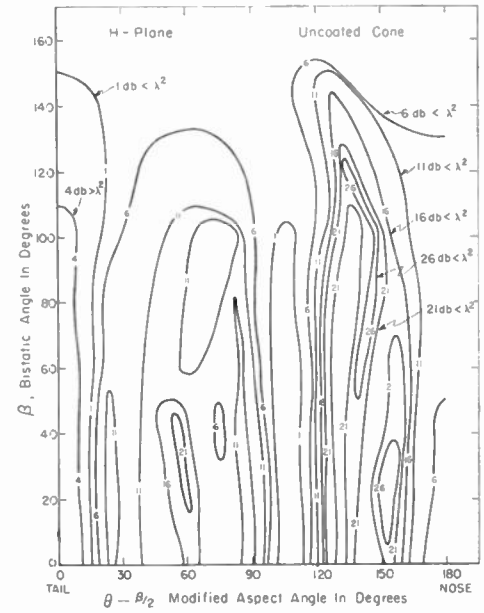

Fig. 15—Contour map for uncoated cone rotated with its longitudinal axis perpendicular to the vertical axis of rotation, vertical polarization of E field, $f=9.375$ kMc, $\lambda=3.2$ cm.

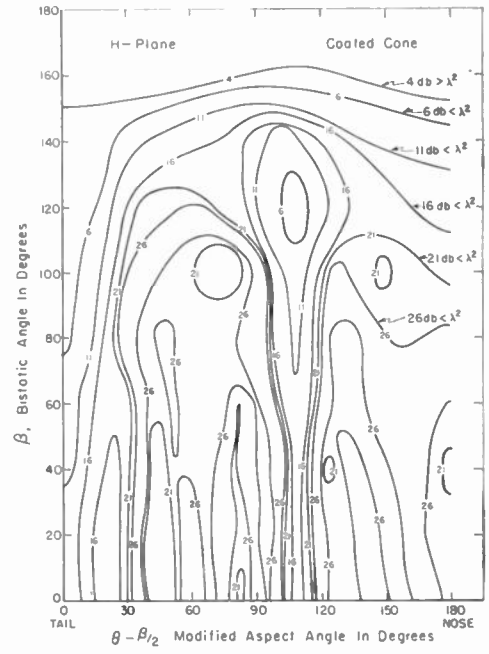

Fig. 16—Contour map for coated cone rotated with its longitudinal axis perpendicular to the vertical axis of rotation, vertical polarization of E field, $f=9.375$ kMc, $\lambda=3.2$ cm.

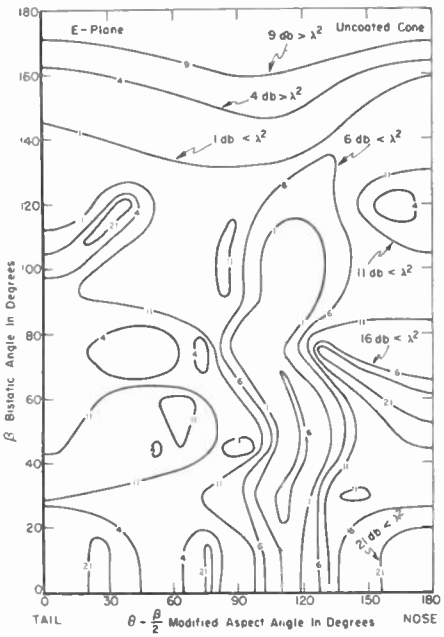

Fig. 17—Contour map for uncoated cone rotated with its longitudinal axis tilted 45° from the vertical axis of rotation, horizontal polarization of E field, $f=9.375$ kMc, $\lambda=3.2$ cm.

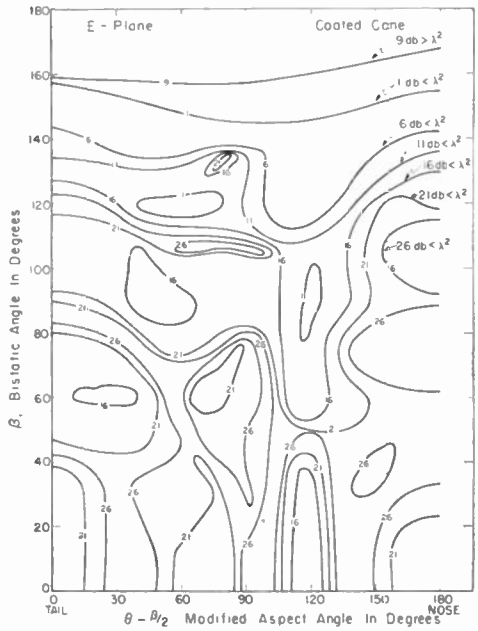

Fig. 18—Contour map for coated cone rotated with its longitudinal axis tilted 45° from the vertical axis of rotation, horizontal polarization of E field, $f=9.375$ kMc, $\lambda=3.2$ cm.

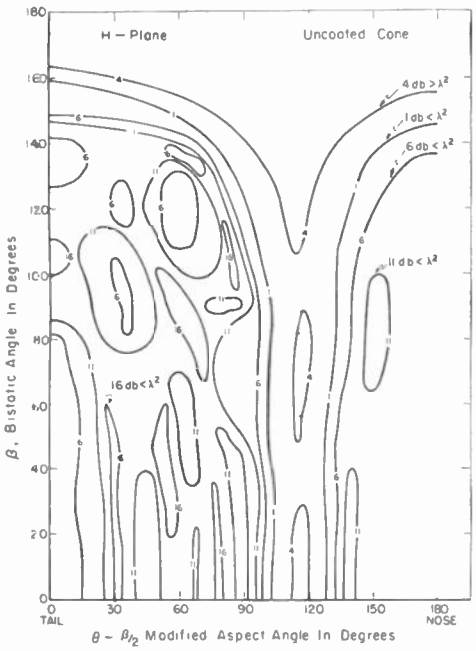

Fig. 19—Contour map for uncoated cone rotated with its longitudinal axis tilted 45° from the vertical axis of rotation, vertical polarization of E field, $f=9.375$ kMc, $\lambda=3.2$ cm.

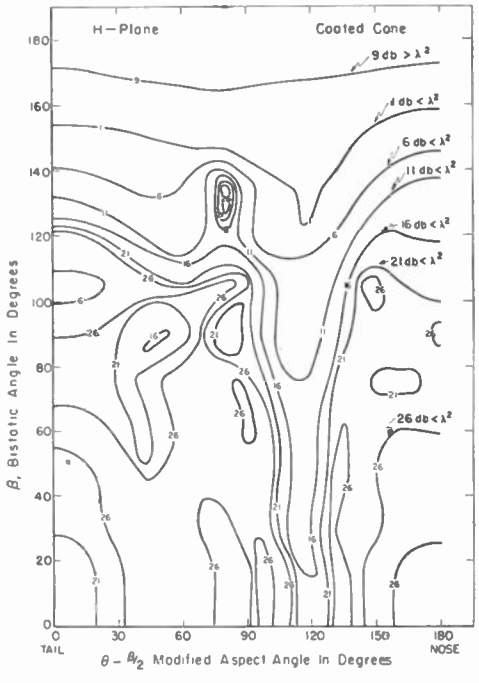

Fig. 20—Contour map for coated cone rotated with its longitudinal axis tilted 45° from the vertical axis of rotation, vertical polarization of E field, $f=9.375$ kMc, $\lambda=3.2$ cm.

The specular reflection from the base of the cone is centered at $\theta-\beta/2$ equal to zero. From Figs. 13 and 14, then, as an example, it is noted that for bistatic angles of less than 100° the base specular reflection is reduced at least 20 db by the absorber coating. Specular reflection from the side of the cone is centered at approximately $\theta-\beta/2$ equal to 108°, as the contour ridge in Fig. 13 clearly demonstrates; and again for bistatic angles of less than 100°, at least a 20-db reduction is noted. Similar comparisons may be made of the scattering at any aspect of the cone for any range of bistatic angles. For large bistatic angles, the contour maps reveal an enhancement of the scattering for the coated cones. The magnitude of the enhancement is not so readily obtained, since forward scatter measurements were not made, and that portion of the contour map is correspondingly sketchy. For bistatic angles of greater than 160°, the contours should be taken only as approximations.

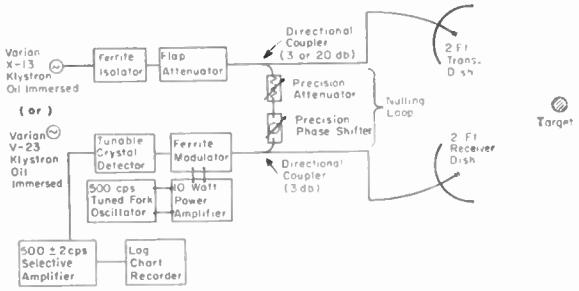

Fig. 21—Schematic diagram of the microwave equipment used for this paper.

Conclusions

In each test performed on bodies in the resonant region experiments show that the absorber coating is effective in reducing scattered energy in the back hemisphere but that in the forward hemisphere scattered energy is increased. It appears that the coated bodies act similarly to lossy lenses which transform some of the energy extracted from the incident wave into heat and reradiate most of the remaining energy into a forward cone. As the body size (in wavelengths) increases, the cone of radiation in the forward direction, within which the scattering from the coated body is greater than that from its uncoated counterpart, becomes narrower.[4]

[4] R. E. Hiatt, K. M. Siegel, and H. Weil, "Forward scattering by coated objects illuminated by short wavelength radar," Proc. IRE, vol. 48, pp. 1630–1635; September, 1960.

Appendix

A schematic diagram of the microwave equipment used to obtain the measured data in this paper is shown in Fig. 21. The system was designed so that either a 250-mw Varian X-13 or a 5-watt Varian V-23 klystron could be used, thus providing for low-power variable frequency or high-power fixed frequency operation. Ferrite modulation was employed in the receiver link to minimize frequency modulation of the source, which is necessary in a null-loop system.

The physical arrangement of the darkroom is shown in Fig. 22. The ceiling and that part of the floor under the target were covered with hairflex. The walls of the room were covered with a combination of hairflex and Plessey, with most of the Plessey located normal to the line of sight from the transmitter. In addition, three

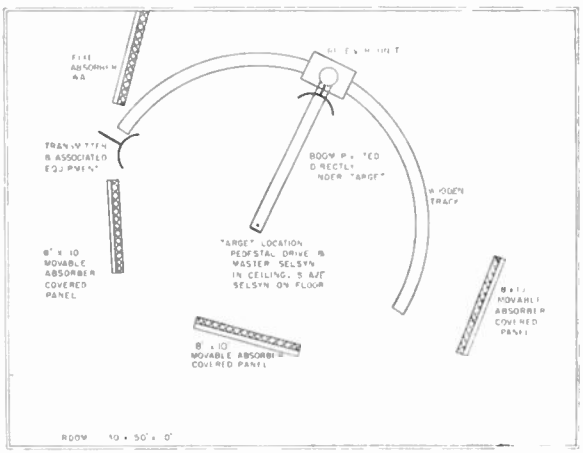

Fig. 22—Physical arrangement of the microwave darkroom.

movable panels of Plessey could be oriented to minimize the background for any bistatic angle.

All measurements presented in this report were made at a range of 15 feet using 2-foot parabolic dishes. The phase and amplitude distributions at the target did not vary more than 22° and 1 db, respectively, over an eight-inch length, and were constant within 10° and ½ db over the targets themselves. Bistatic angles of 165° were measured for all targets, and in some cases 170° angles were possible.

Acknowledgment

The authors wish to acknowledge the helpful discussions of W. Emerson and Dr. R. Wright at the Naval Research Laboratory, who provided us with the targets discussed in this paper. The help of R. Evans, who recorded most of the data, is also appreciated.

IRE Standards on Video Techniques: Definitions of Terms Relating to Television, 1961*

61 IRE 23.S1

COMMITTEE PERSONNEL

Subcommittee on Definitions

1954–1956

G. L. Fredendall, *Chairman*

R. F. Cotellessa S. Deutsch J. M. Eglin W. C. Espenlaub

Video Techniques Committee

1956–1958

J. L. Jones, *Chairman* 1956–1957
S. Doba, Jr., *Chairman* 1957–1959
S. Doba, Jr., *Vice Chairman* 1956–1957
G. L. Fredendall, *Vice Chairman* 1957–1959

I. C. Abrahams
S. W. Athey
A. J. Baracket
J. M. Barstow
J. H. Battison
E. E. Benham
K. B. Benson
E. M. Coan
L. B. Davis
J. R. DeBaun
V. J. Duke
J. R. Hefele
R. T. Petruzzelli
C. G. Pierce
W. J. Poch
H. O. Saunders

Standards Committee

1960–1961

C. H. Page, *Chairman*
J. G. Kreer, Jr., *Vice Chairman*
H. R. Mimno, *Vice Chairman*
L. G. Cumming, *Vice Chairman*

J. H. Armstrong
J. Avins
G. S. Axelby
M. W. Baldwin, Jr.
W. R. Bennett
J. G. Brainerd
A. G. Clavier
S. Doba, Jr.
R. D. Elbourn
G. A. Espersen
R. J. Farber
D. G. Fink
G. L. Fredendall
E. A. Gerber
A. B. Glenn
V. M. Graham
R. A. Hackbusch
R. T. Haviland
A. G. Jensen
R. W. Johnston
I. Kerney
E. R. Kretzmer
W. Mason
D. E. Maxwell
R. L. McFarlan
P. Mertz
H. I. Metz
E. Mittelmann
L. H. Montgomery, Jr.
S. M. Morrison
G. A. Morton
R. C. Moyer
J. H. Mulligan, Jr.
A. A. Oliner
M. L. Phillips
R. L. Pritchard
P. A. Redhead
C. M. Ryerson
G. A. Schupp, Jr.
R. Serrell
W. A. Shipman
H. R. Terhune
E. Weber
J. W. Wentworth
W. T. Wintringham

Definitions Coordinator

H. R. Mimno

* Approved by the IRE Standards Committee, July 10, 1958. At the request of Committee 23, publication was withheld until additional terms had been standardized. This Standard includes revisions of the 1948 list of definitions. However, the revisions contained in 55 IRE 23.S1 are not repeated. Reprints of this Standard 61 IRE 23.S1 may be purchased while available from the Institute of Radio Engineers, 1 East 79th Street, New York, N. Y., at $0.50 per copy. A 20 per cent discount will be allowed for 100 or more copies mailed to one address.

Aspect Ratio. The ratio of the frame width to the frame height.

Brightness Channel (Deprecated). See *Luminance Channel.*

Camera Tube. A tube for conversion of an optical image into an electrical signal by a scanning process.

Chrominance Channel. In a color television system, any path which is intended to carry the chrominance signal.

Chrominance Channel Bandwidth. The bandwidth of the path intended to carry the chrominance signal.

Chrominance Signal Component. A signal resulting from suppressed carrier modulation of a chrominance subcarrier voltage at a specified phase, by a chrominance primary signal.

Color Sync Signal. A signal used to establish and to maintain the same color relationships that are transmitted.

Note: In the FCC Rules covering Radio Broadcast Services, Part 3, the color sync signal consists of a sequence of color bursts which is continuous except for a specified time interval during the vertical interval, each burst occurring on the back porch.

Contrast Ratio. The ratio of the maximum to the minimum luminance values in a television picture or a portion thereof.

Note: Generally the entire area of the picture is implied but smaller areas may be specified as in "detail contrast."

Deflection Yoke. An assembly of one or more coils, whose magnetic field deflects an electron beam.

DC Restoration. The re-establishment by a sampling process of the dc and the low-frequency components of a video signal which have been suppressed by ac transmission.

DC Restorer. A device for re-establishing by a sampling process the dc and low-frequency components of a video signal which have been suppressed by ac transmission.

Note: The sampling process can be accomplished either by the video signal itself or by external pulses.

DC Transmission. A form of transmission in which the dc component of the video signal is transmitted.

Note: In an amplitude-modulated signal with dc transmission, the black level is represented always by the same value of envelope. In a frequency-modulated signal with dc transmission, the black level is represented always by the same value of the instantaneous frequency.

Flyback. The rapid return of the beam in the direction opposite to that used for scanning.

Geometric Distortion. The displacement of elements in the reproduced picture from the correct relative positions in the perspective plane projection of the original scene.

Gray Scale. An optical pattern in discrete steps between light and dark.

Horizontal Hold Control. A synchronization control which varies the free-running period of the horizontal deflection oscillator.

Interlace Factor. A measure of the degree of interlace of nominally interlaced fields.

Note: In a two-to-one interlaced raster, the interlace factor is the ratio of the smaller of two distances between the centers of adjacent scanned lines to one-half the distance between centers of sequentially scanned lines at a specified point.

Jitter. Abrupt spurious deviations in a signal or in the position of a repeated display of an observed quantity.

Limiting Resolution. In television, a measure of resolution usually expressed in terms of the maximum number of lines per picture height discriminated on a test chart.

Note: For a number of lines N (alternate black and white lines) the width of each line is $1/N$ times the picture height.

Linearity Control. A control to adjust the variation of scanning speed during the trace interval to correct geometric distortion.

Luminance Channel. In a color television system, any path which is intended to carry the luminance signal.

Luminance Channel Bandwidth. The bandwidth of the path intended to carry the luminance signal.

Monochrome Channel. Any path which is intended to carry the monochrome signal.

Monochrome Channel Bandwidth. The bandwidth of the path intended to carry the monochrome signal.

Number of Scanning Lines. The ratio of line frequency to frame frequency.

Nominal Line Pitch. The average separation between centers of adjacent lines forming a raster.

Pairing. In scanning, the condition in which lines appear in groups of two instead of equally spaced.

Picture Tube. A cathode-ray tube used to produce a television image.

Progressive Scanning. A rectilinear process in which adjacent lines are scanned in succession.

Overshoot. Overshoot is the initial transient response to a unidirectional change in input, which exceeds the steady-state response. (ASA Definition 65.02.085.)

Raster. A predetermined pattern of scanning lines which provides substantially uniform coverage of an area.

Rectilinear Scanning. The process of scanning an area in a predetermined sequence of straight parallel scanning lines.

Resolution in Television. In television, a measure of ability to delineate picture detail.

Note: Resolution is usually expressed in terms of a number of lines discriminated on a test chart. For a number of lines N (normally alternate black and white lines) the width of each line is $1/N$ times the picture height.

Resolution Wedge. A narrow-angle wedge-shaped pattern calibrated for the measurement of resolution and composed of alternate contrasting strips which gradually converge and taper individually to preserve equal widths along any given line at right angles to the axis of the wedge.

Note: Alternate strips may be black and white of maximum contrast or strips of different colors.

Return Interval. The interval corresponding to the direction of sweep not used for delineation.

Retrace Interval. See *Return Interval.* This item is deprecated.

Return Trace. The path of the scanning spot during the return interval.

Sawtooth Wave. A periodic wave whose instantaneous value varies substantially linearly with time between two values, the interval required for one direction of progress being longer than that for the other.

Scanning Line. A single continuous narrow strip which is determined by the scanning process.

Scanning Linearity. A measure of the uniformity of scanning speed during the unblanked trace interval.

Scanning Speed. The time rate of linear displacement of the scanning spot.

Staircase Signal. A waveform consisting of a series of discrete steps resembling a staircase.

Note: The staircase signal is the electrical equivalent of a gray scale. The heights of the steps may vary, monotonically increasing or decreasing.

Step Wedge (Deprecated). See *Gray Scale.*

Spot Wobble. A process wherein a scanning spot is given a small periodic motion transverse to the scanning lines at a frequency above the picture signal spectrum.

Trace Interval. The interval corresponding to the direction of sweep used for delineation.

Undershoot. Undershoot is the initial transient response to a unidirectional change in input, which precedes the main transition and is opposite in sense.

Vertical Hold Control. A synchronization control which varies the free running period of the vertical deflection oscillator.

The Elimination of Intersymbol Interference by Input Signal Shaping*

I. GERST† AND J. DIAMOND‡

Summary—**Given a time-invariant linear system, the problem of determining those input wave shapes which result in outputs that are zero after a finite time (pulse outputs) is studied. Conditions characterizing these input, pulse-output pairs associated with a linear system are given in terms of their Laplace transforms and the system function. These conditions are then applied in two cases: 1) the general lumped-parameter system, and 2) the general transmission line, to determine classes of suitable input waves for each of these systems. It is shown that the input itself may be taken to be a pulse for all the systems of case 1, and in case 2 for the distortionless infinite line and the general finite line. Furthermore, in case 1 and also for the general RC finite line, the lengths of the associated input and output pulses can be made arbitrarily small.**

I. Introduction

WHEN a pulse, defined here as a waveform which exists in a time interval and vanishes outside the interval, is passed through a linear system, the output generally has a tail or asymptote which stretches out to infinity. This tail makes more difficult the resolution of succeeding pulses, especially in the presence of noise, and so limits the minimum spacing which may be used between pulses. Thus any technique which reduces the tail increases the possible pulse rate, at least in a purely binary system in which only the presence or absence of a pulse conveys information, not pulse shape (leading edge, etc.).

One possible technique is design of the system to reduce the tail. This is the transient synthesis problem and is not the approach we propose.

Rather, for a given system function $F(s)$, we consider the effect of the input wave shape $e_i(t)$ (not necessarily a pulse) on the output tail.[1] Specifically, in Sections II and III, we formulate conditions on $e_i(t)$ under which the output tail can be *eliminated completely.* Then, in Sections IV and V, we show that these conditions can be satisfied, respectively, in the case of a lumped-element constant parameter system and for the general transmission line, finite or infinite; and we give various methods for constructing the requisite inputs. Thus it follows, surprisingly, that by proper choice of the input

* Received by the IRE, September 19, 1960; revised manuscript received, March 7, 1961. The research reported in this paper was performed at RCA for IT&T Communications Systems, Paramus, N. J., in connection with the Air Force 480-L program under Contract No. AF-30(635)-12857.

† Surface Communications Systems Labs., RCA, New York, N. Y.

‡ Autometric Corp., New York, N. Y. Formerly of RCA, New York, N. Y.

[1] Another approach is used by L. A. MacColl (U. S. Patent 2,056,284; 1936). He proposed eliminating intersymbol interference by inserting corrections at the receiver, the transmitted wave shape and the transient response of the system being known.

wave the outputs of the aforementioned systems can be made pulses.

Furthermore, in the lumped parameter case the input wave may also be taken as a pulse of the same length as the output, and this length may be made as narrow as desired. As regards the transmission line, a pulse input is possible in the cases of the distortionless infinite line and the general finite line. In the latter case, arbitrarily small input and output pulse lengths may be attained for the RC line.

II. The Finite Laplace Transform

Consider the time-invariant linear system of Fig. 1 and assume that $e_i(t)$ and $e_o(t)$ have Laplace transforms $E_i(s)$ and $E_o(s)$ respectively, so that, with zero initial conditions, we may write

$$E_o(s) = F(s)E_i(s). \tag{1}$$

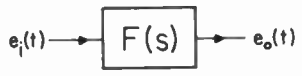

Fig. 1.

We inquire into the possibility of choosing an input $e_i(t)$, such that the output $e_o(t)$ is a function which is identically zero for $t>a$, $a>0$.

A function $g(t)$ with $g(t)\equiv 0$ for $t<0$ and for $t>a$, $a>0$, will be called a pulse of length a. Thus we require $e_o(t)$ to be a pulse of length a, and then it follows that integral defining the Laplace transform of $e_o(t)$ acquires a finite upper limit, so that

$$E_o(s) = \int_0^a e_o(t)e^{-st}dt.$$

Such a transform will be called a *finite Laplace transform* of length a.

Referring now to (1), it is seen that, given the system function $F(s)$, the problem of determining an input $e_i(t)$ yielding a pulse output $e_o(t)$ is reduced to finding a Laplace transform $E_i(s)$ for which $F(s)E_i(s)$ is a *finite* Laplace transform.

At this point, in order to be able to proceed further, we must make use of certain results concerning the finite Laplace transform

$$G(s) = \int_0^a g(t)e^{-st}dt. \tag{2}$$

These will now be considered briefly. As a basis for our discussion, we will assume a development of Laplace transform theory along the lines of Doetsch's[2] recent treatment and will refer to this work whenever necessary for further amplification.

As is well known, a finite integral such as the one in (2) converges for all complex s, defining an analytic function with no singularities in the finite plane, *i.e.*, an entire function. However, this condition on $G(s)$ alone is not sufficient to insure that $g(t)$ be a pulse. For example, the Laplace transform of e^{-t^2}, $t\geq 0$, a nonpulse, is also an entire function.

A theorem giving conditions which characterize the Laplace transform of a pulse has been proved by Doetsch[3] and in our terminology may be stated as follows (here $s=x+iy$, x, y real and C is a positive constant):

Theorem 1

Necessary and sufficient conditions that a Laplace transform $G(s)$ be a finite Laplace transform of length "a" are

a) *$G(s)$ is an entire function,*
b) $|G(x+iy)|\leq C$, *for* $x\geq 0$,
c) $|G(x+iy)|\leq Ce^{ax}$, *for* $x<0$.

The additional conditions b and c require respectively that $G(s)$ be bounded in the right-half plane, and that $e^{as}G(s)$ be bounded in the left-half plane.

Theorem 1 is quite general in that it permits pulses $g(t)$ which are unbounded at a finite number of points in $(0, a)$, as long as $g(t)$ is absolutely integrable at these points. A classic example of this is the pulse $g(t)$ of length 2, defined as

$$g(t) = \frac{1}{\sqrt{t(2-t)}}, \qquad 0<t<2$$
$$= 0, \text{ elsewhere,}$$

which is unbounded at $t=0$, $t=2$ and for which the corresponding finite Laplace transform is $\pi J_0(is)$ [J_0 is the Bessel function of zero order].

Theorem 1 can be modified so that it applies to more restricted classes of pulses which have additional properties of interest for the applications. We mention one of these modifications which is useful in constructing finite Laplace transforms whose corresponding pulses are differentiable.

Theorem 2

Necessary and sufficient conditions that a Laplace transform $G(s)$ be a finite Laplace transform of length "a" corresponding to a pulse $g(t)$ having a generalized nth derivative[4] in the interval $(0, a)$ which is Laplace transformable and for which $g(0^+)=g'(0^+)=\cdots=g^{(n-1)}(0^+)=0=g(a^-)=g'(a^-)=\cdots g^{(n-1)}(a^-)$, are

a) *$G(s)$ is an entire function,*
b) *$s^nG(s)$ is a finite Laplace transform.*

By properly assigning the values of the derivatives at the end points of the interval[5] $(0, a)$, the pulse $g(t)$ of

[2] G. Doetsch, "Theorie und Anwendung der Laplace Transformation," Birkhauser, Basel, Switzerland; 1958.

[3] *Ibid.*, p. 177.

[4] A function $f(t)$ is said to have a generalized first derivative $f^{[1]}(t)$ if $f(t)=f(0)+\int_0 f^{[1]}(t)dt$. Higher-order generalized derivatives $f^{[n]}(t)$ are defined in an analogous manner, cf., *ibid.*, pp. 49–51.

[5] *Ibid.*, p. 51.

Theorem 2 may be described as having continuous derivatives up to order $(n-1)$ and a generalized nth derivative, for all t. This alternative description of $g(t)$ in Theorem 2 will be used in the sequel.

The proof of Theorem 2 follows readily from the fact that under the given conditions on $g(t)$, $\mathcal{L}[g^{[n]}(t)] = s^nG(s)$, and this argument can be reversed. The details will be omitted here.

We now prove the following result which exhibits explicitly a class of finite Laplace transforms of common occurrence.

Theorem 3

If $P_i(s)$, $(i=1, 2, \cdots, k)$ and $D(s)$ *are polynomials in* s *with the* $P_i(s)$ *of lower degree than* $D(s)$, *and if* a_i, $(i=1, 2, \cdots, k)$ are *non-negative real numbers, then the function*

$$G(s) = \frac{1}{D(s)} \cdot \sum_{i=1}^{k} e^{-a_i s} P_i(s)$$

is a finite Laplace transform of length $a = \max a_i$, $(i=1, 2, \cdots, k)$ *if, and only if, it is entire.*

Proof:

By Theorem 1, it is necessary that $G(s)$ be entire. Conversely, suppose that $G(s)$ is entire. Since $|e^{-a_i s}| \leq 1$ for Re $(s) \geq 0$. and since by hypothesis it follows that $P_i(s)/D(s) \to 0$ as $s \to \infty$, we conclude that $G(s)$ is bounded in Re $(s) \geq 0$. Similarly, $e^{as}G(s)$ is bounded in Re $(s) < 0$, since, if s is replaced by $-s$, this function is of the same form as the original $G(s)$. Finally, as is well known, $G(s)$ is a Laplace transform. Thus all the conditions of Theorem 1 are satisfied and it follows that $G(s)$ is a finite Laplace transform. This concludes the proof of Theorem 3.

By admitting impulses of any order as part of the pulse function, Theorem 3 can be extended to cover the case when the $P_i(s)$ are not of lower degree than $D(s)$.

As a final observation, we mention that it follows directly from Theorem 1 that the class of finite Laplace transforms is closed under addition and multiplication. More precisely, we have that: 1) The sum of two finite Laplace transforms of lengths a and b, respectively, is a finite Laplace transform of length $c \leq \max(a, b)$; 2) The product of two finite Laplace transforms[6] of lengths a and b, respectively, is a finite Laplace transform of length $c \leq (a+b)$.

III. The Basic Conditions

We come back now to the question, raised in Section II, of determining a Laplace transform $E_i(s)$ such that $F(s)E_i(s)$ is a *finite* Laplace transform. We see, in the light of Theorem 1, that $E_i(s)$ must be chosen so that the following *basic conditions* hold:

a) $F(s)E_i(s)$ is a Laplace transform;
b) $F(s)E_i(s)$ is an entire function;
c) $F(s)E_i(s)$ satisfies the boundedness conditions b and c of Theorem 1.

Conversely, if these conditions are satisfied $F(s)E_i(s)$ will be a finite Laplace transform.

In the remaining sections of this paper, it will be shown that input transforms $E_i(s)$ exist for which these conditions can be met when $F(s)$ is the system function of a lumped element network or of a transmission line. By way of orientation, we conclude this section by making several remarks relevant to the fulfillment of the basic conditions.

The verification of condition c of Section III will seldom be necessary. In most simple situations where it is possible to obtain an inverse easily, it will generally suffice to establish conditions a and b, since explicit inversion will usually indicate whether or not a pulse is present.

If $F(s)$ has poles, then b requires that these be cancelled by zeros of $E_i(s)$. Many solutions can be found simply by constructing $E_i(s)$ with the requisite zeros. $E_i(s)$ itself may have poles, but only if these poles are cancelled by zeros of $F(s)$. In that case, the input has a tail but the output has none. If the input is also to be a pulse then evidently conditions a–c must be satisfied with $E_i(s)$ a *finite* Laplace transform.

If $E_i(s)$ and $E_o(s)$ correspond to a solution of (1) with $E_o(s)$ a finite Laplace transform, other solutions can be generated by multiplying both sides of (1) by any finite Laplace transform $G(s)$, giving a new input $E_i(s)G(s)$ and a new output $E_o(s)G(s)$. In the time domain this means that the new input is $e_i(t)*g(t)$ and the new output $e_o(t)*g(t)$, where $*$ indicates convolution.

IV. The Lumped-Element Constant Parameter System

In this section, we restrict $F(s)$ to be the system function of a lumped-element constant parameter network. Then $F(s)$ is a rational function which may be written in any of the forms

$$F(s) = \frac{N(s)}{D(s)} = \frac{\sum_{i=0}^{m} k_i s^i}{\sum_{i=0}^{n} h_i s^i} = \frac{N(s)}{\prod_{i=1}^{n} (s - \gamma_i)} \cdot \tag{3}$$

Here $N(s)$ and $D(s)$ are real polynomials with no common factor, and we assume[7] that $m \leq n$, $n \geq 1$, and $h_n = 1$.

We will show that: *For each fixed* $F(s)$ *of the form* (3), *there exist input pulses of arbitrary length* a, *such that the corresponding outputs of the system are pulses of the same length* a. In this result, the fact that the pulse

[6] For this rule to hold in general, the pulses corresponding to the transforms are allowed to be improperly integrable only at $t=0$. *Ibid.*, pp. 54–55.

[7] The restriction $m \leq n$ is made for simplicity. The procedure to be used when $m > n$ will be evident from the discussion in this section.

length is arbitrary and hence can be made arbitrarily small could be of some interest for the applications.

As a consequence of our discussion in Section II, the above statement will be proved if we construct a pair of finite Laplace transforms $E_i(s)$, $E_o(s)$ $(=F(s)E_i(s))$ of arbitrary length a. We give two methods for doing this, the first of which is concerned with the transform domain alone, while the second considers certain mutual relationships of time and transform domains.

A. Method of Zero Insertion in Transform Domain

Consider the entire function

$$E_i(s) = \frac{1 - e^{-\epsilon s}}{s} \cdot \prod_{j=1}^{n} |1 - e^{-\epsilon(s-\gamma_j)}|, \tag{4}$$

where ϵ is an arbitrary positive number and the γ_j are as in (3). Then by Theorem 3 of Section II, $E_i(s)$ is a finite Laplace transform of length $(n+1)\epsilon$. This is the desired input transform.[8]

Since $E_i(\gamma_j)=0$, $F(s)E_i(s)$ is an entire function and, by Theorem 3 of Section II, is a finite Laplace transform of length $(n+1)\epsilon$. With $a=(n+1)\epsilon$, this proves the statement made at the beginning of this section, since n is fixed.

The inversion of $E_i(s)$ and $E_o(s)=F(s)E_i(s)$ to get $e_i(t)$ and $e_o(t)$ presents no difficulty and will be omitted, particularly since an alternative solution of the problem is given in Section IV-B.

Several observations regarding the method given above follow:

1) Instead of the factor $(1-e^{-\epsilon s})/s$ in (4), we can use any finite Laplace transform $G(s)$ of the form given in Theorem 3 of Section II.
2) If the input $e_i(t)$ is not required to be a pulse, we can multiply $E_i(s)$ in (4) by $1/\Pi(s-\delta_i)$ where the δ_i range over some or all of the zeros[9] of $N(s)$, and still get a pulse output.
3) The input pulse defined by (4) will, in general, be discontinuous within the interval $(0, a)$ as well as at the end points. If one desires an input pulse which shall be of class C^n for all t (*i.e.*, have continuous derivatives up to order n for all t, so that, in particular, these derivatives are zero at 0 and a), then (4) can easily be modified to provide such an input. Namely, by Theorem 3 of Section II, the function $E_1(s)=E_i(s)\cdot(1-e^{-\epsilon s})^{n+1}/s^{n+1}$, with $E_i(s)$ as in (4), is a finite Laplace transform which by Theorem 2 of Section II corresponds to an input pulse having the desired differentiability properties. The output transform $E_o(s)=F(s)E_i(s)$ is again of the form given in Theorem 3 and so corresponds to a pulse.

[8] The pulse $e_i(t)$ corresponding to $E_i(s)$ is a real function, since the presence of complex conjugate γ_j in (4) will result in $E_i(s)$ having real coefficients when the product in (4) is multiplied out and $E_i(s)$ is expressed in the form given by Theorem 3 of Section II.

[9] Complex zeros are, of course, to be taken in conjugate pairs.

B. Direct Method in Time Domain

We now consider a second method of obtaining pulse outputs and associated pulse inputs, when $F(s)$ is the system function given in (3). The development here will be largely heuristic. A formal proof of the fundamental representations (5) and (6) is given in Appendix I.

From (3) and (1) we have

$$E_i(s)\frac{N(s)}{D(s)} = E_o(s).$$

There is a temptation to write $E_i(s)=D(s)$, thus removing all the poles of $F(s)$. The trouble is that the resulting $e_i(t)$ will be a sum of higher-order impulses which we do not consider an acceptable solution. But it must be possible to write

$$E_i(s) = E_1(s)D(s),$$
$$E_o(s) = E_1(s)N(s),$$

where $E_1(s)$ is entire, because $E_i(s)$ must contain all the factors of $D(s)$. Thus,

$$E_i(s) = h_0E_1(s) + h_1sE_1(s) + \cdots + h_ns^nE_1(s)$$

and, formally, an inversion of this equation leads to

$$e_i(t) = h_0e_1(t) + h_1e_1'(t) + \cdots + h_ne_1^{(n)}(t). \tag{5}$$

Similarly, we get

$$e_o(t) = k_0e_1(t) + k_1e_1'(t) + \cdots + k_me_1^{(m)}(t). \tag{6}$$

It will be shown in Appendix I that (5) and (6) give a representation for all input and output pulse pairs associated with the system function $F(s)$. In these equations $e_1(t)$ is any pulse of length a having a generalized nth derivative for all t, but is otherwise arbitrary.

V. Transmission Lines

In this section, we consider the determination of input and pulse-output pairs for system functions $F(s)$, which are associated with uniform transmission lines having lumped-element terminations. We shall discuss only the case of $F(s)$ as a voltage transfer ratio, since the other cases are treated in an analogous manner.

Then, for the general infinite line with source impedance Z_0 and characteristic impedance Z_c, we have

$$F(s) = \frac{Z_c}{Z_c + Z_0}e^{-qx}; \tag{7}$$

and for the finite line of length l with, in addition, a load impedance Z_l, the voltage transfer function with respect to the end of the line is [10]

$$F(s) = \frac{Z_cZ_l}{(Z_c^2 + Z_0Z_l)\sinh ql + Z_c(Z_0 + Z_l)\cosh ql}. \tag{8}$$

[10] *Cf.*, E. Weber, "Linear Transient Analysis," John Wiley and Sons, Inc., New York, N. Y., vol. 2, pp. 279, 379, 400; 1956.

Here

$$q = \sqrt{\alpha s^2 + \beta s + \gamma},$$

$$Z_c = \frac{q}{G + sC},$$

and $\alpha = LC$, $\beta = LG + RC$, $\gamma = RG$ where L, G, R, C are the constants of the line.

We assume now that Z_0 and Z_t are lumped-element impedances. Then, expressing Z_0 and Z_t as quotients of polynomials, *viz.*, $Z_0 = N_0/D_0$, $Z_t = N_t/D_t$, (7) and (8) become

$$F(s) = \frac{\dfrac{P_1(s)}{P_1(s) + \dfrac{P_2(s)}{q}}}{} e^{-qx}, \qquad x > 0 \tag{9}$$

and

$$F(s) = \frac{P_3(s)}{P_4(s)\cosh ql + P_5(s)\dfrac{\sinh ql}{ql}}. \tag{10}$$

respectively. Here the $P_i(s)$, $(i = 1, \cdots, 5)$ are polynomials which are defined by

$$P_1 = D_0, \qquad P_2 = (G + sC)N_0,$$

$$P_3 = N_t D_0 (G + sC), \qquad P_4 = (N_t D_0 + N_0 D_t)(G + sC),$$

$$P_5 = q^2 D_0 D_t + N_0 N_t (G + sC)^2.$$

For simplicity, it is convenient to normalize the expressions in (9) and (10).

As is well known, q may be transformed into the form $q = \sqrt{s^2 - \lambda^2}$, $\lambda^2 \geq 0$ or $q = \sqrt{s}$ according as $\alpha \neq 0$ or $\alpha = 0$ respectively (*i.e.*, according as wave propagation or diffusion is present), and simultaneously x and l may each be taken to be unity in (9) and (10), respectively. These normalizations can be achieved by replacing s successively by $s + c_1$, and $c_2 s$, where c_1 and c_2 are suitably chosen positive constants. As a result of these operations, polynomials in s remain polynomials in the transform domain, while pulses corresponding to finite Laplace transforms remain pulses in the time domain. We may therefore, without loss of generality, suppose that (9) and (10) are already in normal form with q as above and $x = l = 1$.

In proceeding to determine suitable inputs associated with the given system functions (9) and (10), it is immediately evident that we are faced with different situations in these two cases. For the infinite line [see (9)], $F(s)$ will in general have branch points, and the relation $E_o(s) = F(s)E_i(s)$ with $E_o(s)$ a finite Laplace transform cannot be satisfied if $E_i(s)$ is entire. Thus the inputs, $e_i(t)$, cannot, in general, be pulses. The only exception is the distortionless line when $\lambda = 0$ and $q = s$.

On the other hand, the system function $F(s)$ of (10) for the finite line is a meromorphic function of s and thus input pulses are possible. We will show that this possibility actually may be realized.

Since the rationale of our method has been detailed in the previous sections, we now restrict ourselves simply to listing one family of inputs leading to pulse outputs for each of the cases which must be considered. The representation of these inputs is analogous to that used in Section III-B for the lumped-parameter case. We do not go into the question of totality of solutions here.

A. Infinite Line:

1) $\alpha = LC \neq 0$; $F(s)$ given by (9) with $q = \sqrt{s^2 - \lambda^2}$, $\lambda^2 \geq 0$, $x = 1$. We may take

$$e_i(t) = P_1(D)\{h_1(t) * e_1(t) + e_1(t)\} + P_2(D)\{h_2(t) * e_1(t)\}. \tag{11}$$

Here $e_1(t)$ is *any* Laplace transformable pulse of length a, which, for all real t, has at least as many derivatives as the larger of the degrees of P_1 and P_2. The functions $h_1(t)$ and $h_2(t)$ are defined as

$$h_1(t) = -\lambda(t^2 - 2t)^{-1/2} I_1[\lambda(t^2 - 2t)^{1/2}],$$

$$h_2(t) = I_0[\lambda(t^2 - 2t)^{1/2}],$$

where I_0 and I_1 are the modified Bessel functions, while $*$ denotes convolution and $D = d/dt$.

Using the transform pairs[11]

$$\mathcal{L}[h_1(t)] = e^{q-s} - 1,$$

$$\mathcal{L}[h_2(t)] = \frac{e^{q-s}}{s},$$

one easily calculates from (11) and (9) that

$$E_o(s) = F(s)E_i(s) = P_1(s)e^{-s}E_1(s),$$

where $E_1(s) = \mathcal{L}[e_1(t)]$; and hence

$$e_o(t) = P_1(D)e_1(t - 1).$$

Thus $e_o(t)$ is a pulse of length $1 + a$ which is zero for $0 \leq t \leq 1$.

Note that for $\lambda = 0$, (11) reduces to

$$e_i(t) = P_1(D)e_1(t) + P_2(D)\left[\int_0^t e_1(\tau)d\tau\right],$$

so that by further restricting the pulse $e_1(t)$ to have $\int_0^a e_1(\tau)d\tau = 0$, the input $e_i(t)$ is also a pulse.

2) $\alpha = LC = 0$; $F(s)$ given by (9) with $q = \sqrt{s}$, $x = 1$. We may take

$$e_i(t) = P_1(D)\left[h_3(t) + \frac{1}{\sqrt{\pi}} t^{-1/2} * \frac{dh_4(t)}{dt}\right] + P_2(D)\left[h_4(t) + \frac{1}{\sqrt{\pi}} t^{-1/2} * h_3(t)\right], \tag{12}$$

[11] A. Erdélyi, *et al.*, "Tables of Integral Transforms," McGraw-Hill Book Co., Inc., New York, N. Y., vol. 1, p. 250; 1954.

where

$$h_3(t) = \sum_{n=0}^{\infty} \frac{e_1^{(n)}(t)}{(2n)!}, \quad h_4(t) = \sum_{n=0}^{\infty} \frac{e_1^{(n)}(t)}{(2n+1)!}, \tag{13}$$

and $e_1(t)$ is *any* Laplace transformable pulse of length a, which is infinitely differentiable for all real t, and for which the infinite series implicit in (12) converge and may be Laplace transformed termwise in order to get $E_i(s)$. Here superscripts denote time derivatives, while the remainder of the notation has its previous meaning.

In Appendix II we will show that the pulse of length a defined as

$$g(t) = e^{-(1/t+1/(a-t))} \quad (0 < t < a),$$
$$g(t) = 0, \quad \text{elsewhere},$$

is an admissible function for $e_1(t)$; and more generally we may take $e_1(t) = g(t)h(t)$ where $h(t)$ is any function analytic in a sufficiently large region containing the segment $0 \leq t \leq a$.

By straightforward Laplace transform calculus, we find from (9) and (12) that

$$E_o(s) = P_1(s)E_1(s),$$

which yields

$$e_o(t) = P_1(D)e_1(t),$$

a pulse of length a.

B. Finite Line

1) $\alpha = LC \neq 0$; $F(s)$ given by (10) with $q = \sqrt{s^2 - \lambda^2}$, $\lambda^2 \geq 0$, $l = 1$. Take

$$e_i(t) = \frac{P_4(D)}{2}\left[\tilde{h}_1(t) * e_1(t) + e_1(t) + e_1(t-2)\right] + \frac{P_5(D)}{2}\left[\tilde{h}_2(t) * e_1(t)\right]. \tag{14}$$

Here, $e_1(t)$ is *any* Laplace transformable pulse of length a which, for all real t, has at least as many derivatives as the larger of the degrees of P_4 and P_5; while $\tilde{h}_1(t)$ and $\tilde{h}_2(t)$ are pulses defined in terms of the functions $h_i(t)$ $(i = 1, 2)$ of (11) as follows:

$$\tilde{h}_i(t) = h_i(t), \quad 0 \leq t \leq 2 \ (i = 1, 2)$$
$$\tilde{h}_i(t) = 0, \quad \text{otherwise}.$$

Evidently $e_i(t)$ as given by (14) is a pulse of length $2+a$. One readily calculates the transform pairs

$$\mathfrak{L}[\tilde{h}_1(t)] = (e^{q-s} - 1) + e^{-2s}(e^{-(q-s)} - 1),$$
$$\mathfrak{L}[\tilde{h}_2(t)] = \frac{1}{q}\left[e^{q-s} - e^{-q-s}\right],$$

from which follows

$$E_o(s) = P_3(s)e^{-s}E_1(s)$$

and, finally,

$$e_o(t) = P_3(D)e_1(t-1).$$

Thus $e_o(t)$ is a pulse of length $1+a$ which is identically zero for $0 \leq t \leq 1$.

2) $\alpha = LC = 0$; $F(s)$ given by (10) with $q = \sqrt{s}$, $l = 1$. Take

$$e_i(t) = P_4(D)h_3(t) + P_5(D)h_4(t). \tag{15}$$

where $h_3(t)$ and $h_4(t)$ are pulses of length a defined by (13) in A-1. The discussion regarding $e_1(t)$ in that case applies here as well. Evidently $e_i(t)$ is a pulse of length a. By direct calculation one finds that

$$E_o(s) = P_3(s)E_1(s),$$

and so the output,

$$e_o(t) = P_3(D)e_1(t),$$

is a pulse of the same length a as the input $e_i(t)$.

VI. Example

Consider the network of Fig. 2(a), for which the transfer function is

$$F(s) = \frac{\alpha^2 + \beta^2}{(s+\alpha)^2 + \beta^2}, \quad \alpha = \frac{R}{2L}, \quad \beta^2 = \frac{1}{LC} - \left(\frac{R}{2L}\right)^2$$

We will assume that $\beta^2 > 0$.

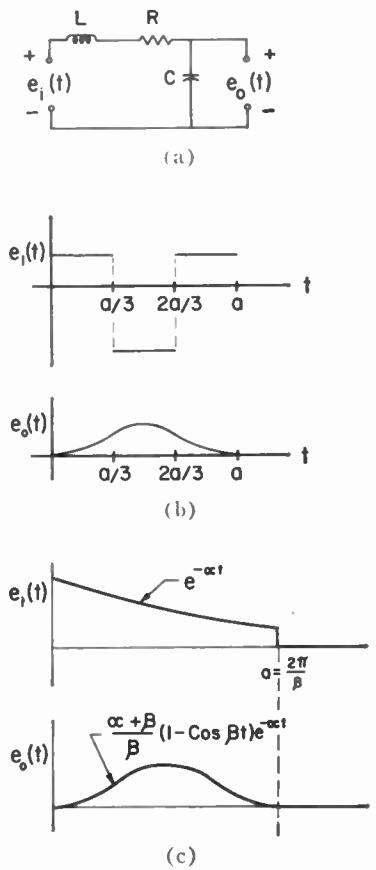

Fig. 2.

Suppose that an input pulse of arbitrary length a is desired. The method of Section IV-A, in which one works in the transform domain, will be illustrated first. Then using (4), we have

$$E_i(s) = \frac{(1-e^{-as/3})(1-e^{-a(s+\alpha-j\beta)/3})(1-e^{-a(s+\alpha+j\beta)/3})}{s}. \quad (16)$$

since $F(s)$ has the poles $-\alpha \pm j\beta$, and $n=2$, $\epsilon = a/3$. Multiplying out the factors in (16) and inverting gives

$$e_i(t) = u(t) - c_1 u\left(t - \frac{a}{3}\right) + c_2 u\left(t - \frac{2a}{3}\right) - c_3 u(t-a),$$

where

$$c_1 = 1 + 2e^{-a\alpha/3}\cos\frac{a\beta}{3}, \qquad c_2 = e^{-2a\alpha/3} + 2e^{-a\alpha/3}\cos\frac{a\beta}{3},$$

$$c_3 = e^{-2a\alpha/3},$$

and $u(t)$ is the unit step function.

Thus the input consists of three rectangular pulses whose amplitudes are respectively 1, $1-c_1$, $1-c_1+c_2$, and which are defined in the intervals $(0, a/3)$, $(a/3, 2a/3)$, $(2a/3, a)$, respectively [*cf.*, Fig. 2(b)].

The output pulse is found to be

$$e_o(t) = h(t) - c_1 h(t - a/3) + c_2 h(t - 2a/3) - c_3 h(t-a),$$

where

$$h(t) = u(t) - e^{-\alpha t}\left(\cos\beta t + \frac{\alpha \sin\beta t}{\beta}\right), \qquad t \geq 0$$
$$= 0 \qquad t < 0.$$

Since $s^2E_o(s) = s^2E_i(s)F(s)$ is a finite Laplace transform, Theorem 2 of Section II implies that the pulse $e_o(t)$ has an ordinary first derivative for all t. Thus, the slope of $e_o(t)$ is zero at both ends of the pulse interval. Fig. 2(b) pictures $e_o(t)$ when a is small compared to $1/\alpha$ and $1/\beta$.

As indicated in Section IV-A, a choice of $E_i(s)$ may be made in many different ways and this gives us the freedom to impose additional restrictions on the type of input pulse we desire. For example, suppose the pulse length a is immaterial but we desire the input to be in "one piece." A glance at (16) shows that the separate "pieces" of our first solution arose because of the various exponential terms in the numerator. Therefore, we attempt to find a suitable $E_i(s)$ by using just one exponential in the numerator. The simplest such finite Laplace transform is of the form

$$E_i(s) = \frac{1 - e^{-a(s+\delta)}}{s+\delta},$$

where $a > 0$ and δ are to be determined so as to make the output a pulse.

The requirement that $E_i(s)$ must be zero at the poles of $F(s)$ leads to the condition

$$a(-\alpha + j\beta + \delta) = 2n\pi j, \qquad n \text{ an integer.}$$

The choice $\delta = \alpha$, $n = 1$, $a = 2\pi/\beta$ can be used here. The resulting input and output pulses of length $2\pi/\beta$ are shown in Fig. 2(c).

Next, we consider the method of Section IV-B where the solution is represented directly in the time domain. Since $N(s) = \alpha^2 + \beta^2$ and $D(s) = \alpha^2 + \beta^2 + 2\alpha s + s^2$ in our example, (5) and (6) become, respectively,

$$e_i(t) = (\alpha^2 + \beta^2)e_1(t) + 2\alpha\frac{de_1(t)}{dt} + \frac{d^2e_1(t)}{dt^2}$$

and

$$e_o(t) = (\alpha^2 + \beta^2)e_1(t).$$

Here $e_1(t)$ may be any pulse of length a having at least a generalized second derivative for all t. For an input pulse without jumps, $e_1(t)$ must have an ordinary second derivative for all t. For example, a suitable function $e_1(t)$ of this latter class would be

$$e_1(t) = (1 - \cos\omega t)^2, \qquad 0 \leq t \leq a$$
$$= 0, \qquad \text{otherwise,}$$

where $a = 2\pi/\omega$. This choice of $e_1(t)$ leads to the input pulse

$$e_i(t) = \frac{3}{2}(\alpha^2 + \beta^2) + 2(\omega^2 - \alpha^2 - \beta^2)\cos\omega t + 2\alpha\omega\sin\omega t + \tfrac{1}{2}(\alpha^2 + \beta^2 - 4\omega^2)\cos 2\omega t - \alpha\omega\sin 2\omega t, \qquad (0 \leq t \leq a)$$
$$= 0, \quad \text{otherwise.}$$

This sort of pulse shape has the advantage that it can be produced by gating a continuous wave rather than by generating the individual pulse.

Appendix I

The Fundamental Equations of Section IV-B

We must show that the relation

$$E_o(s) = \frac{N(s)}{D(s)}E_i(s) \quad (17)$$

with

$$N(s) = \sum_{i=0}^{m} k_i s^i, \quad D(s) = \sum_{i=0}^{n} h_i s^i, \quad h_n = 1, \; m \leq n, \; n \geq 0,$$

$N(s)$ and $D(s)$ relatively prime, plus the assumptions that $E_i(s)$ and $E_o(s)$ satisfy the conditions in Theorem 1 of Section II, imply that

$$e_i(t) = h_0 e_1(t) + h_1 e_1'(t) + h_2 e_1''(t) + \cdots + h_n e_1^{[n]}(t), \quad (18)$$

$$e_o(t) = k_0 e_1(t) + k_1 e_1'(t) + k_2 e_1''(t) + \cdots + k_m e_1^{(m)}(t). \quad (19)$$

Here $e_1(t)$ is a pulse having a Laplace transformable generalized nth derivative [denoted by $e_1^{[n]}(t)$] in the pulse interval $(0, a)$, and satisfying the conditions

$e_1(0^+) = e_1'(0^+) = \cdots = e_1^{(n-1)}(0^+) = 0 = e_1(a^-) = e_1'(a^-) = \cdots = e_1^{(n-1)}(a^-)$ at the ends of this interval.[4,5]

In (17), since $E_0(s)$ and $E_i(s)$ are entire, we must have

$$E_i(s) = D(s)E_1(s), \tag{20}$$

where $E_1(s)$ is an entire function.

We will show that $E_1(s)$ satisfies the conditions of Theorem 2 of Section II. We already have condition a of that theorem. There remains the proof that $s^nE_1(s)$ is a finite Laplace transform.

From (20), we have

$$s^nE_1(s) = \frac{s^n}{D(s)} \cdot E_i(s) = E_i(s) + \frac{N_1(s)}{D(s)} \cdot E_i(s), \tag{21}$$

where $N_1 = s^n - D(s)$ is of lower degree than $D(s)$. Now $N_1(s)E_i(s)/D(s)$ is an entire function and is a Laplace transform by the convolution theorem. Also, since $N_1(s)/D(s) \to 0$ as $s \to \infty$, the inequalities b and c of Theorem 1, Section II, hold for $N_1(s)E_i(s)/D(s)$ and with the same constant a as for $E_i(s)$. Thus by Theorem 1 of Section II, $N_1(s)E_i(s)/D(s)$ is a finite Laplace transform. Then, by (21), $s^nE_1(s)$ is a finite Laplace transform of length a.

We may therefore apply Theorem 2 of Section II to $E_1(s)$ and infer that $e_1(t)$ is a pulse having the differentiability properties stated above. As a consequence of this, $\mathcal{L}[e_1^{(k)}(t)] = s^kE_1(s)$, $(k = 0, 1, \cdots, n)$. Therefore, inverting (20) termwise yields (18). Eq. (19) is obtained by eliminating $E_i(s)$ between (17) and (20) and inverting the resulting equation for $E_o(s)$.

The converse result, that pulses $e_i(t)$ and $e_o(t)$ defined by (18) and (19) are solutions of (17), with $e_1(t)$ as *any* pulse having the stated properties, is immediate.

Eqs. (18) and (19) can be extended in an obvious way to include inputs which may have impulses of any order.

Appendix II

The Convergence of (12) and (15)

If the indicated differentiations $P_1(D)$, $P_2(D)$, etc., in (12) and (15) are carried out, there result expressions which involve a finite number of infinite series of the two general forms:

$$S_1 = \sum_{n=0}^{\infty} \frac{e_1^{(n+k)}(t)}{(2n)!}, \qquad S_2 = \sum_{n=0}^{\infty} \frac{e_1^{(n+k)}(t)}{(2n+1)!},$$

where k may vary from series to series, but in any one series is a fixed non-negative integer.

To begin, we suppose that $e_1(t)$ is a function defined as

$$\begin{aligned} g(t) &= e^{-(1/t - 1/(a-t))}, && 0 < t < a \\ &= 0, && \text{otherwise.} \end{aligned} \tag{22}$$

We will show that, for this choice of $e_1(t)$, the series S_1 and S_2 are absolutely and uniformly convergent in the closed interval $0 \le t \le a$. This not only establishes that these series have meaning, but also justifies calculating the Laplace transform of S_1 and S_2 by transforming the series termwise.

The proof will depend upon the establishment of the following inequality for $g^{(n)}(t)$:

$$|g^{(n)}(t)| \le (n+1)!n^n\beta^n, \quad (n = 0, 1, 2, \cdots,), \ 0 \le t \le a, \tag{23}$$

where β is a constant such that $0 < \beta < 1$. Assuming for the moment that (23) holds, then the stated result can be obtained readily. It suffices to consider S_1. Then, using simply the rough inequality $2n! \ge n!n^n$, we have

$$\left|\frac{g^{(n+k)}(t)}{(2n)!}\right| \le \frac{(n+k+1)!(n+k)^{n+k}\beta^{n+k}}{n!n^n}$$

$$= (n+k+1)(n+k)\cdots(n+1)(n+k)^k(1+k/n)^n\beta^{n+k}.$$

Since

$$\left(1 + \frac{k}{n}\right)^n \to e^k \text{ as } n \to \infty,$$

we have

$$\left|\frac{g^{(n+k)}(t)}{(2n)!}\right| \le CP(n)\beta^{n+k},$$

where C is a bound for

$$\left(1 + \frac{k}{n}\right)^n \text{ and } P(n) = (n+k+1)\cdots(n+1)(n+k)^k$$

is a polynomial in n of fixed degree. Thus S_1 is majorized for all $0 \le t \le a$ by the convergent series $C\beta^k\sum P(n)\beta^n$, and our result follows.

The remainder of this section therefore will be devoted to the proof of (23). We consider first the simpler function $f(t)$ defined as

$$\begin{aligned} f(t) &= e^{-1/t}, && t > 0, \\ &= 0, && \text{otherwise.} \end{aligned}$$

Then $f(t)$ has derivatives of all orders and $f^{(n)}(0) = 0$, $(n = 0, 1, \cdots)$. The function $e^{-1/t}$ considered as a function of a complex variable t is analytic everywhere except at $t = 0$ where it has an essential singularity.

Let z be any positive number. Then by the Cauchy integral formula:

$$f^{(n)}(z) = \frac{n!}{2\pi i}\int_C \frac{e^{-1/t}dt}{(t-z)^{n+1}},$$

where for C we take the circle $C: t = z + re^{i\theta}$, $0 \le \theta \le 2\pi$, with $0 < r < z$ (see Fig. 3).

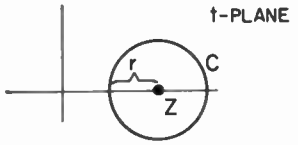

Fig. 3.

By a standard inequality,

$$|f^{(n)}(z)| \leq \frac{n!}{2\pi}\cdot\max\left|\frac{e^{-1/t}}{(t-z)^{n+1}}\right| \text{ on } C\cdot 2\pi r,$$

$$\leq \frac{n!}{r^n}\cdot\max|e^{-1/t}| \text{ on } C.$$

But on C,

$$|e^{-1/t}| = e^{-(z+r\cos\theta)/(z^2+r^2+2rz\cos\theta)}$$

$$= e^{-1/2z}\cdot e^{-A/(z^2+r^2+2rz\cos\theta)},$$

where $A=(z^2-r^2)/2z>0$. Therefore,

$$\max|e^{-1/t}| \text{ on } C = e^{-1/2z}\cdot e^{-A/(z+r)^2} = e^{-1/(z+r)}.$$

Thus,

$$|f^{(n)}(z)| \leq \frac{n!}{r^n}e^{-1/(z+r)}. \tag{24}$$

Up to this point, r has been independent of z, subject only to the condition that $0<r<z$. We now take $r=\alpha z$ where α, a constant subject to the inequality $0<\alpha<1$, is to be determined later. Then (24) becomes

$$|f^{(n)}(z)| \leq \frac{n!}{\alpha^n z^n}e^{-1/(1+\alpha)z}, \qquad z>0. \tag{25}$$

This inequality holds also for $z=0$ if we interpret the right member as $\lim_{z\to 0^+}$, since both members are then zero.

We now determine a bound for the right member of (25) which is independent of z. Consider the function

$$h(z) = \frac{1}{z^n}\cdot e^{-1/(1+\alpha)z}$$

for $z\geq 0$, $n\geq 1$. Then

$$\frac{dh(z)}{dz} = \left[\frac{1}{(1+\alpha)z} - n\right]\frac{e^{-1/(1+\alpha)z}}{z^{n+1}}. \tag{26}$$

It follows from (26) and from the fact that

$$h(0) = h(\infty) = 0,$$

that $h(z)$ attains its maximum at $z=1/(1+\alpha)n$, so that

$$\max h(z) = (1+\alpha)^n n^n e^{-n}, \qquad z\geq 0.$$

Thus (25) becomes

$$|f^{(n)}(z)| \leq n!n^n\beta^n, \qquad \beta = \frac{1+\alpha}{\alpha e}, \tag{27}$$

for $z\geq 0$, $n\geq 1$. By inspection, $|f(z)|\leq 1$ for all z, and if 1 is the value assigned to the right member of (27) when $n=0$, (27) holds also for $n=0$. Trivially, (27) holds for $z<0$.

Since $(1+\alpha)/\alpha e<1$ if $\alpha>1/(e-1)$ and since this last inequality can be satisfied with an α such that $0<\alpha<1$ (*e.g.*, $\alpha=\frac{3}{4}$), it follows that we may suppose that $0<\beta<1$. The inequality (27), except for the presence of $n!$ instead of $(n+1)!$ is (23) for the function $f(t)$.

Next consider $f_1(t)$ defined by

$$f_1(t) = e^{-1/(a-t)}, \quad t<a,$$

$$= 0, \quad \text{otherwise.}$$

Then since $f_1(t)=f(a-t)$ and $|f_1^{(n)}(t)|=|f^{(n)}(a-t)|$, $f_1^{(n)}(z)$ is also subject to the inequality (27) for all z.

Finally, noting that $g(t)=f(t)f_1(t)$, we apply Leibniz's rule for the nth derivative of a product to $g(t)$ and find

$$g^{(n)}(t) = \sum_{i=0}^{n}\binom{n}{i}f^{(i)}(t)f_1^{(n-i)}(t).$$

Then in view of (27), which holds for both $f(t)$ and $f_1(t)$, we get

$$|g^{(n)}(t)| \leq \sum_{i=0}^{n}\binom{n}{i}|f^{(i)}(t)|\,|f_1^{(n-i)}(t)|$$

$$\leq \sum_{i=0}^{n}\binom{n}{i}i!i^i\beta^i\cdot(n-i)!(n-i)^{n-i}\beta^{n-i}.$$

As

$$\binom{n}{i} = n!/(n-i)!i!,$$

and $(n-i)^{n-i}i^i\leq n^n$, it follows that

$$|g^{(n)}(t)| \leq (n+1)\cdot n!n^n\beta^n.$$

This is (23).

The convergence of the series S_1 and S_2 may also be proved when, more generally, $e_1(t)=g(t)h(t)$ where $h(t)$ is any function analytic in a region which contains the rectangle R:

$$-\beta^{-1}\leq \operatorname{Re}(t)\leq a+\beta^{-1}, \quad -\beta^{-1}\leq \operatorname{Im}(t)\leq\beta^{-1}.$$

Here β is the constant in (23) and a is the pulse length of $g(t)$.

For, if t is any real number in the interval $0\leq t\leq a$ then, as is well known, we have $|h^{(n)}(t)|\leq n!M_t/r^n$, where M_t is the maximum of $|h(t)|$ on a circle of radius r with center at t. The circular disk of radius r centered at t must be interior to the region of analyticity of $h(t)$. Since this regior contains R, we can choose $r=\beta^{-1}$. Also $M_t\leq M$ where M is the maximum of $|h(t)|$ on the boundary of R. There results the inequality

$$|h^{(n)}(t)| \leq Mn!\beta^n. \tag{28}$$

If we now apply the Leibniz formula to get $d^n[g(t)h(t)]/dt^n$ and employ (23) and (28), we find

$$\left|\frac{d^n}{dt^n}[g(t)h(t)]\right| \leq M\sum_{i=0}^{n}\binom{n}{i}(i+1)!i^i\beta^i(n-i)!\beta^{n-i},$$

$$\leq Mn!n^n\beta^n\sum_{i=0}^{n}(i+1) = \frac{M}{2}(n+2)!n^n\beta^n.$$

Since this inequality is essentially like (23) with the right member there multiplied by $(n+2)$, the argument given at the beginning of this section is unaffected when $g(t)$ is replaced by $g(t)h(t)$.

Correspondence

Generation of Nanosecond Carrier Pulses at *X*-Band with Tunnel Diodes*

A gallium antimonide[1] point contact[2] tunnel diode has been used to obtain nanosecond carrier pulses at a 10-Mc rate in *X*-band waveguide. The RF pulse of Fig. 1 was generated directly from the switching of this tunnel diode with the 10-Mc pulse. Fig. 1(b) shows a single pulse of Fig. 1(a) in an expanded time scale.

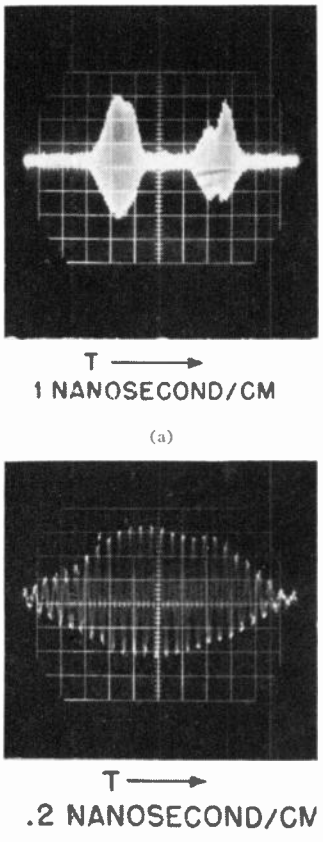

Fig. 1—(a) RF pulses from GaSb tunnel diode. (b) RF cycles in pulse.

Since the waveguide acts as a high-pass or differentiating circuit, one RF pulse is generated as the rising edge of the driving pulse causes the diode to switch to the high-current state; a second pulse is generated as the falling portion of the driving pulse returns the diode to the zero-current condition. The separation between pulses depends on the time that the driving pulse amplitude exceeds the valley voltage.

The pulses were observed on the electronic band-pass stroboscope described by A. F. Dietrich in his letter.[3] Examination of Fig. 1(b) shows there are $2\frac{1}{4}$ RF cycles per cm. Since the horizontal sensitivity is 2×10^{-10} sec/cm, the pulse has a carrier frequency of 11 Gc.

The gallium antimonide diode was mounted without encapsulation directly across a 0.015 inch×0.9 inch *X*-band waveguide (Fig. 2). The diode was formed[1] after assembly in the guide. The I-V characteristics of this diode are shown in Fig. 3. The 10-Mc pulse was coupled to the coaxial line leading to the diode by a broad-band ferrite transformer. For this pulsed operation no dc bias was used.

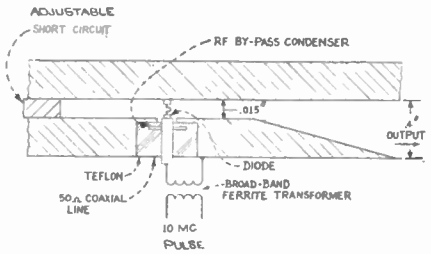

Fig. 2—Tunnel diode pulse circuit.

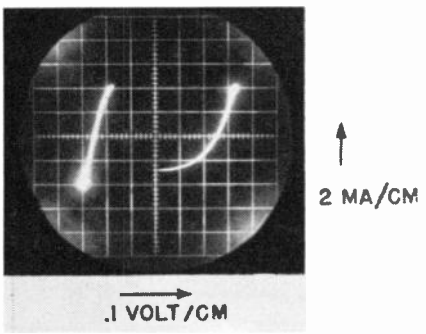

Fig. 3—Gallium antimonide tunnel diode I-V characteristic.

The power output, conversion efficiency and the results of operation of higher carrier frequencies will be reported in the near future.

L. U. Kibler
Bell Telephone Labs., Inc.
Holmdel, N. J.

* Received by the IRE, April 12, 1961.

[1] C. A. Burrus, "Gallium antimonide Esaki diodes for high frequency applications," to be published.

[2] C. A. Burrus, "Esaki diodes for high frequency applications," to be published in *J. Appl. Phys.*

[3] A. F. Dietrich, "8 and 11 Gc nanosecond pulses produced by harmonic generation," accepted for publication in Proc. IRE.

Circuit Control of Tunnel Diode Negative-Resistance Characteristics*

The February, 1961, Paris Conference on Semiconductor Devices included a discussion by S. Amer and W. Fulop concerning a distributed junction tunnel diode in which lateral current flow in one degenerate region, provided with two ohmic contacts, controlled the tunnel negative-resistance curve. This parallels some studies at the Carnegie Institute of Technology in which the emphasis has been on similarly controlling several small area junctions alloyed to the same wafer, or a number of separate lumped circuit elements. Long rectangular junctions involve inconveniently large peak currents and capacitances, and appear to us to possess no compensating advantages.

A typical circuit studied is shown in Fig. 1 where I_d and V_d represent the output quantities, while I_c and V_c are the control parameters. Current I_c in the resistances R_{c1} and R_{c2} biases the individual tunnel junctions, and results in output characteristics with controlled variation of negative resistance as shown in Fig. 2. The resistances R_{c1} and R_{c2} are usually chosen about equal to the negative resistance of a single junction: for example, 300 ohms for the germanium $\frac{1}{3}$-ma peak current units of Fig. 2. The cur-

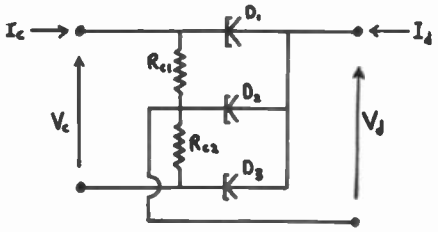

Fig. 1—Three-diode circuit giving control of the tunnel characteristics I_d and V_d.

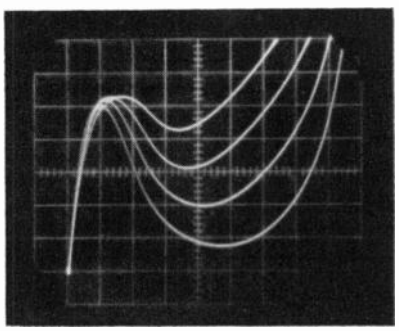

Fig. 2—Tunnel diode current I_d vs voltage V_d for control currents I_c of 0.4, 0.65, 0.9, and 1.15 ma with the circuit of Fig. 1. Vertical and horizontal scales are 0.2 ma and 50 mv per large division respectively.

* Received by the IRE, April 14, 1961.

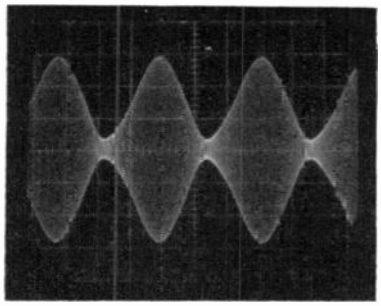

Fig. 3—Modulation of a 100-kc oscillation produced by a sinusoidal control signal superimposed on I_c in Fig. 1. The vertical and horizontal scales are 50 mv and 5 msec per large division, respectively.

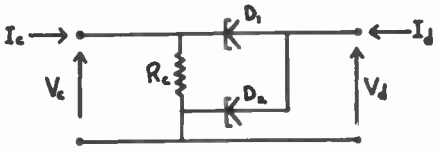

Fig. 4—Two-diode control circuit with common input-output line.

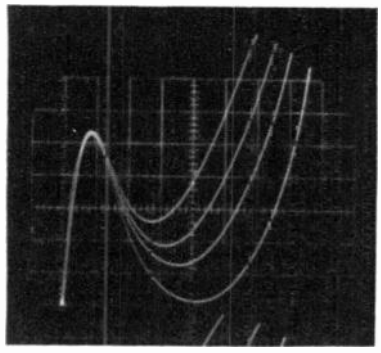

Fig. 5—Tunnel diode current I_d vs voltage V_d for control current I_c values of 0.40, 0.55, 0.70, and 0.85 ma in Fig. 4. Vertical and horizontal scales are 0.1 ma and 50 mv per large division, respectively.

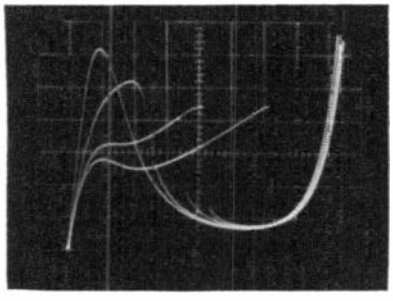

Fig. 6—Control characteristics I_d vs V_d obtained with the circuit of Fig. 4. R_c values are 0, 125, 300, and 550 ohms with $I_c=0$. Vertical and horizontal calibrations are 0.1 ma and 50 mv per large division, respectively.

rent required for full control tends to be about the same magnitude as the peak tunnel current that is controlled. If higher sensitivity is required, the possibility exists for field-effect transistor or bipolar transistor control of I_c.

The control of negative resistance and peak-to-valley ratio that has been demonstrated makes possible many useful circuit functions including variable gain amplification, variable swing relaxation oscillators, and variable threshold switching gates. Fig. 3 illustrates amplitude modulation of a 100-kc oscillation obtained with an LC tank circuit and dc bias in series with the output terminals of Fig. 1, and 60-cps modulation of I_c.

If a common input-output line is required, the even simpler two diode circuit of Fig. 4 is available. Here, there is a little more difficulty in selecting diodes to give the characteristic change required. Fig. 5 shows the curves obtained for matched 0.25 ma peak-current germanium-tunnel diodes with R_c about 200 ohms, and I_c as the parameter. Curves of unusual shape may be produced by a deliberate mismatching of the diodes with respect to characteristics or material. The magnitude of R_c is also a control factor as shown in Fig. 6, where the diodes are mismatched by 2:1, the control current is zero, and R_c is changed in steps to several times the normal value.

Partial support of these studies by the Westinghouse Semiconductor Division, Youngwood, Pa., is gratefully acknowledged.

W. N. Carr
A. G. Milnes
Dept. of Elec. Engrg.
Carnegie Inst. Tech.
Pittsburgh, Pa.

Sensitivity of the Degenerate Parametric Amplifier*

The noise temperature of a degenerate parametric amplifier (double channel) is approximately equal to half that for a nondegenerate amplifier[1] using the same varactor at the same signal frequency and pumped at its optimum pump frequency. The optimum pump frequency (for minimum noise) in a nondegenerate amplifier is approximately equal to γf_{co}, where γ is a capacitance modulation coefficient[1] and f_{co} is the cutoff frequency for the mean operating capacity. For good varactors at the present day, γf_{co} is well above 20 kMc. For radiometric applications, there is thus an advantage in using a degenerate amplifier rather than a nondegenerate one requiring a high pump frequency.

A degenerate parametric amplifier has its input circuit tuned to half the pump frequency f_p, so that the signal and "idler" frequency channels coincide. For a signal at frequency f, the amplified output consists of a component reflected from the input at frequency f, and a component converted to (f_p-f). For high gain these components are equal in amplitude and have in general equal band-pass characteristics symmetric with respect to the frequency $\frac{1}{2}f_p$. If the input is noise, the result is that the noise in the frequency band below $\frac{1}{2}f_p$ is fully correlated with the noise in the frequency band above $\frac{1}{2}f_p$. This correlation can be shown to lead to an increase in the post-detector fluctuations, and so to an increase in the minimum detectable signal.

The reflected narrow-band noise signal can be represented by

$$X_R(t) = X_c(t)\cos\tfrac{1}{2}\omega_p t + X_s(t)\sin\tfrac{1}{2}\omega_p t, \quad (1)$$

where $X_c(t)$ and $X_s(t)$ are independent, slowly fluctuating quantities which have equal rms values and equal normalized autocorrelation functions, $c(s)$. For a pump waveform $\cos(\omega_p t+\phi_p)$, a reflected Fourier component $A_n\cos(n\omega t+\phi_n)$ is accompanied at high gain by a converted component $A_n\cos(\omega_p t-n\omega t-\phi_n+\phi_p)$. Then the degenerate noise output, which is the sum of the reflected and converted components, can be represented by

$$X_D(t) = 2X_a(t)\cos(\tfrac{1}{2}\omega_i t + \tfrac{1}{2}\phi_p), \quad (2)$$

where

$$X_d(t) = X_c(t)\cos\tfrac{1}{2}\phi_p - X_s(t)\sin\tfrac{1}{2}\phi_p$$

and so has the same autocorrelation function as $X_c(t)$ and $X_s(t)$. The post-detector noise fluctuations can be calculated most easily in the case of a quadratic detector followed by an RC filter of time constant τ. If the relative rms fluctuation in the filtered output is $\sqrt{\alpha}$,[2] then when the degenerate noise output (2) is applied to the detector, we have

$$\alpha \doteq 2/\tau\int_0^\infty c^2(s)ds,$$

which is just twice as large as in the case when only the nondegenerate noise signal (1) is applied to the detector.

The increase in the post-detector fluctuations in a degenerate amplifier by a factor $\sqrt{2}$ has been verified experimentally. Since α is inversely proportional to the amplifier bandwidth, the effective bandwidth for noise may be thought of as halved for the degenerate noise output.

If we therefore compare a degenerate amplifier with an optimum nondegenerate amplifier using the same varactor, we find that the capability of detecting a weak noise signal is only $\sqrt{2}$ better in the degenerate case if the signal bandwidths are equal. Another case is that where a degenerate amplifier is followed by a receiver with a pass band narrower than that of the amplifier, which is of practical concern for multiple-tuned[3,4] amplifiers. When the receiver is tuned completely to one side of $\frac{1}{2}f_p$

* Received by the IRE, April 7, 1961. This work has been carried out under the auspices of the Netherlands Foundation for Radio Astronomy [supported by the Netherlands Organisation for Pure Research (ZWO)] and the Radiophysics Laboratory of CSIRO, Australia.

[1] K. L. Kotzebue, "Optimum noise performance of parametric amplifiers," Proc. IRE, vol. 48, pp. 1324–1325; July, 1960.

[2] A. van der Ziel, "Noise," Prentice-Hall, Inc., New York, N. Y., ch. 13; 1954.

[3] B. T. Vincent, "A high-performance X-band parametric amplifier," Proc. IRE, vol. 49, pp. 511–512; February, 1961.

[4] A. G. Little, "A wide band single diode parametric amplifier using filter techniques," Proc. IRE, in press.

("quasi-degenerate"), the sensitivity for wide-band noise will be $\sqrt{2}$ better than when the receiver is centered on $\frac{1}{2}f_p$, provided that the antenna and circulator can pass both the signal and "idler" frequencies. These comparisons hold whatever the value of the antenna temperature.

The increase in the noise fluctuations is a particular case of the limitations imposed by the loss of spectral information when a degenerate amplifier is used.

J. T. DE JAGER
B. J. ROBINSON
Radio Observatory
Dwingeloo
The Netherlands

Stability Criteria for Tunnel Diodes*

The tunnel diode provides network designers with a simple and practical two-terminal negative resistance device whose equivalent circuit, when operating in the linear mode, is that shown in Fig. 1. This representation appears to be valid up to at least 10 kMc. In several recent papers[1-4] devoted to the analysis of amplifiers incorporating tunnel diodes in a passive environment, it has been shown that large gains, wide bandwidths and relatively low noise figures are compatible and achievable with practical configurations.

In order that a two-terminal element, $z_d(p)$, be usable as a basic component in the synthesis of an amplifier, it must be capable of operating in a stable manner under at least one passive termination (Fig. 2). This leads to the following definition.

Definition: A two-terminal device, $z_d(p)$, is *potentially stable* if there exists at least one finite positive real function $Z(p)$ such that the equation

$$Z(p) + z_d(p) = 0 \tag{1}$$

has no solutions in the closed right-half p-plane, Re $p \geq 0$. $Z(p)$ is said to stabilize $z_d(p)$. In the contrary case, $z_d(p)$ is called *totally unstable*

Thus, if $Z(p)$ stabilizes $z_d(p)$, the current I circulating in the closed loop of Fig. 2 is zero for all p in Re $p \geq 0$. On the other hand, a totally unstable $z_d(p)$ will always oscillate (or burn out) when placed in a passive environment and therefore is useless as far as linear controlled amplification is concerned.

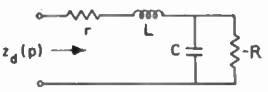

$0 \leq r$ = junction spreading resistance, Ω
$0 \leq L$ = series inductance, h
$0 \leq C$ = junction capacitance, f
$0 \leq R$ = magnitude of negative resistance shunting C, Ω

Fig. 1—Equivalent circuit of a tunnel diode operating in the linear mode.

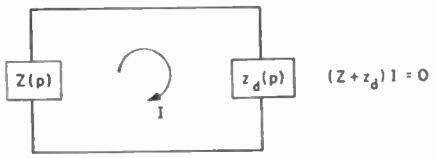

$Z(p)$ = passive impedance
$z_d(p)$ = 2-terminal active device

Fig. 2—Schematic illustrating the meaning of potential stability.

Here we collate and discuss various stability criteria for the tunnel diode depicted in Fig. 1. The results are stated in the form of theorems and all proofs are omitted.

Theorem 1: The two conditions

$$\frac{r}{R} < 1 \tag{2}$$

and

$$\frac{L}{R^2C} < 3 \tag{3}$$

are both necessary for the potential stability of a tunnel diode.

The first inequality (2) is automatically satisfied for all present-day commercially available diodes ($r/R \approx 0.01$), but the second is not and must be checked. For example, the GE ZJ61-22 diode which is ordinarily used in high-speed switching applications has a ratio $L/R^2C = 3.75$.

Theorem 2:[1] For dissipationless tunnel diodes ($r=0$), the condition

$$\frac{L}{R^2C} < 3 \tag{4}$$

is necessary and sufficient for potential stability.

The authors previously gave a rigorous derivation of (4) and proved its sufficiency by exhibiting a stable reflection amplifier design.[1] Now, of course, r is never zero, so that Theorem 2 does not quite cover all practical situations. The next theorem is much sharper; but before stating it, it is necessary to introduce some abbreviations:

$$f_r = \frac{1}{2\pi RC}\sqrt{\frac{R}{r} - 1} \tag{5}$$

$$\theta = \frac{1}{2\pi f_r RC} = \sqrt{\frac{r/R}{1 - r/R}}, \tag{6}$$

$$F(\theta) = \frac{\theta^3}{1+\theta^2} \cdot \frac{1}{\theta - \arctan\theta}. \tag{7}$$

where f_r is the familiar resistive cutoff frequency. The function $F(\theta)$ plays a leading role in Theorem 3 and is plotted in Fig. 3 as a function of the parameter r/R. Note that its maximum value, 3, is attained for $r=0$ and its minimum value, 1, for $r=R$. The transition between the two extremes is monotonic.

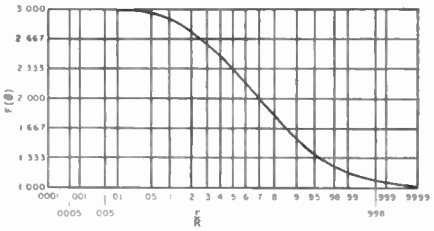

r = junction resistance, Ω
L = series inductance, h
C = junction capacitance, f
R = magnitude of negative resistance, Ω
$L < F(\theta)$.
R^2C

Fig. 3—Plot of $F(\theta)$ vs r/R.

Theorem 3:[5] For a tunnel diode, the two conditions

$$\frac{r}{R} < 1 \tag{8}$$

and

$$\frac{L}{R^2C} < F(\theta) \tag{9}$$

are both necessary for potential stability.

The inequality (8) is the same as (2) and contributes nothing new. But since $F(\theta) \leq 3$, Theorem 3 improves Theorem 1. Work now in progress seems to indicate that (8) and (9) are actually necessary and sufficient. This conjecture is true when $r=0$, for then $\theta = 0$, $F(\theta) = 3$ and (9) collapses into $L/R^2C < 3$, which according to Theorem 2 is indeed necessary and sufficient for potential stability. For additional discussion, the reader should consult the authors' report.[5] To date, (8) and (9) appear to be the most complete set of criteria available for checking stability of a general tunnel diode.

To see how Theorem 3 works, consider the Hoffman HT-10 tunnel diode. The corresponding parameters (typical values) are

$r = 1\ \Omega$
$L = 20\ \text{m}\mu h$ (at 1/4-inch lead length)
$C = 10\ \mu\mu f$
$R = 39\ \Omega (\pm 20$ per cent).

By direct calculation, $r/R = 0.025$, $L/R^2C = 1.32$ and $F(\theta) = 2.97$. Thus, $L/R^2C < F(\theta)$ and the diode may be potentially stable. Observe that Hines' test (Theorem 4) is not applicable.

The next and final theorem is probably the earliest known sufficient condition for the potential stability of a tunnel diode.

* Received by the IRE, March 31, 1961. The work reported in this paper was sponsored by the Rome Air Dev. Ctr. Air Res. and Dev. Command under Contract No. AF-30(602)-2213.

[1] L. I. Smilen and D. C. Youla, "Exact theory and synthesis of a class of tunnel diode amplifiers," *Proc. NEC* vol. 16, pp. 376–404; October, 1960.

[2] D. C. Youla and L. I. Smilen, "Optimum negative resistance amplifiers," *Proc. Symp. on Active Networks and Feedback Systems*, Polytechnic Inst. of Brooklyn, Brooklyn, N. Y., vol. 10, pp. 241–318; April, 1960.

[3] H. J. Carlin and D. C. Youla, "Network synthesis with negative resistors," *Proc. Symp. on Active Networks and Feedback Systems*, Polytechnic Inst. of Brooklyn, Brooklyn, N. Y., vol. 10, pp. 27–67; April, 1960.

[4] E. W. Sard, "Gain-bandwidth performance of maximally flat negative resistance amplifiers," *Proc. Symp. on Active Networks and Feedback Systems*, Polytechnic Inst. of Brooklyn, Brooklyn, N. Y., vol. 10, pp. 319–344; April, 1960.

[5] L. I. Smilen and D. C. Youla, "On the Stability of Tunnel Diodes," Networks and Waveguide Group, Microwave Res. Inst., Polytechnic Inst. of Brooklyn, Brooklyn, N. Y., Memorandum 49, PIBMRI-889-61; in preparation.

Theorem 4:[6] The two conditions

$$r < R \tag{10}$$

and

$$\frac{L}{R^2C} < 1 \tag{11}$$

are sufficient for the potential stability of a tunnel diode. Moreover, the diode may be stabilized with a positive resistor R_s. Any value of R_s satisfying the inequalities

$$1 > \frac{r + R_s}{R} > \frac{L}{R^2C} \tag{12}$$

suffices.

Since the minimum value of $F(\theta)$ is unity, any diode satisfying (10) and (11) certainly passes the test of Theorem 3. Hence, if Theorem 3 can be proved sufficient as well as necessary, it will contain Theorem 4 as a corollary. Any new results will be reported in future letters.

L. I. Smilen
Microwave Res. Inst.
Polytechnic Inst. of Brooklyn
Brooklyn, N. Y.
D. C. Youla
Dept. of Elec. Engrg.
Polytechnic Inst. of Brooklyn,
Brooklyn, N. Y.

[6] M. E. Hines, "High-frequency negative-resistance circuit principles for Esaki diode applications," *Bell Sys. Tech. J.*, vol. 39, pp. 477–513; May, 1960.

On the Possibility of Drift-Tunnel Oscillations in High-Power Klystrons*

During the design and development of the Stanford University high-power klystron [1] in 1953, some 5.2-cm wavelength (5770 Mc) spurious signals were radiated from both input and output terminals with no RF drive signal applied. These spurious signals were accurately measured and they were not second harmonics of the design frequency of the klystron. Tuning the klystron cavities changed the frequency and amplitude of the spurious oscillations. It is conjectured that the oscillation frequencies are governed by 1) the dimensions of the drift tunnels, 2) the internal geometry of the terminating cavities, and 3) a negative resistance derived from long transit angles of a transversally-displaced electron beam in the drift tunnel.

Negative resistances have been generated between cathode and anode in planar [2, 3] and inverted spherical [4] diodes when the electron transit time is about $n+\frac{1}{4}$ ($n=1, 2, 3 \cdots$) RF cycles. In these diodes the direction of the RF electric field is substantially in the direction of the electron beam.

In a different type of electron tube, where the RF electric field is perpendicular to the direction of the electron beam, Fank [5] has calculated that negative resistances can be generated provided a transversally-displaced electron beam can deliver energy to a fringing longitudinal RF electric field after a transit time of $n+\frac{1}{4}$ RF cycles. For the present analysis of the Stanford klystron, Fank's parallel-plate gap can be replaced by a circular drift tunnel which supports a resonant transverse-electric $TE_{11}°$ mode and the qualitative behavior is quite similar in the two configurations. Thus, negative resistances may be generated when the transit time in the tunnel is $n+\frac{1}{4}$ cycles. This infers that drift tunnel oscillations should depend on beam voltage.

In a circular waveguide, the cutoff frequency f_c of the dominant $TE_{11}°$ mode is given by

$$f_cD = 6917\text{-Mc inches},$$

where

f_c = cutoff frequency, megacycles,
D = diameter, inches.

The normalized resonant frequency of an open-ended circular waveguide neglecting fringing fields is given by

$$\frac{f}{f_c} = \sqrt{1 + \left(\frac{mc}{2Lf_c}\right)^2} = \sqrt{1 + 0.728\left(\frac{mD}{L}\right)^2}, \tag{1}$$

where

m = integer, number of half-guide wavelengths,
c = velocity of light, 1.1802×10^{10} inches per second,
L = tunnel length, inches.

Eq. (1) is plotted in Fig. 1 for convenience.[1] In a klystron, the cavities terminating the drift tunnels will present impedances differing from that of an open circuit. Hence, the resonant frequency of the tunnel may differ from that given by (1) and cavity tuning should vary the tunnel resonant frequency.

As stated above, negative resistances may be generated when the transit time is approximately equal to $n+\frac{1}{4}$ RF cycles. Thus a frequency f which will meet this criterion under relativistic conditions [6] can be determined from the following:

$$\frac{fL}{n + 0.25} = 11.802\sqrt{1 - 1/(1 + V/511)^2}\ \text{Mc}. \tag{2}$$

where

V = beam voltage, kilovolts.

For convenience, (2) is plotted in Fig. 2.[1] Since the frequencies which yield negative resistance occur in narrow bands [2–4], (2) gives only approximate values.

In the Stanford klystron, $D = 1.25$ inches, $V = 400$ kv and the drift tunnels were 3.94 and 7.88 inches long. Using Figs. 1 and 2, the data shown in Table I was obtained. The frequencies below 5540 Mc cannot propagate in the 1.25-inch diameter tunnel. This tabulation leads to the conclusion that the 5770-Mc oscillation is associated with the $m=1$ and $n=2$ conditions in the shorter drift tunnel.

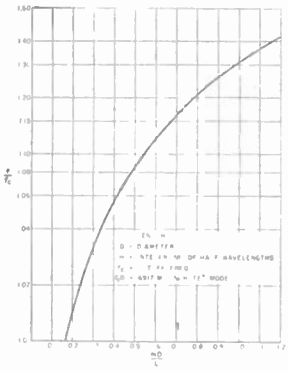

Fig. 1—Normalized resonant frequency of $TE_{11}°$ mode in circular drift tunnel.

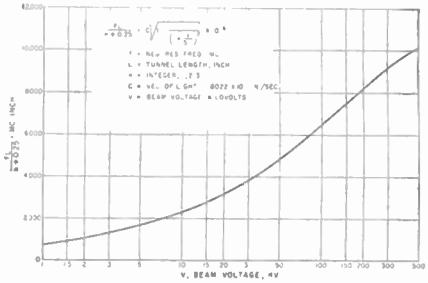

Fig. 2—Negative resistance frequencies in drift tunnel.

TABLE I

Tunnel Length		3.94-inch	7.88-inch
Tunnel Resonant Frequencies	$m=1$	5740 Mc	5590 Mc
	$m=2$	6300	5740
	$m=3$	7150	5985
Negative Resistance Frequencies	$n=1$	3100 Mc	1550 Mc
	$n=2$	5580	2790
	$n=3$	8120	4060
	$n=4$	—	5260
	$n=5$	—	6500

It appears that a large ratio of beam-to-tunnel diameters will yield a larger magnitude of negative resistance than will a small ratio and, hence, larger beams will more likely cause oscillations. A stronger longitudinal magnetic focusing field will reduce the amount of transverse beam displacement which in turn reduces the value of negative resistance. The Q of the tunnel resonant mode is also significant, and proximity to cutoff will result in a lower Q. A comprehensive analysis of the problem, although desirable, is beyond the scope of the present paper.

There is little question that these spurious oscillations with large amplitudes can adversely affect the performance of a klystron since the beam is coupled to both fundamental and spurious frequencies. The adverse effect may be phase and amplitude in-

* Received by the IRE, April 11, 1961.

[1] Full-size copies of the original with fine grid may be obtained from the author.

stability at the fundamental frequency. It is also conceivable that beam interception may increase, and the maximum RF efficiency would undesirably decrease.

K. TOMIYASU
General Engrg. Lab.
General Electric Co.
Schenectady, N. Y.

REFERENCES

[1] M. Chodorow, E. L. Ginzton, I. R. Neilsen, and S. Sonkin, "Design and performance of a high-power pulsed klystron," PROC. IRE, vol. 41, pp. 1584–1602; November, 1953. See especially p. 1601.
[2] F. B. Llewellyn and A. E. Bowen, "The production of ultra-high frequency oscillations by means of diodes," *Bell Sys. Tech. J.*, vol. 18, pp. 280–291; April, 1939.
[3] F. B. Llewellyn, "Electron Inertia Effects," Cambridge University Press, London, Eng., 2nd ed., chs. 3 and 5; 1943.
[4] K. Tomiyasu and M. P. Forrer, "Diode oscillations in high voltage klystrons," submitted for publication.
[5] B. Fank, "Investigation of the Transverse-Field Klystron," Stanford Electronics Labs., Stanford University, Calif., Tech. Rept. No. 305-1; March 10, 1958.
[6] W. W. Harman, "Special relativity and the electron," PROC. IRE, vol. 37, pp. 1308–1314; November, 1949.

Noise in Beam-Type Parametric Amplifiers*

Beam-type parametric amplifiers employing separate input and output couplers or transducers are matched and unconditionally stable.[1] The reason, as is well known, is that the beam passively loads the transducers and is capable of carrying signal power only in the direction of drift. Thus the combination of beam and properly matched lossless transducers can be thought of as a perfect isolator.[2] The property of an isolator radiating thermal noise only in the direction of isolation is preserved, since the input transducer strips existing fast wave noise from the beam and sends it to the generator load. Ideally, no beam noise appears in the output transducer.

The purpose of this letter is to point out that the above picture must be modified to include a small frequency-dependent forward attenuation which arises because of the finite electron temperature and size of the beam. The following comments will be restricted to the transverse beam modes in O-type geometry. The culprit in the following model is the axial velocity spread. Signal power is transferred to a mode on the beam by a transducer and is distributed among a large number of beamlets, each associated with a different axial velocity class. As a result of the variation in velocities, a phase slip occurs among the beamlets which decreases the available signal power; that is, the power can no longer be completely coupled out of the beam. This is equivalent to attenuation. At the same time, noise appears on the beam at a rate which depends on the intrinsic noise temperature of the mode in question and the amount of attenuation. Lea-Wilson[3] and Kompfner[4] have noted that an axial velocity spread will introduce noise into the cyclotron wave.

We find that the attenuation $\alpha(l)$ for a beam that has drifted a distance l is given by

$$\alpha(l) = \left| \sum_{n=1}^{N} (I_n/I_0) \exp - i\beta_n l \right|^2 \qquad (1)$$

in which I_0 is the total beam current, I_n is the current of the nth beamlet, β_n is the propagation constant of the mode determined from the velocity of the nth beamlet, and N is the total number of velocity classes or beamlets.

The noise temperature of the beam at l is found to be

$$T(l) = \alpha(l)T(0) + [1 - \alpha(l)]T_i \qquad (2)$$

in which $T(0)$ is the noise temperature at $l=0$ and T_i is the intrinsic noise temperature for the mode in question. For the cyclotron modes $T_i=(\omega/\omega_c)T_{e\perp}$ in which ω is the angular noise frequency, ω_c is the electron cyclotron frequency and $T_{e\perp}$ is the transverse electron temperature. For the synchronous modes, $T_i=m\omega\omega_c D^2/8k$ for a uniform cylindrical beam of diameter D, in which m is the electron mass and k is Boltzmann's constant. The above expressions are valid for beams whose diameter is small compared to the wavelength of the transverse mode. Eq. (2) follows from consideration of beam dynamics and is identical to the expression for a transmission line attenuator at temperature T_i.

The noise temperature of the beam as it leaves the gun is not necessarily equal to T_i, although the noise temperature immediately in front of the cathode equals T_i, as has been shown by Adler and Wade[5] for cyclotron waves. T_i is invariant for slow changes in magnetic field and increases for rapid changes.[6]

The attenuation has been evaluated for three cases:

Case I. Thermal Axial Velocity Spread

$$\alpha(l) = [1 + (kT_{e\parallel}/mv_0^2)^2\beta_0^2 l^2]^{-1} \qquad (3)$$

in which $T_{e\parallel}$ is the longitudinal electron temperature, v_0 is the average drift velocity of the beam and β_0 the average propagation constant; $\beta_0=(\omega-\omega_c)/v_0$ for the cyclotron modes, $\beta_0=\omega/v_0$ for the synchronous modes.

Case II. Potential Depression Resulting From Space Charge

$$\alpha(l) \simeq \sin^2\theta/\theta^2, \quad \theta = \beta_q^2 l^2 \beta_0 l/32 \qquad (4)$$

in which $\beta_q=\omega_q/v_0$, ω_q being the plasma frequency.

Case III. Single-Anode Plane-Parallel Gun

$$\alpha(l) \simeq \sin^2\phi/\phi^2, \qquad \phi = 4\pi\theta. \qquad (5)$$

In most cases, thermal velocity spreads produce the largest attenuation. In all cases, $1-\alpha$ increases for increasing relative velocity spread.

Note that in degenerate Adler tubes[1] for which $\beta_0=0$, at centerband, there is no appreciable attenuation arising from velocity spread. If the magnetic field is not perfectly uniform, noise from this source can be observed since β_0 is not everywhere zero. Ashkin[7] has observed noise which can be attributed to this effect for a low-drift energy beam (<2 ev).

In nondegenerate amplifiers for which at least one of the signal or idler waves has $\beta_0\neq 0$, the noise arising from axial velocity spread may not be trivial.[8] One obvious solution is an increase of the beam drift energy since the relative velocity spread decreases. However, this can be carried only so far since the pumping process converts synchronous wave noise into cyclotron wave noise in an amount proportional to beam drift energy. This follows from the known fact that the increase in the input noise temperature of the amplifier from the synchronous wave mixing is

$$\Delta T = (Xv_0/L\omega_c)^2[T(\omega_s) + T(\omega_i)(\omega_s/\omega_i)] \qquad (6)$$

in which $T(\omega_s)$ and $T(\omega_i)$ are the noise temperatures of the slow synchronous wave at the signal and idler frequency and L is the pump length. The quantity X is given by $X=\cosh^{-1}\exp(G/8.68)$, in which G is the decibel gain in the quadrupole section; $X=3$ for $G=20$ db. The factor $(Xv_0/L\omega_c)^2$ is of order 10^{-3} in Ashkin's tube[7] and 10^{-2} in Adler's tube.[1] In either case, the noise contribution should be of order 10°K.

It is worth noting from (2) that the noise temperature of the transverse waves always can be made equal to the intrinsic noise temperature. This can be done by providing suitable low-velocity drift regions in which $B_0\neq 0$.

One can use the beamlet concept to compute the increase in input noise temperature which results when electrons, because of their thermal velocity spread, are pumped unequally as proposed by Ashkin.[7] For $\beta_0=0$ it can be shown that

$$\Delta T = \tfrac{1}{4}X^2 \tanh^2 X[2kT_e/mv_0^2]^2 T_i. \qquad (7)$$

For Ashkin's tube with a 10-volt beam and $kT_e=0.1$ ev, $\Delta T \geqq 2\times 10^{-4}\ T_i$. Since for the cyclotron waves $T_i \simeq 10^{3}$°K, $\Delta T \simeq 0.2$°K. For Adler's tube, with a 3.8-ev beam, $\Delta T \simeq 2$°K.

EUGENE I. GORDON
Bell Telephone Labs., Inc.
Murray Hill, N.J.

* Received by the IRE, April 24, 1961.

[1] R. Adler, G. Hrbek, and G. Wade, "The quadrupole amplifier, a low-noise parametric device," PROC. IRE, vol. 47, pp. 1713–1723; October, 1959.
[2] G. L. Cuccia, "An electron coupler," *RCA Rev.*, vol. 10, pp. 270–303; June, 1949.
[3] C. P. Lea-Wilson, "Some possible causes of noise in Adler tubes," PROC. IRE (Correspondence), vol. 48, pp. 255–256; February, 1960.
[4] R. Kompfner, private communication; 1960.
[5] R. Adler and G. Wade, "Beam refrigeration by means of large magnetic fields," *J. Appl. Phys.*, vol. 31, pp. 1201–1203; July, 1960.
[6] E. I. Gordon, "Transverse electron beam waves in varying magnetic fields," *Bell Sys. Tech. J.*, vol. 39, pp. 1603–1616; November, 1960.
[7] A. Ashkin, "A low-noise microwave quadrupole amplifier," PROC. IRE, vol. 49, pp. 1016–1019; June, 1961.
[8] R. Adler and B. Crumley, private communication; 1960.

Pull-In Frequency of the Phase-Controlled Oscillator*

If a phase-locked oscillator is mistuned far enough to throw it out of lock, and the mistuning is then slowly decreased, a point is reached where the oscillator synchronizes with the input signal. The value of mistuning for which this occurs is called the pull-in frequency.

Recently, Rey[1] presented a derivation of the pull-in frequency of a phase controlled oscillator with a sinusoidal comparator. He assumes that, in the marginal asynchronous case, the time derivative of the phase error is zero when the phase comparator output is maximum.

Goldstein[2] analyzed the case of the sawtooth comparator with a phase lag filter (Fig. 1), and found the stable asynchronous mode with the lowest mistuning frequency. In this marginal mode, in general, the phase error approaches the comparator discontinuity with a nonzero, positive slope. The pull-in frequency derived by Goldstein is appreciably lower than that resulting from the zero slope assumption, except for the degenerate RC filter case ($R_2=0$). In this special case, the assumption is correct.

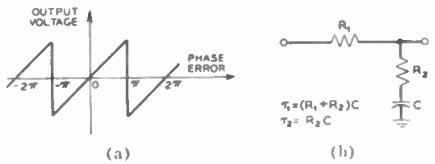

Fig. 1 — (a) Sawtooth comparator. (b) Phase lag filter.

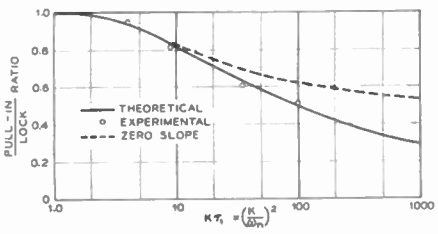

Fig. 2—Normalized pull-in frequency of the phase-controlled oscillator with a sawtooth comparator and phase lag filter. The damping ratio is unity.

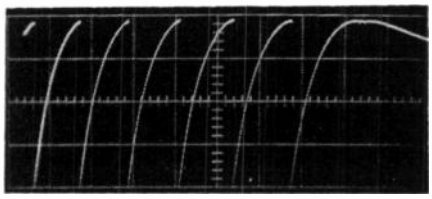

Fig. 3—Phase error during pull-in. The mistuning frequency has been slowly decreased below the pull-in frequency just before this picture was taken. The mistuning was constant during the time shown.

* Received by the IRE, March 6, 1961.

[1] T. J. Rey, "Automatic phase control: theory and design," PROC. IRE, vol. 48, pp. 1760–1771; October, 1960.

[2] A. J. Goldstein and C. J. Byrne, "The phase-controlled loop with a sawtooth comparator," *1960 Northeast Electronics Res. and Engrg. Mtg. Convention Record*, pp. 64–65; November, 1960.

An experimental investigation by Byrne has shown that Goldstein's values of pull-in are correct (Fig. 2), and that the marginal asynchronous mode has the properties predicted by him. When the mistuning is decreased below the marginal value, the mode becomes unstable. After passing through several discontinuities, the circuit synchronizes with the input signal (Fig. 3). The mode with zero slope was not observed. This mode is unstable.

We conclude that, for the case of the sawtooth comparator with a phase lag filter, the assumption of zero slope yields only an upper bound for the pull-in range, and Goldstein's analysis must be used instead.

We do not know whether a similar effect occurs in the case of the sinusoidal comparator, but the possibility should be recognized. Rey has published experimental data which indicates that any error due to his assumptions is small in the region investigated.

A. J. GOLDSTEIN
C. J. BYRNE
Bell Telephone Labs.,
Murray Hill, N. J.

Fourier Series Derivation: A Comment*

Gadsden,[1] in a rebuttal to a note by Ferris,[2] invites comment on the validity of a term-by-term inversion of an infinite series of transforms. This is done very simply in the light of distribution theory[3] which, of course, should have been used by both authors all along. Their quibbles and difficulties with such worn out problems show how little of the modern theory of transforms is known by the people who would most benefit by it.

The famous theorem that, in distribution theory, all convergent infinite series of integrable functions, measures, and/or distributions are always differentiable term by term, is sufficient proof of the validity of the term-by-term inversion. In any case, one can directly derive the Fourier series from the Fourier transform. A periodic function is of the form

$$T = (Y_0 - Y_h)T_* \sum_n \delta_{nh} \qquad (1)$$

where Y_h is Heaviside's step function starting at x equal h, and δ_{nh} is Dirac's delta function placed at x equal nh. The star is for convolution product.

Now the Fourier transform of the Dirac delta function is

$$F\delta_h(x) = \exp - 2i\pi(h\cdot y). \qquad (2)$$

* Received by the IRE, April 21, 1961.

[1] C. P. Gadsden, "Discussion of Fourier series derivation," PROC. IRE, vol. 49, pp. 828–829; April, 1961.

[2] C. D. Ferris, "Discussion of Fourier series derivation," PROC. IRE, vol. 49, pp. 827–828; April, 1961.

[3] L. Schwartz, "Théorie des Distributions," vols. 1 and 2, Herman and Co., Paris, France; 1950.

so that

$$F\left(\sum_n \delta_{nh}(x)\right) = \sum_n \exp - 2i\pi(nh\cdot y). \qquad (3)$$

But the right-hand side is well known to be

$$\sum_n \exp - 2i\pi(nh\cdot y) = h\sum_n \delta_{nh}(y). \qquad (4)$$

thus

$$F\left(\sum_n \delta_{nh}(x)\right) = \frac{1}{h}\sum_n \delta_{nh}(y). \qquad (5)$$

The Fourier transform of (1) is thus

$$FT = \frac{1}{h}\left(\sum_n \delta_{nh}(y)\right) F((Y_0 - Y_h)T), \qquad (6)$$

or

$$FT = \frac{1}{h}\sum_n \delta_{nh}(y) \cdot\left(\int_0^h T(\exp - 2i\pi(x\cdot nh))dx\right). \qquad (7)$$

The integrals are independent of y and x. They are constants in the inverse transformation. Because the inverse Fourier transform of the Dirac delta function is

$$\bar{F}\delta_h(y) = \exp 2i\pi(h\cdot x), \qquad (8)$$

one obtains from (7)

$$T = \frac{1}{h}\sum_n (\exp 2i\pi(x\cdot nh)) \cdot\left(\int_0^h T(\exp - 2i\pi(x\cdot nh))dx\right), \qquad (9)$$

which is the usual form of the Fourier series.

The integrals in (9) having a finite domain of integration will be meaningful for any integrable function, measure or distribution T. The right-hand side of (9) must, however, be convergent when projected on the ϕ functions of the Class D defined as: all continuous functions with compact domains which are indefinitely differentiable, and such that the derivatives also belong to the class. The class must also be endowed with a pseudotopology to the effect that a convergent sequence of ϕ functions can be differentiated term by term any chosen number of times, provided the domains of the ϕ functions are all subsets of the same compact subset of the continuum.[3]

Projecting (9) on a ϕ function

$$T(\phi) = \frac{1}{h}\sum_n\left[\int_R (\exp 2i\pi(x\cdot nh))\phi(x)dx\right] \cdot\left(\int_0^h T(\exp - 2i\pi(x\cdot nh))dx\right), \qquad (10)$$

with R for the continuum. The terms on the right-hand side are always meaningful. The series, however, must be convergent (equal to zero or to a finite value) for all ϕ's of the Class D. It is sufficient, however, to choose ϕ functions with quasi-punctual domains.

Finally, all trigonometric series are Fourier series. The ones which are not Fourier series of periodic integrable functions or measures are Fourier series of periodic distributions.

P. A. CLAVIER
Aeronutronic
Newport Beach, Calif.

Traveling-Wave Maser with Instantaneous Bandwidths in Excess of 100 Mc*

An *S*-band traveling-wave maser has been operated with 3-db amplification bandwidths as great as 126 Mc centered at a frequency of 2280 Mc, with electronic gains greater than 16 db. The maser utilized a comb-type slow-wave structure loaded on both sides of the comb with 6½ inches of X-ray oriented ruby of nominal 0.05 per cent chromium concentration. The external magnetic field was oriented at $\theta = 90°$ to the ruby c axis, and the helium bath temperature was 1.8°K.

These broad bandwidths, more than twice the nominal 60-Mc intrinsic linewidth of ruby,[1] were obtained by stagger-tuning the applied external magnetic field (H_{dc}). The staggered field causes the imaginary part of the magnetic susceptibility $\chi''(f)$, which is usually assumed to have a Lorentzian line shape, to broaden and take on a new effective shape dependent upon the distribution of the magnetic field. This results in a corresponding change in the maser gain vs frequency characteristic $G(f)$, since $G(f) = K\chi''(f)$, where $G(f)$ is the gain in db and K is a constant determined by the microwave propagating structure. An analysis of this technique has been independently presented by Ostermeyer.[2]

Photographs of oscilloscope displays of maser amplification bandwidth under increasing staggered-field conditions are shown in Fig. 1. The field staggering was accomplished by periodically shimming one of the pole pieces of an electromagnet with thin rectangular slabs of high-permeability material. The amplitude of the peak-to-peak field variations on the ruby were controlled by adjusting the proximity of the shimmed pole piece to the slow-wave structure. The average value of the external field for all the measurements was approximately 2.46 kilogauss, and the peak-to-peak variations were as high as 70 gauss. It should be pointed out that under homogeneous field conditions, the maser yielded net gains of 30 db (with a net reverse loss of 100 db), an instantaneous bandwidth of 21 Mc, and an electronic tuning range in excess of 240 Mc.[3]

A detailed bandwidth measurement of the trace shown in Fig. 1 (c) is plotted in terms of net gain in Fig. 2. It can be seen that a maximum net gain of 11 db is obtained with a 3-db bandwidth of 100 Mc. The structure loss was 7.5 db. This high structure loss was due, in part, to the magnetic broadening in some of the ferrite isolator disks produced by the inhomogeneous field.

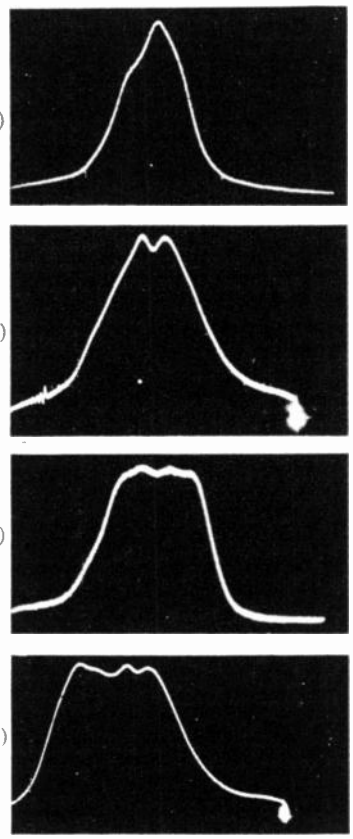

Fig. 1—Oscilloscope display of the maser amplification bandwidth under different field staggering conditions (center frequency≈2280 Mc). (a) 3-db bandwidth = 46 Mc; electronic gain = 25.5 db. (b) 3-db bandwidth = 58 Mc; electronic gain = 23.5 db. (c) 3-db bandwidth = 100 Mc; electronic gain = 18.5 db. (d) 3-db bandwidth = 126 Mc; electronic gain = 16.5 db.

It is believed that with proper ferrite disk design, this loss can be reduced.

All of the above broad bandwidth measurements were obtained with one CW pump source operating at a fixed frequency of 12.62 kMc. This single-frequency source of power sufficiently saturated the wings of the pump transition so that no serious bandwidth degradation effects occurred. A qualitative picture of the degree of wing saturation is shown in the plot of Fig. 3, where the relative gain of a similar maser (with a homogeneous field) is plotted as a function of signal frequency for a fixed CW pump frequency and optimized magnetic field.[4] From this curve, it can be seen that the signal can be tuned over a 120-Mc band before the gain decreases by 3 db. If maser bandwidths much greater than 120 Mc are desired with high gain-bandwidth efficiency, it might be necessary to employ two pump sources operating at different frequencies, or to use one pump source that is frequency modulated at a rate much greater than the pump-transition relaxation time.

It is worthwhile mentioning that two different stagger-tuned field configurations were successfully used.

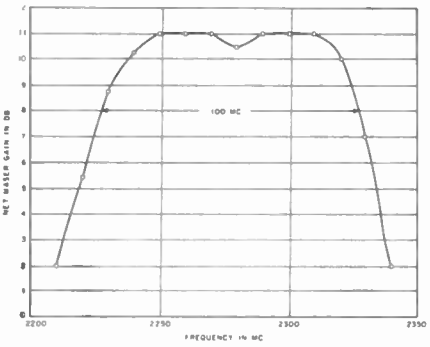

Fig. 2—Detailed amplification band of stagger-tuned TWM [see Fig. 1(c)].

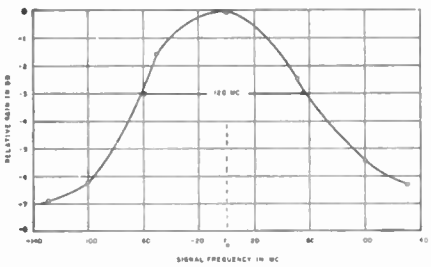

Fig. 3—Relative gain vs signal frequency for fixed pump frequency and optimized magnetic field. $f_0 = 2250$ Mc; $f_p = 12.65$ kMc; pump power = 200 mw; H_{dc} = optimized for maximum gain; $T_{bath} = 1.8°K$.

1) Periodic staggering along the direction of propagation.
2) A linear field variation perpendicular to the direction of propagation.

Either of the above configurations are desirable for low-noise considerations. (It would be undesirable to have a portion of the signal spectrum traveling through a significant length of slow-wave structure experiencing loss before being amplified.) In the first configuration, the periodic staggering effectively divides the structure into many sections, each of which yields gain to the entire signal spectrum. The second configuration has the effect of dividing the ruby into long parallel filaments, each filament yielding gain to a small portion of the frequency band over the entire length. It is believed that this latter technique is more effective in maintaining the maser low-noise properties.

It should also be pointed out that the conditions desired in the staggered field for broadbanding are a variation in the amplitude of the H_{dc} vector and an unperturbed angular orientation. When the angular orientation of the field varies, broadening is obtained but with the additional decrease in gain caused by the reduced transition probability. This is an expensive trade of gain for bandwidth. Unfortunately, in the experiments discussed in this note, a considerable amount of angular inhomogeneity was present. Further work is being done to correct this situation.

S. Okwit
J. G. Smith
Airborne Instruments Lab.
Melville, L. I., N. Y.

* Received by the IRE, April 24, 1961. This work was supported in part by the USAF Aeronautical Systems Div., under Contract AF33(600)-38862.

[1] J. E. Geusic, R. W. DeGrasse, E. O. Schulz-DuBois and H. E. D. Scovil, "The Three Level Solid State Maser," Bell Telephone Labs., Murray Hill, N. J., 9th Interim Rept. on Microwave Solid-State Devices, U. S. Army Signal Corp Contract DA-36-039-sc-73224, pp. 7-10; May, 1959.

[2] F. W. Ostermeyer, "Stagger Tuning of Traveling Wave Masers," Bell Telephone Labs., Murray Hill, N. J., Rept. No. 2, U. S. Army Signal Corps Contract DA-36-039-sc-85357, pp. 17-24; December, 1960.

[3] S. Okwit, J. G. Smith, and F. R. Arams, "Tunable *s*-band traveling-wave maser for telemetry systems," PROC. IRE (Correspondence), vol. 49, pp. 1078-1079; June, 1961.

[4] S. Okwit, F. R. Arams, and J. G. Smith, "Design of a Molecular Amplifier Group," Airborne Instruments Lab., Melville, L.I., N.Y., Rept. No. 5945-2; June, 1960.

The Propagation of Wide-Band Signals Through the Ionosphere*

In connection with wide-band active satellite relaying techniques, consideration must be given to the dispersive characteristic of the ionosphere even at UHF. The phenomenon of Faraday rotations has already been studied in great detail by many including Millman[1] and Garriott.[2] We will, therefore, restrict our consideration here to the question of differential group delay across the frequency band.

For the evaluation of group delay, one can disregard the small effect due the earth's magnetic field and use the following formula for the refractive index of ionosphere.

$$n^2 = 1 - (f_p/f)^2, \tag{1}$$

where n is the refractive index, f_p is the plasma frequency and f is the operating frequency. The plasma frequency f_p depends on certain universal constants (such as charge and mass of the electron) and on the number density of the electrons. As might be expected, it is highly variable. It is characterized by reasonably regular diurnal, seasonal and sunspot cycle variations as well as highly irregular, random fluctuations. A fair estimate of the range of values for f_p through the regular ionosphere is 3 Mc to 12 Mc. For the frequencies of interest,

$$n \cong 1 - f_p^2/2f^2. \tag{2}$$

The propagation constant k is given by $k = k_0 n$ where $k_0 (= \omega/c)$ is the free-space propagation constant. The total phase change ϕ between transmitter and receiver is

$$\phi = k_0 \int n ds = \frac{\omega}{c} \int n ds, \tag{3}$$

where the integral is taken along the path from transmitter to receiver. The group delay τ through the ionosphere is then

$$\tau = \frac{d\phi}{d\omega} = \frac{1}{c} \int [1 + f_p^2/2f^2] ds$$
$$= \frac{R}{c} + \frac{1}{2cf^2} \int f_p^2 ds, \tag{4}$$

where R is range between transmitter and receiver. A fairly simple approximate expression for the group delay $\Delta\tau$ across the band Δf can be obtained by taking the total differential on both sides of (4).

$$\Delta\tau = \frac{\Delta f}{cf^3} \int f_p^2 ds. \tag{5}$$

Until the problem can be studied in finer detail, it would appear that a reasonable requirement for the maintenance of signal fidelity is that $\Delta\tau \ll 1/\Delta f$, where Δf is of the order of the RF bandwidth, since the delay $\Delta\tau$ occurs at RF. Actually, Δf may have to be defined differently for different modes of modulation. The criterion for maintenance of fidelity (or no distortion) can, therefore, be written

$$\Delta\tau\Delta f = \frac{(\Delta f)^2}{cf^3} \int f_p^2 ds \ll 1. \tag{6}$$

This criterion is very conveniently a function of three independent factors, namely, Δf, f, and $\int f_p^2 ds$. The last of these is a characteristic of the ionosphere only. Because the above criterion is very sensitive to frequency (f^{-3}), changes in operating frequency by factors of two or three can bring one from regions with noticeable distortion to regions of negligible distortion, and vice versa.

To obtain a quantitative estimate for the parameter $\Delta\tau\Delta f$, we approximate the integral in (6) by $\langle f_p^2 \rangle R$, where $\langle f_p^2 \rangle$ is the average value of the square of plasma frequency in the ionosphere and R is the slant range through the ionosphere. With this approximation, (6) gets simplified still further.

$$\Delta\tau\Delta f \cong \frac{(\Delta f)^2}{cf^3} \langle f_p^2 \rangle R. \tag{7}$$

For low angles of elevation (*i.e.*, when the satellite is near the horizon) the slant range through the ionosphere may approach 2000 km. A typical number for the average plasma frequency f_p is about 7 Mc. Thus, for one television channel occupying roughly a 10-Mc bandwidth (both sidebands) operating at 1000 Mc, (7) yields $\Delta\tau\Delta f = 3 \times 10^{-2}$. This is indeed small compared to unity. However at 400 Mc, $\Delta\tau\Delta f$ would be almost 0.5, and distortion may turn out to be a problem at this frequency.

To obtain a better estimate of the integral in (6), use was made of an earlier report[1] that in effect evaluated $\int f_p^2 ds$. From the curves in Fig. 24 and Fig. 28 of the report (corresponding to daytime ionospheric conditions and low angles of incidence), the estimate for $\Delta\tau\Delta f$ at 400 Mc varies from 0.4 to 2.0, depending on the assumptions one makes about the structure of the ionosphere. This is consistent with the simple expression in (7) derived earlier.

It is well known in the communication art that channel capacity is related to both bandwidth and signal-to-noise ratio and that, within limits, one of these can be traded for the other. Since power is at a premium in an active satellite, some thought is going into the development of very wide band systems for active satellite relaying. Although high-modulation index FM is not one of the most efficient modulation schemes, it is one of the simplest. For a modulation index of ten, one TV channel would occupy approximately 100 Mc of RF bandwidth. For this case, $\Delta\tau\Delta f$ increases one hundredfold over the previous calculation, and even at 1000 Mc, distortion would become a serious problem. Under these conditions, frequencies above 3500 Mc may be needed. If one looks ahead several years to satellites having the capability of handling the baseband equivalent of several TV channels (the entire baseband FM modulated on one carrier), the problem of delay distortion through the ionosphere will become even more serious.

Relaying to synchronous satellites (*i.e.*, those at a height of 22,300 miles, which remain stationary over a fixed point on earth) does not appear to introduce any additional difficulty. Although the range through the exosphere (that part of the earth's atmosphere which lies beyond the ionosphere) to a synchronous satellite is greater than the range through the ionosphere by a factor of 20, $\langle f_p^2 \rangle$ in the exosphere is reduced from that in the ionosphere by a factor of at least 10^{-2}.

One final note of caution may be in order at this point. The previous discussion restricted itself to a reasonably regular ionosphere. Very intense solar flares occasionally may disrupt the ionosphere sufficiently so as to introduce greater delays than those presented here, especially during sunspot maxima. It would, therefore, behoove us to design some satellite tests in the not too distant future to obtain quantitative estimates for group delay distortion in wideband systems.

H. Staras
RCA Labs.
Princeton, N. J.

* Received by the IRE, May 1, 1961.

[1] G. H. Millman, "An Analysis of Tropospheric, Ionospheric and Extra-Terrestial Effects on V.H.F. and U.H.F. Propagation," T.I.S. Report No. R56EMH31, GE Co., Syracuse, N. Y.; October, 1956 (Unclassified).

[2] O. K. Garriott, "The determination of ionospheric electron content and distribution from satellite observations. Parts 1 and 2," *J. Geophys. Res.*, vol. 65, pp. 1139–1157; April, 1960.

Noise Measure of Lossy Tunnel-Diode Amplifier Stages*

The influence of losses on the noise figure of tunnel-diode amplifiers has been dealt with by several authors.[1] Some [1]–[5] have taken only circuit losses into account, others [6], [7] have included losses caused by the series resistance of the diode only. The author [8] has included both types of losses, but his result was obtained for a series circuit, which is not necessarily stable. Though this may not alter the results, it is worthwhile to repeat the calculation for the stable parallel circuit by a slight extension of Nielsen's approach [7].

First consider the lumped circuit case. The extension of Nielsen's equivalent circuit [7] is shown in Fig. 1. The negative con-

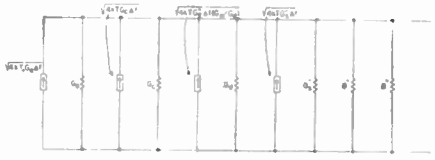

Fig. 1.

ductance of the junction proper is $-G_d$; $-G_d''$ is the transformed junction conductance as seen from the diode terminals, G_s'' is the input conductance caused by the diode series resistance R_s, G_c is the circuit conductance, G_a is the source conductance, B'' the apparent diode susceptance as seen between the terminals, and B the circuit susceptance needed to tune to the desired

* Received by the IRE, April 14, 1961.

[1] Many authors, *e.g.*, Chang [1], [2], Sommers, *et al.* [9], and Tiemann [10] count the noise of the load as belonging to the tunnel diode stage. That problem will be dealt with elsewhere [12]. Trambarulo [11] has reported microwave values of the noise figure.

frequency. The values of $-G_d''$, G_s'', and B'' can be obtained from Nielsen's work [7]. The circuit is stable if $(G_a+G_c+G_s'')>G_d''$; it will be assumed that this condition is satisfied.

The conductances G_a, G_c and G_s'' show thermal noise; the noise associated with G_d'' is represented by a current generator $\sqrt{4kTG_c''\Delta f(G_c/G_d)}$, where G_c is the equivalent noise conductance of the junction proper. $G_c=(eI_0/2kT)$, if the junction current shows full shot noise.

For $(G_a+G_c+G_s'')>G_d''$, the available gain is

$$g_{av}=\frac{G_a}{(G_a+G_c+G_s''-G_d'')}, \tag{1}$$

and the noise figure F is

$$F=1+\frac{4kTG_c\Delta f+4kTG_d''\Delta f\dfrac{G_c}{G_d}+4kTG_s''\Delta f}{4kT_0G_a\Delta f}$$

$$=1+\frac{T}{T_0}\left(G_c+G_d''\frac{G_c}{G_d}+G_s''\right)\frac{1}{G_a}. \tag{2}$$

The noise measure M of the circuit is

$$M=\frac{F-1}{1-1/g_{av}}=\frac{T}{T_0}\left|\frac{\dfrac{G_c}{G_d}G_d''+G_c+G_s''}{G_d''-G_c-G_s''}\right|$$

$$=\frac{T}{T_0}\left|\frac{\dfrac{G_c}{G_d}+\dfrac{G_c}{G_d''}+\dfrac{G_s''}{G_d''}}{1-\dfrac{G_c}{G_d''}-\dfrac{G_s''}{G_d''}}\right|. \tag{3}$$

This expression is useful only if $(G_c+G_s'')<G_d''$, for otherwise the amplifier does not have gain.

For the lossless case $G_c=0$, $R_s=0$ (hence, $G_s''=0$ and $G_d''=G_d$) the noise measure becomes

$$M=M_0=\frac{T}{T_0}\frac{G_c}{G_d}, \tag{3a}$$

corresponding to what is obtained by Sommers, *et al.*, [9] and by Tiemann [10]. For $G_c=0$ but $R_s\neq 0$ the result obtained is identical with the one obtained by Penfield [6] and by Nielsen [7]. For $G_c\neq 0$ and $R_s=0$ (and hence, $G_s''=0$ and $G_d''=G_d$), the result corresponds to the one found by Chang [1], [2], when the contribution of the noise of the loud conductance G_L is eliminated from the latter.[2] For $G_c\neq 0$ and $R_s\neq 0$, the result can be transformed into what was calculated by van der Ziel [8] Nielsen has expressed the noise figure for high gain very conveniently in terms of the diode cutoff frequency. This is easily done for the term $(1-G_s''/G_d'')$, but it is more difficult if the term G_c/G_d'' is taken into account.

The same result (3) is obtained for a reflection-type amplifier using a circulator. Fig. 2 shows the circuit; for the sake of simplicity the noise sources are omitted. Let the notation be the same as before and let G_a again be the source impedance (=transformed characteristic impedance of the line). Following Hines and Anderson [3], the value of the gain that takes the place of the available gain in the noise measure M, is the square of the reflection coefficient of the line:

$$g_p=\left(\frac{G_a-G_c-G_s''+G_d''}{G_a+G_c+G_s''-G_d''}\right)^2. \tag{4}$$

The noise figure F is[3]

$$F=1+\frac{T}{T_0}\frac{4G_a}{(G_a-G_c-G_s''+G_d'')^2}\cdot\left(\frac{G_c}{G_d}G_d''+G_c+G_s''\right). \tag{5}$$

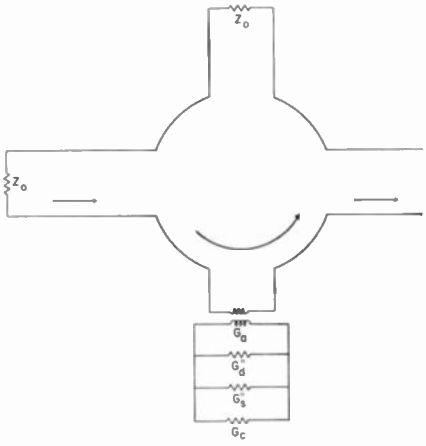

Fig. 2.

When it is observed that g_p corresponds to the expression g_{av} of the previous case, so that $M=(F-1)/(1-1/g_p)$, and the corresponding substitutions are made, one obtains again (3). It is noted that (3) shows considerable similarity with what is obtained for a lossy, distributed, active line [13].

For $R_s=0$ (and hence $G_s''=0$, and $G_d''=0$), (4) and (5) agree with the results obtained by Hines and Anderson [3], Jariv, *et al.* [4], and with Sie's corrected results [5]. Jariv, *et al.*, could express their result in terms of the power gain g_p and of measurable Q factors of the circuit. This becomes more difficult if the losses caused by the series resistance of the diode are taken into account.

The expression

$$F=F_\infty=M+1 \tag{6}$$

corresponds to the noise figure for infinite gain. For the particular case $T=T_0$, (6) reduces to

$$F_\infty=\frac{1+G_c/G_d}{1-G_c/G_s''-G_s''/G_d''}; \tag{6a}$$

it is useful for $(G_c+G_s'')<G_d''$, for otherwise the amplifier does not have gain. For the lossless case ($G_c=0$, $R_s=0$), (6a) reduces to the well-known expression

$$F_\infty=1+\frac{G_c}{G_d}. \tag{6b}$$

A. VAN DER ZIEL
Elec. Engrg. Dept.
University of Minnesota
Minneapolis, Minn.

REFERENCES

[1] K. K. N. Chang, "Low-noise tunnel-diode amplifiers," PROC. IRE, vol. 47, pp. 1268–1269; July, 1959.
[2] K. K. N. Chang, "The optimum noise performance of tunnel diode amplifiers," PROC. IRE, (Correspondence), vol. 48, pp. 107–108; January, 1960.
[3] M. E. Hines and W. W. Anderson, "Noise performance theory of Esaki (tunnel) diode amplifiers," PROC. IRE (Correspondence), vol. 48, p. 789; April, 1960.
[4] A. Jariv, J. S. Cook, and P. E. Butzien, "Operation of an Esaki diode microwave amplifier," PROC. IRE (Correspondence), vol. 48, p. 1155; June, 1960.
[5] J. J. Sie, "Absolutely stable hybrid-coupled tunnel-diode amplifier," PROC. IRE (Correspondence), vol. 48, p. 1321, July, 1960; correction, PROC. IRE (Correspondence), vol. 48, p. 1783; November, 1960.
[6] P. Penfield, "Noise performance of tunnel diode amplifiers," PROC. IRE (Correspondence), vol. 48, pp. 1478–1479; August, 1960.
[7] E. G. Nielsen, "Noise performance of tunnel diodes," PROC. IRE (Correspondence), vol. 48, pp. 1903–1904; November, 1960.
[8] A. van der Ziel, "Noise measure of lossy tunnel diode amplifiers," PROC. IRE (Correspondence), vol. 48, pp. 1321–1322; July, 1960. (The original title of the paper has an obvious misprint that is here corrected.)
[9] H. Sommers, *et al.*, "Tunnel diodes for low-noise applications," 1959 IRE WESCON CONVENTION RECORD, pt. 3, pp. 3–8.
[10] J. J. Tiemann, "Shot noise in tunnel diode amplifiers," PROC. IRE, vol. 48, pp. 1418–1423; August, 1960.
[11] R. F. Trambarulo, "Esaki diode amplifiers at 7, 11, and 26 kMc," PROC. IRE (Correspondence), vol. 48, pp. 2022–2023; December, 1960.
[12] A. van der Ziel, "Noise measure of distributed negative-conductance amplifiers," this issue, p. 1212.
[13] A. van der Ziel, to be published.

Noise Measure of Distributed Negative-Conductance Amplifiers*

Haus and Adler [1] have introduced the concept of the noise measure M of an amplifier stage by the definition

$$M=\frac{(F-1)}{(1-1/g_{ex})}, \tag{1}$$

where F is the noise figure of the stage and g_{ex} is the exchangeable gain. This note shows how their discussion has to be modified for distributed negative-conductance circuits in which the characteristic impedance Z_0 of the circuit has a reactive part. It formalizes the procedure developed by Hines [2] for the distributed tunnel-diode problem. Chang [3] has discussed the general theory of a negative-resistance transmission-line amplifier with distributed noise sources from a somewhat different point of view.

* Received by the IRE, April 14, 1961.

[2] Instead of M, many authors use the expression $(M+1)$, the noise figure for infinite gain. After correcting Chang's result for the effect of the load conductance G_2, his expression corresponds to $(T_0/T)M(1-G_c/G_d)$.

[3] The noise figure is here defined as $F=1+P_d/P_a$, where P_d is the noise power delivered to the line by the diode and the circuit, and $P_a=kTdfg_p$ is the reflected noi e power coming from the source.

If a signal source, or the output of an amplifier, is represented by an EMF E and an internal impedance Z, then the exchangeable power P_e is defined as

$$P_e = \frac{1}{4}\frac{EE^*}{(Z+Z^*)}. \tag{2}$$

where the asterisk denotes the conjugate complex quantity. If Z has a positive real part, P_e represents the power that can be pushed into a (passive) matched load Z^*. If Z has a negative real part, P_e is negative and represents the power that can be pushed into the source by a matched (active) load Z^*. One can thus define the exchangeable source power P_{es} and the exchangeable output power P_{eo} of an amplifier stage. The exchangeable gain g_{ex} is then defined as

$$g_{ex} = \frac{P_{eo}}{P_{es}}, \tag{3}$$

and the noise figure F is defined by

$$F = \frac{\text{exchangeable output noise power}}{g_{ex}kTdf}. \tag{4}$$

Difficulties arise, however, in distributed active circuits. To avoid reflections, the active distributed line is terminated in its characteristic impedance Z_0 on both sides of the line. If Z_0 is real and positive, the termination into Z_0 represents a maximum power transfer. If Z_0 has a reactive part, this is no longer the case, for the line should now be terminated in Z_0 instead of in Z_0^*. This means that definitions (1)–(4) have to be modified.

The most convenient way to do so is to put the discussion on a *current* (not a *power*) basis. Let an active distributed line of length l be terminated on both ends by its characteristic impedance $Z_0=(R_0+jX_0)$, and let $\gamma=(-\alpha+j\beta)$ be the propagation constant of the line. If i_i and i_o are the input and output current, respectively, then $i_o=i_ie^{-\gamma l}$. Hines [2] defines the square of the current gain $|i_o/i_i|$ as the *internal gain* g_i of the active line:

$$g_i = \left|\frac{i_o}{i_i}\right|^2 = e^{2\alpha l}. \tag{5}$$

The noise figure F is defined as

$$F = 1 + \frac{\text{mean-square output noise current due to line}}{\text{mean-square output noise current due to source}}. \tag{6}$$

To calculate F, the noise sources are now introduced. Let a section of the line of length dz have a series impedance $(R_1+jX_1)dz$ and a parallel admittance $(G_1-G_d+jB_1)dz$, where R_1, G_1 and $-G_d$ are the loss resistance, the loss conductance and the negative conductance per unit length, respectively. The noise of a section of length dz can be represented by an EMF $\sqrt{4kTR_1dfdz}$ in series with the line section and by independent current generators $\sqrt{4kTG_1dfdz}$ (thermal noise of G_1) and $\sqrt{4kTG_ndfdz}$ (G_n being the equivalent noise conductance of the noise of the negative conductance $-G_d$) in parallel with the section. The characteristic impedance Z_0 and the propagation constant γ of the line are defined as

$$Z_0 = R_0 + jX_0 = \frac{R_1+jX_1}{G_1-G_d+jB_1};$$
$$\gamma = -\alpha+j\beta = (R_1+jX_1)(G_1-G_d+jB_1). \tag{7}$$

The mean-square output noise current of the source is

$$\overline{i_0^2} = kT_0dfR_0/|Z_0|^2. \tag{8}$$

The noise contributions of $-G_d$, G_1 and R_1 are, respectively,

$$\overline{i_{G_d}^2} = kTG_ndf\left(\frac{g_i-1}{2\alpha}\right), \tag{9}$$

$$\overline{i_{G_1}^2} = kTG_1df\left(\frac{g_i-1}{2\alpha}\right), \tag{10}$$

$$\overline{i_{R_1}^2} = \frac{kTR_1df}{|Z_0|^2}, \tag{11}$$

as is found by taking the contribution of each section dz and then integrating over the length l of the line (compare Hines [2]). Substituting (8)–(11) into (6) gives

$$F = 1 + \frac{T}{T_0}\left(\frac{g_i-1}{g_i}\right)\left(\frac{|Z_0|^2G_d}{2\alpha R_0}\right)\cdot\left[\frac{G_n}{G_d}+\frac{G_1}{G_d}+\frac{R_1}{G_d|Z_0|^2}\right]. \tag{12}$$

If the losses of the distributed line are small, that is, if $R_1 \ll X_1$ and $G_1 \ll G_d$, one finds

$$\frac{2\alpha R_0}{G_d|Z_0|^2} \sim \left[1-\frac{G_1}{G_d}-\frac{R_1}{G_d|Z_0|^2}\right] = 1-\frac{G_1}{G_d}-\frac{G_1'}{G_d}, \tag{13}$$

where $G_1'=R_1/|Z_0|^2$ is the distributed equivalent conductance of the distributed series resistance R_1 of the line. Eq. (12) may thus be written

$$F = 1 + \frac{T}{T_0}\left(1-\frac{1}{g_i}\right)\frac{\left[\frac{G_n}{G_d}+\frac{G_1}{G_d}+\frac{G_1'}{G_d}\right]}{\left[1-\frac{G_1}{G_d}-\frac{G_1'}{G_d}\right]}. \tag{12a}$$

The noise measure M of the active line is now defined as

$$M = \frac{F-1}{(1-1/g_i)} = \frac{T}{T_0}\frac{\left[\frac{G_n}{G_d}+\frac{G_1}{G_d}+\frac{G_1'}{G_d}\right]}{\left[1-\frac{G_1}{G_d}-\frac{G_1'}{G_d}\right]}. \tag{14}$$

For the lossless case ($R_1=0$, $G_1=0$),

$$M = M_0 = \frac{T}{T_0}\frac{G_n}{G_d}. \tag{14a}$$

The result for the lossless case is completely equivalent with the noise measure of the lossless lumped-circuit case, whereas the result for the lossy active line is fully comparable to that of the lossy lumped-circuit case [4].

It is thus seen that (6) is the most convenient expression for the noise figure F, and that

$$M = \frac{F-1}{1-1/g_i} \tag{15}$$

is the proper definition for the noise measure M of the distributed active circuit. For the case of real positive Z_0, (15) reduces to (1), as expected.

A. VAN DER ZIEL
Elec. Engrg. Dept.
University of Minnesota
Minneapolis, Minn.

References

[1] H. A. Haus and R. B. Adler, "Circuit Theory of Linear Noisy Networks," John Wiley and Sons, Inc., New York, N. Y.; 1959.
[2] M. E. Hines, "High-frequency negative-resistance circuit principles for Esaki diode applications," *Bell Sys. Tech. J.*, vol. 39, pp. 477–516; May, 1960.
[3] K. K. N. Chang, "Theory of a negative-resistance transmission line amplifier with distributed noise generators," *J. Appl. Phys.*, vol. 31, pp. 871–875; May, 1960.
[4] A. van der Ziel, "Noise measure of lossy tunnel-diode amplifier stages," this issue, p. 1211.

Full Binary Adder With One Tunnel Diode*

A basic operation performed by the arithmetic section of a digital computer is the addition of binary numbers. This is commonly done by a full binary adder consisting of 16 diodes arranged in four levels of logic serially-driven. The circuit shown in Fig. 1(a) performs full binary addition by employing a single tunnel diode and three resistors in a Wheatstone bridge network. Fig. 1(b) illustrates a tunnel diode I-V characteristic and the operating points indicated by A, B, and C to be achieved by the various values V for one, two and three inputs, respectively. The circuit is voltage-driven. When a voltage pulse V_a is applied to any or all of the inputs X, Y, Z, the voltages V_{FG} and V_{EF} have the logical properties of SUM and CARRY, respectively, provided suitable choices of V_a, R_1, R_2 and R_3 are made for a given R_a and tunnel diode. The circuit can be reduced by Thevenin's theorem to a voltage e applied in series with resistance R_t and the tunnel diode, where R_t is the equivalent resistance of the circuit.

The required operating points A, B and C can be established by e_A, e_B, and e_C (with $e_A:e_B:e_C=1:2:3$, since e is proportional to V_a), and an appropriate choice of R_t. To fulfill the logical functions, R_1 is chosen equal to V_1/i_1 and R_2 is made equal to R_3. R_2 is now the disposable parameter available to establish the correct value of R_t.

The voltage developed across R_2 has the required properties of the SUM since it will be equal to i_1R_2 for both one and three in-

* Received by the IRE, April 11, 1961; revised manuscript received, May 4, 1961.

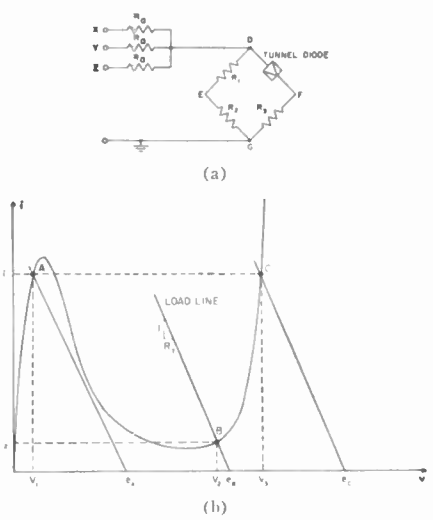

(a)

(b)

Fig. 1—(a) Full binary adder circuit. (b) Tunnel-diode characteristics showing the load line and operating points A, B and C.

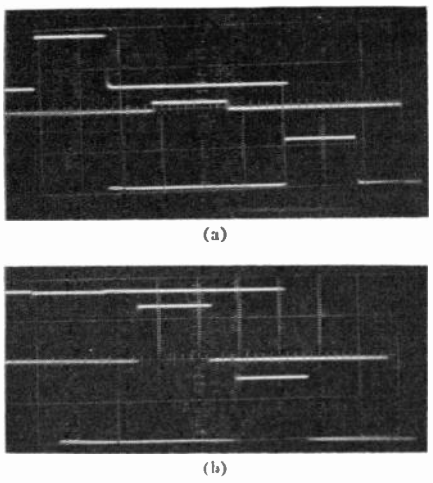

(a)

(b)

Fig. 2—Oscilloscope display of (a) the SUM output, 0.1 v/cm vertically, (b) the CARRY output, 0.2 v/cm vertically. In each picture the upper curve is for a single input, the center curve for two inputs and the lower curve for three inputs. The horizontal scale is 5 μsec/cm

puts, while it has a considerably lower value of i_2R_2 for two inputs. A suitable tunnel diode with a high peak-to-valley ratio can make the SUM output with two inputs 10–20 times below that for one and three inputs. An output corresponding to the CARRY is obtained between terminals E and F of the bridge. With one input, the tunnel diode presents resistance $V_1/i_1=R_1$ to the bridge which is thus balanced, and no output appears between C and D. With two or three inputs present, the resistance that the tunnel diode presents to the bridge is V_2/i_2 and V_3/i_3, respectively. In both cases this is greater than R_1, and the bridge is unbalanced so that there is a voltage output between E and F. These SUM and CARRY outputs fulfill the complete requirements of a full binary adder.

The design analysis will now be outlined. Since there is a broad valley in the tunnel-diode characteristic, state B is certain to be at a current i_2 close to the minimum valley current. It can readily be shown that

$$V_a = v + iR_2 + \left[i + \frac{v + iR_2}{R_1 + R_2}\right]\frac{R_a}{3}. \quad (1)$$

where v is the voltage across the tunnel diode for current i through it. For state A, $V_a=V/3$, $v=V_1$, $i=i_1$, and for state C, $V_a=V$, $v=V_3$, $i=i_1$. Substituting into (1) and eliminating V yields

$$\frac{R_a}{3(R_1+R_2)}\left[R_1 + 2R_2 - \frac{V_3 - 3V_1}{2i_1}\right] = \frac{V_3 - 3V_1}{2i_1} - R_2. \quad (2)$$

Since R_a is necessarily positive, the range of R_2 is given by

$$R_1 + 2R_2 \geq \frac{V_3 - 3V_1}{2i_1} \geq R_1. \quad (3)$$

The left-hand equality corresponds to $R_a\to\infty$ and the right-hand equality to $R_a\to 0$. Since R_1, V_3, V_1 and i_1 are all given by the diode characteristic (choosing i_1 as close to the peak current as is practical with regards to possible component variation), the I-V characteristic of the tunnel diode and source impedance determine the necessary value of R_2.

The carry K is found to be

$$K = \frac{R_2}{R_1 + R_2 + \frac{1}{3}R_a} \cdot \left[V_a - i(R_1 + R_2 + \tfrac{2}{3}R_a)\right]. \quad (4)$$

Since in state A, $V_a=V/3$ and $K=0$, (4) can be written

$$K = \frac{R_2}{R_1 + R_2 + \frac{1}{3}R_a}\left(V_a - \frac{1}{3}V\frac{i}{i_1}\right). \quad (5)$$

For state B, $V_a=2/3V$ and $i=i_2$, and for state C, $V_a=V$, $i=i_1$, thus

$$K_B = \frac{\left(2 - \frac{i_2}{i_1}\right)VR_2}{R_a + 3R_1 + 3R_2} \quad (6)$$

and

$$K_C = \frac{2VR_2}{R_a + 3R_1 + 3R_2}. \quad (7)$$

Also the sum

$$S_A = S_C = \frac{VR_2}{2R_a + 3R_1 + 3R_2}. \quad (8)$$

Experimental results have been obtained using a 1.25-ma peak-current germanium tunnel diode, 1N2939, in the circuit shown in Fig. 1(a) with $R_2=120\Omega$, $R_1=39\Omega$ and $R_a=120\Omega$. A pulse generator was used to simulate the required conditions so that positions of a switch could then simulate the simultaneous arrival of one, two or three pulses to X, Y and Z. The operating points of Fig. 1(a) were then A: $i_1=1.1$ ma, $V_1=45$ mv; B: $i_2=0.15$ ma, V_2 in the valley of the tunnel-diode characteristic, C: $i_1=1.1$ ma, $V_3=470$ mv. An oscilloscope display of the results is shown in Fig. 2. The operating speed was measured by applying a step input of the proper amplitude and having a rise time less than 10 nsec. The SUM and CARRY output was observed with a 100-Mc Tektronix scope and the results obtained showed the transient response to be no greater than 10 nsec. It also appears that the SUM output for two inputs is giving the worst transients. These experimental results agree well with the analytical predictions of the circuit, assuming a linearized tunnel-diode I-V characteristic and neglecting any inductances in the circuit. It should be noted that the CARRY output is above ground. A transformer has been used successfully to convert it to a single-ended output. The circuit offers the advantages of simplicity, potential high-speed operation, no steady-state dissipation and low-switching energy.

B. Rabinovici
C. A. Renton
RCA Surface Communications
New York, N.Y.

Parametric Amplification with a Low-Frequency Pump*

The regenerative, three-frequency parametric amplifier consisting of a varactor, a pump, a signal tank, and an idler tank is well known. The degenerate version of this amplifier results when signal and idler tanks are replaced by a single tank tuned to one-half the pump frequency. This note is to demonstrate the possibility of regenerative signal amplification, or oscillation, with a pump frequency lower than the signal frequency by a specified rational fraction. Leon[1] has shown the possibility of regeneration at an idler frequency greater than the pump frequency, but his findings seem indirectly related to the case discussed here.

Assume a varactor whose displacement q (charge, flux linkage) is a single-valued function of the force v (potential, current), such that

$$q = \sum_{n=1}^{\infty} C_n v^n. \quad (1)$$

the C_n being constants. Let $v=v_p+v_s$, where $v_p=E_p\cos pt$, $v_s=E_s\cos(st+\phi)$. If $C_n\neq 0$, it can be shown that the nth term of (1) is responsible for an average power, delivered by the pumping force v_p and absorbed by the signal force v_s, of

$$W_n = nsC_n(E_p/2)^{n-1}E_s^2/2 \quad (2)$$

provided

$$\begin{cases} \phi = -(\pi/4), (3\pi/4) \\ s/p = (n-1)/2. \end{cases} \quad (3)$$

It is therefore possible, given a sufficiently large C_n, to amplify at a signal frequency s with a pump frequency $2s$, $2s/3$, $2s/5$, $2s/7$, etc. Only odd denominators have been chosen; even denominators represent signals harmonically related to the pump,

* Received by the IRE, May 4, 1961.

[1] B. J. Leon, "Exact Analysis of Linear Parametric Amplifiers," presented at URSI Joint Meeting, Washington, D. C., May 3, 1960; submitted to IRE Trans. on Circuit Theory.

and these would ordinarily be obscured by harmonic generation in the varactor. Oscillators powered by a low-frequency pump may be useful as computer storage elements, for in common with parametron oscillators there are two stable choices for the oscillation phase ϕ.

A general theory of the two-frequency varactor can be constructed with the method outlined above. If the single varactor assumed is part of a network in which all other elements are linear, there are only two possible modes of energy transfer from v_p to v_s. The first mode is nonregenerative, *i.e.*, the network can be considered a stable source of current at frequency s. The second is regenerative, and the network presents a negative conductance to v_s at frequency s. One of the negative conductances is represented by the coefficient of E_s^2 in (2). Other useful results of the theory are: 1) two-frequency nonregenerative frequency dividers (subharmonic generators) are not possible, and 2) two-frequency regenerative frequency dividers are not possible, except for division by 2.

With variable-capacitance diodes of the type designed for high-frequency tuning, oscillations have been produced at 9 kc with a 6-kc pump, and at 15 Mc with a 10-Mc pump. The magnitude of C_4 was thus sufficient to demonstrate the effect with the single-tuned circuits available. No oscillations have been obtained using these diodes with the pump at 2/5, or less, of the signal frequency.

G. Franklin Montgomery
Natl. Bur. of Standards
Washington, D. C.

100-Mc Tunnel-Diode Ring Counter*

Ring counters[1] are characterized by the fact that the "one" state is transferred from one stage to the next at each input. In an N-stage ring counter, each stage is required to operate every N counts. It is triggered to the "one" state every N counts but is reset to the "zero" state at the next count. Thus, with this type of arrangement, each stage has a time interval corresponding to $N-1$ counts in which to be reset. It was this fact that motivated the design of the circuit described below.

The logical layout of this ring counter is shown in Fig. 1. It consists of a series of bistable tunnel-diode AND circuits connected in a ring with a small delay between each stage. The input to each stage is a short transient from the input line and a dc input from the preceding AND stage. Thus, stage i cannot be triggered to its "one" state unless stage $i-1$ is already in its "one" state. The reset circuit will reset stage $i-1$ when stage i is triggered. The next input will trigger stage $i+1$ which will reset stage i. Because the AND gates are arranged in a ring, the "one" state will be transferred from one stage to the next at each input. If we have N stages, the ring counter will be in its base state (the first stage in state "one" and all the rest in state "zero") after every N inputs, thus dividing the input count by a scale of N. The delay between successive stages is required to insure that only one count is achieved for each input. An all transistor decade counter based on a similar logical layout has been reported in the literature.[2]

A schematic diagram of a typical stage is shown in Fig. 2. The tunnel diode in series with its load resistor R_1+R_2 is the basic bistable threshold gate which has been discussed in the literature many times.[3] Resistors R_1, R_2, R_4, and R_5 are chosen to give currents I_0, I_1, and I_2 in diode D_i with peak current I_p such that: $I_0+I_1<I_p$; $I_0+I_2<I_p$; $I_0+I_1+I_2>I_p$, where I_2 is the peak value of the transient input current i_2. This defines the basic AND function, and when the preceding stage is in the "high" or "one" state, diode D_i can be triggered by input current i_2. When this stage goes high it saturates transistor T_i, which resets the preceding stage. Capacitors C_2 and C_3 are commutating capacitors to speed the reset. Diode D_2 is required to eliminate reverse current when D_{i-1} is low and D_i is high. Sufficient delay between successive stages is obtained from the finite switching time of each tunnel diode.

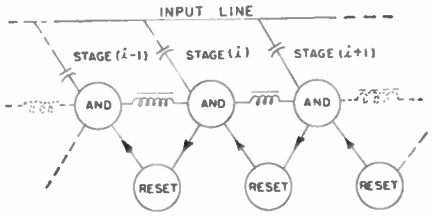

Fig. 1—Logical layout of ring counter.

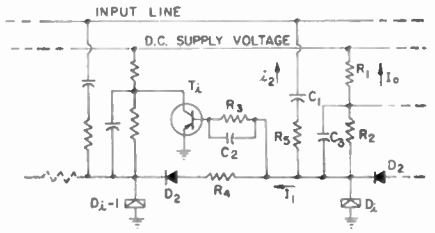

$R_1=3K$ $C_1=2.2\mu\mu f$ $D_i=5$ ma. germanium tunnel diode
$R_2=270\Omega$ $C_2=100\mu\mu f$
$R_3=820\Omega$ $C_3=56\mu\mu f$ $D_2=$ germanium diode
$R_4=68\Omega$ supply voltage $=-11$ volts
$R_5=270\Omega$ $T_i=2N501$ transistor

Fig. 2—Schematic diagram of a typical stage in the ring counter.

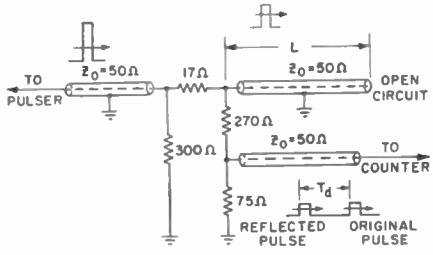

Fig. 3—Circuit used to generate a doublet of narrow pulses.

The input circuit is a 50-ma gallium arsenide diode in series with a 50-ohm resistor, which was chosen to terminate properly the transmission line used for the input cable. Each time the input voltage passes -2.5 volts, the tunnel diode fires and a one-volt step is generated at the input line. This is differentiated by the capacitor C_1 in Fig. 2 and appears as a transient input to all the AND gates. Thus, the counter responds each time the input voltage passes a reference level of -2.5 volts, making the count independent of the input waveshape.

Using the circuit shown in Fig. 3, a doublet of 3-nsec-wide pulses of the same polarity and amplitude was produced. The input pulse was generated by a mercury relay pulse generator. The separation between the original pulse and its reflection is equal to twice the time delay associated with the open-circuited delay line (whose length is adjustable). This doublet was fed into a decade counter using 2N501 transistors; a minimum double pulse resolution time of 10 nsec was observed for reliable counter operation. A smaller double pulse resolution time of 8 nsec was observed using 2N769 transistors for the reset elements, but it is felt that the circuit layout is limiting the minimum resolution time and not the transistors. This same unit was operated successfully using a 100-Mc sine wave input.

Fred P. Heiman
Electronic Res. Lab.
RCA Labs.
Princeton, N. J.

Concerning the Partition Theory and Associated Transform Methods*

In the recent literature there has been considerable discussion of supposedly new transform methods.[1] Wolf, in his discussion, fails to make a distinction between the definition of a transform and methods of application so that his statements and claims are not all valid. His definition of the Laurent-Cauchy transform is given by[2]

$$h_n = \frac{1}{2\pi j}\int_c H(\rho)\rho^{n-1}d\rho \qquad (1)$$

* Received by the IRE, April 27, 1961; revised manuscript received, May 8, 1961.

[1] For a general discussion, see J. Millman and H. Taub, "Pulse and Digital Circuits," McGraw-Hill Book Co., Inc., New York, N. Y., ch. 2; 1956.

[2] "100-Mc solid-state gated counter," *Electronic design*, vol. 8, pp. 58–59; October 12, 1960.

[3] See, for instance, M. H. Lewin, "Negative-resistance elements as digital computer components," *1959 Proc. Eastern Joint Computer Conf.*, no. 16, pp. 15–27; December 1–3, 1959.

* Received by the IRE, February 10, 1961; revised manuscript received, March 13, 1961.

[1] E. V. Bohn and A. A. Wolf, "The equivalence of the Taylor-Cauchy and Laurent-Cauchy transform analysis with conventional methods," Proc. IRE, vol. 49, pp. 358–361; January, 1961.

[2] Y. H. Ku, and A. A. Wolf, "Laurent-Cauchy transforms for analysis of linear systems described by differential-difference and sum equations," Proc. IRE, vol. 48, pp. 923–931; May, 1960.

and

$$H(\rho) = \sum_{n=0}^{\infty} h_n \rho^{-n}. \tag{2}$$

This can be compared with Jury's[3] definition of the Z transform

$$h(nT) = \frac{1}{2\pi j} \int_{\Gamma} H(Z) Z^{n-1} dZ \tag{3}$$

and

$$H(Z) = \sum_{n=0}^{\infty} h(nT) Z^{-n}. \tag{4}$$

That these transforms are identical can be seen by setting $T=1$, $\rho=Z$, and $h(nT)=h_n$. Wolf's reference to sample functions and sequence functions is not relevant. The Z transform cannot distinguish between them. Jury[4] has also commented on the identity of the two transforms in discussing alternate means of deriving some of Wolf's expressions. Wolf makes a comparison with the Laplace and Fourier transforms. That these transforms are different becomes evident when a unit step function is considered. The Fourier transform of a unit step function does not exist. No simple change in notation can convert the Laplace transform, which is $1/s$, into a nonexistent value. There is no justification for the statement that the transform pairs 1, 2 and 3, 4 are generally different. With reference to the Taylor-Cauchy transform, Wolf defines this by[5]

$$H^{(k)}(\lambda) = \sum_{n=0}^{\infty} w_{n,k} \lambda^n \tag{5}$$

and

$$w_{n,k} = \frac{1}{2\pi j} \int_{\Gamma} \frac{H'^{(k)}(\lambda) d\lambda}{\lambda^{n+1}}. \tag{6}$$

Using the substitutions $f(t) = H'^{(k)}(\lambda)$ and $n! w_{n,k} = a_n$, it becomes evident that the Taylor-Cauchy transform pair represents nothing more than a simple power (Taylor) series and the coefficient of the nth power of t. For example, from Wolf's tables, the Taylor-Cauchy transform of $e^{\alpha t}$ is $\alpha^n/n!$. His statement that the Taylor-Cauchy transform arises from the partition theory is erroneous. The Taylor series (5) and Cauchy's integral formula (6) were both well established before the development of the partition theory.

Wolf's claim that the partition theory represents a new and distinct development is based largely on his discussion of backward recurrence relations. This is only an apparent difficulty which can be eliminated by simply converting the integro-differential equation into a differential equation by means of the substitution

$$D^{-N} y(t) = x(t), \tag{7}$$

where D^{-N} is the highest-order integral operator. The nonlinear differential equation will then have the form

$$u_n = f_n(u_0, u_1, \cdots, u_{n-1}, t) \tag{8}$$

where the notation

$$u_n = u_n(t) = \frac{d^n x(t)}{dt^n} \tag{9}$$

is used. The solution of (8) is to be represented by a power series:

$$x(t) = \sum_{n=0}^{\infty} \frac{a_n}{n!} t^n. \tag{10}$$

It follows from (9) and (10) that

$$a_k = u_k(0). \tag{11}$$

The values $a_0, a_1, \cdots, a_{n-1}$ can be specified as initial conditions. The remaining a_k can be found by differentiating (8) successively with respect to t and then substituting $t=0$. This yields

$$\begin{aligned} u_{n+1} &= \frac{\partial f_n}{\partial u_0} u_1 + \cdots + \frac{\partial f_n}{\partial u_{n-1}} u_n + \frac{\partial f_n}{\partial t} \\ &= f_{n+1}(u_0, u_1, \cdots, u_{n-1}, u_n, t) \end{aligned} \tag{12}$$

and, for $t=0$,

$$\begin{aligned} a_n &= f_n(a_0, a_1, \cdots, a_{n-1}, 0) \\ a_{n+1} &= f_{n+1}(a_0, a_1, \cdots, a_{n-1}, a_n, 0). \end{aligned} \tag{13}$$

$$\vdots$$

There is no difficulty in solving these equations for the a_k's.

To see the equivalence of this conventional method with that of Wolf, it should be noted that he sets

$$\frac{d^n x}{dt^n} = \sum_{k=0}^{\infty} w_k t^k, \tag{14}$$

and obtains recurrence relations for the w_k's. From (10) and (14) the following relation is obtained:

$$w_k = \frac{a_{n+k}}{k!}; \qquad (k \geq 0). \tag{15}$$

Wolf's recurrence relations for the w_k's are obtained by using (15) to eliminate the a_k's from (13). In all the examples discussed the use of the a_k's is more straightforward. In view of the simple relation (15), it is difficult to justify Wolf's statement that the methods are distinctly different. His comments concerning the numerical method used by Dietz[6] is not relevant to this discussion which concerns itself with transforms. Dietz solves the nonlinear integral equation

$$x(t) = \int_0^t g(\tau) h(t-\tau) d\tau - \int_0^t F[x(t)] \cdot h(t-\tau) d\tau, \tag{16}$$

where g, h and F are known functions using numerical procedures. This is very distinct from the transform method which assumes a power-series solution of (16) and obtains recurrence relations for the coefficients.

As a final comment, it should be noted that stochastic inputs are considered by postulating probability-density functions for the coefficients of the power series. The usefulness of this approach is very limited even in the case of linear systems. Wolf states that his methods are principally useful for theoretical and systematic studies. It is difficult to agree with this, in view of the fact that a power-series representation is generally of little use and that all examples cited by him are more readily solved by conventional methods.

E. V. Bohn
Dept. of Elec. Engrg.
University of British Columbia
Vancouver, B. C., Canada

[3] E. Jury, "Sampled-Data Control Systems," John Wiley and Sons, Inc., New York, N. Y.; 1958. See, in particular, Eqs. 1.87, 1.90.

[4] E. Jury, "Laurent-Cauchy transforms for analysis of linear systems described by differential-difference and sum equations," PROC. IRE, vol. 48, pp. 2026–2027; December, 1960.

[5] Y. H. Ku, A. A. Wolf, and J. H. Dietz, "Taylor-Cauchy transforms for analysis of a class of nonlinear systems," PROC. IRE, vol. 48, pp. 912–922; May, 1960.

[6] Y. H. Ku, A. A. Wolf, and J. H. Dietz, "On a systematic approximation to the partition method for analysis of a class of non-linear systems," *Trans. AIEE*, vol. 49, pp. 183–189; July, 1960.

A Theoretical Comparison of Average- and Spot-Noise Figure in Transistor Amplifiers*

It is the purpose of this note to calculate the average-noise figure of a transistor from an assumed functional relationship for the spot-noise figure. From this calculation, the dependence of average-noise figure on noise bandwidth and certain transistor parameters may be obtained and the conditions under which the average-noise figure and spot-noise figure are essentially identical will be evident.

Theory

In Fig. 1, spot-noise figure F_{AO} is plotted as a function of frequency f. In Region I, F_{AO} is assumed to decrease at 3 db per octave increase of frequency. In Region II, F_{AO} is independent of frequency with the value of F_0. In Region III, F_{AO} increases at 6 db per octave. The critical frequency that defines the boundary between Region II and Region III is $(\sqrt{1-\alpha_0})f_{\alpha b}$. The analysis here will be restricted to $f \leq f_{\alpha b}$ so that the variation

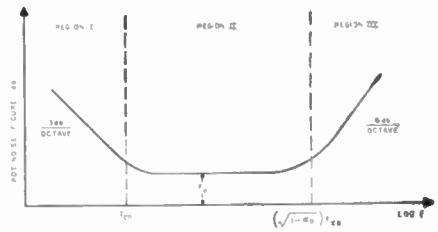

Fig. 1.

* Received by the IRE, March 5, 1961; revision received, March 15, 1961.

shown for Region III holds for the common-emitter, common-base and common-collector connections.

The variation of F_{AO} with f, shown in Fig. 1, defines the functional relationship (1).

$$F_{AO} = \frac{f_{cn}}{f} F_0 + F_0 + \frac{f^2}{(1-\alpha_0) f_{ab}^2} F_0, \quad (1)$$

where f is the frequency at which F_{AO} is specified. Now $f_{cn} \ll (\sqrt{1-\alpha_0}) f_{ab}$ so that it is possible to consider two separate cases.

Case 1

For this case

$$F_{AO} = F_0 \left(1 + \frac{f_{cn}}{f}\right). \quad (2)$$

The average noise figure, F_A, is

$$F_A = \frac{\int_{fa}^{fb} G(f) F_{AO}(f) df}{\int_{fa}^{fb} G(f) df}, \quad (3)$$

where the $f_a < f_b$, and $G(f)$ is the available power gain.

$G(f)$ is determined by the transistor and frequency selective networks associated with the particular amplifier circuit being considered. With the $F_{AO}(f)$ necessary to describe transistor spot-noise figure, (3) may be integrated in closed form for only very simple $G(f)$. In particular we may take $G(f)$ as

$$G(f) = \begin{cases} G_0; & f_a \le f \le f_b \\ 0; & f < f_a, f > f_b. \end{cases} \quad (4)$$

Substituting (4) into (3) and carrying out the indicated integration gives

$$\frac{F_A}{F_{AO}} = \frac{1}{1 + \frac{f_{cn}}{f_0}} \left[1 + \frac{f_{cn}}{f_0} \frac{f_0}{\Delta f} \ln \left(\frac{2 + \frac{\Delta f}{f_0}}{2 - \frac{\Delta f}{f_0}} \right) \right], \quad (5)$$

where $\Delta f = f_b - f_a$ and

$$f_0 = \frac{f_a + f_b}{2}.$$

Eq. (5) is plotted in Fig. 2. F_A/F_{AO} is shown as a function of $\Delta f/f_0$ with f_{cn}/f_0 as a parameter.

Case 2

$$f_{cn} \ll f \gtrless (\sqrt{1-\alpha_0}) f_{ab}, \quad f < f_{ab}. \quad (6)$$

For this case we have

$$F_{AO} = F_0 \left(1 + \frac{f^2}{(1-\alpha_0) f_{ab}^2}\right). \quad (7)$$

Taking $G(f)$ as in (4) and substituting (4) and (7) into (3) gives

$$\frac{F_A}{F_{AO}} = \frac{1 + \frac{3 f_0^2}{(1-\alpha_0) f_{ab}^2} \left[1 + \frac{1}{12} \left(\frac{\Delta f}{f_0} \right)^2 \right]}{1 + \frac{3 f_0^2}{(1-\alpha_0) f_{ab}^2}} \quad (8)$$

where Δf and f_0 are defined as before. Eq. (8) is plotted in Fig. 3. F_A/F_{AO} is plotted as a function of $\Delta f/f_0$ with

$$1 + \frac{3 f_0^2}{(1-\alpha_0) f_{ab}^2}$$

as a parameter.

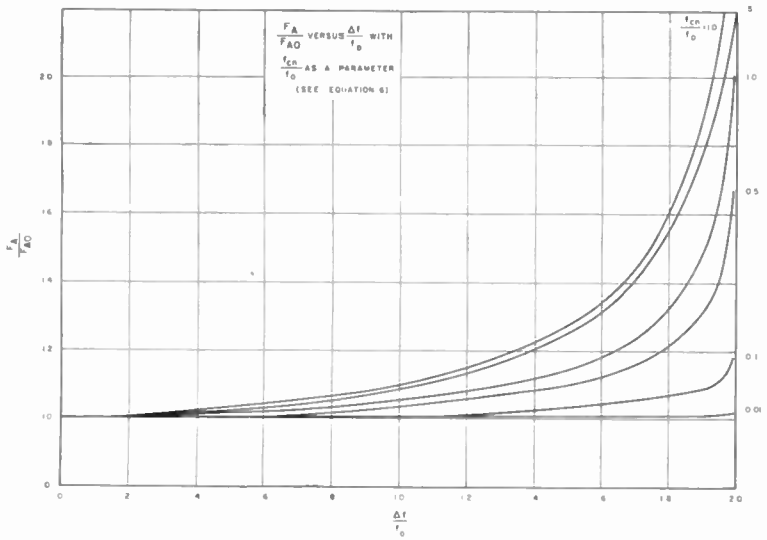

Fig. 2.

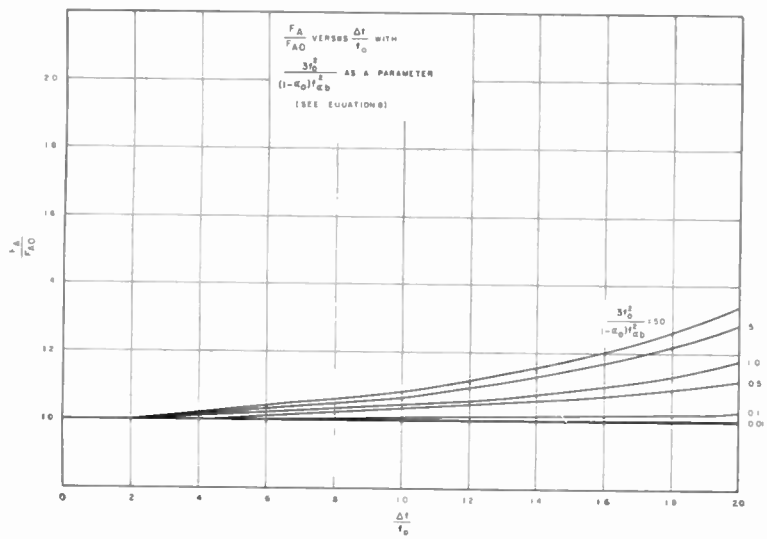

Fig. 3.

Results and Conclusions

By using a particularly simple form for $G(f)$ and approximate expressions for spot-noise figure, equations are derived which relate average-noise figure to spot-noise figure. For both the low-frequency and high-frequency cases the average-noise figure is higher than the spot-noise figure.

For the low-frequency case, F_A will be within 0.5 db of F_{AO} for $\Delta f/f_0 \le 1$ and $f_{cn}/f_0 \le 10$. In the high-frequency case F_A will be within 0.5 db of F_{AO} when $\Delta f/f_0 \le 1.2$ and

$$\frac{3 f_0^2}{(1-\alpha_0) f_{ab}^2} \le 50.$$

In practice the idealized $G(f)$ of (4) can never be realized. However, since the difference between F_A and F_{AO} is so small for $\Delta f/f_0 \le 0.1$, if a filter is chosen such that the ratio of the effective noise bandwidth to the center frequency is small, the difference between the measured noise figure and the actual spot-noise figure will be small.

J. A. Ekiss
J. W. Halligan
Philco Corp.
Lansdale Div.
Lansdale, Pa.

The Calculation of Cutoff Frequencies of Minority-Carrier Transport Factors in Drift Transistors when the Mobilities are not Constant*

The cutoff frequency of minority-carrier transport factor in a drift transistor has been calculated on the assumption that the mobility of an injected minority carrier is independent of the density of impurity in the base region.[1]

Actually, the mobility depends on the density of impurity. In this note, the mobility of holes is assumed as (1) and a cutoff frequency is calculated for a p-n-p drift transistor.

$$\mu_p = \mu_{p_0}\left(\frac{N_d}{N_{d_0}}\right)^{-\nu}, \tag{1}$$

where μ_p is the mobility of holes, μ_{p_0} is the mobility at the front of a collector junction, N_{d_0} is the density of donors at the front of the collector junction, and N_d is the density of donors in the base.

For simplicity, the geometries of a transistor are assumed to be one-dimensional.

In the base region, the current is given as

$$j_p = \mu_p\left(qEp - kT\frac{\partial p}{\partial x}\right), \tag{2}$$

where j_p is the density of hole current, q is the electronic charge, E is the intensity of electric field, p is the density of hole, k is Boltzmann's constant, T is the temperature in Kelvin, x is the coordinate; and the distribution of donor density is given by

$$N_d = N_{d_0}e^{-qE/kT(x-a_0)}. \tag{3}$$

The continuity equation of current is

$$\frac{1}{q}\frac{\partial j_p}{\partial x} = -\frac{\partial p}{\partial t} - \frac{1}{\tau_p}\left\{p - p_0 e^{qE/kT(x-a_0)}\right\} \tag{4}$$

where τ_p is the lifetime of holes and p_0 is the hole density in thermal equilibrium.

From the above equations, the equation giving the distribution of holes in the base region is

$$\frac{\partial^2 p}{\partial x^2} - (1-\nu)\frac{\partial p}{\partial x} - \left\{\frac{1}{{L_{p_0}}^2}e^{-(2/f)(x-a_0)} + \left(\frac{2}{f}\right)^2\nu\right\}p - \frac{1}{D_{p_0}}e^{-2\nu/f(x-a_0)} = -\frac{p_0}{{L_{p_0}}^2}e^{2/f(1-\nu)(x-a_0)}, \tag{5}$$

where ${L_{p_0}}^2$ is $D_{p_0}\tau_p$, f is $2kT/qE$, and D_{p_0} is $\mu_{p_0}kT/q$.

Now, provided that the hole density is divided into three terms as shown in (6), each term satisfies the following boundary conditions:

$$p = p_1 + p_2\frac{q\mu_e}{kT}e^{j\omega t} + p_3 b_1 U_e e^{j\omega t}, \tag{6}$$

where the emitter is located at

$$x = a_0 + a_1 e^{j\omega t} \doteq a_0,$$

the collector at

$$x = b = b_0 + b_1 e^{j\omega t}$$

as shown in Fig. 1 and U_e, and U_c is the amplitude of the sinusoidally-varying junction voltage, the angular frequency of which is ω.

The boundary conditions are as follows:

$$p_1(a_0) = p_2(a_0) = p_0 e^{qV_e/kT}, \tag{7a}$$

$$p_1(b_0) = p_2(b_0) = 0 \tag{7b}$$

$$p_3(a_0) = 0 \tag{8a}$$

$$p_3(b_0) = -p_1'(b_0), \tag{8b}$$

where V_e is the dc voltage of the emitter junction.

If new variables u_1, u_2, u_3, η and ζ, which are defined by (9 a and b), (10 a and b) and (11 a and b), are introduced,

$$p_{1_0} = p_0 e^{2/f(x-a_0)} + \frac{p_0}{{L_{p_0}}^2}e^{1/f(1-\nu)(x-a_0)}u_1 \tag{9a}$$

$$\eta = \frac{\nu}{\nu L_{p_0}}e^{-\nu/f(x-a_0)}, \tag{9b}$$

$$p_2 = e^{1/f(1-\nu)(x-a_0)}u_2 \tag{10a}$$

$$\zeta = \frac{1}{\nu\lambda}e^{\nu/f(x-a_0)}, \tag{10b}$$

where

$$\frac{1}{\lambda^2} = \frac{1+j\omega\tau_p}{{L_{p_0}}^2} \tag{11a}$$

$$p_3 = e^{1/f(1-\nu)(x-a_0)}u_3, \tag{11b}$$

then it is easily seen that the equations giving u_1, u_2 and u_3 are equal to the equations of modified Bessel functions as follows:

$$\eta^2\frac{d^2u_1}{d\eta^2} + \eta\frac{du_1}{d\eta} - (\eta^2+n^2)u_1 = 0, \tag{12}$$

where

$$n = 1 + \frac{1}{\nu}.$$

$$\zeta^2\frac{d^2u_2}{d\zeta^2} + \zeta\frac{du_2}{d\zeta} - (\zeta^2+n^2)u_2 = 0 \tag{13}$$

$$\zeta^2\frac{du_3}{d\zeta^2} + \zeta\frac{du_3}{d\zeta} - (\zeta^2+n^2)u_3 = 0. \tag{14}$$

Therefore, the hole density is

$$p_1 = p_0 e^{2/f(x-a_0)} + p_0 e^{1/f(1-\nu)(x-a_0)} \times \frac{(e^{qV_e/kT}-1)\left[K_n(\eta_b)I_n(\eta) - I_n(\eta_b)K_n(\eta)\right] + e^{1/f(1+\nu)d}\left[K_n(\eta_a)I_n(\eta) - I_n(\eta_a)K_n(\eta)\right]}{I_n(\eta_a)K_n(\eta_b) - I_n(\eta_b)K_n(\eta_a)} \tag{15}$$

$$p_2 = p_0 e^{qV_e/kT}\frac{K_n(\zeta_b)I_n(\zeta) - I_n(\zeta_b)K_n(\zeta)}{I_n(\zeta_a)K_n(\zeta_b) - I_n(\zeta_b)K_n(\zeta_a)}e^{1/f(1-\nu)(x-a_0)} \tag{16}$$

$$p_3 = p_1'(b_0)e^{1/f(1-\nu)(x-b)}\frac{K_n(\zeta_a)I_n(\zeta) - I_n(\zeta_a)K_n(\zeta)}{I_n(\zeta_a)K_n(\zeta_b) - I_n(\zeta_b)K_n(\zeta_a)}. \tag{17}$$

where I_n and K_n are the first and the second kind of modified Bessel functions of nth order, respectively, the subscripts a and b indicate the values at $x=a$ and b, and d is equal to $b-a$.

From (16) and (17), the ac hole current can be calculated, and the transport factor of hole is calculated from the ratio of the hole current at the collector to the hole current at the emitter.

Then the transport factor β is

$$\beta = \frac{\frac{\nu}{f}e^{d/f(1+\nu)}}{\frac{1}{f}(1+\nu)\left[I_n(\zeta_a)K_n(\zeta_b) - I_n(\zeta_b)K_n(\zeta_a)\right] + \frac{1}{\lambda}\left[I_n'(\zeta_a)K_n(\zeta_b) - I_n(\zeta_b)K_n'(\zeta_a)\right]}. \tag{18}$$

Unfortunately, (18) is very complicated because the variables are complex. Provided that τ_p is infinitely long, I_n and K_n are expanded to the sum of *ber* and *bei*, and the sum of *ker* and *kei*, respectively. Then the numerical calculations are greatly simplified.

For $N_d \geq 10^{16}$, the mobility in germanium varies roughly as $N_d^{-1/3}$.[2] Therefore, ν is chosen to be $\frac{1}{3}$ for a germanium p-n-p drift transistor.

For an example, if d/f is chosen to be 4, which is a typical value for a germanium p-n-p transistor, the numerical calculation of the transport factor indicates that the cutoff frequency f_α is approximately given by

$$f_\alpha \doteq 0.3 f_{\alpha_0}. \tag{19}$$

Here f_{α_0} is the cutoff frequency calculated from the simple theory, in which the mobility is assumed to be constant.

It must be emphasized that the cutoff frequency in a drift transistor is greatly reduced due to the decreased mobility of minority carrier at the neighborhood of the emitter.

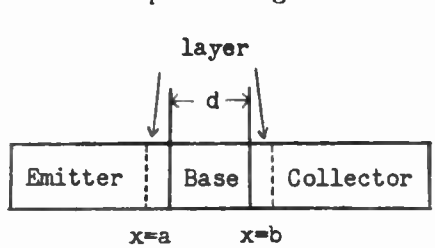

Fig. 1—Geometries of the transistor.

T. Sugano
F. Koshiga
Dept. of Electronic Engrg.
University of Tokyo
Tokyo, Japan

* Received by the IRE, March 7, 1961.

[1] H. Krömer, "Zur theorie des diffusions- und des drifttransistors, I. II. III," *AEÜ*, vol. 8, pp. 223–228, May; pp. 363–369, August; and pp. 499–504, November, 1954.

[2] L. J. Varnerin, "Stored charge method of transistor base transit time analysis," PROC. IRE, vol. 47, pp. 523–527; April, 1959.

Logarithmic Compression of Binary Numbers*

As probes are launched deeper into interplanetary space, it becomes essential to transmit to earth only information of significance and to strain out unneeded data before it reaches a transmitter. This correspondence describes a device that can accept at its input a large binary number and convert this number into a smaller number related to its logarithm. Specifically, we wish to describe here a converter that accepts an input binary number of up to nineteen digits and compresses this to an eight-bit output binary number. This output, by virtue of its coding, indicates the value of the input to an accuracy of better than ±3 per cent throughout its entire range.

Basically the device gives as its output the significant digits of the input plus other digits that indicate where the decimal point should be placed. For a 19-to-8 bit converter, the four most significant figures of the output number are the total number of digits of the input number minus four. The four least significant figures of the output number are the 2nd, 3rd, 4th, and 5th most significant figures of the input. Specifically if the input binary number is "abcdefghi," where "a" is a "1" then the output number will be "Nbcde" where N equals the total number of digits minus four. In the example N=5 which is the binary 101. Therefore, the output is 101bcde. Specific examples are:

Input	Output
1111111111111111111	11111111
10000000000000000000	11110000
10110011011001010110	11110110
00000000011000000000	01011000
00000000000000010000	00010000.

For input numbers with four binary digits or less, the device will provide an output number simply equal to the input number.

Fig. 1 is a plot on semilog paper of output vs input for the 19-to-8 bit converter. The square indicated in Fig. 1 is shown in detail in Fig. 2. Any other plot of input values between 2^n and 2^{n+1} where n is greater than 5 will have the same form as Fig. 2. The notation on the right and top of the figure generalizes the plot so that it is applicable for any input number greater than 32. From zero to thirty-two the output is equal to the input.

A block diagram of the device is shown in Fig. 3. The input number is presented in serial form with the most significant digits presented first. A data pulse in coincidence with a clock pulse is a "one." A clock pulse alone is "zero."

Five clock pulses after the first *data* pulse has been received, a "one" has propagated through the shift register and into the switching flip-flop. This binary changes state and stops generation of switching pulses by its action on the shifting pulse gate. This stops the shift register from any further shifting action, leaving all information in the register intact.

When the switching flip-flop changes state, it also puts the counter gate into a condition to pass clock pulses, including the clock pulse that activated it. Therefore, the total number of digits less four are counted by the counter.

When the conversion is completed the 2nd, 3rd, 4th, and 5th most significant figures of the input are in the shift register, while the counter contains the number of input digits less four.

Other similar schemes can be used to obtain different accuracies or different ranges. The larger the shift register, the more closely the actual value of the input number is known. The larger the counter, the greater the range of input numbers that can be converted.

It is also possible to accept counts rather than a binary number at the input of a different sort of device and to present an output identical to that described above. This device will be described in a later communication.

David H. Schaefer
Head, Computer Sec.
Flight Data Systems Branch
Goddard Space Flight Ctr.
Greenbelt, Md.

* Received by the IRE, February 1, 1961; revision received, March 15, 1961.

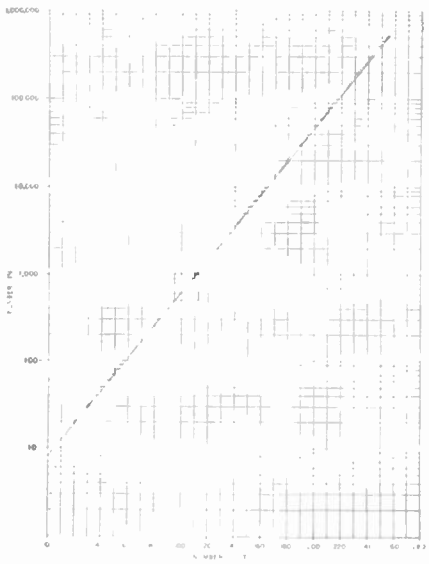

Fig. 1—Output vs input for 19-to-8 bit logarithmic converter.

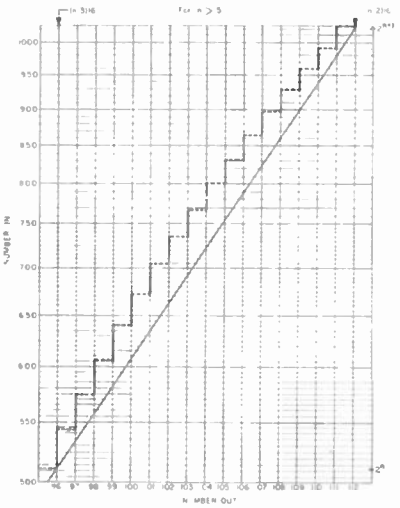

Fig. 2—Detail of square shown in Fig. 1. This figure can be generalized by use of the notation on the right and top of the figure.

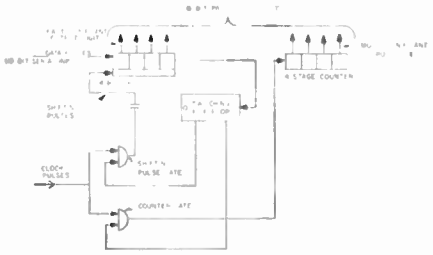

Fig. 3—Converter block diagram. At the beginning of a cycle all flip-flops are in their zero condition.

Converter Efficiency and Power Output of a Tunnel-Diode Relaxation Oscillator*

This brief note is to consider the efficiency and power output of a tunnel diode operated as a dc to ac converter. Such a converter is especially suitable for use in conjunction with thermoelectric generators because both are low impedance devices and the voltage required to bias the tunnel diode into the negative resistance region is obtainable from single-cell thermoelectric generators like lead telluride. A tunnel diode has a characteristic negative resistance region[1,2] as shown in Fig. 1(a). For the purpose of analysis, the characteristic in and near the negative resistance region is approximately represented by

$$i = -ae + be^3, \tag{1}$$

where i and v are the incremental values of current and voltage with regard to their respective quiescent values I_0 and V_0, that is, $i=I-I_0$ and $V=V-V_0$. To obtain a symmetrical ac waveform, we assume that $V_0=(V_1+V_2)/2$ and $I=(I_1+I_2)/2$, the meaning of I_1, I_2, V_1 and V_2 being self-explanatory from Fig. 1(a). By setting $di/de=0$ and

$$i = -(I_1 - I_2)/2 \text{ at } V = (V_2 - V_1)/2,$$

we obtain

$$a = \frac{3}{2}\frac{I_1 - I_2}{V_2 - V_1} \text{ and } b = 2\frac{I_1 - I_2}{(V_2 - V_1)^3}. \tag{2}$$

Suppose that we connect the tunnel diode to a G-L-C circuit as shown in Fig. 2(a). Thus, we have

$$i = -(i_L + i_C + i_G) = -\frac{1}{L}\int edt - C\frac{de}{dt} - Ge = -ae + be^3 \tag{3}$$

* Received by the IRE, March 13, 1961.

[1] L. Esaki, "New phenomenon in narrow germanium p-n junctions," *Phys. Rev.*, vol. 109, pp. 603–604; January, 1958.

[2] I. A. Lesk, N. Holonyak, U. S. Davidsohn, and M. W. Aarms, "Germanium and silicon tunnel diodes—design, operation and application," 1959 IRE WESCON Convention Record, pt. 3, pp. 9–31.

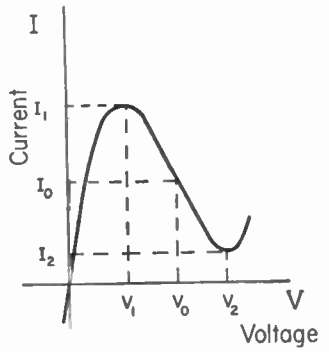

(a)

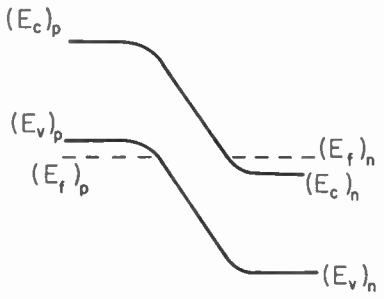

(b)

Fig. 1—(a) Tunnel diode current-voltage characteristic. (b) Tunnel diode energy-band diagram.

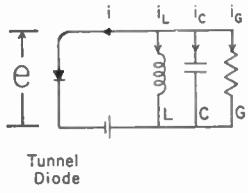

(a)

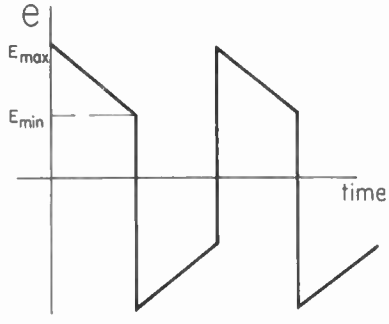

(b)

Fig. 2—(a) Tunnel diode converter circuit. (b) Relaxation oscillation waveform with $\alpha \gg 1$ in (3).

or

$$\frac{d^2e}{dt^2} - \alpha(1 - \beta e^2)\omega_0 \frac{de}{dt} + \omega_0^2 e = 0, \qquad (3)$$

where

$$\omega_0 = (LC)^{-1/2}, \qquad \alpha = (a - G)/\omega_0$$

and

$$\beta = 3b/(a - G).$$

The solution of (3), known as the Van der Pol equation, has been discussed extensively in the literature.[3] For $\alpha \gg 1$, the solution has a waveform shown in Fig. 1(b) and is known as relaxation oscillation. The voltage decreases almost linearly from $E_{max} = 2/\beta^{1/2}$ to $E_{min} = 1/\beta^{1/2}$ and then suddenly changes to $-E_{max}$. Assuming a linear decrease from E_{max} to E_{min}, we find the rms value of the voltage, $E_{rms} = (7/3)^{1/2} E_{min}$ or the ac power output

$$P_{ac} = E_{rms}^2 G = \frac{7}{9} \frac{(a - G)}{b} G. \qquad (4)$$

For a maximum P_{ac}, $G = \frac{1}{2}a$. Thus

$$(P_{ac})_{max} = \frac{7}{36} \frac{a^2}{b} = \frac{7}{32}(I_1 - I_2)(V_2 - V_1). \qquad (5)$$

The dc input into the circuit is

$$P_{dc} = I_0 V_0 = \tfrac{1}{4}(I_1 + I_2)(V_1 + V_2), \qquad (6)$$

and therefore, the efficiency of conversion is

$$\eta = \frac{7}{8} \frac{(I_1 - I_2)(V_2 - V_1)}{(I_1 + I_2)(V_2 + V_1)}. \qquad (7)$$

A typical germanium tunnel diode has peak point voltage and current, $V_1 = 60$ mv and $I_1 = 1$ ma, and valley point voltage and current, $V_2 = 300$ mv and $I_2 = 0.1$ ma. This will give us a conversion efficiency of 48 per cent. For high conversion efficiency, we want to make I_1/I_2 and V_2/V_1 as large as possible. For commercial tunnel diodes, the ratio peak to valley current may vary from 5:1 to 40:1. The current near the valley region is at present not well understood. There is a possible suggestion that impurity states in the forbidden band might contribute extra tunneling current in addition to the normal tunneling and diffusion currents. A reduction of this extra current certainly will help the conversion efficiency. The peak and valley point voltages are determined by the amount of doping used in both sides of the junction. Here again, the valley point voltage may be shifted to larger values due to the existence of the extra tunneling current. Assuming no extra tunneling current, it is clear from Fig. 1(b) that $V_2 = (E_f)_n - (E_c)_n + (E_v)_p - (E_f)_p$. If the n and p sides are equally degenerate, it is expected that $V_1 = (E_f)_n - (E_c)_n = (E_v)_p - (E_f)_p$ and $(V_2 - V_1)/(V_2 + V_1) = \frac{1}{3}$. For $I_1/I_2 = 10$, this will give us a conversion efficiency at 23 per cent. For power conversion, it may be necessary to connect several tunnel diodes in parallel to give the needed current. A further reduction of efficiency may result if the diodes do not have identical characteristics. It should also be pointed out that (1) is an oversimplified representation of the diode characteristic. For accurate representation, even terms, which will produce unsymmetrical waveform, and additional odd terms, may be needed. However, we find in our laboratory that the experimental value of E_{max} agrees well with the theoretical value based upon (1). Apparently, (1) is a fairly good approximation.

The author wishes to thank F. Gevert for a discussion of the experimental work which lends support to the present analysis.

SHYH WANG
University of California
Berkeley, Calif.

[3] See, for example, W. J. Cunningham, "Introduction to Nonlinear Analysis," McGraw-Hill Book Co., New York, N. Y., chap. 6; 1958.

Vertical Incidence Doppler Ionogram*

The measurements of vertical movements of the E layer of the ionosphere described by Ogawa, Ando and Yoshida[1] are closely similar to those made by the author and published in a series of papers.[2–4] The technique used in the author's measurements of phase path changes differs somewhat from those described[1] and has the advantages that both the sense and magnitude of phase path changes can easily be determined. Also, the phase of echoes returned from the E layer is often irregular in its time time variation due to irregularities in the layer itself.[2] The technique used by the author was derived from suggestions in papers by Hafstad and Tuve[5] and Ranzi.[6]

J. W. FINDLAY
Deputy Director
Natl. Radio Astronomy Observatory
Green Bank, W. Va.

Authors' Comment[7]

It seems the essential difference between Findlay's method and ours is that the change in the phase path ΔP is observed, or the time derivative of the phase path dP/dt is observed. Therefore, the former has the advantage in the case of the slow and large movement of the ionosphere and the latter has in the case of the rapid and small movement. When the former and the latter have the errors of $\delta(\Delta P)$ and $\delta(dP/dt)$, respectively, and if the change in the phase path is $\delta(\Delta P)$ in the time interval of more than $\delta(\Delta P)/\delta(dP/dt)$, it cannot be observed by the latter; on the other hand, if the speed of the change of the phase path is $\delta(dP/dt)$ in the time interval of less than $\delta(\Delta P)/\delta(dP/dt)$ it cannot be observed by the former.

The sense of the change would be easily observed in our method if a 90° phase shifter for the reference signal and a phase sensitive detector would be added to our system, which was pointed out in our note.

TORU OGAWA
Mass. Inst. Tech.
Cambridge, Mass.
Formerly at Doshisha Univ.
SADAO ANDO
ATSUSHI YOSHIDA
Elec. Engrg. Dept.
Doshisha Univ.
Kyoto, Japan

* Received by the IRE, March 20, 1961.

[1] T. Ogawa, S. Ando, and A. Yoshida, "Vertical incident Doppler ionogram," PROC. IRE, vol. 49, p. 643; March, 1961.

[2] J. W. Findlay, "The phase and group paths of radio waves returned from region E of the ionosphere," *J. Atmos. and Terr. Phys.*, vol. 1, no. 5/6, p. 353; 1951.

[3] J. W. Findlay, "An investigation of sudden radio frequency near 2 Mc/sec," *J. Atmos and Terr. Phys.*, vol. 1, no. 5/6, p. 367; 1951.

[4] J. W. Findlay, "Moving clouds of ionization in region E of the ionosphere," *J. Atmos. and Terr. Phys.*, vol. 3, no. 2, p. 73; 1953.

[5] L. R. Hafstad and M. A. Tuve, "An echo interference method for the study of radio paths," PROC. IRE, vol. 17, pp. 1786–1792; October, 1929.

[6] I. Ranzi, *Nature*, vol. 132, p. 14; July, 1933.

[7] Received by the IRE, April 24, 1961.

On Scattering Matrices Normalized to Complex Port Numbers*

This paper is concerned with the following practical question. Suppose a linear, time-invariant $2n$-terminal network N (Fig. 1) is excited at its n ports by n generators $E_1, E_2, \cdots, E_n$, with prescribed internal impedances $z_1(j\omega), z_2(j\omega), \cdots, z_n(j\omega)$, respectively. How does one decide upon an appropriate electrical description for N when interest centers mainly on the distribution of average ac power throughout the structure? More specifically, if the z's are not real and positive but are complex over the frequency band under consideration, is it still possible to describe N in terms of a "normalized" $n\times n$ scattering matrix, $S=(s_{kl})$, which is unitary when N is lossless and such that under matched terminations (Fig. 2) the transducer power gain, $G_{kl}(\omega^2)$, from port k to port l is measured by[1]

$$G_{kl}(\omega^2) = |s_{lk}(j\omega)|^2? \tag{1}$$

Interestingly enough, the answer turns out to be in the affirmative if the z's have positive real parts over the frequency range of interest. Before embarking on the proof we introduce some matrix notation.

Let A be an arbitrary matrix. Then A' and $\overline{A}'=A^*$ denote the transpose and the complex conjugate transpose (also called the adjoint) of A, respectively. Column vectors are written $\boldsymbol{a}, \boldsymbol{b}, \boldsymbol{x}$ etc., and in the alternative form $\boldsymbol{x}=(x_1, x_2, \cdots, x_n)'$ whenever it is desirable to exhibit the components explicitly. The matrices 1_n and 0_n are, in the same order, the $n\times n$ identity matrix and the $n\times n$ zero matrix. For an hermetian matrix $A=A^*$, $A\geq 0_n$ means that A is the matrix of a non-negative quadratic form.

Refer to Fig. 1 and assume that the internal impedances $z_1(j\omega), z_2(j\omega), \cdots, z_n(j\omega)$ have positive real parts over the frequency band W; *i.e.*,

$$\text{Real } z_k(j\omega) = r_k(\omega) > 0, \qquad \omega\epsilon W, \quad (k = 1, 2, \cdots, n). \tag{2}$$

The normalized incident and reflected wave amplitudes a_k and b_k impinging on the kth port of N are defined as linear combinations of the associated port voltages and currents according to the scheme:

$$2\sqrt{r_k}\,a_k = V_k + z_k I_k, \tag{3}$$

$$2\sqrt{r_k}\,b_k = V_k - \bar{z}_k I_k, \quad (k = 1\ 2, \cdots, n). \tag{4}$$

All square roots have been chosen positive. The $n\times n$ scattering matrix $S(j\omega)$ of N, normalized with respect to the n impedances $z_1(j\omega), z_2(j\omega), \cdots, z_n(j\omega)$, is defined by means of the linear matrix equation

$$\boldsymbol{b} = S\boldsymbol{a}, \tag{5}$$

where $\boldsymbol{a}=(a_1, a_2, \cdots, a_n)'$ and $\boldsymbol{b}=(b_1, b_2, \cdots, b_n)'$. A more explicit expression for $S(j\omega)$ appears later.

* Received by the IRE, February 18, 1961. Revised manuscript received, March 8, 1961.

[1] H. J. Carlin, "An Introduction to the Use of the Scattering Matrix in Network Theory," Microwave Res. Inst., Polytechnic Inst. of Brooklyn, Brooklyn, N. Y., Rept. R-366-54, PIB-300; 1954.

$$\underline{a} = (a_1, a_2, \cdots, a_n)'; \quad \underline{b} = (b_1, b_2, \cdots, b_n)'$$

$$\underline{V} = (V_1, V_2, \cdots, V_n)'; \quad \underline{I} = (I_1, I_2, \cdots, I_n)'$$

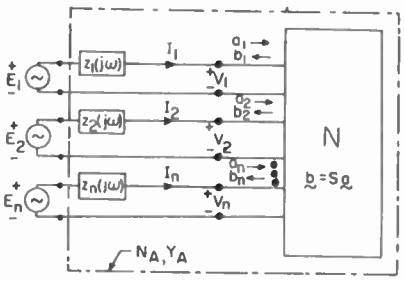

Fig. 1—Schematic of a linear, time-invariant $2n$ terminal network excited at its n ports by n generators $E_1, E_2, \cdots, E_n$ with respective internal impedance $z_1, z_2, \cdots, z_n$.

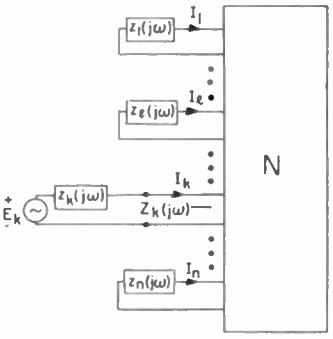

$$z_m(j\omega) = r_m(\omega) + j\,x_m(\omega),$$

$$(m = 1, 2, \cdots, n).$$

$$G_{kl}(\omega^2) = \frac{r_l |I_l|^2}{\dfrac{|E_k|^2}{4r_k}}, \quad l \neq k.$$

Fig. 2—Schematic illustrating the meaning of the transducer power gain $G_{kl}(\omega^2)$ from port k to port l under matched terminations.

Let P_k equal the average power entering N through port k, *i.e.*, $P_k=\text{Real}\,(\overline{V}_k I_k)$. Using (3) and (4), an easy calculation yields

$$P_k = |a_k|^2 - |b_k|^2, \quad (k = 1, 2, \cdots, n). \tag{6}$$

Thus, P_{AV}, the total average power absorbed by N, is given by

$$P_{AV} = \sum_{k=1}^{n} P_k = \sum_{k=1}^{n} |a_k|^2 - \sum_{k=1}^{n} |b_k|^2 = \boldsymbol{a}^*\boldsymbol{a} - \boldsymbol{b}^*\boldsymbol{b}, \tag{7}$$

which, with the aid of (5), transforms into

$$P_{AV} = \boldsymbol{a}^*(1_n - S^*S)\boldsymbol{a}. \tag{8}$$

Consequently, if N is lossless over W, $P_{AV}(\omega^2)=0$, $\omega\epsilon W$, for any $\boldsymbol{a}$, and this, in turn implies that

$$1_n - S^*(j\omega)S(j\omega) = 0_n; \tag{9}$$

i.e., $S(j\omega)$ is unitary for $\omega\epsilon W$. Again, if N is dissipative, $P_{AV}(\omega^2)\geq 0$ for all $\boldsymbol{a}$, and so

$$1_n - S^*(j\omega)S(j\omega) \geq 0_n, \tag{10}$$

$\omega\epsilon W$. Thus the normalization procedure subsumed in (3) and (4) has succeeded in preserving two of the most important properties possessed by a scattering matrix normalized to real positive port numbers.[1]

Let all ports of N except the kth port be closed on their respective normalization impedances and suppose that port k is driven as shown in Fig. 2. Then.

$$V_l = -z_l I_l, \qquad l \neq k. \tag{11}$$

According to (3), (11) is equivalent to

$$a_l = 0, \qquad l \neq k. \tag{12}$$

Hence, from (5),

$$b_l = s_{lk}(j\omega)a_k, \qquad (l = 1, 2, \cdots, n),$$
$$= s_{lk}(j\omega)\frac{E_k}{2\sqrt{r_k(j\omega)}}. \tag{13}$$

since, as is obvious from Fig. 2, $E_k=V_k+z_k I_k$. Eq. (11) coupled with (4) yields

$$b_l = -\sqrt{r_l(j\omega)}\,I_l, \qquad l \neq k, \tag{14}$$

and therefore [see (13)]

$$|s_{lk}(j\omega)|^2 = \frac{r_l(j\omega)|I_l|^2}{\dfrac{|E_k|^2}{4r_k(j\omega)}} = G_{kl}(\omega^2), \qquad l \neq k, \tag{15}$$

the transducer power gain from port k to port l. To determine $s_{kk}(j\omega)$, let $Z_k(j\omega)$ represent the impedance seen looking into port k under matched terminations (Fig. 2). Then $V_k=Z_k I_k$ and the division of (4) by (3) yields, with the help of (13),

$$\frac{b_k}{a_k} = s_{kk}(j\omega) = \frac{V_k - \bar{z}_k I_k}{V_k + z_k I_k} = \frac{Z_k - \bar{z}_k}{Z_k + z_k}. \tag{16}$$

It is possible to express S in terms of $Y_A(j\omega)$, the admittance matrix of N_A, the "augmented" n port associated with N. From Fig. 1,

$$I = Y_A E = Y_A(V + ZI).$$
$$\therefore V - \overline{Z}I = (V + ZI) - (Z + \overline{Z})I$$
$$= V + ZI - 2RI$$
$$= (1_n - 2RY_A)(V + ZI). \tag{17}$$

Hence,

$$2R^{1/2}\boldsymbol{b} = 2(1_n - 2RY_A)R^{1/2}\boldsymbol{a}.$$
$$\therefore S = 1_n - 2R^{1/2}Y_A R^{1/2}. \tag{18}$$

Under our assumptions, Y_A certainly exists if N is passive. Now if N is reciprocal, Y_A is symmetric ($Y_A=Y_A'$) and therefore S is also symmetric since $R^{1/2}$ is diagonal. For a more complete discussion the reader should consult Youla.[2]

D. C. Youla
Dept. of Elec. Engrg.
Polytechnic Inst. of Brooklyn
Brooklyn, N. Y.

[2] D. C. Youla, "Solution to the Problem of Complex Normalization," Microwave Res. Inst., Polytechnic Inst. of Brooklyn, Brooklyn, N. Y. Memo. 48, Contract AF-30(602)-2213; January, 1961.

TM Modes in Parallelogramic Waveguides*

A paper by Swift and Higgins[1] contains comments on a previous article of Malvano,[2] to the effect that a waveguide of parallelogramic cross section cannot support a TM mode free of nodal lines. This implies the possibility that rapid attenuation of the TM_{11} mode in rectangular guide occurs when the guide is deformed into one of parallelogramic cross section and hence we have the characteristic of a mode filter. However, the implication that a slight deformation of a rectangular guide would suppress the mode TM_{11} conflicts with intuition, because it seems that a mode free of nodal lines, as shown in Fig. 1, could exist in a parallelogramic guide.

In order to resolve this argument, the following experiment has been performed. A waveguide section one meter long having a side ratio $\sqrt{2}/2$ (as considered by Malvano) was fabricated with flexible joints so that parallelogramic cross sections of varying angle could be easily obtained. At both ends of this waveguide section, a short-circuiting brass plate was located, properly clamped, so that a good contact was assured along the edge of the guide. At the center of the figure of each shorting plate (*i.e.*, at the intersection of the diagonals of the waveguide cross section), an axial probe was placed. One of the probes was acting as an exciter, and the other as a pick-up for the radiation transmitted along the waveguide. The choice of the axial probe was suggested by the geometry of the expected field, and in consideration of the fact that for a rectangular waveguide the TM_{11} mode is efficiently excited by such a probe. The waveguide cutoff was obtained by measuring the variation of insertion loss vs frequency for constant angle of parallelogramic cross section.

In order to establish that there is a smooth transition from the TM_{11} mode of rectangular guide to the modal pattern depicted in the sketch, measurements of field intensity along the inner surface of the guide around a cross section were made by probing the field with a small electric probe. The field intensity measurements have shown that a TM mode free of nodal lines does exist in guides of parallelogramic cross section.

The experimental data of f_c as a function of α for the fabricated guide are shown in Fig. 2. In the same figure is shown the plot of the equation

$$f_c = \frac{b^2 \sin^2 \alpha + a^2}{\sqrt{\epsilon\mu}\, 2ab \sin \alpha},$$

obtained by considering the TM_{11} cutoff frequency of a rectangular guide having the same base but a height equivalent to the projection of the inclined side of the parallelogramic guide. One can observe that the difference between this curve and the experimental value is less than three per cent for angles from 90° to 30°.

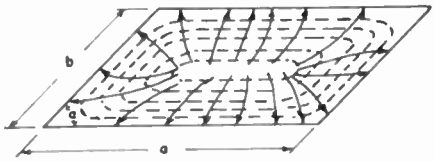

— ELECTRICAL FIELD LINES

--- MAGNETIC FIELD LINES

Fig. 1—Conjectured field pattern of dominant mode in a parallelogramic guide; solid lines represent electric field lines, and dashed lines magnetic field lines.

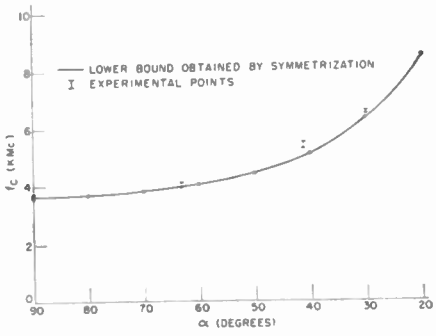

Fig. 2—Cutoff frequency of dominant TM mode vs acute angle of a parallelogramic guide.

This surprisingly good approximation might be interpreted in terms of the geometric operation called "symmetrization," which has been applied by Pólya[3] to the analogous case of vibrating membranes clamped at the edges. Properly applying this operation to a rectangular membrane, one can determine upper and lower bounds for the principal frequency of vibration in a rhombic membrane, and also establish the lower bound for the case of a general parallelogramic membrane. In his article,[3] Pólya demonstrates that symmetrization of a plane figure about a line always decreases the principal frequency of vibration. Hence, symmetrization of a parallelogramic membrane about a line parallel to its vertical will result in a rectangular membrane having a principal frequency which determines a lower bound for the cutoff frequency of the parallelogram. The formula for f_c shown above coincides with the equation defining the lower bound obtained by symmetrization. Unfortunately, there is no line about which a general parallelogram itself (excepting a rhombus and rectangle) is symmetric; hence, one cannot establish an upper bound by this technique.

R. J. Dovtak
D. J. Lewis
P. P. Lombardini
The Moore School of Elec. Engrg.
University of Pennsylvania
Philadelphia, Pa.

* Received by the IRE, March 3, 1961; revised manuscript received, March 16, 1961.

[1] W. B. Swift and T. H. Higgins, "Electromagnetic propagation through waveguides of rhombic cross-section," *Proc. NEC*, vol. 8, pp. 273–284; October, 1952.

[2] R. Malvano, "Guida d'onda metallica a sezione parallelogramma," *Nuova Cimento*, series 9, vol. 6, pp. 265–273; July, 1949.

[3] G. Pólya, "Torsional rigidity, principal frequency, electrostatic capacity and symmetrization," *Quart. Appl. Math.*, vol. 6, pp. 267–277; April, 1948.

A Nondirectional Ferrite Rod Antenna Arrangement Suitable for AM Radios*

This note describes a ferrite rod antenna arrangement suitable for a standard AM radio, and the method by which it is possible to obtain an essentially nondirectional polar pattern. The arrangement is schematically illustrated in Fig. 1, and consists of two mutually-perpendicular, separately-tuned, conventional ferrite rod antennas. By quadrature addition of the two separate antenna signals thus obtained, a perfectly circular polar pattern may be produced. However, even if the addition is not entirely in quadrature, substantial advantages are gained—as is shown by the following development.

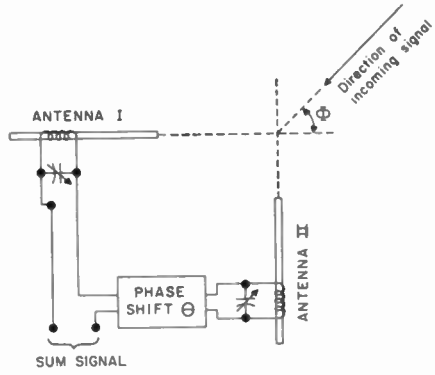

Fig. 1—Nondirectional ferrite rod antenna arrangement.

If the two antennas are identically constructed and tuned to the same frequency, their output signals may be expressed as:

$$S_1(t) = A_0 \cos \omega t \sin \Phi, \tag{1}$$

$$S_2(t) = A_0 \cos \omega t \cos \Phi, \tag{2}$$

where A_0 is a suitable amplitude factor, ω is the angular speed of the received signal, and Φ is the angle between the axis of the ferrite rod of Antenna I and the direction of the incoming signal. If the output from Antenna II is subjected to a phase shift θ and then added to the signal from Antenna I, the amplitude of the resulting sum signal may be obtained by vectorial addition, yielding

$$A_r = A_0 \sqrt{1 + \sin 2\Phi \cos \theta}, \tag{3}$$

which is an expression for the polar pattern of the antenna arrangement shown in Fig. 1.

From (3), it is seen that the ratio between maximum and minimum amplitudes, as obtained when rotating the whole antenna arrangement, can be expressed as

$$R = \sqrt{\frac{1 + |\cos \theta|}{1 - |\cos \theta|}}. \tag{4}$$

From (4) it is found that even if θ deviates fom 90° by as much as ±35°, the resulting polar pattern is still circular within ±3 db.

* Received by the IRE, March 3, 1961; revised manuscript received, March 16, 1961.

This implies that no great accuracy is required in the phase-shifting network, and also that it is not imperative to have perfect tracking between the two tuned circuits when they are tuned over a frequency band.

There are many ways in which to affect the required 90° phase shift. One particularly attractive possibility appears to be that of critically coupling the one antenna to the other. It is well known that in this case the voltage induced in one of the tuned circuits will couple across to the other one with a 90° shift in phase. Consequently, by using the output from either one of the two tuned circuits thus coupled, the effect of a perfectly circular polar pattern should result.

In an experiment performed, critical coupling was established through mutual inductance, and simply by placing the two individual antennas in close proximity to one another. The signal strength across the tuned circuit of Antenna II was then recorded as the whole antenna arrangement was rotated 360° in a plane perpendicular to the direction of polarization of the received signal. Fig. 2 shows the resulting polar patterns as they were obtained at three different frequencies in the AM band. It is to be emphasized that no adjustment in the coupling between the ferrite rod antennas was made during the experiment.

When, as above, the 90° phase shift is established by means of critical coupling, it is to be expected that the effective bandpass characteristics of the antenna arrangement will change with direction of the incoming signal. In Fig. 3 are shown the selectivity curves obtained with the direction of the incoming signal either perpendicular or parallel to the axis of Antenna II. These curves indicate, however, that the changes are not large enough to affect materially the overall selectivity characteristics of a conventional AM radio.

O. K. Nilssen
Scientific Lab.
Ford Motor Co.
Dearborn, Mich.

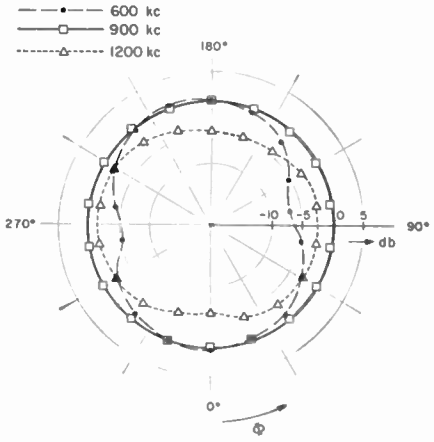

Fig. 2—Experimentally-obtained polar patterns.

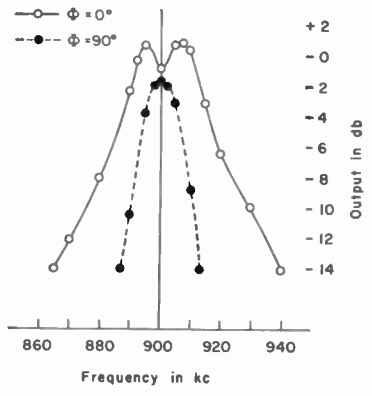

Fig. 3—Selectivity of antenna arrangement for different directions of incoming signal.

"Noisemanship"—The Art of Measuring Noise Figures Nearly Independent of Device Performance*

Almost everyone who has measured the noise performance of a sensitive amplifier or converter has found it possible to read noise-figure values considerably lower or higher than expected. The more exacting experimenters among us have refined their measurement techniques to eliminate such ambiguities and can even obtain accurate noise-figure values for the new, exotic, negative-resistance devices such as parametric amplifiers, masers, and tunnel diode amplifiers and converters. However, as yet, only a few astute practitioners have recognized the tremendous practical value of being able to read noise-figure values much lower or higher than actual. For example, when evaluating their own devices, they can manage to read unusually low noise figures by following certain experimental procedures. (Do not be anxious about their results being much better than theoretical, since they can usually postulate some plausible explanation such as space-charge smoothing.) Conversely, when evaluating their competitors' devices, they can just as readily manage to read exceptionally high noise figures. (Here, however, they usually do the gentlemanly thing and make the magnitude of the noise figures inversely proportional to their competitors' abilities.) To encourage the practice of noisemanship, and thereby bring these very effective practical advantages to all those interested in advancing the state of the art of low-noise devices, we have compiled a partial list of the correct experimental procedures to follow in these two cases.

Case I—Procedures to Be Followed for High-Noise-Figure Readings

1) Use a post-receiver that is very nearly saturated; this makes the output indication almost completely independent of the device under test. By varying the degree of saturation, this one technique alone can lead to almost any desired high noise-figure value.
2) Place a grid-dip meter or sweep generator near the receiver IF amplifier; this is not as effective as procedure 1), but less readily detected by unfriendly observers.
3) Use an argon-discharge noise tube, but use a calibration chart for a neon tube. Since the argon tube has about 3-db less effective output-noise power, an error of 3 db in your favor is easily obtainable. This technique is especially useful if skilled unfriendly observers are present, since the discharge is not visible in any commercial noise generator (because the noise lamp is always located inside a waveguide or coaxial structure) and, therefore, they cannot tell the type of discharge present from its characteristic color.
4) Use a noise generator having the biggest possible difference in source impedance at the two reference noise levels (assuming that a *Y*-factor measurement is made, which is generally true above a few hundred megacycles where noise diodes are no longer useful). This causes a difference in the gain of the device for the two reference conditions. Here, however, one must be careful that the gain decreases when the higher reference temperature is connected. One should also allow sufficient time between the two reference readings so that the output indicator drifts well down scale before the high temperature reference is connected. The use of a badly mismatched noise generator may also cause an unstable device to break into oscillation; if so, an immediate victory is scored.
5) Orient the noise generator for maximum TV, FM, and police radio pickup.
6) Assume that the device has at least three equal spurious responses and, therefore, add 5 db to the measured-noise-figure value. This gives you a knowledgeable air and usually impresses those present.

There are an unusually large number of these procedures, which are too numerous to list here. However, by the use of the few techniques listed above, one can readily pin the noise-figure indicator on the infinite end of the scale. For those pessimists who have only lately entered the low-noise arena, these techniques are guaranteed to lead to immediate positive results.

Case II—Procedures to Be Followed for Low-Noise-Figure Readings

1) Undo procedures 1), 2) and 5) above.
2) Reverse procedures 3) and 4) above.
3) Neglect any spurious responses and quote only the radio-astronomy noise figure.
4) If the observers are aware of the above procedures, place a carefully measured 100-db pad between the noise generator and the device under test. This will eliminate the gain variations caused by noise-generator mismatch, but when 100 db is sub-

* Received by the IRE, March 27, 1961.

tracted from the over-all reading, a low-noise figure is sure to result. An alternate procedure is to use a post-receiver with a 100-db noise figure and then carefully subtract its noise contribution.

Again there are too many of these procedures to list here, but if only the few above are followed, noise figures below 0 db can easily be obtained. This may be a little embarrassing in the presence of theoretically inclined antagonists, but again one can postulate some elaborate thermodynamic mechanism as the probable cause. (If you are anxious about such a procedure, use only one or two of the above procedures, and the noise figure indicator will rest just slightly above the 0-db mark, which is much more readily explained.) For those adventurers who have only lately entered the low-noise arena, these techniques guarantee an immediate entrance into the innermost ring.

In conclusion, techniques have been listed to encourage the rapid growth of noisemanship. Here, however, we think it appropriate to paraphrase Oscar Wilde, who noted that people only like to give advice they will not follow themselves, and with his characteristic wit denoted such advice as the depth of generosity.

J. C. GREENE
Airborne Instruments Lab.
Division of Cutler-Hammer, Inc.
Melville, N. Y.

A Liquid-Helium-Cooled Coaxial Termination*

A 50-ohm coaxial termination has been constructed with a voltage standing-wave ratio less than 1.05 at 960 Mc when cooled by immersion in liquid helium (4.2° K). This termination is very "quiet" in terms of available thermal noise power, which equals kTB, where k is Boltzmann's constant (1.38×10^{-23} joules/°K), T is the temperature (in °K), and B is the bandwidth (in cps). The available noise power from a 4.2°K termination is 5.8×10^{-17} watts, or -132 dbm, over a 1-Mc bandwidth. This instrument has proved to be invaluable in the accurate evaluation of low-noise-amplifier performance, antenna temperature measurements, and radio-astronomy calibrations.

A Stoddart Aircraft[1] 50-ohm "N" connector termination was modified by replacement of the resistive insert with a 63-ohm room-temperature unit. Several inserts were tried until the VSWR desired was obtained when the termination was cooled to the temperature of liquid helium.

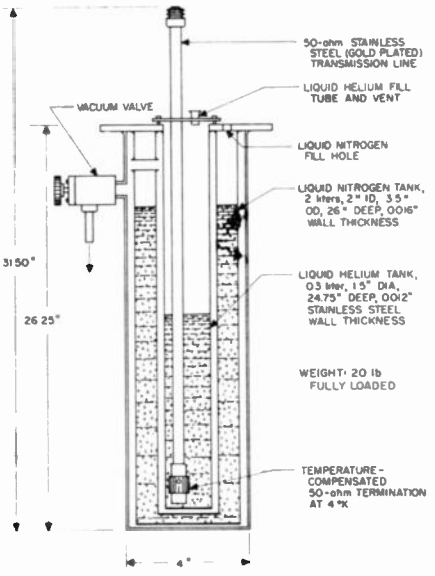

Fig. 1. Construction details of liquid-helium dewar.

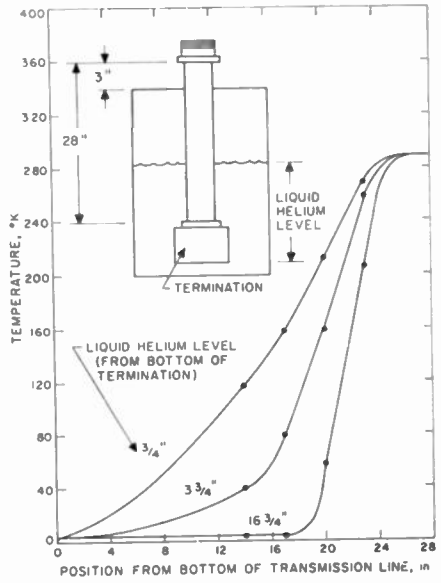

Fig. 2. Plot of temperature distribution on center conductor of coaxial transmission line with liquid-helium-cooled termination.

A 28-inch-long coaxial line was constructed from stainless steel tubing with an inner conductor of 0.188-inch OD, 0.035-inch wall thickness, and an outer conductor of 0.500-inch OD and 0.035-inch wall thickness. Both were plated with 50 micro-inches of copper and 40 micro-inches of gold.

A portable dewar was constructed from standard stainless-steel tubing to hold $\frac{1}{3}$ liter liquid helium and to give approximately 6 hours of active use between refills. The details of the construction are shown in Fig. 1.

The temperature distribution along the transmission line was measured with thermocouples and plotted as shown in Fig. 2 as a function of liquid-helium level. The insertion loss of the transmission line was measured with a Weinschel[2] dual-channel

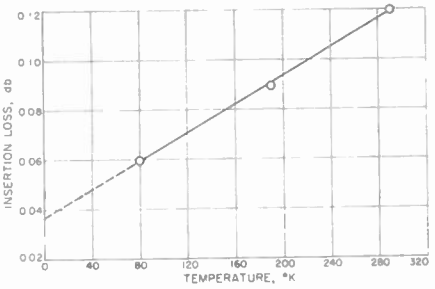

Fig. 3—Insertion loss of plated coaxial line plotted vs temperature.

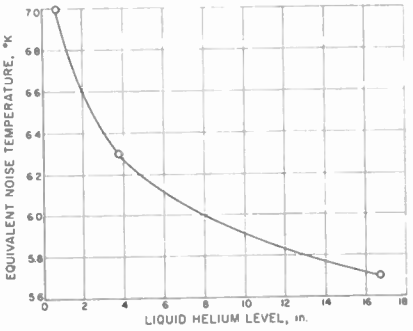

Fig. 4—Calculated equivalent noise temperature of plated coaxial line and liquid-helium-cooled termination plotted vs liquid-helium level.

insertion-loss test set at three temperatures, as shown in Fig. 3. The high insertion loss was assumed to be caused by insufficient plating thickness. The equivalent noise temperature of the transmission line and termination was calculated by separating the line into five sections, each with an average temperature and transmission coefficient. The equivalent noise temperature for a termination and five sections is

$$T = (1 - t_5)T_5 - (1 - t_4)t_5T_4 + (1 - t_3)t_4t_5T_3 + (1 - t_2)t_3t_4t_5T_2 + (1 - t_1)t_2t_3t_4t_5T_1 + t_1t_2t_3t_4t_5T_t,$$

where

T = equivalent noise temperature,
T_n = thermal temperature of nth section from the termination,
t_n = transmission coefficient of nth section from the termination,
T_t = termination temperature.

The equivalent noise temperature was calculated and plotted as shown in Fig. 4 as a function of liquid-helium level.

A second unit is under construction for use at 2388 Mc. The coaxial transmission line will have a larger diameter and thicker plating in order to reduce line loss and, hence, temperature variation with liquid-helium level.

ACKNOWLEDGMENT

The author wishes to acknowledge the assistance of G. Levy, who suggested the project, R. Clauss, who constructed the dewar, and K. Wallace, who performed the measurements.

C. T. STELZRIED
Jet Propulsion Lab.
California Institute of Technology
Pasadena, Calif.

* Received by the IRE, March 1, 1961; revised manuscript received, March 27, 1961. This paper presents the results of one phase of research carried out at the Jet Propulsion Lab., Calif. Inst. Tech., Pasadena, under contract no. NASw-6, sponsored by the Natl. Aeronautics and Space Administration.

[1] Stoddart Aircraft Radio Co., Inc., Hollywood, Calif.

[2] Weinschel Engineering Co., Kensington, Md.

Additional Negative-Resistance Oscillation Modes*

Several modes of oscillation can exist in negative-resistance oscillators. A relaxation mode, a mode operating within the negative-resistance region of the characteristic, and a cosecant mode have been reported.[1] A different set of modes (in effect "class-C" modes) operate around bias points at the peak and valley of the tunnel-diode negative resistance characteristics. Fig. 1 illustrates such a class-C oscillation in a simple parallel LC circuit connected in series with a tunnel diode of characteristics shown in Fig. 2. The output voltage developed across the tank circuit with this mode of oscillation is shown in Fig. 3. Normally the mode is self starting, but under certain bias conditions an external trigger voltage pulse may be used to start the oscillation. Similar oscillations have been achieved around the valley point with voltage swings of 350 mv (peak to peak) for germanium diodes. The operation at frequencies above a few megacycles has not been explored. The lower frequency limit where sinusoidal waveforms have been observed is below 1 cps.

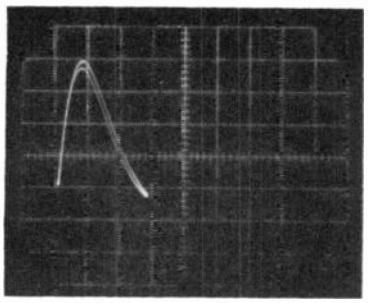

Fig. 1—A class C oscillation cycling about the characteristic curve of diode No. 355 when the dc bias point is at the current maximum. The vertical and horizontal calibrations are 0.1 ma and 50 mv per large division, respectively.

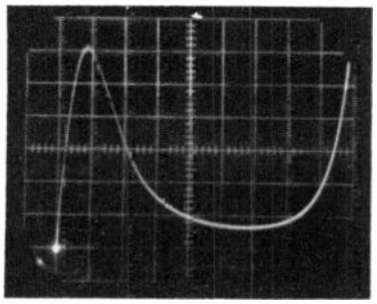

Fig. 2—Germanium tunnel diode No. 355 at room temperature. The vertical and horizontal calibrations are 0.1 and 50 mv per large division, respectively.

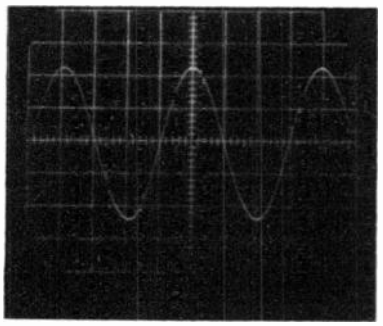

Fig. 3—Voltage output across the tank circuit with the limit cycle of Fig. 1. The total harmonic distortion here is less than 1 per cent. The vertical and horizontal calibrations are 50 mv and 50 μsec per large division, respectively.

* Received by the IRE, March 17, 1961.

[1] C. Brunetti, "Clarifications of average negative resistance with suggestions of its use," PROC. IRE, vol. 25, pp. 1595–1616; December, 1937.

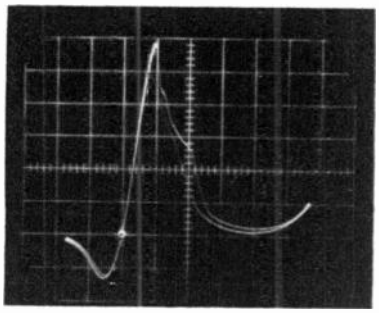

Fig. 4. The oscillation cycling about the characteristic curve of diode Nos. 357 and 383 connected back to back in a simple oscillating circuit. The bias point is at the peak of the tunnel current in the diode with the larger current. The vertical and horizontal calibrations are 0.1 ma and 100 mv per large division, respectively, with the origin being the bright spot.

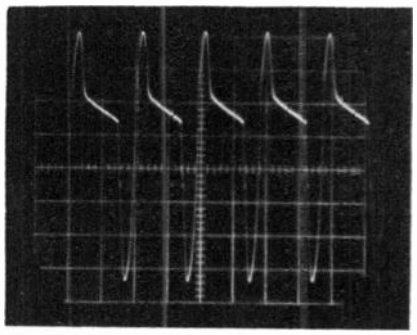

Fig. 5—The output voltage developed across the tank circuit in the oscillation described in Fig. 4. The vertical and horizontal calibrations are 100 mv and 50 msec per large division, respectively.

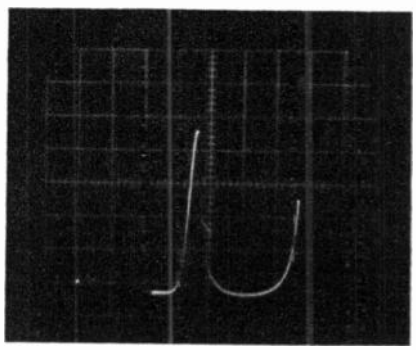

Fig. 6—The oscillation cycling about the characteristic curve of diode Nos. 357 and 390 connected in series. The horizontal scale is 100 mv per large division.

If two tunnel diodes are connected back to back (*i.e.*, in series opposition), the oscillation around the peak point of one diode may extend into the negative-resistance region of the second diode (see Fig. 4) particularly if this diode is of lower peak current. The swing may be as large as 750 mv (peak to peak) and a typical waveform is shown in Fig. 5. Oscillation amplitudes of over a volt may be obtained with a tunnel diode in series with a nontunneling forward-biased diode and the tank circuit as before. With a bias point near the peak of the tunnel diode, the oscillation may extend beyond the tunnel diode characteristic and into part of the nontunelling diode curve as indicated in Fig. 6.

The modes of oscillation in Figs. 4 and 6 require rather large peak-to-valley ratios, and therefore the germanium units used were lowered in temperature to improve the ratio to above 20:1. Such ratios are more commonly obtained at room temperature in gallium-arsenide diodes. A more complete discussion and analysis of oscillation modes in negative-resistance devices is in process.

W. N. CARR
T. C. MATTY
Dept. of Elec. Engrg.
Carnegie Inst. Tech.
Pittsburgh, Pa.

Tunnel-Diode Down Converters*

Similarities exist in two recent papers on tunnel-diode down converters[1,2] if considered in terms of the model shown in Fig. 1. Differences lie in the magnitude and variations assigned to the shot-noise current generator i_{nd}. The shunt-resonant conductance of the input and output circuits tuned to frequency ω_1 and ω_2 respectively, is represented by G_1 and G_2. The diode is represented by a two-port model bridged by a shot-noise generator. A similar model[3] shows that the diode admittance with a relatively large local oscillator voltage applied could be expressed in a Fourier series as

$$g_d = G_0 + 2G_{T_1}\cos\omega_3 t + 2G_{T_2}\cos 2\omega_3 t + \cdots . \quad (1)$$

In addition to the local oscillator voltage at frequency $\omega_3 (=\omega_1+\omega_2)$, only two other voltages at frequencies ω_1 and ω_2 are allowed to exist across the diode by its associated circuits. When these voltages are small compared with the local oscillator voltage, the small signal diode currents are given by taking the product of the small signal diode voltage (v_1-v_2) and the diode conductance g_d. In this product, the signal currents of interest are those selected by the input and

* Received by the IRE, March 20, 1961; revised manuscript received, May 15, 1961.

[1] K. K. N. Chang, *et al.*, "Low-noise tunnel-diode down converter having convers on gain," PROC. IRE, vol. 48, pp. 854–858; May, 1960.

[2] D. I. Breitzer, "Noise figure of tunnel-diode mixer," PROC. IRE (Correspondence), vol. 48, pp. 935–936; May, 1960.

[3] M. J. O. Strutt, "Noise figure reduction in mixer stages," PROC. IRE, vol. 34, pp. 942–950; December, 1946.

TABLE I
EQUIVALENT ANALYSIS SYMBOLS

This Analysis	G_0	G_1	G_2	G_0	G_L	$\bar{G}_1$	$\bar{G}_2$	$(G_{T_1}/\bar{G}_1)^2$	G_{e_0}	G_{e_1}	T_0	T
Chang, *et al.*	G_0	G_1	G_2	G_0	G_L	$\bar{G}_1$	$\bar{G}_2$	$\bar{G}_2\lambda/\bar{G}_1$	$G_e = \frac{e(I_0 - I_{0r})}{2kT}$	—	T_0	T
Breitzer	g_0	—	—	$\frac{1}{r_1}$	$\frac{1}{r_2}$	—	—	γ^2	$\frac{q(I_{0f} + I_{0r})}{2kT}$	$\frac{q(I_{1f} + I_{1r})}{2kT}$	T_1	T_2

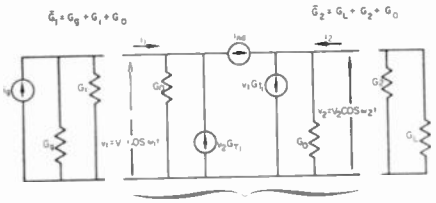

Fig. 1—Noise model of tunnel-diode down converter.

output circuits and are obtained by ignoring all components except those at frequency ω_1 and ω_2

$$i_1 = (G_0V_1 - G_{T_1}V_2)\cos\omega_1 t,$$
$$i_2 = (-G_{T_1}V_1 + G_0V_2)\cos\omega_2 t. \quad (2)$$

Eqs. (2) are the equations used by Breitzer and corresponds to Chang's (2) and (3) at resonance with the changes in the sign of G_{T_1} and v_2 to match the assumed directions for currents and voltages. The most significant terms of (1) here correspond to the two terms obtained from taking the derivative of Chang's (1) with respect to the local oscillator voltage (Table I shows equivalence of terms). Chang assumes that the equivalent saturated diode current for computing G_e was the diode current at the operating point $I_0 = I_{0f} - I_{0r}$ Breitzer assumes not only that the equivalent saturated diode current has an average value given by the sum of the absolute values of the avalanche breakdown current I_{0r}, and the Esaki current I_{0f} at the operating point, but that the equivalent saturated diode current is amplitude modulated by the local oscillator.

Computing the noise figure for Chang's assumptions from Fig. 1, we obtain

$$F = 1 + \frac{T}{T_0}\left\{\frac{G_1}{G_0} + \left(\frac{\bar{G}_1}{G_{T_1}}\right)^2\frac{G_2 + G_L}{G_0} + \left[1 + \left(\frac{\bar{G}_1}{G_{T_1}}\right)^2\right]\frac{G_e}{G_0}\right\}. \quad (3)$$

In (3), the first term results from noise in the signal source, the second term from input-preselector circuit noise, the third from output-tuned circuit and load noise, and the last term from diode noise. Eq. (3) is different in form but identical in content with (26) of Chang *et al.*

Evaluation of the individual terms of (3) for Chang's two examples, results in

$$F_{Ge} = 1 + 0 + 2.32 + 0.30 = 3.62$$
$$= 5.6 \text{ db}^4 \text{ with } 6.0 \text{ db transducer gain} \quad (3a)$$

$$F_{GaAs} = 1 + 0 + 1.14 + 0.21 = 2.35$$
$$= 3.7 \text{ db with } 22.7 \text{ db transducer gain.} \quad (3b)$$

If *LO* modulation of the equivalent saturated diode current is considered, G_e becomes a function of time and may be expressed in a Fourier series as indicated by Breitzer's (6)

$$g_e(t) = G_{e_0} + 2G_{e_1}\cos\omega_3 t + 2G_{e_2}\cos 2\omega_3 t + \cdots. \quad (4)$$

Breitzer has shown that this consideration results in a different noise-figure expression. Using the substitution shown in Table I and adding the terms to account for G_1 and G_2, Breitzer's (5) becomes

$$F = 1 + \frac{T}{T_0}\left\{\frac{G_1}{G_0} + \left(\frac{\bar{G}_1}{G_{T_1}}\right)^2\frac{G_2 + G_L}{G_0} + \left[1 + \left(\frac{\bar{G}_1}{G_{T_1}}\right)^2\right]\frac{G_{e_0}}{G_0} - \frac{\bar{G}_1}{G_{T_1}}\frac{2G_{e_1}}{G_0}\right\} \quad (5)$$

Eq. (5) has one more term than (3). This term results from shot-noise currents in one of the two allowed frequency bands being amplitude modulated by the *LO* which produces correlated shot-noise currents in the other allowed frequency band. When these correlated shot-noise currents are converted to the same frequency band by the small signal properties of the device, the correlation is negative as is shown by the sign of the last term of (5).

Evaluation of the individual terms of (5), in the same order, for the two operating points of a GE ZJ56 (germanium) given by Greene[5] results in

$$F_{Ge_1} = 1 + 0 + 0.58 + 14.92 - 1.24 = 15.3$$
$$= 11.8 \text{ db with } 5.4 \text{ db transducer gain} \quad (5a)$$

$$F_{Ge_2} = 1 + 0 + 0.36 + 9.30 - 1.51 = 9.15$$
$$= 9.6 \text{ db with } 3.0 \text{ db transducer gain.} \quad (5b)$$

In (3a), the shot-noise term is small compared to the G_L/G_0 term. We see here the relative unimportance of the shot-noise term; *i.e.*, whether

$$G_e = \frac{q}{2kT}(I_{0f} - I_{0r}) \quad (6)$$

or

$$G_{e_0} = \frac{q}{2kT}(I_{0f} + I_{0r}) \quad (7)$$

is employed for the equivalent diode shot-noise conductance; the calculated noise figure is essentially unchanged. In (5a) and (5b) terminations have been selected to reduce the load-conductance noise resulting in a large shot-noise term, which makes important the proper choice of (7) for shot-noise conductance.

The noise-figure expression derived by Breitzer differs in two ways from that derived by Chang. The effects of these differences, however, are made small by using high-conductance terminations as Chang, *et al.*, have done in their experimental examples. By allowing the equivalent shot-noise conductance to approach, or exceed, either or both of the input or output conductances, the diode noise is not suppressed. Therefore the more exact noise-figure expression derived by Breitzer gives better agreement with experimental measurements made with other than near-optimum terminations. It appears, then, that Breitzer has derived the more exact noise-figure expression, which Chang, *et al.*, have better minimized.

DON G. PETERSON
Communication and Controls Res. Dept.
Lockheed Missiles and Space Div.
Palo Alto, Calif.

Excess Noise in Microwave Mixer Crystals*

Investigations of noise in dc biased silicon and germanium diodes have shown[1-6] that excess noise is usually the dominating factor, particularly at low frequencies, with a spectral distribution given by

$$W(f) = K(1/f^\alpha), \quad (1)$$

where K and α are constants, and f is the frequency. Most of the measurements have

* Received by the IRE, April 7, 1960.

[4] The reason for the difference between this computed noise figure and the 4.4 db computed by Chang, *et al.*, is not clear, but both agree reasonably well with the measured value of 5.2 db given by Chang, *et al.*

[5] J. C. Greene and E. W. Sard, "Experimental tunnel-diode mixer," PROC. IRE (Correspondence), vol. 49, pp. 350–351; January, 1961.

[1] P. H. Miller, "Noise spectrum of crystal rectifiers," PROC. IRE, vol. 35, pp. 252–256; March, 1947.
[2] H. C. Torrey and C. A. Whitmer, "Crystal Rectifiers," MIT Rad. Lab. Ser., McGraw-Hill Book Co., Inc., New York, N. Y., vol. 15; 1948.
[3] H. C. Montgomery, "Electrical noise in semiconductors," *Bell. Sys. Tech. J.*, vol. 31, pp. 950–975; September, 1952.
[4] F. J. Hyde, "Measurements of noise spectra of a point contact germanium rectifier," *Proc. Phys. Soc.* (London), vol. B66, pp. 1017–1024; December, 1953.
[5] D. K. Baker, "Flicker noise in germanium rectifiers at very low- and audio-frequencies," *J. Appl. Phys.*, vol. 25, pp. 922–924; July, 1954.
[6] A. Hendry, "The temperature dependence of noise temperature ratio in germanium diodes," *Brit. J. Appl. Phys.*, vol. 9, pp. 458–460; November, 1958.

been performed at frequencies below 1 Mc and those made at higher frequencies have been restricted to the normally used intermediate frequencies of microwave receivers. It is found that α is close to unity.[7] However, measurements with dc excitation can give only a qualitative indication of the noise performance to be expected of a mixer crystal in normal use since the actual dynamic operating conditions of a large-amplitude RF drive with a small reverse bias are rather different. The few data which are available of excess noise with RF excitation are restricted to certain fixed frequencies,[2,7-9] and indicate that (1) holds at least up to 45 Mc with $\alpha=1$. The only measurements covering a range of frequencies,[10] 10 to 60 Mc, also indicate that $\alpha\simeq 1$. In view of the comparatively few results available at the higher frequencies, and the important and wide application of these devices, measurements of noise temperature of silicon point-contact diodes have been made over the wide frequency range of 25 cps to 80 Mc.

In the first series of measurements a batch of new, and previously unused, silicon point-contact crystals of types SIM2 and SIM5 (CV2154/5) were tested in broadband mixers over the frequency range 300 kc to 80 Mc. At the higher frequencies the source noise was removed by a cavity filter, and at low frequencies by means of a balanced mixer technique. In each case the crystal noise was compared with that from a standard noise diode. The incident microwave power was adjusted to give a rectified crystal current of 1 ma, which is typical of the values normally used. The resistance of the dc network associated with the mixers was 80 ohms, resulting in a reverse bias of 0.08 volt. Some reverse bias is inevitable, and gives rise to a small increase in crystal noise. The value is quoted here for comparison purposes.

Some typical crystal noise measurements are illustrated in Fig. 1. The results obtained with each crystal are consistent and repeatable, but the imperfection of the manufacturing techniques, even with present-day resources, is shown by the wide variation from crystal to crystal. It may also be seen that none of the crystals tested obeys the $1/f$ rule over the whole frequency range. The curves are all of the same general shape showing that at low frequencies the slope increases to give a value for $\alpha\simeq 1$, while at high frequencies the crystal noise becomes nearly constant and presumably equal to the sum of thermal and shot noise. Extrapolation seems to indicate that excess noise becomes negligible at a frequency of about 100 Mc. For the best crystal tested the $1/f$ law is not obeyed even at frequencies as low as 300 kc; for the bulk of the crystals this relation is only approached below 5 Mc. Thus the view that (1) holds with $\alpha\simeq 1$ at frequencies up to 45 Mc and above must be revised. Extrapolation of the curves indicates that the contributions of thermal and shot noise together correspond to a noise temperature ratio of 0.6 db for the best specimen and 3.0 db for a "typical" crystal.

In order to check how accurately, and over what range, the f^{-1} variation holds at lower frequencies, the noise temperature of one of the crystals was measured over the wide frequency range 25 cps to 30 Mc and for various values of the microwave driving power. The results, of which Fig. 2 is typical, show that the $1/f$ law is obeyed quite accurately from 25 cps to about 300 kc. It is thought that these are the first measurements taken continuously over such a wide frequency range.

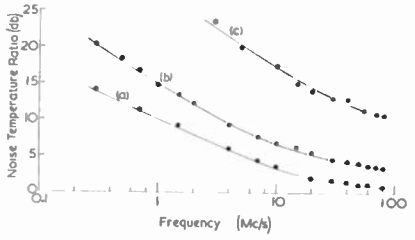

Fig. 1—Variation of noise temperature ratio with frequency. (a) Best crystal. (b) "Average" crystal. (c) Worst crystal.

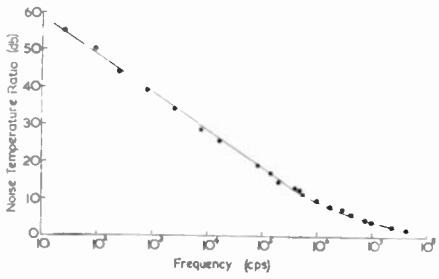

Fig. 2—Variation of noise temperature ratio over frequency range 25 cps to 80 Mc.

It is clear that where the highest sensitivities are required the choice of a mixer crystal for a microwave receiver must be made with great care, and a large number should be tested before the final selection is made since the variation in performance is considerable. Furthermore, when a good crystal is available the noise factor of a receiver can often be further reduced by a reduction in the IF frequency, although the latter also depends on other factors. It appears that although at present excess noise makes a large contribution to mixer noise, further improvement in manufacturing techniques will move the transition region between $\alpha=1$ and $\alpha=0$ to progressively lower frequencies.

B. G. Bosch
W. A. Gambling
T. H. Wilmshurst
Dept. of Electronics,
University of Southampton
Southampton, England

[7] P. D. Strum, "Some aspects of mixer crystal performance," Proc. IRE, vol. 41, pp. 875–889; July, 1953.
[8] G. R. Nicoll, "Noise in silicon microwave diodes," *Proc. IEE*, vol. 101, pt. 3, pp. 317–324; September, 1954.
[9] L. K. Anderson and A. Hendry, "An investigation of the properties of germanium mixer crystals at low temperatures," IRE Trans. on Microwave Theory and Techniques, vol. MTT-6, pp. 393–398; October, 1958.
[10] M. E. Sprinks, G. T. G. Robinson, and B. G. Bosch, "The frequency dependence of noise temperature ratio in microwave mixer crystals," *Brit. J. Appl. Phys.*, vol. 8, pp. 275–277; July, 1957.

WWV and WWVH Standard Frequency and Time Transmissions*

The frequencies of the National Bureau of Standards radio stations WWV and WWVH are kept in agreement with respect to each other and have been maintained as constant as possible with respect to an improved United States Frequency Standard (USFS) since December 1, 1957.

The nominal broadcast frequencies should, for the purpose of highly accurate scientific measurements, or of establishing high uniformity among frequencies, or for removing unavoidable variations in the broadcast frequencies, be corrected to the value of the USFS, as indicated in the table below. The corrections reported have been arrived at by means of improved measurement methods based on LF and VLF transmissions.

The characteristics of the USFS, and its relation to time scales such as ET and UT2, have been described in a previous issue,[1] to which the reader is referred for a complete discussion.

The WWV and WWVH time signals are also kept in agreement with each other. Also they are locked to the nominal frequency of the transmissions and consequently may depart continuously from UT2. Corrections are determined and published by the U. S. Naval Observatory. The broadcast signals are maintained in close agreement with UT2 by properly offsetting the broadcast frequency from the USFS at the beginning of each year when necessary. This new system was commenced on January 1, 1960. A retardation time adjustment of 20 milliseconds was made on December 16, 1959; another retardation adjustment of 5 milliseconds was made at 0000 UT on January 1, 1961.

WWV Frequency
With Respect to U. S. Frequency Standard

1961 April	Parts in 10†
1	−150.7
2	−150.8
3	−150.4
4	−150.0
5	−150.2
6	−150.2
7	−150.4
8	−150.5
9	−150.6
10	−150.5
11	−150.2
12	−150.0
13	−150.3
14	−150.8
15	−150.3
16	−150.2
17	−150.2
18	−150.0
19	−149.9
20	−149.8
21	−149.7
22	−149.7
23	−149.8
24	−149.3
25	−149.6
26	−149.2
27	−149.5
28‡	−149.2
29	−150.3
30	−150.2

† A minus sign indicates that the broadcast frequency was low. The uncertainty associated with these values is $\pm 5\times10^{-11}$.
‡ The frequency was decreased 0.8×10^{-10} at 1900 UT on April 28, 1961.

National Bureau of Standards
Boulder, Colo.

* Received by the IRE, May 25, 1961.
[1] "National Standards of Time and Frequency in the United States," Proc. IRE, vol. 48, pp. 105–106; January, 1960.

On the Hues Seen in Fox-Color Images*

At a session of the National Academy of Sciences, November 20, 1957,[1] Dr. E. H. Land showed fine color pictures projected from only two monochrome slides, astounding the audience, particularly—I would think—those of us who had given much thought to rendition of color, such as in color television. A person or object had been photographed simultaneously with two cameras on black-and-white film, once through a red filter Wratten No. 24, and once through a green filter Wratten No. 58. Copied on slides, the two images were projected in register, the former through red filter No. 24, the other without color filter. The results were very pleasing polychrome images comprising not only red and green (=minus red) but, unexpectedly, also yellow and blue.

The effect had first been noted by W. F. Fox in 1914.[2] He had aimed at two-color pictures with alternate frames using a red and a green filter both for exposure and projection. When the image was too dim he removed the green projection filter, and not only gained light, but also saw many more hues than the mixtures of red and green he had seen before. In 1930, A. Bernardi thought of the same trick for the same reason, had the same surprise ("the theory of the method is perhaps incomplete"[3]). Not for all objects do these images show such unexpected hues. Dr. Land, in his study of images that do show them, has demonstrated that even remarkably modified clues can still make us see them; he and others[4] have tried to find laws relating the colors seen to the stimuli shown. I, myself, to begin with was willing to credit the mind of the viewer with undreamt-of skill in the interpretation of clues. My aim was to find out how many hues a scheme with such limited information can render faithfully, and where it had to fail. If, as we think, definition of a color requires three parameters, either the intensity of three primaries or else a value for the dominant hue (wavelength), for brightness, and for its saturation, then how can we by this method manage with only two parameters for each area, the brightnesses of two superimposed projections? And if we can, one should confidently seek for much simplified color television systems. In 1958, I began a series of systematic tests.

As Dr. Land had shown, superimposed projection of a red wedge crossed by a grey wedge merely shows shades of one pink hue. Recognition of objects is a required condition, thus color test charts also fail. I selected 25 measured hues evenly distributed over the spectrum, each sample in three saturations, and mounted them in five rows in color sequence. The resulting Fox-color images showed only one red in various saturations, one green (minus red) in various shades of (less) saturation, and between them a few near-white colorless areas for the yellow samples. Clearly, it was necessary to study numerous and varied images, and then to try and find rules by induction. Since pictures offer much greater diversity than real objects, and are easily available for repeat and comparison, I selected a dozen full page color pictures from well-printed magazines, ranging from simple, strong to pale and subtle colors, from photographs of fruit bowls to people, landscapes, and to abstract color patches, with preference for well-distributed variety of moderate color areas, as distinct from only one or two hues and from important colors in fine details which might suffer from poor registration. All these were photographed through the same lens in daylight on Kodak Plus X panchromatic 35 mm film, two or three exposures varied 1:2, through red filter No. 24, through green filter No. 58, and later also through bluish-green filter No. 64, whose transmissions are plotted from Eastman data in Fig. 1. There were also color photographs on Kodachrome for reference. All negatives were developed in Kodak D 76, 1:1, 8 minutes at 68° F. All tested negatives were equally usable. They were contact-printed on Kodak positive film with various exposures, developed in D 72, 1:2, at 68°F; all prints tested led to the same observations.

Pairs of these prints were first examined by projection with two identical slide projectors side by side with their axes parallel; one without, the other with, red filter No. 24. Fine register is easily obtained, but projection proved not so flexible and convenient as desired. I therefore built a viewer as sketched in Fig. 2. The eye looks through magnifying lens L of 3-inch focal length under 45° at an optically flat glass plate M_1, whose front surface is anti-reflection coated, and whose rear face is mirror-coated for approximately equal transmission and reflection of all colors under 45°. The transmitted image is that of the "red" slide S_2 backed by a spaced diffuser D and red filter F, illuminated via ordinary mirror M_2. The reflected image is that of the "grey" slide S_1 backed by a spaced diffuser D. Parallel light, indicated by arrows, will illuminate both slides equally. Both slides are seen at the same distance; one of these is easily moved about in its plane for very satisfactory register. Ratio of illuminations could be controlled by shading; but it was found more convenient to provide two lamps No. 47, each in its own reflector and with separate control resistor, mounted so that each illuminated only one slide. Change of "white" hue with lamp current proved harmless. All observations were made with this viewer, many later rechecked with the two projectors, but nothing more or different was noted.

All pairs of slides were methodically and repeatedly scrutinized, again with varied light levels and with varied ratios of brightness; it was noted what colors, if any, were seen in each area and how these compared with the original. From all these data I noted:

1) The color effect is not critical with brightness, is washed out in very bright light and lost in very dim pictures; over the wide useable range the hues seen do not change.

2) Moving one's eyes reveals no afterimage.

3) As soon as one fixes one's gaze, the pictures are nearly final, but (while they do not seem to change) one gets a little more conscious in time of colors other than red or green, such as blue or yellow.

4) Keeping the grey image unchanged and raising red, pictures change from drab neutral to "colored," even when no hue besides red is noted; "colored" means pleasantly undrab, not merely tinted as if seen through tinted glasses.

5) I can see all shades of grey and all shades of that red, some shades in green (=minus red), perhaps in yellow, no shades in other hues.

6) Hues other than red and green were noted only (I think) when known, such as yellow bananas, blue sky, also blue water on some pictures. Listing all hues seen: only one hue of red, one of green, one yellow at a time (this most sensitive of hues shifts towards orange when the red image is turned up), one blue, several orange hues, a dull brown and

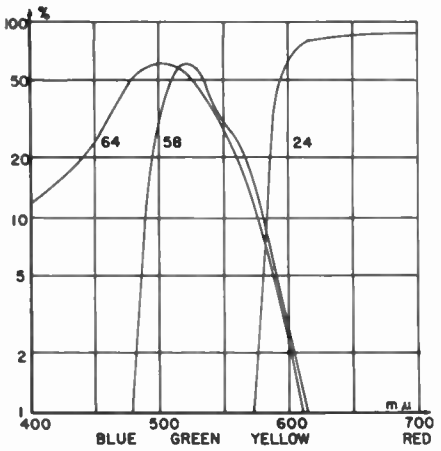

Fig. 1—Transmission of filters no. 24, 58, 64.

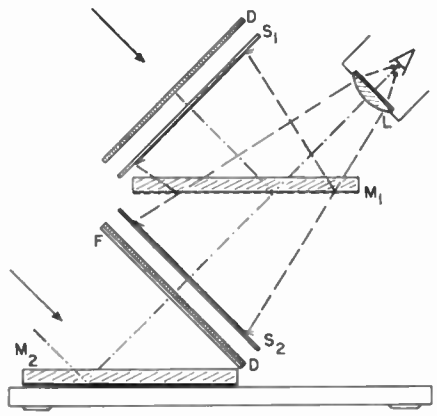

Fig. 2—Optics of slide-pair viewer.

* Received by the IRE, March 27, 1961.

[1] See, for example, E. H. Land, "Color vision and the natural image," *Proc. Natl. Acad. Sciences*, pt. I, vol. 45, pp. 115–129, January, 1959; pt. II, vol. 45, pp. 634–644; April, 1959. Also, "Experiments in color vision," *Sci. Amer.*, vol. 200, pp. 84–99; May, 1959; and letter (by E. H. Land) to *Sci. Am.*, vol. 201, pp. 16, 18, 20 and 22; September, 1959.

[2] W. F. Fox, "Inventor and W. H. Hickey, Manufacturer", British Patent No. 636; July, 1914. I am much indebted to Dr. E. H. Land and to R. T. Kriebel of Polaroid Corp. for this reference and many others.

[3] A. Bernardi, *et al.*, British Patent No. 329,438; May, 1930. Also British Patent No. 335,310; September, 1930.

[4] M. M. Woolfson, "Some new aspects of color perception," *IBM J. Res. & Dev.*, vol. 3, pp. 312–325; October, 1959.

a nondescript color, probably purple, no others.

7) Unless expected, yellow looks white and orange looks red.

8) No hues other than that red and that green can be identified on abstract pictures, even with effort to memorize them.

9) Except for red, then green, yellow and blue, colors are not very strong; one tends to be uncertain about their hue; one notes hues in orange, though not correct.

10) Pictures are (of necessity?) never strident, since seen colors are pleasantly complementary. Indeed one is constantly reminded of Wilhelm Ostwald's ideas on harmonious color combinations,[5] pairs, triples, and quadruples evenly spaced on his 100-hue color circle. As near as I can judge, the red is his No. 79 (>660 mμ), the yellow is his No. 04 (576 mμ), the green is his No. 29 (490 mμ), and the blue is his No. 54 (465 mμ).

11) Since—I suspect—one tends to equate the plausible with the natural, and the strident with the unnatural, one often considers the pleasant hues as natural; yet they are wrong.

12) Pairs of pictures taken with green filter No. 58 render blue very dark, since that filter cuts off blue. Therefore I selected No. 64, a slightly bluer green that passes blue, and repeated most pairs with Nos. 24 and 64. Blue, when seen, *e.g.*, water in a lagoon, is then a bright blue, yellow now a little darker.

13) An order of slides showing most, to few, to no varied hues, corresponds to the order from most familiar to most abstract objects.

14) Since varying of technical conditions such as exposure, printing, and brightness does not, or only slightly, affect these observations, and since the successful and other pairs were all processed alike, I think it most unlikely that I missed one particular set of processing conditions that would have yielded much better results.

The tests led me to suspect that one guesses most of the hues (other than red) from memory. Only a few objects such as fruit were highly successful, many others showed little, and many more no, colors other than red, however long one tries to memorize them. I was pleased only with two out of a dozen images; yet they were not actually correct. My tentative conclusions were that there are two ways to communicate color. The one, according to familiar concepts, informs us without aiding clues, is indispensable at least when we see an object the first time, and requires three parameters. The other transmits much less information (fewer parameters), but relies heavily on the viewer's memory. Indeed it aids the memory rather than is aided by it. One is reminded of a very poor telephone link where one cannot guess words without aid of familiar context. Also that we are unaware of the retinal blind spot shows that our mind can supply what we "see" in these areas.

Since then, there was time to plan some more pointed tests; two occurred to me. The failure to see colors in test charts has been blamed on their extremely unbalanced distribution. Therefore, I assembled the same set of 25 color samples in a seemingly random test chart, actually—for even distribution—so arranged that a), there was in each quarter of the chart at least one hue from each quarter of the spectrum and b), no two patches of similar hue were near each other. This did not improve matters; no more hues can be seen than in the ordered test chart.

Then I wanted to test familiar objects that had been dyed an unfamiliar color. I chose bananas, whose yellow hue is almost irrepressible, and whose even-shaded large surfaces are most convenient. Using filters 24, 58, and 64, photographs as above were taken of mixed heaps of bananas picked for similar size and shape, some bright yellow, some strong green (plantain, Musa paradisiaca) and some mixed-in, painted rather strong skyblue,[6] but approximating the brightness, saturation and surface of their neighbors. While doubting to see them blue, I had expected to see green bananas (a familiar sight here). Actually, with filters 24 and 58, the yellow bananas look a natural yellow, the green plantain look nearly the same yellow, but much less saturated and so look the light-blue bananas, the dark-blue banana tending towards grey-green. With filters 24 and 64, yellow bananas look as before, green plantain as before, the blue bananas rather light, a pale green,—no blue.

As a noted painter[7] wrote: "It would be interesting if some real authority investigated carefully the part which memory plays in painting. . . . The object message . . . has been transmitted in code. . . . It reaches the canvas a cryptogram. Not until it has been placed in the correct relation to everything else that is on the canvas can it be deciphered."

H. E. Kallmann
417 Riverside Drive
New York, N. Y.

[5] W. Ostwald, "Farbkunde," S. Hirzel, Leipzig, Germany, 1923, also "Die Farbenfibel," 2nd ed., UNESMA, Leipzig, Germany, 1917.

[6] Winsor & Newton gouache, cerulean blue and zinc white 1:1; 1:5 thinned with water; a thin, just-opaque coat dries without gloss.

[7] Sir Winston Churchill, quoted in E. H. Gombrich, "Art and Illusion," Bollingen Series, Pantheon Books, Inc., New York, N. Y., pp. 38–39; 1960.

Relative Error Analysis*

In recent years the concept of sensitivity[1] has become one of the useful tools for servo-system design. In another context, that of error analysis, this concept is also quite useful, but its merits do not appear to be widely appreciated. Some of the salient features of this viewpoint are illustrated here.

* Received by the IRE, March 28, 1961.

[1] J. G. Truxal, "Automatic Feedback Control System Synthesis," McGraw-Hill Book Co., Inc., New York, N. Y., pp. 120–127; 1955.

The usual methods for analyzing the propagation of error in an experiment deal with absolute errors and utilize error expressions of the form

$$(\Delta F)_x \approx \frac{\partial F}{\partial x}\Delta x; \qquad (\Delta F)_y \approx \frac{\partial F}{\partial y}\Delta y, \quad (1)$$

where $F = F(x, y)$, and $(\Delta F)_x$ is the absolute error in F resulting from Δx, the absolute error in x. In contrast, sensitivity deals with relative (or per cent) errors and relates the relative error in the results of an experiment to the relative sources of error. These relative errors have the form

$$\frac{\Delta F}{F}; \qquad \frac{\Delta x}{x}; \qquad \frac{\Delta y}{y}.$$

Then if S_x^F is defined as the sensitivity of F to a change in x,

$$S_x^F = \frac{x}{F}\frac{\partial F}{\partial x}, \quad (2)$$

relative error expressions can be written in the form

$$\left(\frac{\Delta F}{F}\right)_x \approx S_x^F \frac{\Delta x}{x}; \left(\frac{\Delta F}{F}\right)_y \approx S_y^F \frac{\Delta y}{y}. \quad (3)$$

Equations having the form of (3) are the key to relative error analysis. Just how the $(\Delta F/F)_i$ for a function, or for an experiment, should be combined to obtain an over-all error figure depends on the use to be made of this figure and also on the nature of the sources of error (*i.e.*, whether independent or correlated, and the shape—Gaussian or otherwise—of each error probability distribution).[2] An outside limit of error can be estimated simply by adding the absolute values of the $(\Delta F/F)_i$.

One simple example of this analysis is a study of the propagation of error in slide rule calculations. Since the scales of a slide rule are of a logarithmic nature, they have the useful property that, for any particular scale, the per cent reading accuracy is the same at all points on the scale. For the C and D scales (and their folded and inverted counterparts) on a ten-inch slide rule, this accuracy is somewhat better than ±0.2 per cent. Now consider the quotient

$$Q = \frac{mno}{pqr}$$

and let it be assumed that the limiting error on each factor is the error in setting the number into the slide rule. The sensitivity of Q to an error in a numerator factor, such as m, is

$$S_m^Q = \frac{m}{Q}\frac{\partial Q}{\partial m} = \frac{m}{\frac{mno}{pqr}}\frac{no}{pqr} = +1.$$

In a similar fashion, the sensitivity of Q to an error in a denominator factor is found to be −1. Hence, the ±0.2 per cent error of setting each factor into the slide rule will contribute ±0.2 per cent to the total error in Q. In addition, there is another ±0.2 per cent error in reading out the answer, Q. Thus, the outside limit of error (as against the prob-

[2] Y. Beers, "Introduction to the Theory of Error," Addison-Wesley, Reading, Mass., pp. 26–36; 1957.

able error, which would be somewhat less) of using a ten-inch slide rule to multiply and/or divide n numbers is simply

$$\% \text{ error} \leq \pm 0.2(n+1)\%.$$

In conclusion, some commonly met sensitivities are tabulated below to suggest the possibilities of relative error analysis. G may be a function of other variables, but not of x.

F	S_x^F
Gx	$+1$
$\frac{G}{x}$	-1
$G \pm x$	$\pm \frac{x}{F}$
Gx^n	n
G^x	x

If M and N are functions of x, then the following relationships may be convenient.

F	S_x^F
MN	$S_x^M + S_x^N$
$\frac{M}{N}$	$S_x^M - S_x^N$
$M \pm N$	$\frac{M}{F} \cdot S_x^M \pm \frac{N}{F} \cdot S_x^N$

John B. Peatman
Dept. Elec. Engrg.
Missouri School of Mines
Rolla, Mo.

Autocorrelation Properties of Convoluted Optimum Finite Code Groups*

There has been a large amount of work done on the problem of finding binary sequences whose autocorrelation functions have uniformly low off-center peaks. This note presents some new results on this topic.

The search for optimum finite code groups has gone on for many years. An optimum code is a sequence of plus and minus ones whose autocorrelation function, as given by the expression

$$R_X(k) = \sum_{i=0}^{N-k} X_i X_{i+k}$$

has the properties:

$$R_X(k) = \begin{cases} N & k = 0 \\ 0 & k \text{ odd} \\ \pm 1 & k \text{ even } k \neq 0, \end{cases}$$

where N is the length of the sequence.

It is known that such sequences exist only for $N = 3, 4, 5, 7, 11$ and 13. In an attempt to produce sequences longer than 13 that have "good" autocorrelation functions, the author has investigated the autocorrelation functions of sequences formed from the convolution of optimum sequences.

The sequences are formed by convolving an optimum sequence of length N, and digit length m, with the same sequence of length N, but of digit length mN. That is, each digit in the original sequence is replaced by the sequence, multiplied by the value of that digit.

If $R_B(k)$ is the value of the autocorrelation function of the original sequence B, at a shift of k digits, then the autocorrelation function of the convolved sequence X, at a delay of k digits, is:

$$R_X(k) = R_B[k(\text{mod } n)]R_B(m) + R_B[n - k(\text{mod } n)]R_B(m+1),$$

where n is the length of the original sequence and m is the integral part of (k/n).

For basic sequences of length 3, 7, and 11, the ratio of $R_X(0)$ to the maximum off-center positive peak of $R_X(k)$ is n^2. A typical correlation function is shown in Fig. 1.

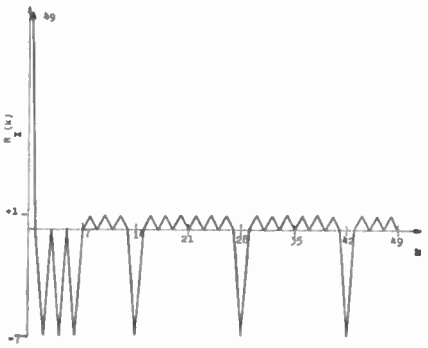

Fig. 1—Autocorrelation function of 7×7 sequence.

The autocorrelation functions of higher-order convolutions are being investigated. From a preliminary study, it would seem that the off-center positive peaks of the correlation functions have the value n^{k-2}, where k is the order of the convolution. Autocorrelation functions of sequences formed from the convolution of different optimum codes are also being investigated.

D. C. Coll
Defence Research Telecommun. Est.
Dept. of Natl. Defence
Shirley Bay
Ottawa, Ont., Can.

References

[1] R. N. Barker, "Group synchronizing of binary digital systems," in "Communication Theory," W. Jackson, Ed., Butterworths Scientific Publications, London, Eng.; 1953.
[2] J. E. Storer and R. Turyn, "Optimum finite code groups," Proc. IRE, vol. 46, p. 1649; September, 1958.

* Received by the IRE, April 14, 1961.

An L-Band Traveling-Wave Parametric Amplifier*

The conventional cavity-type parametric amplifier has a narrow bandwidth and poor stability. The traveling-wave-type parametric amplifier tends to overcome these disadvantages by utilizing a broad-band microwave structure and an amplification mechanism which is unidirectional.[1] This note describes a traveling-wave parametric amplifier which operates around 1.35 Gc and provides a stable gain of approximately 10 db over approximately a 10 per cent band. The amplifier uses 10 Hughes HPA-2810 diodes spaced 3.8 cm apart. Each diode has a series inductance of approximately 4 nanohenries and a static capacitance of about 1 pf for reasonable bias.

The amplifier consists of essentially two circuits: a transmission line for the signal and idling frequencies and a separate circuit for the pump frequency. The signal and idling frequencies propagate on a slab line[2] which is periodically loaded with the semiconductor diodes. Each diode is fed with a pump signal whose phase can be arbitrarily adjusted. The individual pump powers are supplied by a pump generator whose output is divided by means of a power divider into as many lines as there are diodes. Each diode can be individually back-biased by means of an external bias supply.

A drawing of the slab transmission line is shown in Fig. 1(a). The slab line consists of two flat plates and a cylindrical center conductor. The diodes are mounted periodically between the center conductor and one of the flat plates, resulting in a loaded-line impedance of 50 ohms. Each diode is fed with a properly phased pump voltage through a coaxial line. This line contains a bias stub which enables a dc bias voltage to be applied to the diode to cause its static capacitance to be at a desired operating point. A blocking capacitor is placed at the pump input end of each coaxial line to prevent the pump

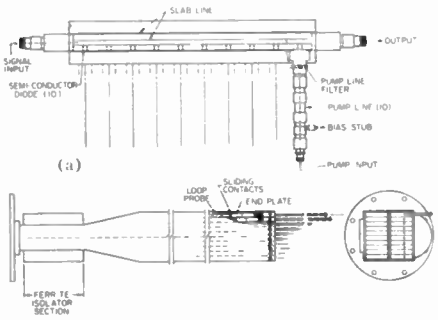

Fig. 1—(a) Signal transmission line of parametric amplifier. (b) Power divider and isolator section.

* Received by the IRE, February 27, 1961; revised manuscript received, March 23, 1961.

[1] C. V. Bell and G. Wade, "Circuit Considerations in Traveling-Wave Parametric Amplifier," 1959 IRE WESCON Convention Record, vol. 3, pt. 2, pp. 75–82.

[2] W. B. Wholey and W. N. Eldred, "A New Type of Slotted Line Section," Proc. IRE, vol. 38, pp. 244–248; March, 1950.

generator from shorting out the bias power supply.

A band-pass filter is located near the diode junction in each pump line. This filter prevents propagation of the signal, idling, and upper sideband frequencies toward the pump power divider while allowing transmission of the pump frequency.

The 10 coaxial pump lines are fed from the 10 outputs of a waveguide power divider, a drawing of which is shown in Fig. 1(b). The pump source is a 2 K 41 klystron which provides a power output of approximately 0.7 watt at a frequency of 2.64 Gc. The pump power is fed into a section of standard height *S*-band waveguide which is then divided into ten 6.35 mm height waveguide outputs. A loop probe is inserted into each waveguide output and attached to an end plate. This shorting plate is moveable and makes electrical contact with the walls by means of attached fingers. Each probe is attached to a rigid Amphenol Subminax connector which in turn connects through a length of Subminax coaxial cable to one of the pump inputs of the slab line. The pump phases are varied by moving the combination waveguide shorts and loop probes in or out.

The biases and pump phases were adjusted for an optimum gain over the band. Fig. 2 shows the forward gain characteristics of the amplifier for an average pump power per diode of approximately 50 mw. With slight readjustment of pump phases or diode biases, the gain near 1.42 Gc can be increased to above 30 db without much change in the rest of the gain curve. It appears that the gain is not due entirely to a pure traveling-wave type of interaction, but that the individual diodes are also contributing to the gain in a nontraveling-wave fashion.

When the amplifier is operating properly, it should have no reverse gain, and preferably a loss. The reverse loss is shown dotted in Fig. 2.

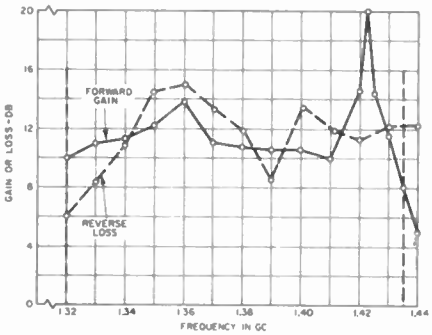

Fig. 2—Forward gain and reverse loss of parametric amplifier.

Noise figure measurements were made with the amplifier operating in the frequency range of 1.34 to 1.39 Gc and for gains varying from 10 to 15 db. The average single-channel noise figure was 4.0 db, with a probable error of ±0.3 db.

ACKNOWLEDGMENT

The authors wish to acknowledge the advice and assistance of H. Heffner, J. Lepoff, and G. Wheeler during the course of this work.

S. J. TETENBAUM
Sylvania Electric Products, Inc.
Mountain View, Calif.
F. A. OLSON
AF Cambridge Res. Labs.
Air Research Dev. Ctr.
Bedford, Mass.
Formerly with Sylvania Electric Products, Inc.
Mountain View, Calif.
A. SAVARIN
G. T. and E. Labs., Inc.
Palo Alto, Calif.
Formerly with Sylvania Electric Products, Inc.
Mountain View, Calif.

Contributors

W. H. CLINGMAN

William Clingman was born in Grand Rapids, Mich., on May 5, 1929. He received the B.S. degree in chemistry in 1951 from the University of Michigan, Ann Arbor, and the A.M. and Ph.D. degrees in chemistry and physical chemistry, respectively, from Princeton University, N. J., in 1954.

In that year, he was employed by American Oil Company, Texas City, as a Research Chemist, and from 1957 to 1959 he served as a Group Leader. His experience with that firm included the effect of radiation on semiconductor catalysts, radiation chemistry, and radioisotope applications; he also did exploratory work in the development of chemical and petroleum processes. He joined Texas Instruments, Inc., Dallas, Tex., in 1959 as Head of the Thermoelectric Section in the Device Research Department, Central Research Laboratories.

Dr. Clingman is a member of the American Chemical Society and Sigma Xi.

❖

J. M. DIAMOND

Joseph M. Diamond (S'44–A'47–M'55) was born in New York, N. Y., on December 26, 1924. He received the B.E.E. degree from Cooper Union, New York, N. Y., in 1944. He then served in the Navy for two years, did television receiver development at Bendix Radio Corp., Baltimore, Md., for a year, and returned to school for graduate work. He received the M.S.E.E. degree in 1949 and the M.A. degree in mathematics in 1950, both from the University of Pennsylvania, Philadelphia. Since that time he has been concerned with circuit theory and circuit design, especially as applied to electronic instrument design. In this capacity he designed a wide range of instruments for laboratory and production use, at the United Transformer Company, New York, N. Y. He also has been active as an instructor of electrical engineering at the University of Pennsylvania and at C.C.N.Y., and has published a number of papers.

Mr. Diamond is a member of Tau Beta Pi.

R. J. GARBACZ

Robert J. Garbacz (S'54–M'59) was born in Buffalo, N. Y., on September 12, 1933. He received the B.S.E.E. degree from the University of Buffalo, Buffalo, N. Y. in 1955 and the M.S.E.E. degree from The Ohio State University, Columbus, in 1957.

Since 1955 he has been a Research Associate of the Ohio State Antenna Laboratory, during which time he has been concerned primarily with microwave circuit theory, flush-mounted antennas, and electromagnetic scattering, and where he is presently working towards the Ph.D. degree.

Mr. Garbacz is a member of Pi Mu Epsilon, and is associated with Sigma Xi.

❖

Irving Gerst was born in New York, N. Y., on May 30, 1912. He received the B.S. degree in mathematics from the College

of the City of New York in 1931. He did graduate work in mathematics at Columbia University, New York, N. Y., receiving the M.A. and Ph.D. degrees in 1932 and 1947, respectively.

IRVING GERST

From 1937 to 1944 he was an instructor in mathematics and applied mathematics, first in the New York City school system and then at the Air Force Technical School, Biloxi, Miss. From 1944 to 1945 he served in the Army Transportation Corps as a technical consultant on logistics problems. From 1946 to 1958 he was at the Control Instrument Company, Burroughs Corporation, Brooklyn, N. Y., first as a research mathematician and later as Head of the Applied Analysis Section. Since 1958 he has been associated with the Surface Communications Systems Laboratory, RCA, New York, N. Y., where he is presently Leader of the Networks and Topology Group. Since 1958 he has also been a lecturer at the Graduate School of Engineering, the College of the City of New York.

Dr. Gerst is an associate editor of the *Journal of the Society for Industrial and Applied Mathematics*. He is a member of the AMS, the Mathematical Association of America, and Sigma Xi.

❖

J. M. Lafferty (M'46–SM'48–F'54) was born in Battle Creek, Mich., on April 27, 1916. He attended Western Michigan University, Kalamazoo, and received the B.S. degree in engineering physics in 1939, the M.S. degree in physics in 1940, and the Ph.D. degree in electrical engineering in 1946, all from the University of Michigan, Ann Arbor.

J. M. LAFFERTY

After aiding in the development of the VT proximity fuse at the Carnegie Institution, Washington, D. C., during 1941, he joined the General Electric Company, Schenectady, N. Y., in 1942. At G.E. he has done research on microwave tubes, electron accelerator guns, boride cathodes, color-television picture tubes, gas-discharge tubes, and measurement of ultra-high vacua. Presently he is Manager of the Physical Studies Section of the General Electric Company's Research Laboratory in Schenectady.

Dr. Lafferty is a member of the American Physical Society, the AIEE, the American Vacuum Society, and Sigma Xi.

❖

David L. Moffatt (S'58–M'59) was born in Wheeling, W. Va., on October 28, 1927. He received the B.E.E. degree in 1958 and the M.S.E.E. degree in 1961, both from The Ohio State University, Columbus.

D. L. MOFFATT

Since 1958 he has been associated with the Antenna Laboratory of the Electrical Engineering Department of The Ohio State University as a Research Associate, working in the fields of flush-mounted antennas and electromagnetic scattering.

Mr. Moffatt is a member of Tau Beta Pi and Eta Kappa Nu.

❖

H. A. Stone, Jr. (SM'55) was born in New York, N. Y., on July 7, 1909. He received the B.S. degree in physics from Yale University, New Haven, Conn., in 1933.

H. A. STONE, JR.

He joined Bell Telephone Laboratories, Inc., Murray Hill, N. J., in 1936 where he was engaged in the design of inductors until 1953, when he became Components Development Engineer in charge of an organization devoted to fundamental development of inductors, capacitors, and resistors. In 1958 he was appointed Director of Components Development with responsibility for the development and design of passive components for Bell System use.

Mr. Stone is an associate member of the AIEE.

T. A. Vanderslice was born in Philadelphia, Pa., on January 8, 1932. He received the B.S. degree in chemistry from Boston College, Boston, Mass., in 1953, and the Ph.D. degree in physical chemistry from the Catholic University of America, Washington, D. C., in 1956. His doctoral thesis work was on free radical chemistry, under the direction of Professor F. O. Rice.

T. A. VANDERSLICE

Since joining the General Electric Company, Schenectady, N. Y., in 1956, he has done research on surface chemistry, gas discharges, mass spectrometry and ultra-high vacua.

Dr. Vanderslice is a member of the American Chemical Society, the American Physical Society, the AAAS, the American Vacuum Society, Alpha Sigma Nu, and Sigma Xi.

❖

R. M. Warner, Jr., (SM'59) was born in Barberton, Ohio, on March 21, 1922. He received the B.S. degree in physics from Carnegie Institute of Technology, Pittsburgh, Pa., in 1947, and the M.S. and Ph.D. degrees from Case Institute of Technology, Cleveland, Ohio, in 1950 and 1952, respectively. He served as physics instructor at both institutions and, during school intervals, worked in the research laboratories of the Pittsburgh Plate Glass Company and the Corning Glass Works.

R. M. WARNER, JR.

He spent 40 months in the Army Signal Corps, serving as radio officer during World War II in both overseas theatres. From 1952 to 1959 he worked on semiconductor device development at Bell Telephone Laboratories and since 1959 has been Chief Engineer, Diode Development, at Motorola Semiconductor Products Division, Phoenix, Ariz.

Dr. Warner is a member of the American Physical Society, AAAS, Sigma Xi, Tau Beta Pi, and Phi Kappa Phi.

Books

High-Frequency Magnetic Materials—Their Characteristics and Principal Applications, by W. J. Polydoroff

Published (1960) by John Wiley and Sons, Inc., 440 Fourth Avenue, New York 16, N. Y. 215 pages +4 index pages +x pages. Illus. 6×9¼. $9.00.

The subject of high-frequency magnetic materials covers a wide variety of materials for a multiplicity of applications. Considerably more than the 215 pages in this book would be required to treat the complete subject with any degree of thoroughness. The author has elected to emphasize several particular applications and materials characteristics related thereto—namely, magnetic core inductors, variable inductors for permeability tuning, and ferromagnetic antennas—and to provide only a cursory treatment of other high-frequency magnetic applications and their respective materials requirements and characteristics.

Following a short first-chapter introduction, the remaining thirteen chapters can be considered either as materials oriented or application oriented. Chapters 2–8 are concerned primarily with materials, their properties, measurement techniques, and methods of preparation; and chapters nine through fourteen deal with the applications of high-frequency magnetic materials.

Materials covered include elemental iron prepared by various processes (carbonyl, electrolytic, hydrogen-reduced, etc.); alloys of iron with other metals such as nickel, aluminum, silicon, tin, and antimony; and ceramic ferrites of the spinel type like nickel zinc ferrite. No mention is made of other types of ferrites, *e.g.*, the oriented-plane hexagonal ferrite. Dense and powdered forms of most of the included categories of magnetic materials are discussed. The account of measurement techniques describes mainly the methods of measuring permeability and loss of high-frequency core materials.

The last seven chapters stress the applications of high-frequency magnetic materials in magnetic core inductors, variable inductors for permeability tuning, and ferromagnetic antennas. The author references and discusses several of his patents in these chapters. A unique case of permeability tuning that was considered involves tuning by using the incremental permeability. Here, an additional winding passing a direct current of controllable magnitude changes the inductance of the coil by superimposing on the core material a steady flux. The author believes that this method possesses great potential for nonmechanical and remote-control tuning of all kinds of radio equipment. He cites as the major obstacle to this method the attainment of a steady direct-current source, but this reviewer feels he does not give due consideration to the deleterious temperature coefficient effects of ferrite core materials if the technique is intended for military equipment and consumer products.

Cursory treatment is given to other high-frequency applications of magnetic materials in the final chapters. These include loaded dipole antennas, delay lines, pulse transformers, memory cores, and microwave ferrites. Although one of the chapters is concerned totally with ferrites in microwave applications, the chapter cannot be interpreted as other than a superficial treatment because of the vastness of this particular field. The microwave chapter does, however, provide the reader with an introductory concept of several microwave applications of ferrites.

In general, the book provides a valuable source of information on magnetic materials, including much tabular and graphical data, and will be particularly useful to the applications engineer designing and employing high-frequency circuit elements such as magnetic core coils, tuners, and antennas. Written with a maximum of practical description and a minimum of complex mathematics, the book has an easy-reading manner of presentation, making it also useful to the novice desirous of general knowledge in this field.

D. L. Fresh
Motorola, Inc.
Scottsdale, Ariz.

Linear Circuits, Part 1: Time-Domain Analysis; Part 2: Frequency-Domain Analysis, by R. E. Scott

Published (1960) by Addison-Wesley Publishing Co., Inc., Reading, Mass. 897 pages +12 index pages +xx pages +bibliography by chapter +6 appendix pages +37 answers to exercises pages. Illus. 6×9¼. Each volume $6.75.

The purpose of this two-volume treatment of linear circuits is to provide depth in network theory in a beginning course with a minimal allotment of time. To this end, the author has directed himself with noteworthy perception, clarity, and enthusiasm. Many subjects rarely found in a first course are concerned.

In both volumes, each chapter contains a summary of the most significant results, references, and an abundance of well-selected problems.

Approximately the first half of Part 1, "Time Domain Analysis," is given to the topology of networks with the elements being limited to resistors. This approach allows study of more complex network configurations without the attendant complexities imposed by reactive elements. The mesh and node equations, network theorems, and four-terminal networks are all considered in this section. Further, the mesh and node equations are extended to cover networks containing ideal current and voltage sources. In view of the fine quality of presentation, it would have been well to extend the mesh equations to non-planar networks in order that the mesh set have the broad utility of the node set.

The second half of this volume introduces the differential equations of reactive networks and considers classical solutions of these equations.

In Part 2, transform domain techniques are considered. About one half the book is devoted to sinusoidal steady-state solutions, with the remainder being given to applications of Fourier Series and the Fourier, Sine, Cosine, and Laplace Transforms.

Even though individual preference might dictate some differences in emphasis and order of presentation, the reviewer feels that this work merits careful examination by all teachers of network theory.

T. W. Culpepper
Michigan State University
East Lansing

Principles of Feedback Control, by C. H. Wilts

Published (1961) by Addison-Wesley Publishing Co., Inc., Reading, Mass. 244 pages +3 index pages +x pages +17 appendix pages. Illus. 6¼×9¼. $8.75.

To summarize this book in the fewest words: very good! As stated in the preface the book gives rigorous treatment to the primary analytical tools of the servo designer. These tools include the Bode, Nyquist and root locus methods.

The complex variable theory is given as the prime mathematical means, with the Laplace transform appearing only often enough to remind the reader of its existence. This makes the book, in this reviewer's opinion. This approach puts the three methods previously mentioned in their proper perspective as mathematical tools useful as guides during feedback design. This is in contrast to the usual presentations where the methods are presented as panaceas.

The development of the book is straightforward and precise. Having the proper definitions in the proper spots is a good feature.

It is not until Chapter 7 that the actual servo design is introduced. The first six chapters logically develop the tools. The book then proceeds through multiloop systems, closed loop response, transient response, and other selected topics. These topics are described by all three methods: Bode, Nyquist, and root locus.

Chapter 11–12 cover sampled-data and nonlinear systems. The Z-transform and the describing function are examined.

It is felt that this book would be of greatest use to those who have had some previous studies in complex variables, both analytically and graphically. In addition, a course in response of physical systems is helpful but not essential.

While no handbook, the book serves a good purpose in training the senior or graduate student and the practicing engineer. It is strongly recommended to those in the control business as well as those wishing to get into this field.

Richard G. Buscher
General Electric Co.
Schenectady, N. Y.

Electronic Equipment Reliability, by G. W. A. Dummer and N. Griffin

Published (1961) by John Wiley and Sons, Inc., 440 Fourth Ave., New York 16, N. Y. 257 pages+4 index pages+xi pages+12 bibliography pages. Illus. 5¼×8¼. $7.50.

This book supplies an excellent introduction to the background of reliability engineering. This rapidly expanding field is loaded with numerous papers but is lacking many good sound texts. Here is a book which covers the many phases of reliability and should be helpful to all those persons presently involved in reliability problems.

If we divide reliability into three major phases: parts and materials, systems, and quality assurance, it should be noted that the book is oriented towards the first of the three. This is good, for it can arouse the designers who must understand the need for reliability. There are valuable descriptions of part failure modes. Environmental effects and part testing methods are treated very well also. The book is not as strong in the latter two areas but it is impossible to expect everything within one volume. However, the sections on reliability predictions and reliability design are brief but concise. Enough information is presented to instruct the designers in the preparation of predictions and redundancy analyses. The subject of quality assurance was not formally presented. Its theme is not a necessary part of this kind of text.

A very valuable section of this book concerned human engineering. This is a very important marriage—human engineering and reliability. The chapter presents a good bit of definite design practices which, if followed, should increase the reliability of equipment operation.

The most severe criticism of the book is its presentation of old data. Most of the referenced articles date to the 1950–1957 era. Reliability techniques and failure rates of parts have changed greatly since that time. However, in contrast to some of the outdated information there is some good data on late techniques such as wire wrap, and some good information concerning printed circuit boards. Another disappointing factor is the lack of transistor data. Evidently the author plans an additional volume to discuss the semiconductors. Many preferred tube circuits are presented. At this point the book digressed into a set of pseudo standards which the reviewer believes is out of order in a text of this type.

M. Raphelson
RCA
Camden, N. J.

Mathematical Handbook for Scientists and Engineers, by Granino A. Korn and Theresa M. Korn

Published (1961) by McGraw-Hill Book Co., Inc., 330 W. 42 St., New York 36, N. Y. 746 pages+29 index pages+xiv pages+bibliography and references by chapter+164 appendix pages+7 glossary pages. Illus. 6¼×9¼. $20.00.

This comprehensive volume represents the first really authoritative attempt to describe mathematical formalism of vital importance to scientists and engineers. By steering a middle course between the facts and formulas which are typical of handbook treatment and the ponderous development which characterizes treatises in special fields, the authors have succeeded in condensing various aspects of modern mathematics into a coherent format. It is truly a remarkable achievement.

In referring to specific chapters, the reader will be highly impressed by the fact that details, which can usually seem too numerous and hopelessly confusing, fall into place with proper emphasis. As a special feature, the authors have thoughtfully included, at the end of each chapter, a cross-reference on those topics which are closely related throughout the handbook. Further, each chapter is very well documented with references and bibliography, and is sufficient in itself.

Chapter 1 begins with algebraic concepts involving real and complex numbers and develops several methods for locating the roots of algebraic equations and for solving simultaneous algebraic equations. Chapter 2 considers the basic concepts of plane analytic geometry and relations involving various geometries. These principles are extended in Chapter 3 to include solid analytic geometry. In Chapter 4, functions of real variables and their representations are described and a thorough treatment of limits, differential calculus, integral calculus, and infinite series is included. Elliptic integrals, Lebesque-Stieltjes integrals, Weierstrass's approximation theorems, Fourier integrals, and Fourier transforms are also discussed. Chapter 5 deals with vector analysis. Representations of scalar and vector functions in terms of curvilinear coordinates are formulated in Chapter 6. This chapter also lists useful equations relating to a number of special orthogonal coordinate systems.

Functions of a complex variable, the Laplace transformation, and other integral transformations, as well as the Schwarz-Christoffel Transformation, are the main topics of Chapters 7 and 8. A striking treatment of ordinary differential equations in Chapter 9 is followed by the development of partial differential equation as part of Chapter 10. This latter chapter also delves deeply into the characteristics and boundary-value problems of hyperbolic, parabolic, and elliptic second-order equations. The use of integral-transform methods is also outlined.

Chapter 11 introduces the reader to methods of solving problems by maximization or minimization techniques involving functions of real variables, definite integrals, and differential equations. Foundations of modern algebra, notably, groups, rings, fields, vector spaces, linear algebras, and Boolean algebras, are summarized in Chapter 12. The content of Chapter 13 relates to matrix algebra and matrix calculus. Chapter 14 reviews the theory of vector spaces and linear transformations. Chapter 15 considers the solution of linear boundary-value problems and eigenvalue problems involving differential equations in addition to potential theory and conformal mapping.

Chapter 16 establishes the basic rules of tensor algebra and analysis as applied to the description of curved spaces and continuous fields in physics. Chapter 17 emphasizes the use of differential geometry in describing curves in Euclidean space. Chapter 18 treats probability theory and random processes, including special procedures for solving probability problems and examples of random processes. Statistical methods are lucidly covered in Chapter 19. A variety of numerical computation schemes are detailed in Chapter 20. The calculus of finite differences is also introduced and applied to deriving numerical solutions. Chapter 21, as the final chapter, summarizes the characteristics of special functions, such as transcendental, gamma, elliptic, cylinder, step, and symbolic impulse functions. Polynomials of the Bernoulli and orthogonal types are also discussed.

Formulas describing plane figures and solids, plane and spherical trigonometry, permutations and combinations, tables of Fourier expansions and Laplace-transform pairs, tables of indefinite and definite integrals, and numerical tables of various functions are respectively introduced in the appendixes.

All in all, this is a timely handbook, written by just the right authors, about a subject of fundamental value to anyone concerned with the exact physical sciences and their applications. It is first rate all the way through.

Anthony B. Giordano
Polytech. Inst. Brooklyn
Brooklyn, N. Y.

1959 Digest of Literature on Dielectrics, Louis J. Frisco and Thomas D. Callinan, Eds.

Published (1960) by the National Academy of Sciences—National Research Council, 2101 Constitution Ave., Washington 25, D. C. 421 pages+xiv pages+bibliography by chapter+1 appendix page. 8½×11. $8.00.

Like its predecessors, this book contains summaries of progress during the year in the broad field of dielectrics. It is the result of the efforts of approximately 50 specialists, and includes material from almost every subdivision of the field. Material is organized into chapters, in which easily-read, concise commentaries of notable results published during 1959 are given. These are amply interspersed with over 2200 references to books, periodicals, and conference papers.

Of the twelve chapters, one is devoted to instrumentation and measurements, one to applications of dielectrics, and the remaining ten to the theory and properties of materials. In addition to coverage of solid, liquid and gaseous conventional dielectrics, the digest includes material on photoconduction and electroluminescence. A large chapter is devoted to magnetic materials. Another covers ferroelectric and piezoelectric materials. Nineteen pages of tables of dielectric constants, dipole moments, and dielectric relaxation times are also included.

The depth of the material summarized makes this book of particular value to the research worker. The reviewer found several such people who were familiar with the volume to be unanimous in their expressions of its usefulness.

P. N. Wolfe
Westinghouse Research Labs.
Pittsburgh, Pa.

The International Dictionary of Physics and Electronics, Second Edition, Walter C. Michels, Editor-in-Chief

Published (1961) by D. Van Nostrand Co., Inc., 120 Alexander St., Princeton, N. J. 1269 pages+85 index pages. Illus. 7¼×10¼. $27.85.

This is a revised and up-dated edition, with a considerable number of new definitions added, particularly in such rapidly-growing fields as thermonuclear research, magnetohydrodynamics, nuclear physics, astrophysics and electronics. It encompasses over 8000 entries, and 300 illustrations and is amply supplied with mathematical expressions for important relationships.

This reviewer has checked a considerable number of entries, particularly in the solid-state and nuclear fields. Also, their conformance to some of the more recent IRE Standards was examined. In general this conformance is good; however, the editor has occasionally fallen into the common fault of revising some existing IRE definitions, possibly by changing only a word here or there. A more serious complaint is that in those IRE definitions which have notes included, these notes have been incorporated into the body of the definition without differentiation. In the proper usage, the notes are intended to be explanatory and do not form part of the actual definition and have no legal standing.

The coverage of the solid-state art is quite inclusive, particularly with respect to transistors. Tunnel diodes, however, were apparently not on the scene at the time of preparation, and are not included. Tunneling and the tunnel effects are, however, defined by reference to penetration probability. Similarly the epitaxial technique is not included directly, although there is a definition of epitaxy which is applicable.

There are some inconsistencies in the use of transistor letter symbols, as, for example, in the occasional use of lower-case subscripts for dc values, even though the section on transistor symbols itself is correct in most places. A few random items in this particular field: avalanche transistor is defined as being another name for a semiconductor controlled rectifier; drift mobility definition is quite different from current IRE definition; impurity definitions are radically different from the 1960 IRE Standard, and slightly different from previous 1954 Standard; and "hole" definition is radically different from IRE.

Coverage in the nuclear field is considerably less comprehensive than in the solid-state field. This reviewer looked in vain for a mathematical treatment of the fission process comparable to that given some of the mathematical concepts (*e.g.*, Elliptic Integral) or physical concepts (*e.g.*, Beta Decay Theory). Various reactivity terms are missing; precursor is mentioned but not defined; the definition of proportional counter reads like the IRE definition of Proportional Counter Tube but omits the "tube"; the definition of proportional counter tube refers to counter tube, proportional, but this is not listed; resolving time is not defined.

A few more items: emitance is defined as impedance and/or admittance, which does not conform to the IRE definition; transmittance is defined only for optics; transfer admittance is not defined as per the latest IRE Standard; "flip-flop" is indicated as being applied to monostable as well as to bistable multivibrators, which is not common practice.

This reviewer appreciates only too well how easy it is to pick out a few examples of errors or inconsistencies out of more than 8000 items and does not intend to imply that the work is, therefore, incorrect. Even where the definitions do not quote IRE exactly, they are usually clear and correct as to content; however, it should be understood that this is a glossary of terms, not a compilation of official definitions. If used in this manner this book will provide the user with an invaluable source of information and will be an indispensable item on many bookshelves.

The introduction is particularly valuable in providing an excellent chronology to the past two centuries' outstanding discoveries in the physical and chemical fields. One feature of particular value is the use of bold type to indicate items which appear in the dictionary proper. This device also serves nicely as a means of locating a particular item in this chronology.

The French-English, German-English, Russian-English and Spanish-English indexes are invaluable, not only as a means of providing cross-references between the various languages involved, but also as a pocket version of the usually much more comprehensive, hence larger, foreign language dictionaries. This can assist anyone with a moderate familiarity with the language to do a reasonable job of translating a technical paper.

In summary, "The International Dictionary of Physics and Electronics" is an excellent compilation of those terms likely to be of most interest to the engineer or physicist who wishes to become more familiar with the other's domain and to keep abreast of progress in his own, provided he uses it for what it is—a dictionary, not a standard.

R. F. Shea
General Electric Co.
Knolls Atomic Power Lab.
Schenectady, N. Y.

Design Fundamentals of Analog Computer Components, by R. M. Howe

Published (1961) by D. Van Nostrand Co., Inc., 120 Alexander St., Princeton, N. J. 261 pages+7 index pages+x pages. Illus. 6×9¼. $7.50.

The author of this volume is writing for those who already have an acquaintance with the modern electronic differential analyzer, and at least a general knowledge of its theory of operation is assumed.

The title is somewhat misleading in that it may appeal only to those who are engaged in the production of analog computer coponents, and not those who operate and maintain them. Such is not the case, and the author makes this clear in his introduction, where he explains why design details are important to the user of the computer. He states " . . . a complete understanding of the capabilities of an electronic analog computer cannot be obtained without considerable knowledge of the component details and how they affect the computer solutions." Thus, the general theme of the book (seven chapters, 261 pages) deals with the inherent imperfections in the electromechanical and electronic devices which comprise the modern analog computer.

Although it would be impossible to produce a book which is completely up to date in the computing field, especially when dealing with new equipment, the author has discussed more thoroughly than is elsewhere available the most common, off-the-shelf components of the several analog computer manufacturers. In particular, the author treats with the design philosophy of Electronic Associates, Inc., Beckman/Berkeley, Reeves and Goodyear Aircraft, the producers of the "PACE," "EASE," "REAC," and "GEAD," respectively.

Over-all system convenience is investigated with respect to patchboard systems, set-up and control methods and problem check circuits. Detailed circuits are given and analyzed for the most common computing elements. Particular emphasis is given to the effect of nonlinearities, finite band-pass, phase shift characteristics and their effects upon problem solution. Specifically, the elements discussed are: dc amplifiers; servo, electronic and diode square law multipliers; function generators; recorders; noise generators and time delay units.

Since ultimately the accuracy of analog simulation must be referred to the operating characteristics of the individual computer components, this volume should prove of considerable value to those who operate and maintain analog computers.

J. E. Sherman
Lockheed Missiles and Space Div.
Sunnyvale, Calif.

Solid State Physics in Electronics and Telecommunications, Vol. 2. Semiconductors, Part II, M. Désirant and J. L. Michiels, Eds.

Published (1960) by Academic Press, Inc., 111 Fifth Ave., New York 3, N. Y., 645 pages+xvii pages+bibliography by chapter. Illus. 6¼×10. Chapters in English, French, and German. $18.00.

This book constitutes the second volume of the *Proceedings of the International Conference on Solid State Physics in Electronics and Telecommunications* held in Brussels (June 2–7, 1958), and sponsored by the International Union of Pure and Applied Physics. The first volume deals with preparation and properties of semiconductors (the principal emphasis being placed on germanium and silicon), solid-state theory, effects of intense electric fields in semiconductors, noise, and surface phenomena. Volume 2 contains 72 papers, the papers being printed in the respective languages of presentation at the Conference. (Forty-one papers are written in English, and the remainder in German and French.)

A major portion of Volume 2 deals with semiconductor compounds (33 papers), their physics, preparation and properties, such as electric, magnetic, Hall-effect, optical, magnetoresistive, thermoelectric, magneto-thermoelectric, electroluminescent, photoconductive, and photoelectric properties. A few papers treat thin film compounds. A second, relatively brief, section (6 papers) deals with a few, apparently somewhat erratically-se-

lected, semiconductor applications. A third, also major, portion of the volume (27 papers) presents papers on semiconductor devices, their properties and methods of fabrication. Discussed are diodes, transistors (including power transistors and avalanche transistors), 4-layer devices, field effect transistors, microwave diodes (including parametric and breakdown types), double base diodes, and other special devices. The fourth section of the book (6 papers) is devoted to semiconductor power rectifiers.

The book contains a great deal of most valuable material and can, in many respects, serve as a useful reference source for people active in the semiconductor field. However, considering that the papers were published in 1958 and that, therefore, much of the knowledge described in the papers was gained in 1956 or so, large portions of the volume can be considered today as outdated or superseded by more recent information. Nevertheless, this reviewer still recommends the volume as a very desirable component of a solid-state library.

ARTHUR P. STERN
General Electric Co.
Syracuse, N. Y.

Semiconductor Abstracts, Vol. VI—1958 issue, J. J. Bulloff and C. S. Peet, Eds.

Published (1961) by John Wiley and Sons, Inc., 440 Fourth Ave., New York, 16, N. Y. 470 pages+57 index pages. 8½×11¼. $14.00.

Since its inception in 1953, "Semiconductor Abstracts" has been a valuable tool for both theorists and practitioners of the state-of-the-art in semiconductors. Furthermore, these abstracts have been available at a reasonable price. The sponsors are to be commended for continuing this series.

A review of this type appropriately is started by taking a look at the table of contents. Here we are able to see the changes that have been reflected in this year's issue of "Semiconductor Abstracts." More emphasis has been placed on the most popular semiconductor topics of the period. For example, Boron, which enjoyed a heading of its own in the 1957 Abstracts, is now found under "Other Inorganics." The work properly starts off with germanium and silicon, covers other elemental semiconductors, the Halides, and then a new grouping is cataloged, entitled "Chalcogenides," which is followed by the group III–V Intermetallics, Other Inorganics, and then Organics.

The next section is concerned with theory of semiconductors. This is followed by an application section, which more properly might be entitled "State-of-the-Art."

Now that we have covered the general organization of this year's "Semiconductor Abstracts," we find upon examining the abstracts in detail that they have improved over those of previous issues and that seldom does one read an abstract with the feeling that not enough information has been given to determine the content of the original paper. The only objectionable criticism that the reviewer can raise with this issue of "Semiconductor Abstracts" is that of incorrectly placing some abstracts. As a specific example, Abstract No. 1074 is entitled "Lifetime of Non-Equilibrium Charge Carriers in Germanium for Arbitrary Injection Levels." Upon reading the title, and further, the abstract itself, it is obvious that this abstract is concerned with semiconductor theory. Yet it has been placed in the section on "Other Inorganics."

In spite of this one basic criticism, the book is a worthwhile and necessary tool for theoretical, experimental, or state-of-the-art investigation into semiconductors.

J. A. SLUSS, JR.
Philco Corp.
Lansdale, Pa.

Field Theory for Engineers, by Parry Moon and Domina Eberle Spencer

Published (1961) by D. Van Nostrand Co., Inc., 120 Alexander St., Princeton, N. J. 515 pages+10 index pages+ix pages+4 appendix pages. Illus. 6½×9¼. $12.75.

This is another addition to the growing volume of books on fields and waves written at the intermediate level. For the most part it deals with Laplace's equation and its solution by separation of variables. The merit of the book lies in the clear and well-illustrated treatment of a large number of boundary-value problems. In addition to covering the usual coordinate systems, the authors also describe bicylindrical, bispherical, and toroidal systems. Interesting applications are made to electromagnetic, acoustical, thermal and gravitational fields. The presentation requires only a rudimentary background in differential equations, vector analysis, and classical physics.

While the book is clearly written, the reader may be baffled at times by the notations. For example, a superscripted asterisk is not used to denote a complex conjugate, but rather, it indicates any complex quantity. Also, cylindrical Bessel functions are denoted by unfamiliar script letters.

JAMES R. WAIT
National Bureau of Standards
Boulder Labs.
Boulder, Colo.

Terrain Scattering Properties for Sensor System Design (Terrain Handbook II), by R. L. Cosgriff, W. H. Peake, and R. C. Taylor

Published (1960) by the Engineering Experiment Station, College of Engineering, The Ohio State University, Columbus. 114 pages+vi pages+3 bibliography pages. Illus. 6×9. $3.00.

The scattering properties of terrain make up as confusing a subject matter as exists in physics. The current theoretical approach to the subject consists of a hodgepodge of "models," each of which depends upon a constant which must be evaluated experimentally for each terrain sample, and which still may or may not "fit." These difficulties arise because the theoretical basis being used is highly oversimplified, and the resulting short algebraic expressions are simply not adequate.

The reasons for these complications are manifold: first and foremost, both the transmitter and the receiver are in the near field; second, the roughness can usually be described only by statistical parameters; third, the terrain is far from a perfect conductor, and its electromagnetic constants vary considerably not only from place to place but also with the seasons of the year.

The idea that the power returned from rough terrain obeys an inverse R^3 law has been with us for some time.[1] Of course the usual (far zone) R-dependence in the radar range equation is R^4, but in the near zone it is R^2. Thus, for example, the radar cross section of a sphere of radius a when the wavelength is small with respect to a and the radar is in the far field is $\sigma=\pi a^2$; if the radar is in the near field and we define the radar cross section to apply to that case, then $\sigma=4\pi R^2$ where R is the range from the transmitter-receiver combination to the specular point on the sphere. Thus in the near field the return is independent of the radius of the sphere to the first order (as long as the principal radii of curvature are large with respect to the wavelength). Physically this is to be expected, since when one is close to the surface of a sphere, locally the sphere looks flat.

Now when we extend these concepts to cover areas which are "rough," the roughness parameters being of the order of, or larger than, the wavelength, and if we remain in the near zone, a combination of laws comes into play. The R-dependence changes due to the relation between the area and the range, the beamwidth, and the product of pulse length and velocity of propagation. These complications must be added to those due to near-zone effects, roughness, and imperfect and varying conductivity and permittivity.

These theoretical difficulties are not adequately faced in the handbook under review. For example, the subject of relationship between scattering properties of a surface and its apparent temperature and applications of the theory, including some experimental results, are all covered in eleven pages. In fact, the theoretical portions would have been better eliminated from this handbook, as it is felt that they do not do justice to the field. To those readers who are interested in understanding models of roughness, the handbook is not considered an adequate source of reference material and is not recommended.

On the other hand, this handbook gives an excellent experimental summary of the present state of terrain scattering technology and is quite valuable for this purpose alone. There is a rather good bibliography, which is reasonably representative as far as experimental work is concerned. But, especially if pertinent theoretical papers were to be included, it would be easy to triple the number of references to U. S. literature and, what is most unfortunate, the key references for the U.S.S.R. are missing.

To summarize this reviewer's opinion: this book is recommended to those who want a quick reference on experimental data on terrain scattering. To those desirous of understanding the theoretical models of terrain scattering, or deriving their own models, this handbook is not recommended as a reference source.

KEEVE M. SIEGEL
University of Michigan
Ann Arbor

[1] L. N. Ridenour, "Radar System Engineering," McGraw-Hill Book Co., Inc., New York, N. Y., p. 86; 1947.

Linear Graphs and Electrical Networks, by Sundaram Seshu and Myril B. Reed

Published (1961) by Addison-Wesley Publishing Co., Inc., Reading, Mass. 292 pages + 5 index pages + x pages + 10 bibliography pages + 8 appendix pages. Illus. 6¼ × 9¼. $9.75.

As stated by the authors, the aim of "Linear Graphs and Electrical Networks" is "to provide, for electrical engineers, an introduction to the theory of linear graphs and to demonstrate the power of these methods in solving network problems." This aim is sufficiently well achieved that the reviewer intends to devote substantial effort to intensive study of some of its chapters. The book is organized along lines of definition, theorem statement and proof, and illustration. While the book is short, only 292 pages, its information density is very high. It will challenge most readers, and at the same time will be rewarding in the sense of extension of the reader's mathematical horizons.

The basic theory of linear graphs is developed in the first five chapters of the book, which account for about one-third of its length. Linear graph theory is a branch of mathematical topology, so it should not be surprising that these five chapters depend heavily upon matrix theory and modern algebra. A background of matrix theory is presupposed. On the other hand, little acquaintance with modern algebra is assumed; hence concepts such as number fields, Boolean Rings, and Abelian Groups are introduced, defined, and illustrated as needed.

The remaining chapters, five in number, are devoted to applications of graph theory. Chapters 6–8 are concerned with graph theory formulations of Kirchhoff's Laws, of energy functions and stability, and of topological considerations of linear networks. Chapter 9 will be of special interest to engineers who are interested in switching theory. Topics such as contact networks, sequential machines, and logic networks are considered. The communications specialist will find an area of interest in Chapter 10, which consists of a brief survey of the applications of graph theory to various types of communications problems.

In the opinion of this reviewer, this is an excellent book. It is worthy of study by network theorists, switching theorists, and communications specialists.

Philip F. Ordung
Yale University
New Haven, Conn.

Physics of Semiconductors, by A. F. Ioffe

Published (1961) by Academic Press, Inc., 111 Fifth Ave., New York 3, N. Y. 432 pages + 4 index pages + xi pages + bibliography by chapter. Illus. 6¼ × 9¼. $12.50.

Professor Ioffe's text, "Physics of Semiconductors," is written from the viewpoint of an experimental physicist. The concepts and mechanisms are developed intuitively with analytical formulations presented in a style which should be appealing to the experimentalist.

The first chapter deals with solid electrolytes and is both historical and introductory in character. The nature of ion and electron currents and their statistical behavior in various solid electrolytes are discussed and the groundwork laid for interpreting some of the phenomena observed in semiconductors which cannot be treated classically.

Chapter 2 contains a brief but concise treatment of the electrical and thermal properties of metals. The presentation is made in the language and pictures of Sommerfeld's theory neglecting the effects of periodic potential variations in the lattice.

Chapter 3 is a general survey of semiconductors containing a phenomenological description of the more important effects found in semiconductors with elementary explanations of the mechanisms. At this stage the only aspect of quantum mechanics employed has been the use of Fermi-Dirac statistics for electrons.

Chapter 4 introduces the modern Quantum Theory of Semiconductors. Here we find a discussion of energy bands; their population; a quantum mechanical treatment of the motion of free electrons and electrons in a periodic field; the concept of effective mass; holes; impurity levels; polarons; excitons; and a critical review of the present state of semiconductor theory.

Chapter 5 is probably the most important section of the text. This chapter, entitled "Physical Phenomena in Semiconductors," discusses crystal properties influencing the more useful semiconductor functions; the nature and influence of imperfections and impurities in the crystal lattice; phonon and electron propagation, scattering, mean free path and mobility; surface states; contact resistance; rectification of barrier layers and junctions; transistors; photoelectric and photovoltaic effects; contact potentials; thermionic and secondary emission phenomena; effects of applied electric and magnetic fields on semiconductors; magnetoresistance; paramagnetism; cyclotron resonance ferro- and antiferromagnetism. In addition to all of these phenomena, this section contains an interesting discussion of thermal conductivity in semiconductors, and under a section on thermoelectricity is a summary of most of the information contained in the author's well-known monograph on "Semiconductor Thermoelements and Thermoelectric Cooling."

Chapter 6 reviews methods which have been developed for measuring the basic properties of semiconductors, including: electrical conductivity, electron and hole mobilities; electron and hole concentrations; band gaps; lifetime and diffusion length; Seebeck coefficient; thermal conductivity; specific heat; velocity of sound; contact potential; Hall coefficient; dielectric constant; magnetic susceptibility.

Chapter 7 contains a summary of known properties of a wide variety of semiconducting materials.

The book contains a final chapter entitled, "Conclusions," in which Ioffe has written a beautiful analysis of the advances which have been made and limitations which remain in developing a completely satisfying theory to explain the phenomena observed in semiconductors.

This book possesses the charm and appeal which most frequently occur when an author writes in an area in which he has, himself, made significant contributions. It contains a summary and digestion of much work which has been published in Russia and is relatively inaccessible outside of Russia.

Lloyd T. DeVore
Hoffman Science Center
Santa Barbara, Calif.

Recent Books

Cahen, Gilbert, and Treille, Pierre, *Nuclear Engineering*. Allyn and Bacon, Inc., College Div., 150 Tremont St., Boston 11, Mass. $8.50.

Elsevier's Dictionary of Automation, Computers, Control, and Measuring. Compiled and arranged on an English alphabetical base by W. E. Clason. Elsevier Publishing Co., Amsterdam, Netherlands. $27.50. (English language distributor: D. Van Nostrand Co., Inc., 120 Alexander St., Princeton, N. J.) In English, Dutch, French, German, Italian, and Spanish.

Murphy, Glenn, *Elements of Nuclear Engineering*. John Wiley and Sons, Inc., 440 Park Avenue South, New York 16, N. Y. $7.50. Presents, at the college level, a survey of the field of nuclear engineering for the purpose of indicating its scope, potentialities, and limitations.

NMR and EPR Spectroscopy. Pergamon Press, Inc., 122 E. 55 St., New York 22, N. Y. $12.00. Papers presented at Varian Associates' Third Annual Workshop on Nuclear Magnetic and Resonance and Electron Paramagnetic Resonance, Palo Alto, Calif.

Pickard, J. K., Warren, F. H., Lowe, W. W., and McLain, S., *Power Reactor Technology*. D. Van Nostrand Co., Inc., 120 Alexander St., Princeton, N. J. $11.25. The Second Geneva Series on the Peaceful Uses of Atomic Energy. Evaluates efforts toward goal of economic nuclear power, with pertinent operating results and technical and economic data for further development.

Savant, C. J., Jr., Howard R. C., Solloway, C. B., and Savant, C. A., *Principles of Inertial Guidance*. McGraw-Hill Book Co., Inc., 330 W. 42 St., New York, 36, N. Y. $9.75. Covers basic concepts of navigation and elements required for automatic navigation; discusses the autonavigation components and computers, platform controllers, ground alignment, and pre-flight testing; and presents theoretical information on inertial navigation principles.

Stout, M. B., *Basic Electrical Measurements, Second Edition*. Prentice-Hall, Inc., Englewood Cliffs, N. J. $11.65. Revision of the original textbook in which Chapter 2 ("Experiments and Statistical Analysis") has been considerably lengthened and updated. Elements discussed are basic passive measuring devices; the more refined and specialized devices using active circuits are not treated.

Scanning the Transactions

A new method of guided propagtion of electromagnetic wave beams has been proposed which has important application to the transmission of millimeter waves. The new technique makes use of the fact that a wave beam emitted by a highly directional antenna has within the Fresnal region a substantially uniform diameter. If a way could be found to form new Fresnal regions exactly like the original at uniform intervals along the beam path, the beam would then pass along with essentially no change in diameter and with little loss. The key ingredient which made this idea workable was the discovery that the cross-sectional amplitude distribution of the beam repeated itself at a certain distance from the origin. Therefore, if the original phase distribution could be made to repeat itself at that point, too, the requirements for forming a new Fresnal region identical to the original would be met. This was accomplished by inserting at that point of the beam a phase transformer, in the form of a dielectric lens, which reconstituted the original phase distribution in the required manner. The result was an open waveguide consisting simply of a series of dielectric lenses spaced at uniform intervals along the beam path. A beam waveguide of this type, consisting of a row of dielectric lenses 20 cm in diameter and spaced one meter apart, was built and tested at 23 kMc, with excellent results. In addition to low loss, an interesting property of the beam waveguide is that it can turn corners easily without introducing any distortions or additional losses because the beam can be deflected by means of reflectors or dielectric wedges. (G. Goubau and F. Schwering, "On the guided propagation of electromagnetic wave beams," and J. R. Christian and G. Goubau, "Experimental studies on a beam waveguide for millimeter waves," IRE TRANS. ON ANTENNAS AND PROPAGATION, May, 1961.)

Management and information theory, two unlikely bedfellows, have been tentatively coupled in an interesting compatibility test to determine whether information theory might be applied to the study of real management situations. Specifically, it was desired to know whether information theory concepts would be at all useful in 1) analyzing the communication system within an enterprise that uses electronic data processing or other automation methods, 2) forecasting demands or other economic factors, and 3) studying production processes. The study was made not without some trepidation. Information theory analogs have been used—perhaps overused—in a wide variety of far removed fields. The question of whether such analogs lead to useful results or practical benefits is a controversial one. The present study was, therefore, noteworthy in two respects. First, it was concluded that information theory was *not* generally useful in situations 1) and 2) above. Secondly, it was concluded that the most promising application of information theory to management control appears to be in viewing the production process as the adding of information to raw materials in order, for example, to measure work in progress in a convenient way. Whether this approach bears fruit must await further studies. Should it prove to yield new insight into management operations, especially those that are not already intuitively understood and practiced, further progress will have been made in formalizing the art of management. (R. C. Hopkins, "Possible applications of information theory to management control," IRE TRANS. ON ENGINEERING MANAGEMENT, March, 1961.)

Land's two-color projection system has been a widely discussed subject during the past two years. Following Land's original demonstration others have conducted similar experiments in an effort to determine whether two-color projection could give as good results as conventional tricolor projection. It was found that generally the quality of two-color pictures was inferior. However, the quality of a picture is a matter of subjective judgment. Since there was a considerable lack of statistical data on this question a further study was recently conducted, using students at the Swiss Federal Institute of Technology as subjects. The results showed that the students judged the two-color pictures inferior to the tricolor pictures. It was also found that in viewing two-color pictures the mechanism of color transformation worked well with most persons when viewing natural scenes, but seemed to fail when looking at abstract pictures. An interesting detail of the results is that a minority of students could detect little or no difference between the two forms of projection. While the results apply only to the particular two-color system used in the experiment, it was concluded that it is improbable that sometime a two-color process might be found which will give the spectator the same quality reproduction as tricolor projection. (C. Burckhardt and M. J. O. Strutt, "Experiments with E. H. Land's two-color projection," IRE TRANS. ON BROADCAST AND TELEVISION RECEIVERS, April, 1961.)

The Citizens Radio Service is experiencing an astounding boom which in the last two years has made it second only to the Amateur Radio Service in the number of licensed stations. Indeed, by the end of this year it will probably have passed the Amateur Service in numbers. The Citizens Radio Service was first set up by the FCC at the end of World War II to make radio communication available to private individuals, and the 460–470 Mc band was allocated for this purpose. By 1958 a modest 36,000 licenses had been issued. By the end of 1960 the number had swelled to 150,000 and was growing at the rate of 10,000 a month. At least 60 manufacturers are now engaged in large scale production and sale of sets or kits of station equipment. The cause of this sudden boom was two actions taken by the FCC in 1958: 1) the more accessible eleven-meter amateur band (about 27 Mc) was turned over to the Citizens Radio Service and 2) a new and technically simpler class of station (class D) was authorized. Today, the average family can install a base station at home and a mobile set in the car for less than half the cost of a good television set. It is this type of base-to-mobile communication, for business as well as family purposes, that accounts for most of the users of the Citizens Band. Sets may be found in boats, airplanes, house trailers, farm tractors, delivery trucks and snow plows, bringing added convenience or important economies to private citizens and to business enterprises. The foresight of the FCC in investing a small portion of spectrum space 15 years ago for use by the general populace is now paying handsome dividends. (I. H. Loucks, "The Citizens Band boom," IRE TRANS. ON VEHICULAR COMMUNICATIONS, April, 1961.)

Abstracts of IRE Transactions

The following issues of TRANSACTIONS have recently been published, and are now available from the Institute of Radio Engineers, Inc., 1 East 79th Street, New York 21, N. Y., at the following prices. The contents of each issue and, where available, abstracts of technical papers are given below.

Sponsoring Group	Publication	IRE Members	Libraries and Colleges	Non Members
Antennas and Propagation	AP-9, No. 3	$2.25	$3.25	$4.50
Bio-Medical Electronics	BME-8, No. 2	2.25	3.25	4.50
Broadcast and Television Receivers	BTR-7, No. 1	2.25	3.25	4.50
Electron Devices	ED-8, No. 2	2.25	3.25	4.50
Engineering Management	EM-8, No. 1	2.25	3.25	4.50
Engineering Writing and Speech	EWS-4, No. 2	2.25	3.25	4.50
Microwave Theory and Technique	MTT-9, No. 3	2.25	3.25	4.50
Product Engineering and Production	PEP-5, No. 1	2.25	3.25	4.50
Vehicular Communications	VC-10, No. 1	2.25	3.25	4.50

Antennas and Propagation

Vol. AP-9, No. 3, May, 1961

John T. Bolljahn, 1918–1960—J. V. N. Granger (p. 234)

The John T. Bolljahn Memorial Award—(p. 235)

Synthesis of Modulated Corrugated Surface-Wave Structures—J. T. Bolljahn (p. 236)

An exact procedure for the design of a surface that will support a prescribed group of surface waves simultaneously is described. The surfaces resulting from the application of this procedure are found to be modulated (*i.e.*, to contain periodic waves in the direction of propagation) and to have surface impedance values that vary periodically in the direction of propagation. Finite-length surfaces of this type are hence reminiscent of Simon's "cigar antenna." Several surface designs are presented, and some general properties of the surfaces and the composite waves they support are discussed. Certain limitations on the design procedure are described.

Magneto-Ionic Faraday Rotation of the Radio Signals on 40 Mc from Satellite 1957α (Sputnik I)—E. V. Sorensen (p. 241)

Some of the fadings of the 40-Mc signals from Sputnik I during morning transits are assumed to originate in Faraday rotation in the ionosphere. This has been investigated for the transit of October 12, 1957, 5:30 GMT, for which the orbit was known with reasonable accuracy.

The fading records show an increasing fading rate during the last part of the transit. This is contrary to the simple theory based on the assumptions of a flat earth and a homogeneous ionosphere, from which a constant fading rate should be expected. The main reason why simple theory did not apply in this case is that the satellite travels through the twilight zone from night towards day, *i.e.*, from low to high ionization.

The Faraday rotation is calculated by means of data for the orbit, magnetic field maps and predictions of the ionosphere conditions. The result is in good agreement with the observation when a high ionization between the altitude of maximum ionization and the satellite is assumed. The effect of refraction is estimated by means of the perturbation theory. It increases the Faraday rotation from 0 to 19 per cent during the transit. The general conclusion is that, even though the fading behavior of a transit near sunrise is explainable to some extent, it is still difficult to deduce detailed information on the state of the ionosphere from it, especially when the frequency is so low that refraction becomes significant.

On the Guided Propagation of Electromagnetic Wave Beams—G. Goubau and F. Schwering (p. 248)

Any field in a half-space can be described by a continuous spectrum of cylindrical waves. If this spectrum comprises substantially only waves whose propagation constant is very close to the plane wave propagation constant, the field can be resolved into a set of elementary wave beams which are characterized by Laguerre polynomials. They satisfy orthogonality relations like the wave modes in a waveguide. The elementary beams or "beam modes" can be reiterated and guided by reconstituting the cross-sectional phase distribution at certain intervals. Reiterative beams are utilized in the beam waveguide. The finite size of the phase resetting devices effects a modification of the reiterative beam modes and causes diffraction losses. These losses decrease very rapidly with increasing diameter of the phasing devices.

Experimental Studies on a Beam Waveguide for Millimeter Waves—J. R. Christian and G. Goubau (p. 256)

The beam waveguide utilizes reiterative wave beams which are guided by resetting the cross-sectional phase distributions at periodic intervals. The major purpose of the measurements was to obtain data concerning the inherent losses of the guide, including the diffraction loss, caused by energy by-passing the phase transformers, and the dielectric and reflection losses of the transformers. Resonance measurements with an "open cavity," consisting of a section of a beam waveguide terminated by plane reflector walls, yielded the over-all losses of the phase transformers. In order to isolate the diffraction loss, pulse measurements were made between two reflectors, slightly curved to reset the phase distribution in the reflected beam. These measurements also gave information of the build-up of the reiterative wave beam. The experimental data support the theory which predicts that the diffraction losses of reiterative beams can be made extremely small.

Parasitic Excitation of Circular Antenna Arrays—T. L. Simpson and J. D. Tillman (p. 263)

A method of calculating the radiation pattern of a circular antenna array of parallel monopoles or dipoles using symmetrical components is presented. The results obtained when only one element of the array is excited are not particularly good. However, if an additional element is added at the center of the array a fairly good directional pattern results. The sidelobe level is dependent upon the tuning of this central element, and a graphical analysis is given which optimizes this tuning. Calculated and measured patterns are shown and compared. Sidelobe levels of 15 db, and a beamwidth of 78° are typical. The principal advantage of this antenna lies in the fact that the pointing of the beam can be changed by simply changing the element that is excited.

Angular Accuracy of a Phased Array Radar—L. E. Brennan (p. 268)

One type of phased-array radar of current interest employs an array of separate receiving elements, each followed by an individual amplifier. These individual signals are combined coherently to form one or more receiving beams for searching, tracking, or performing both functions simultaneously. This paper presents an approach to the theory of angle measurement with a phased array of this type.

In the one-dimensional problem considered here, the receiving antenna consists of a linear array of individual antenna-amplifier elements. The receiver-noise-limited case is considered, in which accuracy is limited by the additive normally distributed noise present in each channel. An expression is derived for the limiting accuracy of angular measurement when a single set of samples is available. This set of samples is obtained simultaneously, one sample from each channel. Next, two methods of implementing the angular measurements are discussed. These are amplitude comparison monopulse and a coherent or phase comparison technique. For large signal-to-noise ratios and for either a square law or a linear envelope detector, the accuracy of amplitude comparison monopulse approaches the theoretical limit. The same accuracy can be achieved with the coherent technique by proper weighting of the individual signals.

A Spiral-Doublet Scanning Array—John R. Donnellan (p. 276)

An array of eight spiral doublets, each doublet consisting of a pair of equally-excited two-wire spirals in the same plane and wound in opposite senses, has been used to scan a beam of horizontal polarization over a $\pm 40°$ range simply by rotations of the spiral doublets. The combination of a microstrip ring network and twin lead provided a balanced feed for each spiral in the array. Sidelobe levels were those

predicted (25 db) for the broadside pattern and —at the test frequency of 1430 Mc—were, in general, below 19 db over the 80° scan. A novel microstrip feed harness provided isolation between the doublets and served to absorb most circulating currents. This printed circuit feedboard consisted of judiciously-grouped microstrip ring networks and provided the desired feeding coefficients to within ±0.1 db. An application of the array for tracking purposes is also described.

Leaky Wave Antennas II: Circular Waveguides—L. O. Goldstone and A. A. Oliner (p. 280)

The propagation characteristics of leaky waves on slotted circular cylinders are derived by the methods described in an earlier paper on leaky rectangular waveguides. The cross section of a typical leaky circular waveguide is represented by a radial transmission line network incorporating a lumped terminating admittance which characterizes the slot discontinuity and the external region. The expression for the lumped admittance is obtained by combining an integral equation solution with a variational procedure. The resonances of this transverse network, which yield the complex propagation constants for the leaky waves, are solved by perturbation techniques to produce results in simple and practical form. Solutions are obtained for leaky waves corresponding to two different excitations of a slotted cylinder and these results are shown to compare favorably with measured values.

A Spiral-Grating Array—J. R. Donnellan and R. T. Close (p. 291)

A problem associated with a two-dimensional spiral doublet array is concerned with the fact that use of the spiral doublet as an element to obtain linear polarization leads to spacing difficulties, since the distance between elements is always twice as much in one dimension as in the other. Thus, the allowable scan is seriously limited in one principal plane. A method is proposed for obtaining linear polarization from a *single* spiral antenna by using it in combination with a polarization grating and a ground plane. Experimental results were obtained by combining eight of these elements in a one-dimensional array. For the broadside position of the main beam, the field was found to be linear, with the cross-polarized component of the main beam being 40 db down from the principal polarization. As the beam was scanned out to ±45°, the linearity decreased quite rapidly (to approximately 10 db at 45°) and the plane of the linear polarization was rotated; sidelobes were higher than predicted. Use of this array rather than an array of doublets would involve a compromise concerning specifications, dependent upon the particular application of the array.

Coupled Surface Waves and Broadside Arrays of End-Fire Antennas—J. L. Yen (p. 296)

The concept of coupled surface waves is introduced to describe the action of element interaction in a broadside array of traveling-wave end-fire antennas. These coupled waves are formulated in terms of an interaction matrix, whose elements either can be determined experimentally, or, for some antenna structures, can be computed. Two methods of pattern evaluation based on two well-known approaches to end-fire antennas are then presented. The roles of interaction in the two methods turn out to be quite different, and the method which assumes radiation at the end of the antenna appears to be more favorable. A criterion on the over-all interaction effect on array pattern is introduced which indicates under what condition coupling can be neglected. Finally, the nature of patterns obtainable with different element spacings is examined.

Bio-Medical Electronics

Vol. BME-8, No. 2, April, 1961

Interconvertibility of certain engineering units and time-motion studies leads to simplifications in simulating the chemist's performance. The system described utilizes a carrier stream into which samples and reagents are injected at controlled intervals. Reactions proceed in transit. Normalization results in replacing volume measurements by time, durations by distances and concentrations by rates of mass flow. Thus, all variables are controllable by means of timers.

The system incorporates a plurality of special plug-in units (pumps, mixers, sampler). Each operating module includes a multi-cam timer programmer. The modules may be arranged in series-parallel arrays. The system is pulse-operated from a random-access keyboard, so that a time-sharing programming method is possible. Setting of the measuring devices (colorimeter, pH-meter, etc.) for sensitivity, scale span and wavelength is automatic. A unique amplifier is utilized. Data logging is conventional. Performance analysis by application of the Sampling Theorem is useful in optimizing the operations. Examples dealing with urine color, albumin, glucose and nonglucose reducers by the peroxidase method, blood RBC and hemoglobin are described.

A recent development of interest in analytical instrumentation provides a system for the continuous automatic determination of a wide variety of biochemically important compounds by colorimetry. The system is controlled by a multichannel, peristaltic proportioning pump which accurately delivers fixed volume ratios of samples and reagents to other components. Purification or separation of the constituent to be analyzed is effected by continuous dialysis and, after appropriate chemical treatment, optical density is measured in a ratio-recording dual beam colorimeter fitted with a flow curette. The system can analyze different samples on a continuous basis or monitor changes in a continuous sample stream. Operations require a minimum of technical attendance.

The system has application in many areas of medical research: routine determination of classical clinical constituents for diagnosis and treatment; study of chemical pharmacology *in vivo* and *in vitro;* biochemical aspects of proteins, amino acids, and enzymes; organ and tissue perusal studies in physiology; microbial metabolism and assay; screening of experimental pharmacodynamic agents.

The design and operation of the instrument system will be treated in general terms and the application and results in the aforementioned fields of research will be discussed. Economies time and financial expenditure will be summarily noted.

A capacitance-resistance bridge for the measurement of the dielectric properties of human blood at 100 kc is described. The use of inductively coupled ratio arms in the bridge greatly reduces the effect of stray impedances to ground. This allows the glass measuring cell to be mounted in a transparent plastic thermostatting box, without metallic shielding. Thus, the physical condition of the blood can be observed throughout the period of coagulation.

Observed changes in the capacitance and resistance of blood sample during coagulation are briefly outlined, particularly the effects observed when the blood samples are taken from donors who are known to have abnormal blood states.

Various efforts to instrument coagulation determinations have proved either excessively costly or practically difficult. An instrument is described which is compact, reasonable in cost, and affords accurate, reproducible, nonsubjective determinations. Operation depends upon rotational sweep of precisely sized and located wires through the reaction mixture. Initial polymerization products are carried by one wire to a precision electrode arrangement which causes a sensitive electronic circuit to stop a timer. "Zero time" is automatically synchronized with the start of the reaction. A selector switch permits electrical adaptation of the electrode arrangement to determination of whole-blood clotting time. Extensive testing of a prototype instrument, confirmed by preliminary results obtained by various laboratories, indicates attainable accuracies of 0.3-second standard deviation.

In radiographic diagnosis of heart disease, it is necessary to synchronize accurately the injection of radio-opaque dye into the circulation with the diastolic portion of the cardiac cycle. Because of the high-energy electrostatic and electromagnetic fields associated with radiographic apparatus, it was decided to make a photosensitive transducer to be clamped on the ear lobe to give an electric signal proportional to the blood flow through the ear. This signal is electronically shaped and amplified, and used to trigger a variable delay timing circuit which then operates the injector.

The basic polarographic circuit and its accuracy are discussed. A bridge-type current amplifier, using one transistor, is presented as one solution to the problem of displaying the very small current flow in a polarographic circuit. A second solution, the insertion of a pH-millivoltmeter directly into the basic control circuit, is evaluated from the medical worker's viewpoint. Techniques and circuits employing four different types of pH-millivoltmeters are described. The direct application of a polarographic cell for continuous measurement of the oxygen partial pressure in the blood of a heart-lung machine is presented.

An air-damped artificial mastoid has been constructed to simulate the mechanical impedance of the human mastoid. The instrument is used to determine the force transmitted through the skull by bone vibrators used in clinical audiometers and bone-conduction-type hearing aids.

A method of measuring cardiac output from dye-dilution curves recorded by an ear oximeter is described. No sampling of blood is necessary to make the dye-dilution curves quantitative. The inaccuracies inherent in the "end-tail" method of calibration are thus avoided and the technical procedure greatly simplified.

Theoretical considerations, circuitry and calibration procedures are discussed.

Forty-one cardiac output estimations were made in 15 subjects. Coomassie blue was used as indicator. Comparison was made between the results obtained by the technique under study and by the end-tail venous method. Seven results had to be excluded from the com-

parison due to manifest inaccuracy of the reference method, which is inherently inaccurate. In spite of this, there was reasonably good agreement. The standard deviation of the differences between simultaneous values by both methods was 14.3 per cent.

Fifty-two dye-dilution curves were recorded in seventeen white subjects at rest and during steady-state exercise at loads up to 600 kilogram-meters per minute. Comparison was made between the cardiac output estimates obtained by the technique described and by the "arterial end-tail" method. The standard deviation of the differences between the simultaneous values from the two methods was 14.2 per cent.

The Transmission of Red and Infrared Light Through the Human Ear—N. M. Anderson, P. Sekelj, and M. McGregor (p. 134)

A study was performed of the light transmission characteristics of the compressed "bloodless" ear in 70 subjects of white, Indian and Negro stock.

It was found that in white children and adults of both sexes, the ratio of light transmission of the red filtered photocells to that transmitted to the infrared photocell was virtually constant when the ear was rendered bloodless by compression. The error introduced by assuming this ratio to be constant was no greater than the errors involved in making the measurement.

If the assumption were made that this ratio was the same in Indian and Negro subjects as it is in white subjects, the estimation of the ratio would be in error in the average Indian subject by approximately −3.38 per cent and in the average Negro subject by −4.73 per cent.

Contributions:

The Normal Fetal Electrocardiogram, with a Proposed System of Standardized Terminology—S. D. Larks and R. Abdul-Karim (p. 136)

A system of standard electrode and patient positions for fetal electrocardiography as suggested by an international *ad hoc* committee, is presented. The variation in the accuracy of the fetal ECG technique during gestation is shown and discussed. Existence of two peaks of high accuracy, at 22 weeks and at term, is shown. Normal values for the duration of the fetal QRS are shown to increase from 0.026 second at 20 weeks to 0.040 second at term. Normal values and ranges for fetal heart rates and the amplitudes of the fetal QRS are reported.

A Theoretical Basis for Determining Heart-Lead Relationships of the Equivalent Cardiac Multipole—D. A. Brody, J. C. Bradshaw, and J. W. Evans (p. 139)

During the past few years, it has been proposed that the electrical behavior of the heart be represented more precisely by the addition of multipolar current singularities to the equivalent cardiac dipole. In this report, we have explored the factors which determine the relationship of each such multipolar component to the various electrocardiographic lead connections. Specifically, we have been able to amplify and generalize the concept of the ideal electrocardiographic lead field by showing that the electrocardiographic contribution of a given multipole component is related solely to the lead-field component of identical degree and order. Thus, the McFee-Johnston proposal for resolving lead fields is reintroduced, and the heart-lead property of each component is particularized. Finally, some brief, speculative remarks are made concerning possible biomedical applications of the generalized lead-field concept.

An Amplitude Distribution Analyzer for Studying Brain Waves—Fred L. Alexander (p. 144)

An amplitude-distribution analyzer which estimates the probability-density and probability-distribution functions of brain wave forms is described. The circuit uses high-gain dc operational amplifiers as its basic component and is simple in design. The theoretical probability-density and probability-distribution functions for a sine wave, a triangle wave and a random signal are discussed and compared with the experimental results of the analyzer.

Broadcast and Television Receivers

Vol. BTR-7, No. 1, April, 1961

The Challenges of TV in Education—T. F. Jones, Jr. (p. 7)

The future excellence of our educational system will depend largely upon the extent to which the capabilities of modern technology are exploited. TV in particular promises to play an important role by solving many problems in elementary, secondary, and higher education. MPATI, a large scale educational experiment involving a TV transmitter in an aircraft, is beginning operations this spring.

Although TV is sufficiently developed to meet many important educational needs, the engineer is challenged to develop techniques and equipment which will meet a broader range of educational needs more effectively and efficiently.

The paper summarizes the problems, the present solutions involving TV, and the challenges which face television engineers to provide improvements and new capability.

Network Design Analysis for Stereo Discriminators—John P. Pietrolewicz (p. 26)

A Foster-Seeley discriminator is used to detect the FM or PM information in a stereo signal. It is desired to design the detector for optimum sensitivity and linearity without excessive sacrifice of gain in the last IF stage.

The complex expressions involved in the transfer function are translated into a single algebraic equation relating the location of the poles to the zero by way of the parameter C_{11}/C_{22}, the ratio of primary to secondary capacitance. The particular case of critical coupling is treated and the problem of locating the zero is graphically presented. The influence of primary and secondary Q and C ratios on zero location and input impedance is described; associated design curves are plotted.

The application of these equations and curves to detector design is made. When increased discriminator linearity is desired, the zero must be moved further toward the "imaginary" axis—with corresponding sacrifice of gain and additional burden on the cost of the transformer. A sample problem is outlined in which bandwidth and zero location are chosen and the circuit parameters and input impedance are to be determined.

Experiments with E. H. Land's Two-Color Projection—C. Burckhardt and M. J. O. Strutt (p. 34)

Since the quality of E. H. Land's two-color pictures has been subject to discussion, two groups of students were asked to judge the quality of Land's pictures. The preparation of the slides and the experimental setup is described. The results show the inferiority of E. H. Land's system in its actual form to ordinary tricolor projection. From the results it appears that the mechanism of color transformation works well with most people tested, but that the lack of information contained in the slide photographed through the blue filter is considered serious. An interesting detail is that a minority of people can detect very little or no d fference between the two forms of projection.

Electron Devices

Vol. ED-8, No. 2, March, 1961

Some Properties of Multiple BWO's—E. A. Ash, L. Solymar, and A. C. Studd (p. 99)

Some of the fundamental properties of multiple BWO's are examined in terms of a simple model. The starting conditions are found for both low and high space-charge conditions and particularly for the case in which there is a small difference between the velocities of the separate beams. The latter results are used to discuss the tolerances which must be met in multiple BWO's. Experiments carried out at X band provide some qualitative confirmation of the theory.

Parametric Amplifier Using a Silver Bonded Diode—S. Kita, T. Okajima, and M. Chung (p. 105)

Recently, the parametric amplifier has merited attention because of its low-noise characteristics. A novel diode has been designed which is suitable for use in a parametric amplifier. The diode is a bonded type and is composed of a silver-gallium whisker and an N-type germanium. The cutoff frequency of the silver bonded diode is higher than 150 kMc. The parametric amplifier was made using these diodes at 6 kMc and 11 kMc, and stable gain of more than 20 db was obtained. The noise figures were approximately 5 db and 6.5 db at 6 kMc and 11 kMc, respectively.

Highly Linear Amplification with Transistors—N. E. Chasek (p. 110)

Highly linear amplification can be obtained with HF diffused-base transistors in the common base configuration. It is the purpose of this paper to 1) present experimental results to demonstrate this, 2) demonstrate the causes for this high degree of linearity and derive expressions for optimum bias voltages and currents (these results can be extended with certain restrictions to the common emitter and common collector configurations), and 3) present a general method for analytically treating nonlinearity in all transistor configurations.

A push-pull amplifier using 2N509- or 2N1195-type transistors provided 13 db of gain, with signal-to-distortion ratios of 70 to 80 db for broad-band white noise signals with +3 dbm of average output power or sine wave signals with +15-dbm peak output power. The stability of this gain and linearity with temperature and interchange of transistors is high. This high degree of linearity is shown to be due to 1) cancellation of current sensitivity nonlinearity in the emitter and collector resistances, 2) collector voltage bias adjusted so that the derivative of the collector conductance with respect to collector voltage is zero, and 3) the use of a high alpha cutoff frequency transistor. An expression derived for optimum bias was in good agreement with experiment. The nonlinear distortion in transistors is shown to be different from that found in most devices, in that there are frequency-sensitive and frequency-insensitive nonlinearities. A general

analysis carried out including these terms was in good qualitative agreement with experiment.

Simulating Parametric Amplifiers—William T. Hatley, Jr. (p. 116)

In this paper, the problems of producing a general simulator model of a parametric amplifier are discussed. This model is to be simple, accurate, and applicable to many forms of parametric amplifiers. A brief discussion of the theory behind parametric amplification is followed by proposals for three models. Each of these is discussed in terms of its limitations and applications. The results of tests on two of these models are presented, and these results are discussed. Some emphasis is placed on the most successful of the models, which has been used to simulate a subharmonic oscillator.

The Reverse Transient Behavior of Semiconductor Junction Diodes—W. H. Ko (p. 123)

The reverse transient behavior of junction diodes after a rectangular pulse of forward current is analyzed and the results verified experimentally. Based on the simplified planar diode model and the diffusion equation, equations are obtained to determine the reverse recovery current and voltage as functions of carrier lifetime and circuit parameters.

The transient behavior of both the open circuit and the closed circuit conditions are shown to be described by some set of equations, and the presently unrelated explanations are unified. The relation between the charge stored by forward current and the charge recovered by reverse current is then derived. These equations are confirmed with an accuracy of 5 per cent or better by experimental data from germinium and silicon alloyed diodes.

Several applications on measurements of diode material properties and on circuit applications (diode amplifiers, modulators, etc.) are suggested.

The Reflex Klystron as a Microwave Detector—B. G. Whitford (p. 131)

The mechanism of detection in a passive reflex klystron is discussed qualitatively on the basis of elementary space-charge theory with emphasis on the character of the anode-repeller potential distribution necessary for detection. Tabulation of tangential sensitivities obtained using several different tube types is included, together with other experimental data. It is shown that there is a possibility of using reflex klystrons as tunable detectors at frequencies where crystal diode performance is relatively poor.

Response of a *P-N* Junction to a Linearly Decreasing Current—M. A. Melehy and W. Shockley (p. 135)

A study is made to determine analytically the time variation of the terminal voltage of a *p-n* junction in response to a terminal current which starts with a large forward value and continues to decrease linearly until the reverse saturation is attained. It is shown that the period between the reversal of current and the reversal of voltage depends exclusively on the lifetime, diffusion length, and thermal equilibrium densities of minority carriers in both regions of the junction. For some cases, the period between the reversal of current and voltage reduces to half the lifetime of either of the two types of minority carriers. This property allows measuring the lifetime of minority carriers for certain *p-n* junctions by relatively simple means.

Tangential Magnetic Field Immersion of a Hollow Beam Electron Gun—E. J. Cook (p. 140)

Harris flow is one of a number of equilibrium electron beams requiring a launching method which imparts angular momentum to the stream. Immersion of the electron gun region in a magnetic field tangent to the cathode and orthogonal to the electron trajectories provides a means of rotation free of the defocusing and discontinuity effects of previous methods. Centrifugal-force spreading is eliminated by electric-field compensation in the gun. This compensation results in field lines at an angle to the stream edges and necessitates gun electrode design by a curvilinear flow method.

An immersed gun of this kind has produced a stable Harris flow beam containing 86 per cent of the total energy in rotational motion. Anode transmission is in excess of 95 per cent.

An Anomalous Flicker Effect in Tubes with Oxide-Coated Cathodes—R. C. Schwantes and A. van der Ziel (p. 150)

An anomalous flicker effect is observed in tubes with oxide-coated cathodes if the grid bias is near zero volts. The time constant deduced from the noise spectrum is of the order of 10^{-2} second. The magnitude of the noise increases strongly with increasing temperature. It is impossible to detect individual noise pulses. It is proposed that the noise is caused by individual positive ions emitted by the cathode and trapped in the space charge. The effect is similar to the anomalous flicker effect in tubes with tungsten cathodes; it differs in the time constant (10^{-2} second instead of 10^{-4} second) and in the magnitude of the ion pulses causing the effect (single ions or small numbers of ions instead of about 10^4 ions per pulse).

Charge Analysis of Transistor Operation Including Delay Effects—A. N. Baker and W. G. May (p. 152)

The charge control concept of transistor operation is extended to include delay effects in an accurate, yet tractable, way. Defining the transit time τ_t as the ratio of the excess base charge to the collector current, the transform of the transit time $\tau_t(s)$ is approximated by $\tau_t(1+s\tau_D)$, where τ_D is the delay time. For a one-dimensional, homogeneous-base transistor, $\tau_D=\tau_t/6$. The results of this technique are in good agreement with exact calculations.

Transfluxor Design Considerations—Walter L. Morgan (p. 155)

The transfluxor is a new magnetic device for use in information handling and nondestructive storage systems. The location and sizes of each of the several apertures determine many of the operating characteristics of the device. This paper discusses the various geometric and magnetic factors that should be considered before deciding upon a core configuration. Two methods, one based on a graphical approach, the other on mathematics, are outlined to determine the optimum shape for a particular application. A procedure may be reversed to predict the performance of existing cores. The flux storage principles are described and the equation $\phi_s=kI_c-k'$ is derived. This equation shows the relationship between the input current I_c and the stored flux ϕ_s. k and k' are design constants depending on the magnetic and physical properties of a core. Comparisons are made between a 346-mil (OD) core and one of 83 mils. Estimates are given as to the practical limits to which core miniaturization may be carried using existing fabrication methods.

A Unidirectional Amplifier with Esaki Diodes—W. J. Grubbs (p. 163)

Two Esaki diodes can furnish unidirectional amplification when used in conjunction with a Hall-effect isolator. The input and output impedances of this amplifier are greater than the absolute value of the negative resistance of the diodes by a factor which is proportional to the voltage gain. The voltage gain-bandwidth product of such an amplifier is $g_T/4\pi RC$, where g_T is determined by the isolator and RC is the usual RC time constant of the Esaki diodes. Typically g_T is between 0.1 and 1. If one of the diodes is removed, the remaining network still amplifies unilaterally, but the impedance at the diode-less end drops to that of the isolator alone. In addition, a Hall-effect gyrator or circulator can be made essentially lossless by the addition of Esaki diodes.

Engineering Management

Vol. EM-8, No. 1, March, 1961

Readers are invited to participate in a data-collection effort, conducted by SCARDE (Study Committee for the Analysis of Research, Development, and Engineering) on the patterns of man-power and money utilization currently found in R and D projects. The aggregated and summarized data should provide valuable insights into current practices in a variety of industries and firms of different sizes, and be useful to researchers interested in a quantitative approach to the management of R and D activities. Strict procedures to safeguard proprietary information have been established. The background and results of a pilot study are indicated, and an example of the possible use of the study results is presented.

Scientists and technologists are in the midst of an enormous social experiment, involving the growth of many new skill groups and the undertaking of very large and complex R and D projects. The boundaries of the engineering profession and a philosophy of organizing complex projects are discussed. Some effects on engineering education are traced. Differences between engineers and scientists are examined in the context of the "research and development explosion." Traditional functional differences are being erased, but some differences in personal and social characteristics are described.

Technological change creates strains within the structure of the firm because it causes shifts in the relative power and influence between groups. The arrival of new groups in an organization such as a research laboratory creates linguistic problems: the language of the laboratory is different from that of the design activity and still different from that of the shop. To bridge the linguistic gap, interpreter or liaison groups are formed. In establishing these groups, management attempts to accommodate organizational strains within the existing structure rather than re-organize to reflect the new technology.

This study is based on the experiences of twenty firms in England and Scotland.

One of the most important functions of research management is to establish objective criteria for measuring the progress and performance of the research effort. Another important aspect is to allocate resources to research projects in the "best" manner. Two systematic procedures were developed in a large research laboratory to assist management in these tasks. The first is a Data Presentation System which provides a means for recording and presenting the status, progress and plans

for the research laboratory in terms of the allocation of resources. The second is an Evaluation System which provides a means for evaluating the technical and economic elements relative to research projects.

Weapon System Phasing for Ready Forces—Herbert K. Weiss (p. 30)

A ready force is defined as one designed to have a decisive capability in a short war in which the decision is reached before reserves and production capability can supplement the forces existing at the time hostilities begin. It is assumed that annual expenditures to equip, train, maintain and operate the ready force are constant. Within this constraint, it is desired to attain maximum effectiveness by balancing quality against quantity of weapons. Maximum quantity of weapons would be attained by selecting one type, and producing this type indefinitely, in view of decreasing unit production costs with number produced. However, rapid advancement of the state-of-the-art creates weapon obsolescence and, periodically, old weapons must be phased out and new weapons phased in. Maximum quality can be attained at the expense of quantity by very small production runs with frequent introduction of new weapons. The optimum program of effective weapons in sufficient quantity represents a compromise between the two extremes.

A model incorporating the variables of production cost, number of weapons produced, operating cost, growth of the state-of-the-art, effectiveness and budgetary limits is developed for a very simple model of warfare, and the relations among the variables for maximum force effectiveness are determined.

Strategy in Research—Alternative Methods for Design of Experiments—D. S. McArthur (p. 34)

Several simulated research problems have been programmed for the IBM 704 computer. Six different empirical research strategies have also been programmed for the computer. The "research problems" are "solved" by the computer using one of the six strategies to learn which is best. The computer uses each research strategy on each problem several times to get a statistical evaluation of its effectiveness. The work is not complete as yet; however, it has already had an influence on the way we are tackling some of our research problems.

Possible Applications of Information Theory to Management Control—Robert C. Hopkins (p. 40)

Several areas of possible application of information theory are discussed: 1) communication in automation, 2) forecasting, and 3) production processes. In the production area, the following possible applications are examined: "reduction of uncertainty" in raw materials and information content of a design. An example is given for a milling machine operation.

Engineering Writing and Speech

Vol. EWS-4, No. 2, May, 1961

The Cover (p. 34)

Human Responses—A Vital Link in Communications Progress. Part II—Beverly Dudley (p. 35)

An interpretation of the communications process is given in terms of stimulus and response. Part I, published in the January, 1961, issue of these Transactions, deals with communications in the physical and behavioral sciences and with the nature of stimulus/sensation under various sensory conditions. Part II deals further with the basic processes of communication and cites an example of underwater communication between submarines.

How to Write Officialese—Brockway McMillan (p. 42)

This paper gives an up-to-date communication basis for the 1961 time frame.

Better Writing: New Answers for an Old Problem—John B. Bennett (p. 44)

Instruction in the mechanics (grammar, spelling, punctuation, and the like) is no key to improved engineering writing. The critical factors in such improvement are correctness, completeness, and comprehensibility. These subjects can be taught through the use of simple student exercises specially designed to permit controlled emphasis on, and objective evaluation of, correctness, completeness, and comprehensibility; the same exercises make it possible to judge student competence in handling the less important mechanics. This approach has been tested and can be widely applied to improve the quality of our engineering writing.

Apply Quality Control to Engineering Writing—Ronald S. Blicq (p. 47)

Quality control can be exercised over engineering writing in the same way that it is exercised over manufacturing and installation/maintenance programs. In the case of writing, however, the "inspector" is the technical editor or a supervisory engineer. His terms of reference are the engineering writing standards laid down in a standards handbook prepared by those responsible for the production of technical publications.

The proposed "quality-controlled" engineering writing program has two major advantages:

1) It is simple to implement since it follows comparable established engineering and quality-control practices, to which engineers are accustomed.
2) It is imposed from within the department directly concerned with engineering writing, and is thus entirely independent of outside control.

Taking the Splatter out of Your Technical Writing—John M. Carroll (p. 52)

Three major ills of engineering writing are use of cliches, round-about expressions, and long, unfamiliar words. Articles containing such words and phrases are lengthy and tiresome to read, and often have their basic meaning obscured. Cliches, round-about expressions, and long words may be likened to solder splatter in a hand-wired chassis. Splatter gives the job an unprofessional appearance and may interfere with circuit operation. This article identifies many of the more common splatter-expressions that creep into engineering writing. It is based on a six-month study during which words and phrases deleted from articles published in *Electronics* magazine were accumulated and tabulated.

Persuasion in Engineering Proposals—Robert B. MacAskill (p. 56)

This article suggests several important methods by which an engineer writer may enhance his proposal in the eyes of the reader and future customer. Consideration is also given to the attitude the writer must take in order to write the successful proposal. The writer must become aware of the elements of persuasion in writing.

Library and Laboratory: Partners in Research—Harold S. Sharp (p. 58)

Duplication of research effort can be prevented when a literature search is made before starting laboratory work. The role of the librarian in assisting the engineer-researcher is discussed, and the services which can be expected of the librarian are stated. This article discusses certain library tools and techniques for the engineer-researcher.

Book Reviews (p. 62)

The Authors (p. 63)

Information for Authors (Inside Back Cover)

Microwave Theory and Techniques

Vol. MTT-9, No. 3, May, 1961

Octave-Bandwidth UHF/*L*-Band Circulator—F. Arams, B. Kaplan, and B. Peyton (p. 212)

Test data are presented on two aluminum-substituted yttrium-iron-garnet (YIG) materials that have low-saturation magnetizations that permit the extension of ferrite devices well into the UHF/VHF region. In particular, one composition has a saturation magnetization of 300 gauss and a line width of 50 oersteds. Measurements are presented that compare the new materials with previously available higher-saturation magnetization materials.

A broad-band UHF/*L*-band four-port circulator that operates over a 2-to-1 frequency band has been developed, using this 300 gauss material. Insertion loss is 1 db or less from 665 to 1320 Mc (with constant magnetic field) and 0.5 db or less from 800 to 1150 Mc. A very compact and favorable circulator package design was obtained by using coaxial hybrids and dielectric-loaded strip transmission line. Data on the broad-band magic-tee used in the circulator are included. Isolator measurements down to 200 Mc are reported. Reverse-to-forward magnetic-loss ratios of 36 at 600 Mc and 12 at 300 Mc were obtained.

A Five-Port Matched Pseudo-Magic Tee—Akira Okaya (p. 216)

The five-port matched pseudo-magic tee consists of an input waveguide, two load arm waveguides which are coupled into the input waveguide with $+90°$ and $-90°$ phase shifts, respectively, and an output waveguide which is split into two load waveguides by a septum.

The improvements include a much broader matching and isolation bandwidth, higher isolation between arms, better matching into arms, and a variety of modifications for different applications.

These characteristics have been obtained by employing frequency-insensitive phase shifters. Hence, frequency coverage is mainly limited by mechanical asymmetry and the characteristics of the directional coupler in the magic tee.

While this type of hybrid junction is not a true magic tee because the loads arms are not used as the input arm, it does have several applications which an ordinary magic tee does not have.

X-, *K*-, and *M*-band models were examined experimentally, and highly sensitive and accurate impedance measurements were made.

Theory of Dielectric-Loaded and Tapered-Field Ferrite Devices—R. F. Soohoo (p. 220)

Loading a ferrite resonance isolator or differential phase shifter with a dielectric or biasing the ferrite with an inhomogeneous dc magnetic field are very useful ways of improving the performance of these ferrite devices. Whereas these methods are very commonly used in transverse-field ferrite devices, no extensive analytical treatment of the subject has appeared in the literature. It is the purpose of this paper to present a theoretical analysis of the problem, chiefly by means of combined boundary-value and perturbation-theory approach. It will be shown that dielectric-loading and tapered-field techniques increase the bandwidth of isolators and phase shifters, the isolation-to-insertion loss ratio of the former, and the phase shift of the latter.

Theory of TEM Diode Switching—Robert V. Garver (p. 224)

The theory of TEM diode switching is presented for the purpose of understanding and designing TEM microwave diode switches. A few experimental results are reported for the purpose of supporting the theory and demonstrating the exceptional bandwidth possible.

An analysis is given of the switching action of one and of two or more diodes as well as the

biasing of the center conductor of a TEM transmission line over broad-frequency bandwidths without interacting with the RF signal. The use of point-contact germanium, varactor, and gold-bonded germanium diodes for TEM switching is discussed. Some considerations of switching speed and maximum power-handling capacity are given.

A coaxial transmission line switch has been constructed in which two gold-bonded diodes provide 26-db or greater isolation and insertion loss ranging from 1.6 db to less than 1 db from 40 Mc to 4000 Mc. The addition of a bias lead should increase the insertion loss 0.4 db or less over the 100-to-1 bandwidth, the maximum increase being at the upper and lower bounds.

Measurement of Small Dielectric Losses in Material with a Large Dielectric Constant at Microwave Frequencies—R. O. Bell and G. Rupprecht (p. 239)

A method is described for measuring dielectric losses at microwave frequencies in materials with a large dielectric constant. By observing a dielectric resonance in a sufficiently large sample, the loss tangent of the material can be obtained. Results on $SrTiO_3$ single crystals at 20 kMc are presented.

On the Existence of Leaky Waves Due to a Line Source Above a Grounded Dielectric Slab—E. S. Cassedy and M. Cohn (p. 243)

The existence of a particular type of leaky wave is verified experimentally. The leaky wave considered is that due to an electric line source above a dielectric slab. Since such a leaky wave cannot exist by itself, it must be detected in the presence of the remainder of the continuous spectrum and often in the presence of a surface wave (or waves). This was done by probing the fields and observing an interference pattern between the leaky wave and the existing surface wave, as predicted by the theory. These results emphasize a need to take leaky waves into account in the design of surface wave components and antennas.

A Broad-Band Glass-to-Metal Coaxial Vacuum Seal—W. M. Nunn, Jr., and L. E. Paul (p. 248)

The design procedure for a broad-band glass-to-metal seal is described, and experimental results are presented for a structure examined over the frequency range of 100 to 11,000 Mc. The seal described is capable of operating at bakeout temperatures as high as 450°C, with higher temperatures being attainable by the use of other materials.

Magnetically-Tunable Microwave Filters Using Single-Crystal Yttrium-Iron-Garnet Resonators—Philip S. Carter, Jr. (p. 252)

A new type of magnetically-tunable band-pass microwave filter that makes use of ferrimagnetic resonance in single-crystal yttrium iron garnet is presented. The 3-db bandwidth can be adjusted from about 6 Mc to 100 Mc at *X* band, and the center frequency can be tuned over a wide range of frequencies, by means of a varying dc field. A theoretical analysis of the operation and behavior of this type of filter is presented. Descriptions of single-resonator and two-resonator filters which can be tuned over the *X*-band frequency range are given and experimental data are presented showing their tuning range, insertion loss, and bandwidth.

Product Engineering and Production

Vol. PEP-5, No. 1, April, 1961

Analytical Dollar Tradeoffs for Development of Electronic Equipment—David Ehrenpreis (p. 2)

This paper presents reasons for the importance of formal documented analytical calculations regarding tradeoff decisions in the design and evolution of electronic and electromechanical equipment.

This paper offers several quantitative tradeoff factors which convert equipment design parameters to equivalent dollar penalties and values.

Solid State Laminants—Barton L. Weller (p. 9)

The technology of producing smaller electronic systems is going in the direction of creating function within single units. Achieving the ultimate in size reduction can come from experience in manufacturing commercial capacitors of porcelain-silver, fused laminants. This means of generating system in solids is described and examples of different three-dimensional structures are shown.

New Method in Vibration, Shock, and Stress Analysis of Electronic Equipment—John J. Albanes (p. 19)

Audio Visual Instructions for Electronics Assembly—A. P. Kromer (p. 31)

Small Lot and Specialty Production Problems—Harold M. Wilson (p. 33)

Value Engineering in Practice—Marvin Kaplan (p. 36)

Trade-Off Considerations in Using Automatic Test Equipment—E. L. Roel (p. 39)

Transportation and Packaging Techniques to Improve Reliability—Anthony Rubertone (p. 45)

An outline is presented of probable environments to be expected in shipping electronic equipment by the following:

1. Aircraft transport vehicles
2. Railroad
3. Trucks
4. Ships

The environmental engineering data are based upon previous studies and military governing specifications. Orders of magnitude are given as yardsticks for shock design inputs in terms of G level shock pulses, pulse shapes, pulse durations, population of pulses and direction of pulses. Test procedures to simulate environment shocks are described. Accelerated life test philosophy is defined.

Similarly, orders of magnitude are given for low frequency vibration inputs as terms of cumulative cycles, frequencies, G levels and amplitude levels. Test procedures are briefly discussed.

Discussion is included regarding electronic equipment resistance to environmental transportation shock and vibration. References are cited for the performance of rigorous analyses for determination of natural frequency and transmissibility. Recommendations are made for qualitative evaluation of electronic equipment resistance in shipping environments.

Transmissibility across suspension system during shock and vibration excitation is discussed. Incompatibility between shock and vibration isolation is discussed.

Vehicular Communications

Vol. VC-10, No. 1, April, 1961

Personal Radio Systems and Applications—John F. Mitchell (p. 1)

This paper is a discussion of the system aspects of radio systems designed to use the new types of Personal Radio Equipments which have been, and are being, introduced to the market in increasing numbers and types. Several actual applications are discussed. These examples cover the two basic types of equipment now in use, which are two-way non-selective call units, and one-way selective calling paging units.

The basic capabilities of the personal equipment are examined insofar as they pertain to Personal Radio System Design. The limitation and advantage of this equipment as well as the new uses and applications of this equipment are treated.

The Citizens Band Boom—Ivan H. Loucks (p. 6)

A Two Way Dial Private Mobile System for Telephone Construction and Maintenance—R. L. Flaminio and W. H. Rice (p. 11)

The assignment of frequencies by the Federal Communications Commission in 1958 for use by the Telephone Industry opened the way for obtaining more efficient plant operations through vehicular communications. The mobile communication system described in this paper was designed to serve the needs of the construction and maintenance forces in the Southwest District of the Bell Telephone Company of Pennsylvania.

The system employs decentralized dispatching which permits the supervisory personnel to use the service directly from their respective job locations. This is accomplished by incorporating the talking and signaling functions of the radio system into the standard Bell System 500 type telephone set normally used for the wire line service.

Since the dispatch points are located in administrative offices where loudspeaker operation must be avoided, mobile to base station dial signaling is employed. Similarly, dial signaling from base to mobile was used to protect the public from indiscriminate loudspeaker operation. Arrangements are also provided for mobile to mobile calls on a dialing basis. This feature is of significant value to the foremen who supervise a number of cable or line crews throughout a relatively large area.

Personal Radio Antennas—N. H. Shepherd and W. G. Chaney (p. 23)

The trend toward personalizing vehicular radio sets has been accompanied by major engineering problems. Of these, one of the most challenging is that of designing an efficient antenna to occupy a small space. Due to these size limitations, personal radio antennas will be referred to as small antennas.

This paper will describe a series of tests made under laboratory conditions followed by a coverage study made under service conditions in city streets to evaluate the relative performance of small antennas and accumulate propagation data for system design.

The laboratory measurements included a study of the properties of ferrite loop antennas, coils, whips and short wire antennas. The field measurements covered actual recorded field strength data from personal carried transmitters using reference quarter-wave whips.

It was concluded that $\frac{1}{4}$-wave whips even when working against as poor a ground plane as the set chassis offered the best performance. However, the 20 to 25 db of shadow loss found in city streets plus a 10 to 15 db antenna loss even with whips will severely restrict the coverage of personal transmitters. Other steps may be necessary if adequate areas are to be reliably covered.

Mechanical Filters for FM Mobile Applications—R. A. Johnson (p. 32)

The Western Division of Collins Radio Company has developed an electromechanical band-pass filter for use in the low frequency IF of split channel FM mobile receivers.

The "Mobile" Filter has a 455 kc center frequency and nominal 3 db and 60 db bandwidths of 13 kc and 28 kc respectively. The filter is fixed tuned, enclosed in a third of a cubic inch package and was engineered with the idea of low price without compromise in performance.

The Mobile Filter gives both the equipment designer and user excellent selectivity and stability, so essential when operating under split channel conditions, along with a flat amplitude response and low loss.

A Modular Approach to the Design of FM Communication Equipment—B. Tennent and G. G. Armitage (p. 38)

Through the use of coils wound on subminiature ferrite bobbins, threaded ferrite cup cores and of newly released P.A.D.T. transistors, the IF strips of an FM communications receiver have been packaged into two compact, hermetically sealed, pre-tuned components. This ensures built-in optimum performance, reliability and standardization of an important section of FM receivers for all frequency ranges and simplified maintenance.

Similar developments for other sections of FM communications equipment and for Citizen's Band Radio are referred to in this paper.

A Selective Ringing Decoder for Mobile Radiotelephone Use—James D. Malone (p. 49)

A Centralized Mobile Telephone Test Panel—John P. Gill (p. 55)

A centralized method of testing Mobile, Test and Base Station Transmitters "Off the Air" has always been considered desirable. With the inauguration of 450 Mc narrowband common carrier telephone service with its more stringent requirements, a centralized method of testing has become almost a necessity.

The Centralized Mobile Telephone Test Panel described herein can be used to evaluate the over-all performance of the Mobile telephone system and can also be used as a tool to insure proper routine operation of a system. Provisions are made in the CMTTP for automatic sampling of each radio channel with statistical evaluation of ON-OFF frequency operation of mobile transmitters.

The present unit is arranged to monitor on the 450 Mc and Personal Signaling (Bellboy) services only. However, the test panel can be readily adapted for the 40 and 150 Mc channels as well.

Control Consoles—The VHF Integrators—Hugh H. Davids (p. 64)

Control circuitry integrates pieces of communication equipment into VHF communication systems. The control functions for simpler systems are adequately provided by standard remote control units, using options to provide for a variety of needs.

More complex systems require special control circuitry and control consoles whose design is part of the overall system design. A duplex backbone system such as used on cross-state turnpikes is typical of such complex systems. Party line vs multi-channel design of such systems is contrasted and use of various devices such as receiver voting discussed.

Console design is illustrated by discussing features of the Massachusetts Turnpike Control Console. Range of control design is indicated by mention of two-way mobile telephone requirements and the potential field of remote control from portable control consoles, such as remote control of a switching locomotive.

A Proposed System for 11 Channel Access in the Mobile Telephone Service—C. A. Rypinski, Jr. (p. 75)

A signaling, supervision and radio technique suitable for multi-channel access in the VHF MTS band is proposed. The logic is based on the continued use of 600/1500 cps transitional signaling and certain existing methods of transmitting supervisory signals to the base terminal. Mobile identification is provided but is neither required or excluded. The availability of a mobile radio equipment which does not deteriorate as a result of continuous channel switching is assumed.

Signaling tone at either frequency is used to mark the idle channel on which the next call will appear or on which the mobile may seize the terminal. If the mobile is not locked on a channel marked idle, the busy indication is given.

The logic of this technique is further detailed in a table and is illustrated by tracing sequences of calls including special cases such as carrier fade, simultaneous seizure and the persistent caller with no answer.

To illustrate feasibility a suitable mobile decoder and control unit is described which provides decoding, supervision and logical control. Component content of this design is tabulated.

A possible configuration of a preferred mobile radio transceiver is proposed which employs synthesis type channel switching, linear detection and full duplex operation. The 13 crystals employed are shared by transmitter and receiver and only one is a high accuracy type.

It is the object of this paper to encourage the adoption of a multi-channel access standard to serve the interval preceding the development of the broad-band service by showing compatibility with existing technique and the feasibility of the required equipment.

The Use of Level Controlling Devices in the Radio-Telephone Service—L. E. Getgen (p. 87)

This paper introduces the subject of speech level control as applied to radio-telephone service by presenting statistical data describing talker level variations and anticipated levels at the telephone central office. Because speech measurements are difficult to make, mention is made of speech to sine wave relationships that are convenient for system line-up. Next, maximum levels are established for the output of the controller and application to the wire-line or the radio transmitter.

The operational characteristics of three available types of level controlling devices are discussed. These are: the Agamp and Vogad which were designed specifically for control of speech levels into radio transmitters; the clipper-limiter commonly used in radio broadcasting; and the Compandor which is familiar in telephone applications.

Recordings were made of these devices in operation. Analysis of these recordings as related to the "ground rules" established in the text allowed conclusions to be drawn concerning the most advantageous use of each.

In discussing the use of level controlling devices, it is necessary to determine the nature of the signals that are to be controlled. Where telephone facilities are to be used, consideration must be given to plant practices. These practices as well as the transmitter input requirements will establish the output level limits for the device. Having an idea of the input and output requirements and taking into account unusual noise and environmental conditions, the next step is to examine the characteristics, and cost, of available units to determine the extent to which they meet the system application.

Measurement of Deviation and Frequency in FM Two-Way Radio Systems—M. Cooper (p. 98)

Sinad System Design—R. A. Farmer (p. 103)

This paper deals with performance parameters used in designing a communication system, black boxes and all, rather than with the circuit parameters needed to design the individual equipments which make up the total system. There is a common language for use in the Land Mobile Services which should, but does not yet, have the stature of CCIF and CCITT specifications used by system designers in the field of point-to-point communications. The Electronic Industries Association (EIA) specifications for Land Mobile equipment are examined and their applicability to system design work is discussed.

Abstracts and References

Compiled by the Radio Research Organization of the Department of Scientific and Industrial Research, London, England, and Published by Arrangement with that Department and the *Electronic Technology* (incorporating *Wireless Engineer* and *Electronic and Radio Engineer*) London, England

NOTE: The Institute of Radio Engineers does not have available copies of the publications mentioned in these pages, nor does it have reprints of the articles abstracted. Correspondence regarding these articles and requests for their procurement should be addressed to the individual publications, not to the IRE.

The number in heavy type at the upper left of each Abstract is its Universal Decimal Classification number. The number in heavy type at the top right is the serial number of the Abstract. DC numbers marked with a dagger (†) must be regarded as provisional.

UDC NUMBERS

Certain changes and extensions in UDC numbers, as published in PE Notes up to and including PE 666, will be introduced in this and subsequent issues. The main changes are:

Artificial satellites:	551.507.362.2	(PE 657)
Semiconductor devices:	621.382	(PE 657)
Velocity-control tubes, klystrons, etc.:	621.385.6	(PE 634)
Quality of received signal, propagation conditions, etc.:	621.391.8	(PE 651)
Color television:	621.397.132	(PE 650)

The "Extensions and Corrections to the UDC," Ser. 3, No. 6, August, 1959, contains details of PE Notes 598–658. This and other UDC publications, including individual PE Notes, are obtainable from The International Federation for Documentation, Willem Witsenplein 6, The Hague, Netherlands, or from The British Standards Institution, 2 Park Street, London, W.1, England.

A list of organizations which have available English translations of Russian journals in the electronics and allied fields appears each June and December at the end of the Abstracts and References section.

The Index to the Abstracts and References published in the PROC. IRE from February, 1953 through January, 1960 is published by the PROC. IRE, June, 1960, Part II. It is also published by *Electronic Technology* (incorporating *Wireless Engineer* and *Electronic and Radio Engineer*) and included in the April, 1960 issue of that Journal. Included with the Index is a selected list of journals scanned for abstracting with publishers' addresses.

ACOUSTICS AND AUDIO FREQUENCIES

534.2 1695

The Effective Dynamic Parameters for Sound Propagation in Inhomogeneous Media—I. A. Ratinskaya. (*Akust. Zh.*, vol. 6, no. 1, pp. 128–131; 1960.) A revision of an earlier analysis [1041 of 1959 (Kalkovich and Khalfin)] is given.

534.2–14 1696

Sound Field of a First-Order Normal-Mode Wave in a Layer of Water—F. I. Kryazhev. (*Akust. Zh.*, vol. 6, no. 1, pp. 65–76; 1960.)

534.2–14 1697

Normal-Mode Waves in a Three-Layer Medium—F. I. Kryazhev and N. A. Petrov. (*Akust. Zh.*, vol. 6, no. 2, pp. 229–236; 1960.) An analysis is given of experimental data on the propagation of sound waves in some shallow waters of the Caspian Sea in the frequency range 8–1000 cps. Waveguide-type propagation occurs at values of $kh > 2.8$, where k is the wave number and h the layer depth.

534.2–14 1698

A Method of Wave Front Determination for a Sound Wave of Approximately Sawtooth Form—L. K. Zarembo. (*Akust., Zh.*, vol. 6, no. 1, pp. 43–46; 1960.) An analysis of the propagation of sawthooth waves in water is given.

534.2–14 1699

Investigation of Low-Frequency Sound Propagation in Shallow Waters—V. S. Grigor'ev and F. I. Kryazhev. (*Akust. Zh.*, vol. 6, no. 1, pp. 34–42; 1960.) A description of an experimental method illustrating the waveguide-type propagation of sound in sea water at frequencies up to 10 kc is given.

534.213.4 1700

Sound Propagation in a Waveguide with Rectangular Grooves in the Walls—A. D. Lapin. (*Akust. Zh.*, vol. 6, no. 2, pp. 237–243; 1960.) A mathematical treatment relating to acoustic filters is given. The optimum size of a transverse channel in a waveguide wall for greatest sound reflection is determined and the frequency characteristics of a waveguide are obtained.

534.213.4–14 1701

Signal Amplitude and Phase Fluctuations Induced by Surface Waves in Ducted Sound Propagation—J. A. Scrimger. (*J. Acoust. Soc. Am.*, vol. 33, pp. 239–247; February, 1961. The dependence of the amount of amplitude and phase fluctuation in received signals on surface wave crest-to-trough height has been determined for frequencies in the range 1–10 kc propagated over a distance of 300 feet in water 10 feet deep.

534.213.4–8 1702

Theory of Ultrasonic Attenuation in Cylindrical and Rectangular Waveguides—E. F. Carome and J. M. Witting. (*J. Acoust. Soc. Am.*, vol. 33, pp. 187–197; February, 1961.) The systems studied consist of a piston source radiating into a bounded inviscid fluid and a receiver the same size as the source. Expressions for receiver output are derived, and acoustic loss as a function of path length is computed for various source and waveguide configurations.

534.22–8–14 1703

The Propagation Velocity of Ultrasonic Wave of Finite Amplitude in Liquids—L. K. Zarembo and V. V. Shklovskaya-Kordi. (*Akust. Zh.*, vol. 6, no. 1, pp. 47–51; 1960.) An application of a phase-comparison method for an investigation of velocity jump is given.

534.232 1704

Experimental Investigation of Cylindrical Focusing Systems—I. N. Kanevskiĭ. (*Akust. Zh.*, vol. 6, no. 1, pp. 123–124; 1960.) Results of measurements made on cylindrical $BaTiO_3$ focusing radiators in the frequency range 600–900 kc with angles of aperture 30°, 60° and 90° are noted.

534.26 1705

Diffraction of a Plane Sound Wave Incident at an Arbitrary Angle on an Infinite Cylindrical Cavity in an Elastic Medium—V. V. Tyutekin. (*Akust. Zh.*, vol. 6, no. 1, pp. 101–106; 1960.)

534.26–14 1706

Scattering of Acoustic Energy by Solid and Air-Filled Cylinders in Water—G. R. Barnard and C. M. McKinney. (*J. Acoust. Soc. Am.*, vol. 33, pp. 226–238; February, 1961.) Results are given of an experimental investigation of the scattering of acoustic energy from solid and hollow cylinders as a function of cylinder length, pulse length and frequency.

534.286–8 1707

Contribution to the Theory of Ultrasonic Absorption in Metals—V. P. Silin. (*Zh. Eksp. Teor. Fiz.*, vol. 38, pp. 977–983; March, 1960.) A theoretical treatment of low-temperature absorption at wavelengths small compared to the electron mean free path is given. In the region of wavelengths which are approximately equal to the thickness of the anomalous skin layer a decrease in the ratio of the absorption coefficient to frequency should be observed with increase of frequency.

534.41:538.652 1708

The Relation between the Magnetic Properties and Sensitivity of Magnetostrictive Receivers of Nickel-Zinc Ferrite—A. D. Sokolov

and Ya. S. Shur. (*Akust. Zh.*, vol. 6, no. 1, pp. 131–133; 1960.) Experimental data are tabulated.

534.52 1709

Sound Field in the Focal Plane of Converging Spherical Beams—B. D. Tartakovskiĭ. (*Akust. Zh.*, vol. 6, no. 1, pp. 96–100; 1960.) The distribution of the oscillation velocity and sound pressure in the focal plane is calculated for a focusing system in which the beams have a nonuniform amplitude distribution over the wave front.

534.6:534.84 1710

Application of Frequency Modulation to Acoustic Measurements—V. A. Zverev and A. I. Kalachev. (*Akust. Zh.*, vol. 6, no. 2, pp. 205–212; 1960.) A CW FM technique is described for measurements in normal rooms. Spectrum and correlation analysis are applied for locating sources of sound and reflections. The autocorrelation process makes it possible to separate the discrete reflections from reverberation signals.

534.61–8:539.2 1711

Phonon-Photon Double-Quantum Transitions as a Detector of Microwave Ultrasonics—N. S. Shiren. (*Phys. Rev. Lett.*, vol. 6, pp. 168–170; February 15, 1961.) A fast intensity detector for microwave ultrasonic pulses is described. The spin systems of Ni^{2+} and Fe^{2+} in MgO crystals at 2°K are used. The absorption of CW microwaves is increased when ultrasonic pulses are transmitted through the crystal. Absolute ultrasonic energy measurements are possible.

534.75 1712

Subdivision of the Audible Frequency Range into Critical Bands (Frequenzgruppen)—E. Zwicker. (*J. Acoust. Soc. Am.*, vol. 33, p. 248; February, 1961.) A note showing the relation between critical-band function and frequency, and defining the proposed frequency limits of the critical bands is given.

534.79 1713

The Loudness of Directional Sound Fields—D. W. Robinson and L. S. Whittle. (*Acustica*, vol. 10, no. 2, pp. 74–80; 1960.) Subjective measurements have been made in the frequency range 1.6–10 kc of the variation of loudness with source direction, together with corresponding measurements of sound pressure. The loudness estimated from the sound pressures at left and right ears agrees well with the observed binaural loudness if a 6-db summation law is assumed.

534.844 1714

Recent Subjective Acoustic Investigations of Reverberation Time—T. Tarnóczy, T. Járfás, and M. Lukács. (*Elektron. Rundschau*, vol. 14, pp. 223–226; June, 1960.) A definition of "subjective reverberation time" is given which is based on a subjective assessment allowing for different musical tempi. Experimental results are discussed.

534.844.1+[621.317.2:538.566.08 1715

The Upper Limits for the Reverberation Time of Reverberation Chambers for Acoustic and Electromagnetic Waves—K. Walther. (*J. Acoust. Soc. Am.*, vol. 33, pp. 127–136; February, 1961.) "The upper limits for the reverberation time and Q factor of acoustic reverberation chambers with perfectly rigid walls with a smooth surface are determined. The reflection factor for a rigid wall of arbitrary thermal conductivity is determined from a consideration of the viscosity and heat conductivity-boundary layer. The cases of isothermal and adiabatic boundary conditions are discussed. See 1393 of May (Meyer, *et al.*).

534.844.1 1716

Measurement of the Degree of Diffusion of a Sound Field in Rooms by Means of a Directional Microphone—V. V. Furduev and Chen Tun. (*Akust. Zh.*, vol. 6, no. 1, pp. 107–115; 1960.) The method is based on a comparison of the directivity characteristics of a microphone in a "dead" room and in the room to be investigated. The theory of measurement using a microphone which is a combination of a pressure type and pressure-gradient type is given. Some results obtained in a reverberation chamber and broadcasting studios are shown.

621.395.61 1717

A Microphone Arrangement of High Directivity—P. Dämmig. (*Acustica*, vol. 10, no. 2, pp. 120–123; 1960. In German.) A parallel arrangement of two groups of slit-tube directional microphones forming a crossed array is described. The half-width of the directional characteristic is 15° at 1 kc and 12° at 4 kc.

621.395.616 1718

Pressure Response of Condenser Microphones at Low Ambient Pressures—J. D. Chalupnik, E. Rule, and F. J. Suellentrop. (*J. Acoust. Soc. Am.*, vol. 33, pp. 177–178; February, 1961.) Pressure response curves at a number of ambient pressures in the range 10^6dyn/cm^2–17×10^4 dyn/cm^2 have been obtained for two commonly used condenser microphones. Features of the response curves are discussed from a qualitative point of view.

621.395.625.3:538.221 1719

The Properties of Modern Magnetic Recording Tapes—P. H. Werner and E. Kohler. (*Tech. Mitt. PTT*, vol. 38, pp. 217–228; July 1, 1960. In French and German.) Mechanical and electrical properties are reviewed and means of reducing print-through effects are discussed.

ANTENNAS AND TRANSMISSION LINES

621.315.212 1720

Continuous Loading of Coaxial Circuits without Air Gap—P. M. Prache. [*Câbles & Trans. (Paris)*, vol. 14, pp. 180–190; July, 1960.] A theoretical determination of the attenuation in a coaxial circuit loaded by toroidal ferrite cores inserted between the two conductors so that there is no air gap is given. Experimental results confirm the theoretical calculations and show that it is possible to reduce coaxial-circuit attenuation in this way, at least for frequencies up to 2 Mc.

621.372.2:621.372.44 1721

Periodic Solutions of the Wave Equation with a Nonlinear Interface Condition—W. L. Miranker. (*IBM J. Res. & Dev.*, vol. 5, pp. 2–24; January, 1961.) An analysis is given of the voltage oscillations in a transmission line when shunted with a diode represented by a nonlinear capacitance.

621.372.8:621.396.44 1722

Characteristics of Waveguides for Long-Distance Transmission—A. E. Karbowiak and L. Solymar. (*J. Res. NBS*, vol. 65D, pp. 75–88; January/February, 1961.) A detailed discussion and analysis of propagation characteristics including effects of bends and other discontinuities are given. 35 references.

621.372.81 1723

The Theory of Waveguides and Cavities: Part 2—Examples of Waveguides and Discussion of Special Points—R. W. Waldron. (*Elektronic Tech.*, vol. 38, pp. 140–147; April, 1961.) The method described in Part 1 (1404 of May) is applied to two examples: a) an air-filled circular waveguide; b) a coaxial line in which the core material is considered as a dielectric.

4621.372.826 172

Sommerfeld and Harms-Goubau Waveguides in the Centimetre and Millimetre Wave Range—H. Severin. (*Arch. elekt. Übertragung*, vol. 14, pp. 155–162; April, 1960.) The calculation of transmission characteristics of surface waveguides for cm and mm λ is made. Curves are included of the radius of the external field and of attenuation as a function of frequency and line parameters. Given a maximum permissible attenuation of 3.5 db/km, Sommerfeld and Goubau lines are not suitable for wavelengths below 5 cm.

621.372.826:537.226 1725

Measurement of the Properties of Dielectric Transmission Lines at Millimetre Wavelengths in an Optically Coupled Resonator—G. Schulten. (*Arch. elekt. Übertragung*, vol. 14, pp. 163–166; April, 1960.) Measurements of dispersion and attenuation of the HE_{11} mode were made at 5 and 8 mm λ on threads of polythene of various diameters for use as dielectric lines of the ordinary or image type [see *e.g.*, 2827 of 1959 (Schlesinger and King)].

621.372.831.2 1726

The Reflection of the Fundamental Mode at Waveguide Discontinuities, particularly with a Gradual Transition from a Rectangular to a Circular Waveguide—K. Schnetzler. (*Arch. elekt. Übertragung*, vol. 14, pp. 177–182; April, 1960.) Theoretical expressions are derived for the reflection of the fundamental mode at waveguide junctions involving smooth transitions with small angles. Calculated values for a rectangular/circular junction agree well with measured values.

621.372.837 1727

A Low-Loss, Semiconductor Microwave Switch—D. L. Rebsch. (Proc. IRE, vol. 49, pp. 644–645; March, 1961.) The superiority of a new semiconductor switch configuration is discussed in which the diode is mounted in the arm of symmetry of an H-plane T-junction.

621.372.853.1 1728

Backward Waves in Waveguide with Anisotropic Dielectric—F. Borgnis. (*Bull. schweiz. elektrotech. Ver.*, vol. 51, pp. 1030–1033; October 8, 1960.) The conditions under which separately excited backward waves can exist in a waveguide are investigated.

621.372.853.2 1729

Backward Waves in Longitudinally Magnetized Ferrite Rods—A. W. Trivelpiece, A. Ignatius, and P. C. Holscher. (*J. Appl. Phys.*, vol. 32, pp. 259–267; February, 1961.) A quasi-static approximation $(\nabla\times\bar{H})=0$ is used to develop a theory of this effect, the waves propagating with a phase velocity $<c$ and in a frequency range where the permeability is negative. Experimental measurements of phase velocity are described. Interaction with an electron beam is considered.

621.396.67(24) 1730

Useful Radiation from an Underground Antenna—H. A. Wheeler. (*J. Res. NBS*, vol. 65D, pp. 89–91; January/February, 1961.) Radiation efficiency is derived simply for a) a vertical loop in a submerged radome, and b) a submerged horizontal insulated wire with each end connected to a ground electrode. A power efficiency of 0.0014 is given in a specific example of b).

621.396.674.3 1731

The Characteristics of Dipole Impedances with Dipole Excitation Varying Exponentially with Time—K. Fränz. (*Arch. elekt. Übertragung*, vol. 14, pp. 167–168; April, 1960.) A mathematical treatment of dipole impedance by variational principles for real frequencies >0 is given.

621.396.677:523.164 1732
An Interferometer for the Measurement of Radio-Source Sizes—Goddard, Watkinson, and Mills. (See 1817.)

621.396.677:621.391.812.63 1733
Launching Over the Sea of Vertically Polarized Waves for Long-Distance Ionospheric Propagation—E. O. Willoughby. [*Proc. IRE, (Australia)*, vol. 21, pp. 591–597; September, 1960.] Simple vertically-polarized antennas from mast heights of 150 feet or less, launching over the sea, are shown to be capable of gains exceeding 14 db over a frequency band of 5 to 15 Mc, with good matching and efficient radiation between 1° and 10° elevation.

621.396.677.3 1734
Linear Aerial Arrays with Attenuated Side Lobes—K. Baur. (*Elektron. Rundschau*, vol. 14, pp. 217–222; June, 1960.) The radiation diagrams of linear antenna arrays are discussed and a method is given for modifying sidelobe maxima, and operating bandwidth and radiation angle by varying the antenna spacing. Examples of 4-, 8- and 16-antenna arrays with unequal antenna spacing are given.

621.396.677.3:621.396.965 1735
A High-Resolution Rapid-Scan Antenna—H. V. Cottony and A. C. Wilson. (*J. Res. NBS*, vol. 65D, pp. 101–110; January/February, 1961.) A description is given of an electronically-scanned broadside receiving array of 7 Yagi elements with spacing 1.4 λ. A 5.8° beam swept over a 41.8° azimuth 20 times per second is produced, operating at 40.92 Mc. Sample records showing ionospheric scatter and reflections from meteor trails and sporadic-E are given.

621.396.677.83:621.396.65 1736
The Deflector as Part of a Directional Aerial System—H. D. Kühne. (*Telefunken Ztg.*, vol. 33, pp. 120–131; June, 1960. English summary, pp. 157–158.) The design of plane or parabolic reflectors used as deflectors in radio-link antenna systems is described [see 45 of January (Münzer)]. Experimental results obtained at 3.3 and 7.5 cm λ are compared with calculated data.

AUTOMATIC COMPUTERS

681.142:538.221:539.23 1737
Patterns in Thin Films make Fast Nondestructive Memories—J. W. Hart. (*Electronics*, vol. 34, pp. 126–129; February 17, 1961.) The Kerr magneto-optic method is used to show that irreversible domains can be formed in thin magnetic films.

681.142:538.221:539.23 1738
The Problem of 'Coupling' in a Switching Circuit System consisting of Thin Magnetic Films—H. Oguey. (*Bull. schweiz. elektrotech. Ver.*, vol. 51, pp. 1004–1010; October 8, 1960.) Problems relating to the design of logic switching circuits formed by magnetic film elements are reviewed.

CIRCUITS AND CIRCUIT ELEMENTS

621.316.86:621.317.332 1739
The Impedance Value of Carbon Film Resistors as a Function of Frequency and D.C. Resistance—A. Debel and L. Hechler. (*Frequenz*, vol. 14, pp. 193–197; June, 1960.) An arrangement is described for impedance measurements in which the dimensions of the mounting are standardized in relation to resistor dimensions so that comparisons are possible between results obtained for resistors of different size. Curves are given of maximum usable frequency as a function of dc resistance, and of skin effect as a function of frequency and surface resistance.

621.318.57:621.382.33:517 1740
Methods of Analysis of Circuit Transient Performance—L. Hellerman and E. J. Skiko. (*IBM J. Res. & Dev.*, vol. 5, pp. 33–43; January, 1961.) A survey is given of some numerical methods for studying the performance parameters associated with transient behavior of switching circuits.

621.319.45 1741
Properties and Characteristics of Tantalum Capacitors with Solid Electrolyte—W. Ackmann. (*Nachrtech. Z.*, vol. 13, pp. 261–265; June, 1960.)

621.372:621.391.822:621.385.2 1742
Nonlinear Thermal Fluctuations in a Diode—N. G. Van Kampen. (*Physica*, vol. 26, pp. 585–604; August, 1960.) As an example of nonlinear noise, the fluctuations in a circuit consisting of a diode and a capacitor are studied and the complete fluctuation spectrum is calculated. See also 1898 of 1960 (Alkemade).

621.372.413 1743
Time Delay and Frequency Response of Resonant Cavities—A. G. Mungall and D. Morris. (*Canad. J. Phys.*, vol. 38, pp. 1510–1515; November, 1960.) "The frequency response and time delay characteristics of resonant cavities are discussed. It is found that a signal travelling through a resonant cavity undergoes a time delay dependent on both the cavity Q and also the difference between the signal and resonant frequencies. The time delay for a frequency-modulated wave is calculated and checked experimentally."

621.372.44:517.512.2 1744
Application of Distortion Functions to Instantaneous Nonlinear Circuits—R. Codelupi. (*Note Recensioni Notiz.*, vol. 9, pp. 489–540; May/June, 1960.) A mathematical treatment of nonlinear nonreactive networks using the functions derived in 3975 of 1960 is given.

621.372.5 1745
The Propagation Coefficient of a General Linear Quadripole—H. Weber. (*Bull. schweiz. elektrotech. Ver.*, vol. 51, pp. 958–960; October 8, 1960.) Current and voltage relations in a quadripole joining two transmission lines are calculated using methods of image-parameter theory.

621.372.5.029.6 1746
Determination of the Characteristic Impedance of Any Quadripole at Microwave Frequencies—S. Lefeuvre. (*Comple rend. Acad. Sci., Paris*, vol. 250, pp. 3288–3289; May 16, 1960.) Measurements made on the quadripole under certain load conditions are used in determining the characteristic impedance by a graphical method.

621.372.54 1747
The Modification of Wide-Band Noise Phenomena by Linear Transmission Systems—H. Schlitt. (*Arch. elekt. Übertragung*, vol. 14, pp. 239–246; June, 1960.) For simple types of filters the distortion of the power spectrum and autocorrelation function is investigated with wide-band noise as input. Relations between parameters of classical and of statistical system theory are derived.

621.372.54 1748
Method of Investigation of the Four-Branch Reactive Ladder-Filter Section—J. Bimont. [*Câbles & Trans.* (Paris), vol. 14, pp. 175–179; July, 1960.] An extension of a graphical method described earlier (3738 of 1960) is given.

621.372.54 1749
Antimetric Ladder Filters—J. E. Colin. [*Câbles & Trans.* (Paris), vol. 14, pp. 200–219; July, 1960.] All parameters of a quadripole antimetric ladder filter are shown to depend on four polynomial functions of p^2 (p being the complex angular frequency) between which a relation exists. The theory is applied to antimetric band rejection filters and to high- and low-pass filters, and tables are given facilitating calculations.

621.372.54 1750
Extension of the Possibilities of Filter Circuit Construction by means of Regions of Imaginary Characteristic Impedance in the Pass Band and Regions of Real Characteristic Impedance in the Stop Band—W. Herzog. (*Nachrtech. Z.*, vol. 13, pp. 291–295; June, 1960.) See also 1434 of May.

621.372.54:621.374 1751
The Choice of Filters with Favourable Transient Characteristics—O. Herrmann and W. Schüssler. (*Arch. elekt. Übertragung*, vol. 14, pp. 183–189; April, 1960.) The design of networks with the desired characteristics for pulse-shaping circuits is based on an analog-computer method [3737 of 1960 (Schüssler)]. Examples are given of filters with idealized response or with transfer function approximated by polynomials.

621.372.54:621.375.13.029.4 1752
Audio-Frequency Comb-Filter—L. H. Bedford. (*Electronic Tech.*, vol. 38, pp. 138–140; April, 1961.) Details are given of the design of a mechanical system consisting of a stretched metallic string for supressing 50-cps hum and associated harmonics in the output of an AF amplifier. Experimental results are noted.

621.372.6 1753
The Scattering Matrix of Generally Interconnected Multipoles—T. A. Abele. (*Arch. elekt. Übertragung*, vol. 14, pp. 262–268; June, 1960.) The scattering matrix of the network is formed by the simple manipulation of matrices based on the scattering matrix of the individual multipoles. See also 3399 of 1960 (Schuon and Wolf).

621.373.029.66 1754
Research on Submillimetre Wave Generation and Techniques—G. E. Weibel. (*Bull. schweiz. elektrotech. Ver.*, vol. 51, pp. 1015–1020; October 8, 1960. In English.) Experiments and experimental equipment are described for investigations on sub-mm-wave generation, including a "tornadotron" in which EM radiation is produced by the action of pulsed magnetic fields, of the order of 100 kg, on a trapped electron cloud. Aspects of instrumentation suitable for these frequencies are briefly discussed.

621.373.4:621.376.32 1755
Frequency Modulation of a Pound Stabilized Oscillator—K. Leibrecht. (*Compt. rend. Acad. Sci., Paris*, vol. 250, pp. 3302–3304; May 16, 1960.) A method is outlined for applying frequency modulation to an improved pound stabilized oscillator [355 of 1956 (Hervé)]. The frequency deviation is limited to about 1 Mc.

621.373.4.072.9 1756
Impulse-Governed Oscillator-Techniques: Part 2—C. J. de Lussanet de la Sablonière. (*Philips Telecommun. Rev.*, vol. 22, pp. 32–46 and 94–101; September, 1960, and January, 1961.) Theoretical aspects of IGO techniques are given. Part 1: 3754 of 1960.

621.373.42.029.6:621.018.41(083.74) 1757
Microwave Generators for the I.E.N. Caesium Standard—G. Zito. (*Bull. schweiz. elektrotech. Ver.*, vol. 51, pp. 1075–1079; October 8, 1960. In English.) Two microwave generators are described which are used in the atomic frequency standard of the Istituto Elettrotec-

nico Nazionale in Turin for Cs resonance excitation by molecular-beam technique. Measurements of phase drift and frequency stability are also considered.

621.373.422 1758
Plate Voltage Control of Phantastron Frequency—W. C. Whitworth. (*Electronics*, vol. 34, pp. 73–74; February 10, 1961.) "Two pentodes, each forming a phantastron circuit, are interconnected so that both mark and space of their combined output waveforms are controlled by linear rather than exponential sweeps. Circuit jitter is less than 0.003% at 5 pulses/sec repetition rate."

621.373.422:621.382.333 1759
Phantastron Circuits using Transistors—N. C. Hekimian. (*Electronics*, vol. 34, pp. 46–47; February 24, 1961.) Arrangements of three transistors to simulate the screen/anode current partition of a pentode enable transitron-type circuits to be designed are given.

621.373.43:621.374.32 1760
The Eccles-Jordan Circuit with Transistors for High-Speed Counters—W. Hilberg. (*Telefunken Ztg.*, vol. 33, pp. 98–108; June, 1960. English summary, p. 156.) A static analysis of a transistor flip-flop circuit is given, and the counting frequency limits for high-speed counters consisting of balanced flip-flop elements are discussed. Circuits operating at frequencies in excess of 20 Mc are described.

621.373.43:621.382.23 1761
One-Tunnel-Diode Flip-Flop—R. A. Kaenel. (PROC. IRE, vol. 49, p. 622; March, 1961.) A note on the operation of a simple bistable device is given.

621.373.43:621.382.23 1762
Designing Tunnel-Diode Oscillators—W. H. Ko. (*Electronics*, vol. 34, pp. 68–72; February 10, 1961.) An analysis of relaxation oscillators and associated circuits for sine-wave and square-wave generation is given.

621.374.3 1763
Mathematical Analysis of Pulse Networks—R. Hofmann. (*Arch. elekt. Übertragung*, vol. 14, pp. 255–261; June, 1960.) Linear systems are analyzed which comprise an element capable of converting a continuous input function into pulses of any desired shape. A pulse-network equation is derived which is applicable to closed-loop control systems.

621.374.3 1764
The Generation of Very Short Needle-Shaped Pulses—H. P. Louis. (*Bull. schweiz. elektrotech. Ver.*, vol. 51, pp. 1067–1072; October 8, 1960.) The design of pulse generators and pulse-shaping networks is discussed. Details are given of a double-differentiating network for the generation of 0.35-nsec pulses of 400-mv amplitude; further improvements by means of tunnel diodes appear possible.

621.374.33:621.387.4 1765
Low-Level Linear Microsecond Gate—P. R. Chagnon. (*Rev. Sci. Instr.*, vol. 32, pp. 68–70; January, 1961.) A six-diode gate, linear over the range 0.01–5 v is described.

621.374.5 1766
A Solenoid Delay Line with Constant Delay—A. J. Giger. (*Bull. schweiz. elektrotech. Ver.*, vol. 51, pp. 960–962; October 8, 1960.) A description is given of a compact delay line which consists of a solenoid wound on a ceramic tube of high dielectric constant with a metal core. Delay can be made independent of frequency with an appropriate tube/core diameter ratio.

621.374.5:534.2–8 1767
The Effect of an Intermediate Layer on the Frequency Characteristics of Ultrasonic Delay Lines—K. S. Aleksandrov, L. S. Gurovits, and E. I. Kamenskiĭ. (*Akust. Zh.*, vol. 6, no. 2, pp. 171–179; 1960.) General expressions are derived for the line conversion factor taking account of an intermediate layer between the transducer and the line. The effect of this layer on the frequency characteristics and transmission band is considered and the relevant characteristics of different transducer and layer materials are tabulated.

621.375.029.6:[621.385.6+621.382.23 1768
Amplification—Modern Trends, Techniques and Problems—Nergaard. (See 2044.)

621.375.432 1769
The Behaviour of a Nonlinear Transistor Amplifier in the Region of its Stability Limit—I. Gumowski. (*Compt. rend. Acad. Sci., Paris*, vol. 250, pp. 3142–3144; May 9, 1960.) An extension of earler work (4150 of 1960 and 801 of March) is discussed. The limit of stability of the amplifier is established from the form of the solution of a first-order differential equation describing the amplifier is given.

621.375.432 1770
Transistor Amplifiers with Feedback—E. R. Hauri. (*Tech. Mitt. PTT*, vol. 38, pp. 185–200 and 228–236; June 1, and July 1, 1960.) An analysis of the properties of transistor amplifiers using the *h* parameters is given. Feedback circuits with special characteristics are reviewed. Over 40 references.

621.375.9:537.311.33 1771
Semiconductor Amplifiers and Generators with Carriers having Negative Effective Mass—N. G. Basov, O. N. Krokhin, and Yu. M. Popov. (*Zh. Eksp. Teor. Fiz.*, vol. 38, pp. 1001–1002; March, 1960.) It is not possible to produce, in a semiconductor, states with negative losses by means of a constant electric field; it is necessary to have a state with negative temperature as achieved in molecular generators or using pulsed excitation by an electric field.

621.375.9:538.569.4 1772
Cross-Relaxation Masers—G. S. Bogle. (PROC. IRE, vol. 49, pp. 573–590; March, 1961.) The ways in which ruby, spinel, rutile and emerald can amplify at frequencies small compared with their zero-field splitting frequencies are surveyed. Cross-relaxation is shown to give a two-fold improvement in maser performance. Analytic expressions for the energies are given.

621.375.9:538.569.4 1773
Seesaw Maser Operation—P. A. Forrester and W. B. Mims. (*J. Appl. Phys.*, vol. 32, pp. 317–320; February, 1961.) "Cross relaxation between adjacent intervals may be used to secure an advantage in maser operation comparable to that obtained by 'push-pull' pumping. Equations for the rate of change of populations in a scheme of four levels (*A*, *B*, *C*, *D*) when *AC* is pumped and cross relaxation takes place between *BC*, *CD* have been formulated, and the steady-state condition corresponding to various assumptions regarding lattice relaxation times is discussed. In an experimental investigat on of maser operation based on this scheme and using ruby as the active material, an inversion of 0.9:1 was obtained at a signal frequency of 14.5 Gc/s when pumping at 24.5 Gc/s."

621.375.9:621.372.44 1774
Travelling-Wave Parametric-Amplifier Analysis using Difference Equations—H. Zucker. (PROC. IRE, vol. 49, pp. 591–598; March, 1961.) A second-order difference equation is derived for both periodically and uniformly distributed parametric amplifiers. Gain and voltage output are calculated. The results are specifically applied to an LC-distributed parametric amplifier.

621.375.9:621.372.44 1775
Effect of Upper Sidebands in Travelling-Wave Parametric Amplifiers—A. Dayem. (*Bull. schweiz. elektrotech. Ver.*, vol. 51, pp. 1054–1061; October 8, 1960. In English.) The effect of higher sidebands on paramagnetic amplification is investigated for circuits of limited bandwidth and infinite bandwidth [see *e.g.*, 3240 of 1959 (Roe and Boyd)].

621.375.9:621.372.44:523.164 1776
Theoretical Considerations regarding the Application of Parametric Amplifiers to Radio Telescopes—W. Druey and H. Rickenbach. (*Bull. schweiz. elektrotech. Ver.*, vol. 51, pp. 1061–1067; October 8, 1960.) The improvement of resolving power obtained by using one parametric amplifier immediately preceding the antenna and another as the preamplifier stage of the receiver is discussed.

621.375.9:621.372.44:523.164 1777
Parametric Amplifier for Space Probe Tracking—C. F. Brett. (*Electronics*, vol. 34, pp. 41–45; January 27, 1961.) A description of the parametric amplifier used with the Jodrell Bank Radio telescope for reception of the Pioneer V space probe signals from distances of over 22×10^6 miles is given. A description of a parametric-amplifier tester using transistors is included.

621.375.9:621.372.44:538.221 1778
Parametric Circuits at Low Frequencies using Ferrites and Thin Magnetic Films—A. Brändli. (*Bull. schweiz. elektrotech. Ver.*, vol. 51, pp. 1046–1053; October 8, 1960. In English.) The design of parametric circuits incorporating ferrite cores and films with nonlinear *B/H* characteristics is discussed. Films appear to be more suitable for operation at higher frequencies. An advantage of the use of ferrite and magnetic-film devices is their resistance to nuclear radiation.

621.375.9:621.372.44:621.385.3 1779
The Reactance Tube as a Parametric Frequency Divider and Amplifier—R. A. Elco and J. Nee. (PROC. IRE, vol. 49, pp. 624–625; March, 1961.) A derivation of the equivalent circuit of a parametric amplifier in which a reactance tube functions as a time-varying inductance is given. If the signal source is removed, the circuit will operate as a frequency divider, where the output is a subharmonic of the pump frequency.

621.375.9:621.372.44:621.385.63 1780
Energy Balance in a Parametric Electron-Beam Amplifier—Grau. (See 2046.)

621.375.9:621.372.44:621.385.63 1781
Coupled-Mode Theory of Electron-Beam Parametric Amplification—Gould and Johnson. (See 2047.)

621.375.9:621.372.44:621.385.63 1782
A Cyclotron Wave Amplifier with Magnetic Pumping—Robson. (See 2048.)

621.375.9.049.75:621.382.23 1783
Designing Tunnel-Diode R.F. Amplifiers—E. D. Long and C. P. Womack. (*Electronics*, vol. 34, pp. 120–123; February 17, 1961.) A strip-line filter and tunnel diode are combined to give low-noise amplification at UHF in a small module.

GENERAL PHYSICS

537.291 1784
Time-Averaged Effects on Charged Particles in A.C. Fields—T. W. Johnston. (*RCA*

Rev., vol. 21, pp. 570–610; December, 1960.) The basic theory is developed and applied to plasmas, including some cases with a dc magnetic field. A bibliography and a critique of theory and experiments are included.

537.32 1785
Transient Response of a Thermocouple Circuit under Steady Currents—A. D. Reich and J. R. Madigan. (*J. Appl. Phys.*, vol. 32, pp. 294–301; February, 1961.)

537.533 1786
Experimental Study of Anomalous Electron Stream Behavior—M. H. Miller and W. G. Dow. (*J. Appl. Phys.*, vol. 32, pp. 274–281; February, 1961.) Experimental measurements on the characteristics of the sole current in a rectilinear crossed-field beam are reported. The sole current may be assigned a kinetic temperature of the order of 10 v corresponding to energy in excess of that corresponding to motion in static fields. The energy exchange leading to this excess energy is believed to be associated with multiple-loop trajectories in the low-potential region near the cathode.

537.54:621.391.822 1787
Noise Generated in the Ion Sheath of a Probe—K. Shimada. (PROC. IRE, vol. 49, pp. 632–633; March, 1961.) The frequency-dependence of I_{eq}, the saturated diode current, is examined theoretically and results obtained are compared with measured values.

537.56 1788
The General Theory of the Motions of Ions and Electrons in Gases—L. G. H. Huxley. (*Aust. J. Phys.*, vol. 13, pp. 718–737; December, 1960.) The chief formulas for the drift velocities and diffusion coefficients of ions and electrons in gases are derived in general form by the application of dynamical principles.

537.56 1789
An Error in the Thermal Conductivity for a Fully Ionized Gas—R. W. Vaughan-Williams and F. A. Haas. (*Phys. Rev. Lett.*, vol. 6, pp. 165–166; February 15, 1961.) A discrepancy between formulas of Marshall and of Rosenbluth and Kaufmann (1703 of 1958) is due to an error in the last collision integral of Marshall.

537.56 1790
The Investigation of High-Frequency Plasmas by means of a D.C. Probe—H. Fetz and H. Oechsner. (*Z. angew. Phys.*, vol. 12, pp. 250–253; June, 1960.)

537.56 1791
Instability of Longitudinal Oscillations of an Electron-Ion Plasma—L. M. Kovrizhnykh and A. A. Rukhadze. (*Zh. Eksp. Teor. Fiz.*, vol. 38, pp. 850–853; March, 1960.) In an isotropic plasma the oscillations are always damped; in an anisotropic medium ion motion may lead to instability.

537.56:537.533 1792
Interaction of an Electron Beam with Plasma—I. F. Kharchenko, Ya. B. Faĭnberg, R. M. Nikolaev, E. A. Kornilov, E. A. Lutsenko, and N. S. Pedenko. (*Zh. Eksp. Teor. Fiz.*, vol. 38, pp. 685–692; March, 1960.) An experimental investigation of modulated and unmodulated beams of high-energy electrons with a high-frequency discharge plasma is reported. When an unmodulated beam moves through the plasma, oscillations are produced in the beam at frequencies close to the plasma frequency.

537.56:537.533 1793
Interaction of an Electron Beam with a Fully Ionized Plasma—M. A. Allen and G. S. Kino. (*Phys. Rev. Lett.*, vol. 6, pp. 163–165; February 15, 1961.) An electron beam, modulated at microwave frequency ω, passes through a thermal Cs plasma (critical frequency ω_p, cyclotron frequency ω_c). Gain in beam modulation amplitude is measured. Theory is outlined which predicts gain for $\omega_c^2<\omega^2<\omega_c^2+\omega_p^2$ with a maximum at $\omega=\omega_p$. Preliminary experiments agree with theoretical predictions. A measured gain >20 db at 3 Gc is reported.

538.24 1794
Magnetic Polarizability of a Short Right Circular Conducting Cylinder—T. T. Taylor. (*J. Res. NBS*, vol. 64B, pp. 199–210; October–December, 1960.) A comprehensive mathematical analysis using a method given earlier (488 of February) is described.

538.311:537.312.62 1795
Production of Magnetic Fields exceeding 15 Kilogauss by a Superconducting Solenoid—J. E. Kunzler, E. Buehler, F. S. L. Hsu, B. T. Matthias, and C. Wahl. (*J. Appl. Phys.*, vol. 32, pp. 325–326; February, 1961.) Experiments with Mo_3Re in wire form are described. Critical-field data are given.

538.561:539.124 1796
Cherenkov Radiation of a Particle Possessing a Charge and an Intrinsic Magnetic Moment—Li Men Kha (Li Meng-Ha). (*Zh. Eksp. Teor. Fiz.*, vol. 38, pp. 934–936; March, 1960.) An analysis, by quantum electrodynamic methods, of the effect of the spin on the intensity and polarization of the radiation produced in a ferrite by a charged particle with an intrinsic magnetic moment is given.

538.566+534.2 1797
Energy-Momentum Tensor for Plane Waves—P. A. Sturrock. (*Phys. Rev.*, vol. 121, pp. 18–19; January 1, 1961.) A general form is established for the energy momentum tensor for plane waves propagating in a homogeneous medium, the field equations of which are derivable from a quadratic Lagrangian function.

538.566+534.2 1798
Limit of Applicability of the Method of "Smooth" Perturbations in the Problem of Wave Propagation through a Medium with Inhomogeneities—V. V. Pisareva. (*Akust. Zh.*, vol. 6, no. 1, pp. 87–91; 1960.) Mean square values of the phase and amplitude fluctuations and of the amplitude correlation function are discussed. Conditions are determined under which the effect of the layer with inhomogeneities on the traversing radiation can be replaced by the perturbation action of an equivalent phase screen.

538.566:535.42]+534.26 1799
Diffraction of a Scalar Wave by a Slit and by a Circular Aperture in a Screen of Arbitrary Thickness—M. V. Butrov. (*Akust. Zh.*, vol. 6, no. 1, pp. 16–22; 1960.) An expression is derived for the transmission coefficient, and its variation as a function of screen thickness and aperture size is plotted.

538.566:535.42 1800
An Electromagnetic Diffraction Problem involving Unidirectionally Conducting Surfaces—R. A. Hurd. (*Canad. J. Phys.*, vol. 38, pp. 1229–1244; October, 1960.) The exact value of the EM field scattered by a unidirectionally conducting surface under plane wave excitation is obtained. The surface, which is an entire plane, is the junction of two unidirectionally conducting half-planes whose conductivity directions are inclined at an arbitrary angle to each other and to the boundary line.

538.566:535.42 1801
On the Theory of Diffraction by a Composite Cylinder—R. D. Kodis. (*J. Res. NBS*, vol. 65D, pp. 19–33; January/February, 1961.) General formulas are developed for the diffraction field around a perfectly conducting cylinder with a dielectric sleeve. These formulas represent the field due to a unit electric line source parallel to the cylinder. Limiting cases are examined.

538.566:537.56 1802
Gyro-resonance Absorption of Electromagnetic Waves in a Plasma—B. N. Gershman. (*Zh. Eksp. Teor. Fiz.*, vol. 38, pp. 912–924; March, 1960.) An earlier analysis (1476 of May) is extended to frequencies near the gyrofrequency and multiples of this, taking account of the thermal motion of electrons.

538.566.029.64:530.17:535.43 1803
Microwave Analogue to the Scattering of Light by Nonspherical Particles—J. M. Greenberg, N. E. Pedersen, and J. C. Pedersen. (*J. Appl. Phys.*, vol. 32, pp. 233–242; February, 1961.) Total scattering cross sections and angular distributions have been measured; some approximate theoretical methods appear to be useful. The results are referred to the effects of interstellar matter on starlight.

538.569.4:535.853 1804
Paramagnetic Resonance Spectroscopy at Zero Magnetic Field—G. S. Bogle, H. F. Symmons, V. R. Burgess, and J. V. Sierins. [*Proc. Phys. Soc.* (London), vol. 77, pp. 561–566; March 1, 1961.] Two spectrometers covering the range 8–18 Gc are described.

538.569.4:535.853:621.316.726 1805
Frequency Stabilization Scheme for the Pound-Watkins R.F. Spectrometer—J. Jeener. (*Rev. Sci. Instr.*, vol. 32, pp. 27–28; January, 1961.) "A scheme is described for locking the frequency of a marginal-oscillator r.f. spectrometer to that of an external standard. This makes it convenient to use such a spectrometer for high-resolution NMR work."

538.569.4:535.853:621.375.9 1806
Comparison of the Sensitivities of the Beam Maser and Cavity Absorption Spectrometers—Y. Beers. (*Rev. Sci. Instr.*, vol. 32, pp. 23–27; Januray, 1961.) A formula is derived for the SNR of the beam maser considering it as a special case of cavity spectrometer. The sensitivity of the maser relative to the spectrometer varies inversely with the frequency.

538.569.4:538.221 1807
Restoration of Stability in Ferromagnetic Resonance—H. Suhl. (*Phys. Rev. Lett.*, vol. 6, pp. 174–176; February 15, 1961.) The threshold RF power for subsidiary absorption can be increased by a small ac modulation of the dc magnetic field.

538.569.4:621.373.421.1 1808
High Level Oscillator for Nuclear Resonance—W. D. Knight. (*Rev. Sci. Instr.*, vol. 32, p. 95; January, 1961.) A modification of the cathode-coupled circuit [see *e.g.*, 1972 of 1960 (Robinson)] which functions at RF levels in the range 1–10 v rms is given.

538.569.4:621.375.9:535.61-1/2 1809
Theory of LASER Oscillation in Fabry-Perot Resonators—J. Kotik and M. C. Newstein. (*J. Appl. Phys.*, vol. 32, pp. 178–186; February, 1961.) An approximate condition for oscillation is derived.

538.569.4:621.375.9:535.61-2 1810
Stimulated Optical Emission from Exchange-Coupled Ions of Cr^{+++} in Al_2O_3—I. Wieder and L. R. Sarles. (*Phys. Rev. Lett.*, vol. 6, pp. 95–96; February 1, 1961.)

538.569.4:621.375.9:535.61-2 1811
Simultaneous Optical Maser Action in Two Ruby Satellite Lines—A. L. Schawlow and G. E. Devlin. (*Phys. Rev. Lett.*, vol. 6, pp. 96–

98; February 1, 1961.) Maser oscillations have been obtained simultaneously at wavelengths of 7,009 Å and 7,041 Å in concentrated ruby.

538.569.4:621.375.9:535.61-2 1812
Population Inversion and Continuous Optical Maser Oscillation in a Gas Discharge containing a He-Ne Mixture—A. Javan, W. R. Bennett, Jr., and D. R. Herriott. (*Phys. Rev. Lett.*, vol. 6, pp. 106–110; February 1, 1961.) Experimental data on the physical properties of the system are discussed.

538.569.4.029.64/.65:546.217 1813
Radio Wave Absorption of Several Gases is the 100 to 117 kMc/s Frequency Range— C. O. Britt, C. W. Tolbert, and A. W. Straiton. (*J. Res. NBS*, vol. 65D, pp. 15–18; January/February, 1961.) An extension of earlier work [2699 of 1960 (Straiton and Tolbert)] to the gases CO, N_2O, SO_2 and NO_2 is given. The gases were contained within a $6\frac{1}{8}$-inch-diameter tube up to 500 feet long, and a wide pressure range was used.

538.569.4.029.65:535.223 1814
Precise Measurement of the Microwave Absorption Frequencies of the Oxygen Molecule and the Velocity of Light—R. W. Zimmerer and M. Mizushima. (*Phys. Rev.*, vol. 121, pp. 152–155; January 1, 1961.) "Ten microwave absorption frequencies of the oxygen molecule in the 60-Gc/s region have been measured with an accuracy of about 10 kc/s. The result is interpreted by successfully refining the existing theory. Comparing the resultant value of the rotational constant B_0 with the value obtained in ultraviolet spectra, the velocity of light is calculated to be 299,773 ±12 km/s."

GEOPHYSICAL AND EXTRATERRESTRIAL PHENOMENA

523.164 1815
A Catalogue of Radio Sources between Declinations −20° and −50°—B. Y. Mills, O. B. Slee, and E. R. Hill. (*Aust. J. Phys.*, vol. 13, pp. 676–699; December, 1960.) This list of 892 sources supplements a previous catalogue for declinations between +10° and −20° (423 of 1959). Angular sizes of 50 of the strongest sources are given, several of these being less than 15-seconds arc in size.

523.164:621.396.62 1816
A 75-cm Receiver for Radio Astronomy and some Observational Results—C. L. Seeger, F. L. H. M. Stumpers, and N. van Hurck. (*Philips Tech. Rev.*, vol. 21, pp. 317–333; September 27, 1960.) A description is given of a superheterodyne receiver in which the HF amplifier contains two disk-seal triode tubes in cascode, the effective cathode resistance of the second tube being made very high by a simple neutralization circuit. A noise factor of 2.5 has been obtained at 400 Mc. Radio-astronomy observations are described which have been made with this receiver and the 25-m parabolic reflector at Dwingeloo. An isophot chart of the sky drawn from these observations is reproduced.

523.164:621.396.677 1817
An Interferometer for the Measurement of Radio-Source Sizes—B. R. Goddard, A. Watkinson, and B. Y. Mills. (*Aust. J. Phys.*, vol. 13, pp. 665–675; December, 1960.) The 85.5-Mc cross-type radio telescope at Sydney [1126*g* of 1958 (Mills, *et al.*)] has been modified to study sources in the range 100 seconds–1 minute arc. The instrument and its operation are described.

523.164:621.396.677.5/.6 1818
Direction-Finding on Diffuse Sources of Electromagnetic Radiation—D. G. Cartwright. (*Aust. J. Phys.*, vol. 13, pp. 712–717; December, 1960.) By combining the characteristics of an Adcock type and rotating-loop type of direction-finder the position and size of an extended source can be determined.

523.164.3 1819
An Attempt to Detect Linear Polarization in the Galactic Background Radiation at 215 Mc/s—J. L. Pawsey and E. Harting. (*Aust. J. Phys.*, vol. 13, pp. 740–742; December, 1960.) Observations of a strip of sky about declination 34°S set an upper limit of 1 per cent to the degree of linear polarization for bandwidths of 1 Mc, 700 and 300 kc.

523.164.32 1820
Recent Developments in Solar Radio Astronomy—A. Maxwell. (*Proc. Natl. Acad. Sciences*, vol. 46, pp. 1260–1269; September, 1960.) A review with 24 references is given.

523.164.32 1821
The Radio Brightness of the Quiet Sun at 21 cm Wavelength near Sunspot Maximum—N. R. Labrum. (*Aust. J. Phys.*, vol. 13, pp. 700–711; December, 1960.) The quiet-sun temperature, measured using pencil-beam and fan-beam techniques, is approximately 140,000°K. This value is twice that for the same wavelength at sunspot minimum.

523.164.32:523.75 1822
Investigation of the Relative Positions of Solar Radio Storm Sources and of Associated Optical Centres of Activity—É. J. Blum and A. M. Malinge. (*Compt. rend. Acad. Sci., Paris*, vol. 250, pp. 3119–3121; May 9, 1960.) A comparison has been made between the mean positions of radio storm centers observed on 169 Mc and optically observed sunspots. Results show a systematic difference between the apparent and true positions of the former and, for more intense storm centers, a directivity effect with latitude.

523.164.32:550.385.4 1823
Solar Radio Emissions and Geophysical Disturbances during July 1959—M. P. Hughes. (*J. Geophys. Res.*, vol. 66, pp. 651–653; February, 1961.)

523.164.4 1824
Cosmological Significance of Angular Measurements of Distant Radio Sources—W. Davidson. (*Nature*, vol. 189, pp. 991–992; March 25, 1961.)

523.165 1825
Solar-Produced Cosmic Rays near the North and South Poles—M. A. Pomerantz, S. P. Duggal, and K. Nagashima. (*Phys. Rev. Lett.*, vol. 6, pp. 123–125; February 1, 1961.) Results of ground observations during the storms of November 12th and 15th, 1960, are presented.

523.165 1826
X Rays from Van Allen Belt Electrons—J. B. Cladis and A. J. Dessler. (*J. Geophys. Res.*, vol. 66, pp. 343–350; February, 1961.) It ought to be possible to detect the X-ray flux, at peak intensity, above the cosmic radiation background at balloon altitudes.

523.165 1827
Electrons in the Primary Cosmic Radiation—P. Meyer and R. Vogt. (*Phys. Rev. Lett.*, vol. 6, pp. 193–196; February 15, 1961.) Extraterrestrial electrons with energies in the range 25–1300 Mev and greater have been observed on three balloon flights.

523.165 1828
Charged Particles in the Inner Van Allen Radiation Belt—A. H. Armstrong, F. B. Harrison, H. H. Heckman and L. Rosen. (*J. Geophys. Res.*, vol. 66, pp. 351–357; February, 1961.) Results are given for the flight through the inner Van Allen belt of emulsion stacks carried in an Atlas rocket. The measured proton energy spectrum was in accord with a cosmic ray albedo source down to 100 Mev. However, below 100 Mev the spectrum exhibits structure with a maximum at 80 Mev and a minimum at 60 Mev. Penetration of solar protons into the belt over a period of days can explain the effect.

523.165:539.16 1829
Hydromagnetic Waves and the Trapped Radiation: Parts 1 & 2—D. G. Wentzel. (*J. Geophys. Res.*, vol. 66, pp. 359–369; February, 1961.) A theoretical discussion and comments on the results of the Argus experiment are given.

523.746.5 1830
An Estimate of the Peak Sunspot Number in 1968—C. M. Minnis. (*J. Atmos. Terr. Phys.*, vol. 20, pp. 94–99; March, 1961.) A detailed analysis was made of the statistical properties of the twenty peaks in the sunspot cycle since 1761, the results of which were given earlier (2341 of 1960).

523.75:523.164.32 1831
Unusual Solar Disturbance—(*Tech. News Bull. NBS*, vol. 44, pp. 138–139; August, 1960.) No solar flare could be observed at the time of a radio disturbance of importance 3+ at 1638 U.T. on June 9, 1959. The flare became observable after a delay of $1\frac{1}{2}$ hours. This and other anomalies are discussed in relation to two assumptions concerning the flare: a) that it occurred on the far side of the sun, b) that it originated at a lower level in the sun's atmosphere than the source of RF emissions.

550.385.37 1832
Geomagnetic Micropulsations—G. R. A. Ellis. (*Aust. J. Phys.*, vol. 13, pp. 625–632; December, 1960.) Simultaneous observations of geomagnetic pulsations at geomagnetic latitudes 28°S, 42°S and 51°S showed no change in period with latitude, but a monotonic increase in amplitude with latitude for periods between 10 and 100 sec. The interpretation of these results is discussed.

550.385.4 1833
The Simultaneity of Geomagnetic Sudden Impulses—M. Yamamoto and H. Maeda. (*J. Atmos. Terr. Phys.*, vol. 20, pp. 212–215; March, 1961.) An analysis of several events during the I.G.Y. shows that sudden impulses are propagated from high latitudes to low latitudes in times of about 1 minute.

551.507.362.2 1834
The Theory of Artificial Satellites in Terms of the Orbital True Longitude—P. Musen. (*J. Geophys. Res.*, vol. 66, pp. 403–409; February, 1961.) Previous theory (1589 of 1960) has been developed in terms of orbital true longitude and leads to faster convergence for large eccentricities and to a smaller number of terms in the series representing the perturbations.

551.507.362.2:621.391.812.3 1835
On the Large-Scale Regions of Irregularities Producing Scintillation of Signals Transmitted from Earth Satellites—J. Frihagen and J. Tröim. (*J. Atmos. Terr. Phys.*, vol. 20, pp. 215–216; March, 1961.) Evidence is presented which indicates that absence of scintillation is not due primarily to high aspect sensitivity scattering from field-aligned irregularities.

551.507.362.2:621.391.812.3 1836
Ionospheric Scattering of Satellite Transmissions—J. Maudsley and I. R. Richards. (*Nature*, vol. 189, pp. 906–907; March 18, 1961.) Reports of observations of nighttime scintillations of satellite transmissions are briefly analyzed in relation to the position of the observing station and the direction of pas-

sage of the satellite. Results demonstrate the ability of field-aligned irregularities to scatter m-λ radio waves in a manner highly sensitive to aspect. See also 1160 of April (Bain).

551.507.362.2:621.391.812.34 1837
Observed Field Strength in the Neighbourhood of the Skip Distance—K. C. Yeh and G. W. Swenson, Jr. (*J. Geophys. Res.*, vol. 66, pp. 654–656; February, 1961.) Examples of ray focusing due to the satellite 1958 δ_2 crossing the skip-distance boundary are given. The skip distance agrees well with values derived from ionograms.

551.510.535 1838
Ion-Neutral Reactions—M. Hertzberg. (*J. Atmos. Terr. Phys.*, vol. 20, pp. 177–182; March, 1961.) A list is given of reactions which may control the chemical composition of positive ions in the ionosphere. Under certain assumptions about reaction rate coefficients, nitrogen is substantially dissociated in the F region, contrary to the theoretical conclusions of other investigators.

551.510.535 1839
A Preliminary Model for the Variations of Upper Air Densities—H. K. Paetzold. (*Nature*, vol. 190, pp. 35–36; April 1, 1961.) A model is proposed covering variations of density with a period greater than one day.

551.510.535 1840
The Highest Parts of the Ionosphere—J. A. Ratcliffe. (*Quart. J. R. Met. Soc.*, vol. 85, pp. 321–331; October, 1959.) The text is given of the Symons Memorial Lecture, 1959, reviewing current theories concerning the formation and structure of the ionosphere above 150 km.

551.510.535 1841
Incoherent Scattering by Free Electrons as a Technique for Studying the Ionosphere and Exosphere: some Observations and Theoretical Considerations—K. L. Bowles. (*J. Res. NBS*, vol. 65D, pp. 1–14; January/February, 1961.) Observations confirm the existence of the incoherent scatter at predicted levels but indicate less Doppler broadening than expected, for which an explanation is offered.

551.510.535 1842
A Possibility for Determining the Existence of a Permanent Form of Magnetic Field-Aligned Ionization Irregularities—R. L. Leadabrand. (PROC. IRE, vol. 49, pp. 639–640; March, 1961.) Incoherent scatter from a direction perpendicular to the earth's magnetic field is discussed.

551.510.535 1843
Internal Atmospheric Gravity Waves at Ionospheric Heights—C. O. Hines. (*Canad. J. Phys.*, vol. 38, pp. 1441–1481; November, 1960.) Irregularities and irregular motions observed in the upper atmosphere are interpreted in terms of a spectrum of waves propagated upwards and modified to produce different dominant modes at different heights.

551.510.535 1844
Vertical Characteristics of Travelling Ionospheric Disturbances—L. H. Heisler. (*Aust. J. Phys.*, vol. 13, pp. 655–664; December, 1960.) A comparison between the occurrence of disturbances on fixed-frequency records and $N(h)$ profiles for the same period reveals that a) there appears to be an upper-limiting height for the occurrence of disturbances on fixed frequency, and b) the direction of travel of disturbances is related to season only and seems unrelated to height in the ionosphere.

551.510.535 1845
The Analysis of Night-Time $h'(f)$ Records—J. Titheridge. (*J. Atmos. Terr. Phys.*, vol. 20, pp. 209–212; March, 1961.) A correction of electron density profiles for errors due to underlying ionization, by the use of the extraordinary ray, is given.

551.510.535 1846
Theoretical World Curves of Maximum F_2 Ionization: Part 2—J. E. C. Gliddon and P. C. Kendall. (*J. Atmos. Terr. Phys.*, vol. 20, pp. 183–188; March, 1961.) A time-dependent solution of the continuity equation, including vertical diffusion of ionization, is used to obtain a theoretical variation of maximum F_2-layer electron density with latitude and local time. Some similarity to experimental data is found, but the equatorial "trough" does not occur in the theoretical solution. See also 2738 of 1960.

551.510.535 1847
On the Influence of Horizontal Motion of the Neutral Air on the Diffusion Equation of the F Region—J. P. Dougherty. (*J. Atmos. Terr. Phys.*, vol. 20, pp. 167–176; March, 1961.) The equations of motion of a plasma in applied fields are discussed with reference to the F region. The plasma sets the neutral air into motion horizontally within about $\frac{1}{2}$ h, but is not free to move vertically. The consequences of this result, on a worldwide scale, are discussed.

551.510.535:550.385.36 1848
Movements of the F Layer of the Ionosphere during Geomagnetic Bay Disturbances—H. Kohl. (*Arch. elekt. Übertragung*, vol. 14, pp. 169–176; April, 1960.) The vertical movement of the F layer during and after geomagnetic disturbances is evaluated from ionospheric soundings made at Lindau, Germany. The movement is treated theoretically on the basis of the plasma theory developed by Lucas and Schlüter (2085 of 1954), and to account for the rise of the layer use is made of Martyn's theory allowing for the influence of the neutral gas. By comparing calculated and measured data, estimates of conductivity and neutral-gas density in the ionosphere can be made.

551.510.535:550.385.4 1849
The Occurrence of the Spread F and the Geomagnetic Field—T. Shimazaki. (*J. Radio Res. Labs., Japan*, vol. 7, pp. 437–450; September, 1960.) Spread-F is more probable in days after a sudden commencement at high latitudes, and less probable at low altitudes, especially at the equinoctial seasons. There is a strong correlation between the magnitude of the geomagnetic field and the occurrence of spread-F at low latitudes; a turbulence mechanism is suggested to explain this.

551.510.535:551.507.362.1 1850
Measurement of Positive-Ion Density in the Ionosphere by Sounding Rocket—T. Ichimiya, K. Takayama, T. Dote, Y. Aono, K. Hirao, S. Miyazaki, T. Sugiyama, and T. Muraoka. (*Nature*, vol. 190, pp. 156–158; April, 1961.) Preliminary results are given of measurements made over the Akita Rocket Range, Japan, in September, 1960. Two rockets were launched, one during the daytime and one at night, each equipped with a spherical Langmuir probe. Ascent and descent records for each flight show close agreement and the values of electron density scaled from $h'(f)$ records agree fairly well with those obtained from rocket measurements.

551.510.535:621.3.087.4 1851
Vertical Incident Doppler Ionogram—T. Ogawa, S. Ando, and A. Yoshida. (PROC. IRE, vol. 49, p. 643; March, 1961.) An improved apparatus has been constructed for the measurement of Doppler shifts produced by vertical movements of the ionosphere.

551.510.535:621.3.087.4 1852
Contribution to an Investigation of Ionospheric Absorption on a Fixed Frequency—G. Pillet. (*Ann. Télécommun.*, vol. 15, pp. 157–184 and 198–219; July/August and September/October, 1960.) A thesis, concerning theoretical and experimental aspects of ionospheric absorption measurements by vertical-incidence sounding is given. Measurements made on a frequency of 3.4 Mc during the period September, 1955–March, 1958, are analyzed. 74 references.

551.510.535:621.391.812.63 1853
Determination of the Ionospheric Absorption from Recordings of Field Strength and Cosmic Noise—H. Schwentek. (*Arch. tech. Messen*, no. 296, pp. 177–180; September, 1960.) Brief descriptions are given of a method of determining the ionospheric absorption index from oblique incidence recordings (see also 2732 of 1959), and of the riometer method using extraterrestrial noise sources [1566 of 1959 (Little and Leinbach)].

551.510.535(98):621.391.812.631 1854
Statistical Study on the Occurrence of Polar Blackouts—I. Kasuya. (*J. Radio Res. Labs., Japan*, vol. 7, pp. 451–465; September, 1960.) The distributions of radio blackouts in both hemispheres are examined using $f_{\min}$ data at 31 stations in the north and 12 stations in the south. The changes of blackout occurrence and times of maximum occurrence frequency with position are studied.

551.510.536 1855
A Theoretical Model of Electron Density Distribution along a Geomagnetic Line of Force in the Exosphere—R. L. Dowden. (*J. Atmos. Terr. Phys.*, vol. 20, pp. 122–130; March, 1961.) A model of electron density in the exosphere is set up by supposing electrons to diffuse along tubes of force. Electron densities in ionosphere and exosphere are related by steady-state solutions. The particle source is in the ionosphere under normal conditions, but during the magnetic storm particles are injected into a tube of force at its furthest point from earth. The role of collisions is discussed.

551.594.5:621.396.96 1856
A Note on the Disposition of Daytime Auroral Ionization in Space—R. L. Leadabrand. (*J. Geophys. Res.*, vol. 66, pp. 421–428; February, 1961.) Radio auroras are classified into two groups according to latitude spread. The properties are compared and their relation to "diffuse" and "discrete" auroras is discussed.

551.594.5:621.396.96 1857
The Slant E_s Echo—a High-Frequency Auroral Echo—H. F. Bates. (*J. Geophys. Res.*, vol. 66, pp. 447–454; February, 1961.) The slant E_s echo is associated with VHF auroral echoes. It is formed by scattering from randomly distributed field-aligned irregularities and is enhanced by least-time focusing and aspect focusing.

551.594.5:621.396.96 1858
Temporal Variations of Auroral Radio-Echo Activity in Subauroral Latitudes—C. D. Watkins. (*J. Atmos. Terr. Phys.*, vol. 20, pp. 140–148; March, 1961.) The diurnal, 27-day, seasonal and 11-year variations in the occurrence of radio auroras are investigated and also the time delay between class-3 flares and the appearance of auroras is measured. The bimodal diurnal distribution may be a consequence of the specular reflection properties of the auroral echoes.

551.594.5:621.396.96:550.386 1859
Auroral Radio Echoes and Magnetic Disturbances—C. D. Watkins. (*J. Atmos. Terr. Phys.*, vol. 20, pp. 131–139; March, 1961.) The occurrence of radio echoes from aurora is strongly correlated with local K-index. The position and motion of individual echo regions

correspond closely with the current systems causing magnetic disturbances.

551.507.362:061.3 1860
Space Research [Book Review]—H. Kallman Bijl, Ed., Interscience Publishers, Inc., New York, N. Y., 1195 pp., 1960, $24.00. (*J. Atmos. Terr. Phys.*, vol. 20, p. 222; March, 1961.) It contains the text, mainly in English, of the scientific papers presented at the First Internatl. Space Science Symp., Nice, France, January, 1960.

551.510.535(084) 1861
An Atlas of Oblique-Incidence Ionograms [Book Review]—V. Agy, K. Davies, and R. Salaman. U. S. Department of Commerce, Washington, D. C., $2.25. (*J. Res. NBS.*, vol. 65D, pp. 35–36; January/February, 1961.) The atlas is published as NBS Technical Note No. 31 (1959) and contains routine records for the paths: a) Washington–St. Louis, b) Washington–Boulder. A discussion of equipment is given, and seasonal variation, layer formation and disappearance, spread echo, MUF extension and other phenomena are illustrated.

LOCATION AND AIDS TO NAVIGATION

621.396.933 1862
A New Assessment of the Gee System—D. H. R. Archer. (*Brit. Commun. Electronics*, vol. 8, pp. 272–275; April, 1961.) Possible applications of the Gee System to long-range navigation and as a basis for a navigation system for areas where the air traffic is dense are discussed in general terms.

621.396.944 1863
Reception and Direction Finding of Electromagnetic Waves in Sea-Water—G. Ziehm. (*Telefunken Ztg.*, vol. 33, pp. 141–150; June, 1960. English summary, pp. 158–159.) VLF wave propagation in sea-water and the limits set to reception by atmospherics and receiver noise at various depths of submersion are discussed. Formulas are derived for the depths at which reception or direction finding is possible, and maximum depths are calculated as a function of transmitter-receiver distance for given transmitter and receiver characteristics.

621.396.96 1864
Radar Picture Transmission—(*Telefunken Ztg.*, vol. 32, pp. 152–181; September, 1959.) English summaries, pp. 208–210.) The following three papers deal with underlying theory including bandwidth compression and the principles of storage-tube design; four such storage tubes are described and details are given of an experimental system.

1) **Principles and Fundamental Problems**—F. Schröter, pp. 152–161.

2) **Storage Tubes**—J. E. Otto and W. Schaffernicht, pp. 162–173.

3) **Frequency-Band Compression of Radar Signals by means of a Line Storage Tube with Circular Deflection of the Electron Beam**—K. Dinter, pp. 174–181.

621.396.96 1865
Technique for Amplitude Modulating a Van Atta Radar Reflector—L. H. Bauer. (Proc. IRE, vol. 49, pp. 634–635; March, 1961.) By introducing phase shifts in the interconnecting lines of a Van Atta array, the radar return can be modulated in amplitude electronically.

621.396.963.3 1866
Combining Remote Radars on a Central Display—G. E. Martin. (*Electronics*, vol. 34, pp. 124–125; February 17, 1961.) Each radar is represented by its own separate sweep on the combined PPI display.

621.396.963.3:621.385.832 1867
Practical Tubes for Bright Radar Displays—Veith. (See 2054.)

621.396.969.3 1868
Techniques and Problems of Tracking Radar—A. F. Braun. (*Bull. schweiz. elektrotech. Ver.*, vol. 51, pp. 689–700; July 16, 1960.) The operating principles of various types of radar are summarized. Problems relating to system and equipment design and to operation under various conditions are discussed.

621.396.969.3 1869
Automatic Beacon Radar Identifies Aircraft—W. L. Woodson. (*Electronics*, vol. 34, pp. 57–61; February 10, 1961.) An automatic aircraft interrogation system using airborne transponders is described.

621.396.969.3 1870
A Radar Observation of a Sea-Breeze Front—E. Eastwood and G. C. Rider. (*Nature*, vol. 189, pp. 978–980; March 25, 1961.) The length and penetration inland of a sea-breeze front have been studied using a 23-cm radar and a photographic time-compression technique. It is probable that both birds and refractive discontinuities contributed to mark the passage of the front.

MATERIALS AND SUBSIDIARY TECHNIQUES

535.215:537.311.33 1871
Determination of Recombination Constants from the Spectral Characteristic of a Photocell with a *p-n* Junction—V. K. Subashiev. (*Fiz. Tverdogo Tela*, vol. 2, pp. 205–212; February, 1960.)

535.215:546.4'682'221 1872
Photoconductivity in Ternary Sulphides—J. A. Beun, R. Nitsche and M. Lichtensteiger. (*Physica*, vol. 26, pp. 647–649; August, 1960.) Measurements on $ZnInS_4$, $CdIn_2S_4$ and $HgInS_4$ are reported.

535.215:546.47'221 1873
The Photovoltaic Effect in Striated ZnS Single Crystals—W. J. Merz. (*Helv. Phys. Acta*, vol. 31, pp. 625–635; October 31, 1958.) The photovoltaic effect was investigated as a function of wavelength, light intensity and temperature. A band model is proposed which provides a qualitative explanation of experimental results.

535.215:546.48'221 1874
Processes Prior to Electrical Breakdown in CdS Sing e Crystals—K. W. Böer and U. Kummel. (*Z. angew. Phys.*, vol. 12, pp. 241–244; June, 1960.) The various stages of breakdown due to thermal effects and high field strengths are discussed and illustrated by photographs obtained with the aid of electro-optical techniques [1636 of 1960 (Böer, *et al.*)].

535.215:546.48'221 1875
A Contribution to the Clarification of the Spectral Distribution of the Photoconductivity CdS Single Crystals—H. Berger, H. W. Böer, and E. H. Weber. (*Mber. dtsch. Akad. Wiss. Berlin*, vol. 2, no. 2, pp. 95–101; 1960.) An interpretation is given of the results of photoconductivity measurements in the region of the absorption edge at room temperature, in which three maxima are usually obtained. See also 1904 of 1959 (Böer and Gutjahr).

535.215:546.48'221 1876
Anomalous Photovoltaic Effect of CdS Single Crystals—S. Ibuki, H. Komiya and H. Yamashita. (*J. Phys. Soc. Japan*, vol. 15, p. 2356; December, 1960.) Photo-voltaic effects observed in a CdS crystal partly coated with an evaporated Cu layer are explained as a combination of *p-n* junction action and electron diffusion.

535.215:546.48'221:539.23 1877
Effect of Oxygen upon Sintered Cadmium Sulphide Photoconducting Films—S. Kitamura. (*J. Phys. Soc. Japan*, vol. 15, pp. 2343–2350; December, 1960.)

535.215:546.682'86 1878
Photosensitivity Spectrum Distribution of *p*-Type Indium Antimonide—D. N. Nasledov, M. P. Pronina and Yu. S. Smetannikova. (*Fiz. Tverdogo Tela*, vol. 2, pp. 239–241; February, 1960.) A note of measurements of photoconductivity and photomagnetic effect in *p*-type samples with acceptor concentrations from 10^{13} to $10^{15}/cm^3$ is given.

535.215:546.817'221 1879
On the Temperature Dependence of the Photoconductive Decay Time of Films of the Lead Salts—F. M. Klaassen, J. Blok, H. C. Booy, and F. J. De Hoog. (*Physica*, vol. 26, pp. 623–628; August, 1960.) A comparison of theory with results of measurements on PbS photodetectors indicates that minority carriers are retrapped repeatedly before recombination occurs.

535.37:537.311.3 1880
The Relation between the Recombination Luminescence and Conductivity under Non-isothermal Conditions—K. K. Rebane. (*Fiz. Tverdogo Tela*, vol. 2, pp. 273–274; February, 1960.)

535.37:546.47'221 1881
Electronic Structure of the Centres in ZnS—J. L. Birman. (*Phys. Rev.*, vol. 121, pp. 144–145; January 1, 1961.)

535.37:546.47'221 1882
Vapour-Phase Growth and Properties of Zinc Sulphide Single Crystals—H. Samelson. (*J. Appl. Phys.*, vol. 32, pp. 309–317; February, 1961.)

535.376 1883
Surface Recombination and Diffusion Processes in Cathodoluminescence and Electron-Bombardment-Induced Conductivity—G. Gergely. (*J. Phys. Chem. Solids*, vol. 17, pp. 112–116; December, 1960.) Values of diffusion length and surface recombination velocity are obtained from an analysis of experimental brightness/voltage curves.

535.376:546.47'221 1884
Electroluminescence of Zinc Sulphide Single Crystals—I. T. Steinberger, V. Bar, and E. Alexander. (*Phys. Rev.*, vol. 121, pp. 118–124; January 1, 1961.) Rectangular voltage pulses were applied to single crystals of ZnS. During the ON period the emission gradually increased to a stationary level. Removal of the voltage resulted in a burst of emission which decayed slowly. A model is suggested which explains this behavior.

535.376:546.48'221 1885
Electroluminescence of CdS Single Crystal—H. Yamashita, S. Ibuki, M. Yoshizawa, and H. Komiya. (*J. Phys. Soc. Japan*, vol. 15, p. 2366; December, 1960.) A description and possible explanation of electroluminescence observations is given.

535.376:546.681'18 1886
Electroluminescence of Gallium Phosphide Crystals—F. G. Ullman. (*Nature*, vol. 190, pp. 161–162; April 8, 1961.) Results obtained with crystals of GaP weakly doped with Zn corroborate the observations of Wolff, *et al.* (1433 of 1956).

537.227 1887
Thermal Conduction in Ferroelectric Ceramics—I. Yoshida. (*J. Phys. Soc. Japan.*, pp. 2211–2219; December, 1960.) Measurements on Pb, Ba, and Sr titanates and on Pb zirconate are described and discussed in relation to crystal structure.

537.227:546.431'824–31 1888
On the Origin of Barkhausen Pulses in BaTiO.—R. C. Miller. (*J. Phys. Chem. Solids*, vol. 17, pp. 93–100; December, 1960.) The domain phenomena which give rise to ferroelectric Barkhausen pulses in $BaTiO_3$ have been investigated experimentally: specific domain phenomena have been correlated with particular Barkhausen pulse shapes.

537.227:621.318.57 1889
The Reversal of the Spontaneous Polarization in Guanidine Aluminium Sulphate Hexahydrate—E. Fatuzzo. (*Helv. Phys. Acta*, vol. 33, pp. 429–436; August 15, 1960.) Crystals have been subjected to electrical and thermal treatment and their switching properties studied under different conditions. These properties may, with some additional assumptions, be described by the model developed by Fatuzzo and Merz (1267 of 1960) for triglycine sulphate. At high electric fields the domain-wall motion time is longer than the nucleation time and hence controls the switching process.

537.311.3:538.21 1890
The Relation between Magnetism and Electrical Conductivity of Compounds with Transition Elements—F. Hulliger. (*Helv. Phys. Acta*, vol. 32, pp. 615–654; December 31, 1959. In German.) A detailed review and discussion are given of theoretical and experimental results. Over 100 references.

537.311.31:538.63 1891
Transverse-Even Voltage: a High-Field Galvanomagnetic Effect associated with Open Orbits in Metals—J. R. Klauder and J. E. Kunzler. (*Phys. Rev. Lett.*, vol. 6, pp. 179–182; February 15, 1961.) The shape of the Fermi surface and the open orbit directions can be determined by measurements in single-copper crystals of even voltages transverse to the current when H is also transverse.

537.311.33+535.215 1892
Carrier Density Fluctuations in Semiconductors and Photoconductors with One Kind of Trapping Centres—F. M. Klaassen, K. M. Van Vliet, and J. Blok. (*Physica*, vol. 26, pp. 605–617; August, 1960.) Expresssions for the matrix elements of carrier density fluctuations and for relaxation times are given.

537.311.33 1893
Volume-Controlled, Two-Carrier Currents in Solids: the Injected Plasma Case—M. A. Lampert and A. Rose. (*Phys. Rev.*, vol. 121, pp. 26–37; January 1, 1961.) Double injection into semiconductors and insulators is studied under conditions where the injected electrons and holes are free. The current is field-driven and volume-controlled. The analysis shows an extended voltage region following the Ohm's law region, over which the current is proportional to the voltage squared. In this region the current is depressed through the increase in the number of minority carriers in thermal equilibrium. This is shown to result from recombination kinetics.

537.311.33 1894
Hydrogen-Like Impurity States in Axially Symmetric Crystals—R. W. Keyes. (*IBM J. Res. & Dev.*, vol. 5, pp. 65–66; January, 1961.)

537.311.33 1895
Influence of Interelectronic Collision on Hall Mobility in Nonpolar Semiconductors—Y. Uchiyama. (*Progr. Theor. Phys.*, vol. 24, pp. 455–456; August, 1960.) The correction due to the interelectronic collision is found to be very small in magnitude.

537.311.33 1896
Structure of the Energy Bands in Semiconductors of the $CdIn_2Se_4$ Type—A. I. Gubanov and F. M. Gashimzade. (*Fiz. Tverdogo Tela*, vol. 2, pp. 255–260; February, 1960.)

537.311.33 1897
Semiconduction in $Li_xNi_{(1-x)}O$—S. van Houten. (*J. Phys. Chem. Solids*, vol. 17, pp. 7–17; December, 1960.) NiO is an insulator which may be made conducting by the addition of LiO. An energy level scheme which explains this behavior is discussed.

537.311.33 1898
Current/Voltage Characteristics of Forward-Biased Long *p-i-n* Structures—R. D. Larrabee. (*Phys. Rev.*, vol. 121, pp. 37–39; January 1, 1961.) The characteristics have been observed in several Ge *p-i-n* structures in which the *n* side was biased negatively and the *p* side positively so as to cause a double injection of electrons and holes.

537.311.33:53.082.7 1899
Thermoelectrically Cooled Probe for the Determination of Semiconductor Type—R. V. Jeanes and K. E. G. Pitt. (*J. Sci. Instr.*, vol. 38, p. 33; January, 1961). A simple Bi_2Te_3 cold-probe device is described for the determination of semiconductor type in a near-intrinsic Ge sample. Because the probe is at a lower temperature than the sample there is no risk of heat transfer and subsequent type inversion typical of the hot-probe method.

537.311.33:535.215 1900
Bulk Photoeffects in Inhomogeneous Semiconductors—C. D. Cox. (*Canad. J. Phys.*, vol. 38, pp. 1328–1342; October, 1960.) Theoretical expressions are derived for the relation between photo-EMF and illumination, and between photo-EMF and resistance decrease. Experimental results for Ge filaments are given.

537.311.33:537.312.9 1901
Effect of High Pressure on Electrical Properties of NiO, CoO, CuO and Cu_2O—A. P. Young, W. B. Wilson, and C. M. Schwartz. (*Phys. Rev.*, vol. 121, pp. 77–82; January 1, 1961.)

537.311.33:537.32 1902
Thermoelectric Behaviour of *p-n* Junctions—M. Cutler. (*J. Appl. Phys.*, vol. 32, pp. 222–227; February, 1961.) Equations are derived for the flow of carriers and electronic heat when a temperature difference and a potential difference exist across a *p-n* junction. Large- and small-signal situations are discussed.

537.311.33:538.569.4 1903
A Note on Date's Paper "Magneto-plasma Resonance in Semiconductors: Part 1"—K. Yamagata. (*J. Phys. Soc. Japan*, vol. 15, p. 2363; December, 1960.) Comment is given on 931 of March considering the effect of anisotropic mass on magneto-plasma resonance.

537.311.33:538.63 1904
Galvanomagnetic Effects and their Application—C. Hilsum. (*Brit. J. Appl. Phys.*, vol. 12, pp. 85–91; March, 1961.) The properties of semiconductors suitable for galvanomagnetic applications are discussed and instruments based on the Hall effect and magnetoresistance are described.

537.311.33:546.23 1905
Dielectric Investigations of Polycrystalline Selenium—W. Ludwig. (*Mber. dtsch. Akad. Wiss. Berlin*, vol. 2, no. 2, pp. 91–92; 1960.) A brief note is given on results of ac bridge measurements on Br-doped high-purity Se at temperatures in the range $+40°$ to $-160°C$.

537.311.33:[546.28+546.289 1906
The Temperature Dependence of the Polarizability of the Free Carriers in Germanium and Silicon—M. Cardona, W. Paul, and H. Brooks. (*Helv. Phys. Acta*, vol. 33, pp. 329–346; August 15, 1960.) The contribution of the free carriers to the total electric polarizability was determined from the reflectivity and an average effective mass for the carriers was deduced. An increase in electron mass with both carrier concentration and temperature was found in both *n*-type Ge and *n*-type Si. No definite conclusions could be drawn about *p*-type Ge owing to transitions between branches of the degenerate valence band. For *p*-type Si the effective mass increases with temperature.

537.311.33:[546.28+546.289 1907
Theory of Solubility of Interstitial Impurities in Germanium and Silicon—K. Weiser. (*J. Phys. Chem. Solids*, vol. 17, pp. 149–161; December, 1960.) A theory of solubility is developed which is based on estimating the change in energy and in entropy when an impurity is placed in an interstitial site in the lattice.

537.311.33:[546.28+546.289]:535.215 1908
Photoelectron Emission from Germanium and Silicon in the Amorphous and Crystalline States—P. G. Borzyak, L. S. Miroshnichenko, and O. G. Sarbei. (*Fiz. Tverdogo Tela*, vol. 2, pp. 314–318; February, 1960.) The spectral sensitivity curve for crystalline Ge shows a dip in the short-wavelength region which is not observed with amorphous films. This effect is less marked in the case of Si.

537.311.33:[546.28+546.289]:539.23 1909
The Preparation of Thin Films of Germanium and Silicon—B. A. Irving. (*Brit. J. Appl. Phys.*, vol. 12, pp. 92–93; March, 1961.) Films about 1000 Å thick, suitable for observing dislocations by transmission electron microscopy, have been prepared from the brittle semiconductors germanium and silicon by a combination of mechanical polishing and chemical etching.

537.311.33:546.28 1910
Surface States on Cleaved Silicon—D. R. Palmer, S. R. Morrison and C. E. Dauenbaugh. (*Phys. Rev. Lett.*, vol. 6, pp. 170–171; February 15, 1961.)

537.311.33:546.28 1911
Acoustic-Mode Mobilities for 'Split *p*-Silicon'—P. J. Price and Y. H. Kao. (*IBM J. Res. & Dev.*, vol. 5, pp. 63–64; January, 1961.)

537.311.33:546.28 1912
Spin Resonance of Electrons on Donors in *p*-type Silicon—G. Bemski and B. Szymanski. (*J. Phys. Chem. Solids*, vol. 17, pp. 173–175; December, 1960.) The resonance was observed using compensated *p*-type Si crystals after the samples had been illuminated with light of about 1 $\mu\lambda$. The amplitude of the resonance gives useful information on the concentration of the donor.

537.311.33:546.28 1913
The Effect of Gold on the Electrical Properties of Silicon—B. I. Boltaks, G. S. Kulikov, and R. Sh. Malkovich. (*Fiz. Tverdogo Tela*, vol. 2, pp. 181–191; February, 1960.) Donor and acceptor levels determined from Hall-effect measurements agree with those reported by Collins, *et al.* (2498 of 1957). Experimental and calculated values of resistivity and carrier concentration in gold-alloyed samples of *n*- and *p*-type Si with different initial resistivity are compared. A nomogram for calculating the resistance of gold-alloyed samples is given.

537.311.33:546.28:535.34–15 1914
The Absorption of Infrared Radiation by Free Charge Carriers in Silicon—V. S. Vavilov. (*Fiz. Tverdogo Tela*, vol. 2, pp. 374–377; February, 1960.) Measurements have been made in

the wavelength range 1–11 μ on single-crystal p- and n-type Si with carrier concentration between 10^{14} and 5×10^{17} cm^{-3}, and on samples with carrier concentration 10^{12} cm^{-3} irradiated with fast neutrons. For highly transparent crystals the $\lambda^{1.5}$ relation for the absorption coefficient was not confirmed.

537.311.33:546.289 1915
Pressure Dependence of the Direct Energy Gap in Germanium—M. Cardona and W. Paul. (*J. Phys. Chem. Solids*, vol. 17, pp. 138–142; December, 1960.) "The pressure dependence of the energy gap corresponding to allowed optical transitions in Ge has been measured at room temperature and pressures up to 7000 kg/cm^2. This direct energy gap is found to increase at a rate of $1.3\pm0.1\times10^{-5}$ eV.cm^2/kg, in agreement with previous approximate determinations and with the pressure coefficient of the same energy gap in group III-V compounds."

537.311.33:546.289 1916
Direct Viewing of Imperfections in Germanium p-n Junctions—M. Tomono. (*J. Phys. Soc. Japan*, vol. 15, pp. 2254–2264; December, 1960.) A copper-plating method is described for making junction imperfections visible. The imperfections are then related to the reverse (electrical) characteristics of the junction.

537.311.33:546.289 1917
Investigation of the Effect of Certain Factors on Formation of Dislocations during Crystallization and on the Dislocation States in Germanium Single Crystals—A. D. Belyaev, V. N. Vasilevskaya, and E. G. Miselyuk. (*Fiz. Tverdogo Tela*, vol. 2, pp. 227–234; February, 1960.) Dislocations dispersed between boundaries of regions with different orientation are displaced toward these boundaries by annealing at 700–800°C. Dislocations at these boundaries are removed only at temperatures close to the melting point. The effect of dislocations of density from 10^3 to 10^7 cm^{-2} on carrier lifetime is determined.

537.311.33:546.289 1918
The Effect of Lead Treatment of Germanium on the Lifetime of Nonequilibrium Charge Carriers—A. K. Mednikov. (*Fiz. Tverdogo Tela*, vol. 2, pp. 235–238; February, 1960.) The diffusion length of minority carriers substantially decreased with the removal of residual Cu from Ge by treatment with molten lead. Increasing the Cu concentration caused the diffusion length first to increase and then to decrease.

537.311.33:546.289 1919
Electron-Electron Interaction in Hot-Electron Problems—J. Yamashita. (*Prog. Theoret. Phys.*, vol. 24, pp. 357–369; August, 1960.) The theory of warm and hot electrons in n-type Ge at 77°K is discussed with reference to Gunn's experiments (*J. Phys. Chem. Solids*, vol. 8, pp. 239–241; January, 1959).

537.311.33:546.289 1920
Donor Concentration at the Surface of a Diffused n-Type Layer on p-Type Germanium—R. Glang and W. B. Easton. (*J. Electrochem. Soc.*, vol. 107, pp. 758–763; September, 1960.) Four methods of evaluating donor concentration have been investigated. All methods assume a complementary error function distribution in the diffused layer and require the use of experimental and published data. With three of the methods, calculated surface concentrations agree within a factor of 2 or 3.

537.311.33:546.289:535.215 1921
Current/Voltage Characteristics of Photoelectric Emission from Germanium—P. G. Borzyak, P. M. Marchuk, and O. G. Sarbei. (*Fiz. Tverdogo Tela*, vol. 2, pp. 306–313; February, 1960.) Experimentally determined I/V characteristics of the emission from Ge films with low work function show no evidence of a bulk photoeffect.

537.311.33:546.3–1'289'28 1922
Electrical Conductivity and Hall Effect of Ge-Si Alloys—G. Busch and O. Vogt. (*Helv. Phys. Acta*, vol. 33, pp. 437–458; August 15, 1960. In German.) Methods of preparation of Ge-Si single-crystal and polycrystalline alloys are described. Hall coefficients and conductivity have been measured in the temperature range 20°–900°C, and electron and hole mobilities and intrinsic carrier concentrations calculated as functions of alloy composition. Typical results are given and discussed.

537.311.33:546.?–1'289'28 1923
Indirect Transition in Narrow Junction of Ge-Si Alloy—K. Ando. (*J. Phys. Soc. Japan*, vol. 15, p. 2360; December, 1960.) Data on indirect transitions are obtained from cusps in junction characteristics measured at liquid helium temperature.

537.311.33:[546.55'221+546.55'231 1924
Relations between the Crystalline Structure and the Electronic Properties of Ag_2S, Ag_2Se, Cu_2Se Compounds—P. Junod. (*Helv. Phys. Acta*, vol. 32, pp. 567–600; December 31, 1959. In French.)

537.311.33:[546.571'221+546.571'231 1925
Brillouin Zones, Chemical Bonds and Conduction Mode of Ag_2S and Ag_2Se—P. Junod. (*Helv. Phys. Acta*, vol. 32, pp. 601–614; December 31, 1959. In French.)

537.311.33:546.681'19 1926
Scattering of Current Carriers in Gallium Arsenide in the Presence of Strong Degeneracy—O. V. Emel'yanenko, T. S. Lagunova and D. N. Nasledov. (*Fiz. Tverdogo Tela*, vol. 2, pp. 192–197; February, 1960.) Results of conductivity and Hall-effect measurements on GaAs samples with n- and p-type impurity conductivity show that the mobility of electrons and holes depends only weakly on the concentration of uncompensated impurities.

537.311.33:546.681'682'19 1927
Electrical and Optical Properties of GaAs-InAs Alloys—J. C. Woolley, C. M. Gillett, and J. A. Evans. [*Proc. Phys. Soc. (London)*, vol. 77, pp. 700–704; March 1, 1961.] Electrical measurements showed that there is mixed conduction in the alloys and hence the Hall mobility is without significance. Optical transmission measurements of optical energy gap give good agreement with values obtained by diffuse-reflection methods.

537.311.33:546.681'682'86 1928
Electrical Properties of GaSb-InSb Alloys—J. C. Woolley and C. M. Gillett. (*J. Phys. Chem. Solids*, vol. 17, pp. 34–43; December, 1960.) The electrical properties have been investigated as a function of composition. Values of extrapolated thermal energy gap, electron mobility and mobility ratio have been determined for some 25 specimens.

537.311.33:546.682'86 1929
Orientation-Dependent Distribution Coefficients in Melt-Grown InSb Crystals—J. B. Mullin and K. F. Hulme. (*J. Phys. Chem. Solids*, vol. 17, pp. 1–6; December, 1960.)

537.311.33:546.682'86 1930
Carrier Lifetime in Indium Antimonide—R. A. Laff and H. Y. Fan. (*Phys. Rev.*, vol. 121, pp. 53–62, January 1, 1961.) The recombination of excess electron-hole pairs in InSb has been studied in the temperature range 200°K–15°K where it is controlled by localized centers. A model for the process is deduced from the analysis of the results, and evidence is obtained that the recombination centers are due to structural defects.

537.311.33:546.682'86:538.63 1931
Galvanomagnetic Effects in Three-Band Semiconductors—Experiments with p-Type InSb—G. Fischer. (*Helv. Phys. Acta*, vol. 33, pp. 463–488; August 15, 1960.) A three-band model is discussed and formulas are given with which it is possible to derive values for the concentrations and mobilities of the various charge carriers from the dependence of the Hall coefficient and resistivity on the magnetic field. This model appears valid for p-type InSb in the extrinsic range.

537.311.33:546.817'241:538.63 1932
Oscillatory Magnetoresistance in n-Type PbTe—C. D. Kuglin, M. R. Ellett, and K. F. Cuff. (*Phys. Rev. Lett.*, vol. 6, pp. 177–179; February 15, 1961.)

537.312.62 1933
Magnetic-Field Dependence of Energy Gap in Superconductors—K. K. Gupta and V. S. Mathur. (*Phys. Rev.*, vol. 121, pp. 107–117; January 1, 1961.) The dependence of the energy gap on static magnetic fields has been derived in a gauge-invariant way from the theory of Bardeen, *et al.* (1386 of 1958). The gap decreases with magnetic field approaching the critical value. Optimum conditions for observation of this effect are discussed.

537.312.62:538.63 1934
Superconductivity in Nb_3Sn at High Current Density in a Magnetic Field of 88 KG—J. E. Kunzler, E. Buehler, F. S. L. Hsu, and J. H. Wernick. (*Phys. Rev. Lett.*, vol. 6, pp. 89–91; February 1, 1961.) Results of observations indicate that superconducting solenoid magnets with fields of 100 kG are feasible.

538.1/.2:061.3 1935
International Colloquim on Magnetism—(*J. Phys. Radium*, vol. 20, pp. 65–442; February/March, 1959.) The text is given of papers presented and subsequent discussions at the colloquim held in Grenoble, France, July 2nd–6th, 1958. 78 papers were presented, of which 44 were in English.

538.22:537.27 1936
Magnetoelectric Effect in Antiferromagnetics—D. N. Astrov. (*Zh. Eksp. Teor. Fiz.*, vol. 38, pp. 984–985; March, 1960.) A note on measurements of the magnetic moment developed in a sample of Cr_2O_3 in an alternating electric field is given. Curves show the temperature dependence of a signal at the output of a measuring amplifier with fields of 230 and 430 v/cm at 10^4 cps.

538.221 1937
Anisotropy on Polycrystalline Sheets of V-Permendur—C. Kuroda. (*J. Phys. Soc. Japan*, vol. 15, p. 2355; December, 1960.)

538.221 1938
The Anisotropy Constants of Ferromagnetic Cubic Crystals—A. S. Viglin. (*Fiz. Tverdogo Tela*, vol. 2, pp. 331–346; February, 1960.) A numerical treatment relating to calculations of anisotropy energy is given.

538.221 1939
On the Mechanism of Reversible Appearance of Residual Magnetization at Low Temperature Transition in αFe_2O_3—K. Siratori, A. Tasaki, and S. Iida. (*J. Phys. Soc. Japan*, vol. 15, pp. 2357–2358; December, 1960.)

538.221:539.23 1940
Depictive Representation of the Coherent Rotation of Magnetization in Thin Ferromagnetic Films—E. Feldtkeller. (*Z. angew. Phys.*, vol. 12, pp. 257–261; June, 1960.) De-

tails of the magnetic reversal process in thin films are discussed and a graphical method is given for determining the direction and rate of change of magnetization at any instant on the basis of the directional characteristics of magnetization energy.

538.221:539.23:537.312.8 1941
Influence of a Magnetic Field on the Electrical Resistance of Thin Ferromagnetic Layers at Low Temperatures—A. A. Hirsch. (*Physica*, vol. 25, pp. 581–589; July, 1959.)

538.221:621.318.124 1942
The Thermomagnetic Behaviour of Cobalt Ferrite—L. F. Bates and A. Pacey. [*Proc. Phys. Soc., (London)*, vol. 77, pp. 567–575; March 1, 1961.] The behavior is similar to that of other materials; a new method of analysis of results is described.

538.221:621.318.134 1943
Low-Loss Ferrites used in Electronics and Telecommunications—Y. Lescroel and A. Pierrot. [*Câbles & Trans.* (Paris), vol. 14, pp. 220–244; July, 1960.] The effects of manufacturing procedure and, in particular, conditions of heat treatment on the permeability and loss factors of Mn-Zn and Ni-Zn ferrites are investigated.

538.221:621.318.134 1944
Manganese-Zinc Ferrites with Spontaneous Isoperm Loop—M. Kornetzki, E. Moser, and E. Röss. (*Naturwiss.*, vol. 47, p. 274; June, 1960.) The magnetization curve of a magnetically isotropic ferrite of composition $Mn_{0.46}Zn_{0.47}Fe_{0.07}O \cdot Fe_2O_3$ is given; the probable causes of the isoperm characteristic are discussed.

538.221:621.318.134 1945
Spontaneous Magnetization of Magnesium Ferrite—Manganite System—K. Muramori and S. Miyahara. (*J. Phys. Soc. Japan*, vol. 15, p. 2354; December, 1960.)

538.221:621.318.134 1946
Interpretation of the Characteristics of Microwave Ferrites by means of the Forced Precession of Gyroscopes—H. Lueg. (*Telefunken Ztg.*, vol. 33, pp. 132–140; June, 1960. English summary, p. 158.) The use of a gyroscope is proposed as an analog of the gyromagnetic properties of ferrites. The validity of the method is checked using results of ferrite measurements by other authors.

538.221:621.318.134 1947
The Irreversible Change of Magnetization produced in 'Square-Loop' Ferrite by Pulsed Magnetic Fields—J. E. Knowles. [*Proc. Phys. Soc., (London)*, vol. 77, pp. 576–586; March 1, 1961.] The experimental results were interpreted in terms of a domain wall model; it was found that the domain wall energy passed through a maximum 25 times in the course of a magnetization reversal.

538.221:621.318.134:538.569.4 1948
Note on Ferromagnetic Relaxation Equations—H. Suhl and R. C. Fletcher. (*J. Appl. Phys.*, vol. 32, pp. 281–282; February, 1961.) The omission of an explicit back-reaction term in "energy" and "number of quanta" formulations is justified provided a large number of spin waves are excited by the scattering centers.

538.221:621.318.134:538.569.4 1949
Suppression of Subsidiary Absorption in Ferrites by Modulation Techniques—T. S. Hartwick, E. R. Peressini, and M. T. Weiss. (*Phys. Rev. Lett.*, vol. 6, pp. 176–177; February 15, 1961.) The prediction of Suhl (1807 above) is confirmed by experiments on Y-Fe garnet. Optimum modulation frequencies of about 1 Mc are found, depending upon the excess of the microwave field above normal threshold.

538.221:621.318.134:538.569.4 1950
Ferromagnetic Resonance in Europium-Iron Garnet—T. Miyadai. (*J. Phys Soc. Japan*, vol. 15, pp. 2205–2210; December, 1960.) A study of g-values and line widths of single-crystal and polycrystalline specimens at 18 Gc and at temperatures from 100°K to the Curie point (565°K) is given.

538.222:534.283–8 1951
Selection Rule for the Interaction of Microwave Ultrasonics with Spins—N. S. Shiren and E. B. Tucker. (*Phys. Rev. Lett.*, vol. 6, pp. 105–106; February 1, 1961.)

538.222:543.283–8 1952
Attenuation of Longitudinal Ultrasonic Vibrations by Spin-Photon Coupling in Ruby—E. B. Tucker. (*Phys. Rev. Lett.*, vol. 6, pp. 183–185; February 15, 1961.) The magnetoelastic coupling constant is determined from the observed attenuation. See 1951 above.

538.222:538.569.4 1953
Spin-Lattice Relaxation in Chromium Corundum—A.A. Manenkov and A.M. Prokhorov. (*Zh. Eksp. Teor. Fiz.*, vol. 38, pp. 729–733; March, 1960.)

538.222:538.569.4 1954
Relaxation in Ruby—R. A. Armstrong and A. Szabo. (*Canad. J. Phys.*, vol. 38, pp. 1304–1317; October, 1960.) "The relaxation of the (1↔2) and (2↔3) transitions in chrome-doped Al_2O_3 (0.015%) has been studied at S-band frequencies, using a pulsed microwave method, over a range of crystal orientations in the magnetic field at temperatures of 77°K to 50°K, and at 4.2°K and 1.6°K."

621.315.6:538.569.3 1955
Electromagnetic Properties of Insulators: Part 2—V. Ambegaokar. (*Phys. Rev.*, vol. 121, pp. 91–103; January 1, 1961.) The system considered is an insulator plus one electron. The main result is that the response of the system to low-frequency electric fields is exactly that of a free electron with a certain effective mass moving in a medium having the dielectric constant of a perfect insulator. Part 1: 2468 of 1960 (Ambegaokar and Kohn).

621.315.61:539.23 1956
Tunnelling through Thin Insulating Layers—J. C. Fischer and I. Giaever. (*J. Appl. Phys.*, vol. 32, pp. 172–177; February, 1961.) Measurements of the tunneling current through thin Al oxide films can be formally explained by a theory of Holm (2455 of 1951), provided an electron mass factor of 1/9 is used.

MEASUREMENTS AND TEST GEAR

621.3.018.41(083.74) 1957
The Significance of the Time Intervals arranged in Geometric Progression for the Standard-Frequency and Time-Signal Transmission of the Physikalisch-Technishe Bundesanstalt via Station DCF 77—U. Adelsberger. (*Nachtech. Z.*, vol. 13, pp. 296–298; June, 1960.) The usefulness of the time intervals of 2 minutes and 3 hours forming the basis of the transmission schedule and their relation to other useful time intervals are discussed. See also 3977 of 1960 (Süss) and back references.

621.3.018.41(083.74) 1958
Characteristics of the Ammonia Beam Maser (AM-1) as an Atomic Frequency Standard at JJY—Y. Saburi and M. Kobayashi. (*J. Radio Res. Labs. Japan*, vol. 7, pp. 425–436; September, 1960.) The construction of the maser and the associated circuit arrangements are described. Comparisons with time signals emitted from WWVH show that the frequency stability is ±2 or 3 parts in 10^{10}.

621.317.2:538.566.08+534.844.1 1959
The Upper Limits for the Reverberation Time of Reverberation Chambers for Acoustic and Electromagnetic Waves—Walther. (See 1716.)

621.317.3.029.64:538.632 1960
On the Method of Measuring Hall Coefficient at Microwave Frequencies—K. Yamagata. (*Sci. Rep. Res. Inst. Tohoku Univ.*, A, vol. 12, pp. 235–246; June, 1960.) A theory of the bimodal or dual-mode cavity without initial unbalance is developed.

621.317.3.029.64:538.632 1961
Measurement of Hall Mobility of Germanium at a Microwave Frequency—K. Yamagata and T. Fukuroi. (*Sci. Rep. Res. Inst. Tohoku Univ.*, A vol. 12, pp. 247–251; June, 1960.) The theory of the dual-mode cavity developed by Yamagata (1960 above) is extended to include the case of initial unbalance, and a report is given of experiments based on a dual-mode cavity with resistive unbalance. The accuracy of measurement of the Hall mobility is limited by the accuracy with which the microwave power level can be measured.

621.317.412 1962
Measurement of Magnetic Susceptibility in Very High Pulsed Fields—R. Stevenson. (*Rev. Sci. Instr.*, vol. 32, pp. 28–31; January, 1961.) The sample is suspended in a nonuniform magnetic field and the force on it when the field changes is measured by a transducer comprising two piezoelectric crystals.

621.317.755:531.76 1963
Zig-Zag Oscilloscope Presentation of Millimicrosecond Accuracy for Microsecond Time Invervals—E. G. Leger, D. Nyberg, K. Graf, and L. Tardif. (*Rev. Sci. Instr.*, vol. 32, pp. 57–61; January, 1961.) The zig-zag wave, the trigger pulses and the time marks 2-mμsec wide at 50-mμsec intervals are derived from a 2-Mc crystal-controlled oscillator; six oscilloscopes can be driven simultaneously or in sequence from delayed triggers.

621.317.794 1964
Cobalt-Manganese Semiconducting Oxide Bolometers—A. L. Burkin and I. T. Sheftel'. (*Fiz. Tverdogo Tela*, vol. 2, pp. 288–296; February, 1960.) Techniques for the measurement of bolometer characteristics are discussed and the design of three types of bolometer as infrared-sensitive devices is described.

621.317.794.029.64/.66:537.312.62 1965
Superconductors as Quantum Detectors for Microwave and Sub-millimetre-Wave Radiation—E. Burstein, D. N. Langenberg, and B. N. Taylor. (*Phys. Rev. Lett.*, vol. 6, pp. 92–94; February 1, 1961.) An analysis of low-voltage tunneling in metal/barrier/superconductor and superconductor/barrier/superconductor structures suggests its application for measuring microwave and submillimeter radiation incident on the barrier region. Limitations due to carrier lifetime are discussed.

OTHER APPLICATIONS OF RADIO AND ELECTRONICS

531.78:537.311.33:537.312.9 1966
Semiconductor Strain Gauges offer High Sensitivity—R. E. Talmo. (*Electronics*, vol. 34, pp. 43–45; February 24, 1961.) Single-crystal Si gives a change in resistance 10–100 times greater for a given strain than metallic gauges. See 3230 of 1960 (Geyling and Forst).

531.79:621.397.331.3 1967
An Automatic Particle Counter and Sizer—H. A. Dell, D. S. Hobbs, and M. S. Richards. (*Philips Tech. Rev.*, vol. 21, pp. 253–267; August 4, 1960.) Methods used for automatic counting and sizing are discussed and commer-

cial equipment is described in which the sample is photographed and the film examined automatically using a flying-spot scanning system.

534.88 1968
Narrow-Beam Echo-Ranger for Fishery and Geological Investigations—M. J. Tucker and A. R. Stubbs. (*Brit. J. Appl. Phys.*, vol. 12, pp. 103–110; March, 1961.) A detailed description is given of a 36-kc acoustic echo-ranger with a range of 800 yards suitable for fish detection and geological investigation of the sea bed. Typical records are shown and discussed.

621.362:621.387 1969
A New Thermionic Generator—D. Gabor. (*Nature*, vol. 189, pp. 868 872; March 18, 1961.) The principle of operation of a vacuum diode using argon vapor is described. The main discharge occurs between the emitter and a large-area collector of cellular construction. Ions are supplied to the main discharge space from an auxiliary discharge between a perforated structure and an auxiliary anode. By controlling this auxiliary discharge, direct generation of ac is possible. An experimental cost figure of 0.05 0.1 w/a has been achieved.

621.362:621.387 1970
Low-Frequency Oscillations in a Filamentary-Cathode Cesium Diode Converter—K. P. Luke and F. E. Jamerson. (*J. Appl. Phys.*, vol. 32, p. 321; February, 1961.) Oscillations at frequencies below 100 kc are reported, and waveforms are given. Some of the characteristics correspond to a plasma potential distribution unlike that in high-frequency oscillations.

621.384.611.3 1971
The Design and Construction of a 29-MeV Microtron—D. K. Aitken, F. F. Heymann, R. E. Jennings, and P. I. P. Kalmus. [*Proc. Phys. Soc., (London)*, vol. 77, pp. 769 785; March 1, 1961.] The microtron has a 20-ton magnet and a pole diameter of 80 inches. An extracted electron beam of 10^{-8} a at an energy of 29 Mev can be focused to a spot about 2 mm in diameter.

621.384.8 1972
Microwave Separator for High-Energy Particle Beams—P. R. Phillips. (*Rev. Sci. Instr.*, vol. 32, pp. 13 16; January, 1961.) 150-Mev electrons were deflected $\frac{3}{4}$ inch at the final focus of the analyzing magnet, using a TM_{012} rectangular cavity with a Q of 15,000 and maximum power dissipation of 1.3 mw.

621.387.4:621.383 1973
The Measurement of Proton Currents by means of Photosemiconductors and Measurements of Polarization Dependence on Composite Photocathodes—P. Görlich. (*Mber. dtsch. Akad. Wiss. Berlin*, vol. 2, no. 2, pp. 67–70; 1960.)

621.396.969.14 1974
Speed Measurement by means of the Electromagnetic Doppler Effect—B. Koch. (*Arch. tech. Messen*, Nos. 293 and 295, pp. 109 112 and 153–156; June and August, 1960.) Details are given of practical applications, following an outline of the principles underlying Doppler-radar measurement methods. 61 references.

77:537.2(083.74) 1975
I.R.E. Standards on Electrostatographic Devices, 1961—(PROC. IRE, vol. 49, pp. 619–621; March, 1961.) Standard 60 IRE 28.S2 defining terms used.

PROPAGATION OF WAVES

621.391.812.34:551.507.362.2 1976
Observed Field Strength in the Neighbourhood of the Skip Distance—Yeh and Swenson. (See 1837.)

621.391.812.61 1977
Attenuation of Electromagnetic Wave due to Rain with Distorted Raindrops—T. Oguchi. (*J. Radio Res. Labs., Japan*, vol. 7, pp. 467–485; September, 1960.) The scattered field is expressed as a function of the deformation of a drop from spherical shape. The deformation as a function of terminal velocity is known and hence a relation between attenuation and rate of precipitation can be found. Greater attenuation is expected for horizontal polarization.

621.391.812.61.029.65 1978
An Analysis of Recent Measurements of the Atmospheric Absorption of Millimetric Radio Waves—C. W. Tolbert and A. W. Straiton. (PROC. IRE, vol. 49, pp. 649–650; March, 1961.) Water-vapour losses are greatly enhanced near the oxygen absorption lines. See 1813 above.

621.391.812.62.029.62 1979
Observation of F-Layer and Sporadic-E Scatter at V.H.F. in the Far East—K. Miya, T. Sasaki, and M. Ishikawa. (*J. Res. NBS*, vol. 65D, pp. 93–99; January/February, 1961.) Measurements made over the paths Okinawa-Tokyo (1480 km) and Philippines-Tokyo (2850 km) at about 50 Mc are described.

621.391.812.621 1980
Correlation of Monthly Median Transmission Loss and Refractive Index Profile Characteristics—B. R. Bean and B. A. Cahoon. (*J. Res. NBS*, vol. 65D, pp. 67–74; January/February, 1961.) An examination of propagation data taken at 100 Mc over 21 paths in the U.S.A. shows that the surface value of atmospheric refractive index is well correlated with the annual cycle of radio transmission loss.

621.391.812.622.029.64 1981
Characteristics of Maritime Advective Duct and their Effect on the Microwave Propagation Beyond the Line of Sight—A. Takabira and H. Irie. (*J. Radio Res. Labs, Japan*, vol. 7, pp. 531–544; September, 1960.) Helicopters were used to make measurements of atmospheric refractive index over the sea along the radio wave path. It is possible to predict the profile of the *M* curve over the sea up to 20 km from the coast line.

621.391.812.624.029.63 1982
Correlation between Amplitudes of Radio Waves of Different Frequencies in U.H.F. Beyond-the-Horizon Propagation—M. Hirai, M. Fukushima, and Y. Kurihara. (*J. Radio Res. Labs., Japan*, vol. 7, pp. 509 529; September, 1960.) Selective fading is caused by interference between multipath waves. This is treated theoretically and expressions are derived for the amplitude correlation coefficient, the distribution of amplitude ratios and the distribution of multiple-path delays. A comparison is made between these theoretical formulas and experimental data.

621.391.812.63 1983
Wave Interaction in Plasma Inhomogeneities—L. Wetzel. (*J. Appl. Phys.*, pp. 327–328; February, 1961.) The perturbation of electron density giving rise to first-order combination frequencies [3847 of 1959 (Ginzburg)] is deduced for the case of a spatially homogeneous plasma and compared with the perturbation normally giving rise to second-order wave interaction in a homogeneous plasma.

621.391.812.63 1984
Focusing of Radio Waves Reflected from a Rough Curved Ionosphere—J. D. Whitehead. (*Aust. J. Phys.*, vol. 13, pp. 621 624; December, 1960.) The increase in echo amplitude due to focusing by a rough curved ionosphere is shown to be given by the same formula as that for a smooth ionosphere (see 914 of 1957), but different areas of reflection are effective in the two cases, and as a result large amplitude increases are not expected in the rough case.

621.391.812.63 1985
Perpendicular Intersections with a Dipole Field—M. H. Cohen and M. L. Dwarkin. (*J. Geophys. Res.*, vol. 66, pp. 411 419; February, 1961.) "This paper deals with the geometry of radio rays originating at an arbitrary point in a force-free dipole magnetic field. The echo surface, defined by the points where the rays intersect the field at right angles, is calculated. The distance from the source point to the echo surface is computed and plotted for various configurations."

621.391.812.63 1986
Radio Wave Reflections from the Mesosphere: Part 1—Heights of Occurrence—J. B. Gregory. (*J. Geophys. Res.*, vol. 66, pp. 429–445; February, 1961.) The height distribution of partial reflections from the lower ionosphere was made in Christchurch, New Zealand, for one year using a frequency of 1.75 Mc. Reflections occur most frequently from regions whose lower boundaries are at 86, 74, 66, 61, 55 km. Some small seasonal trends were noticed. The reflections are thought to be due to turbulent scatter in the presence of a gradient of electron density at certain preferred heights.

621.391.812.63:523.78 1987
Behaviour of Broadcast-Frequency Waves at Oblique Incidence during an Annular Eclipse—R. K. MacCrone and F. R. N. Nabarro. (*J. Atmos. Terr. Phys.*, vol. 20, pp. 200–205; March, 1961.) Abrupt increases in received signal strength for oblique incidence are observed during an annular eclipse. The mechanism suggested is a Chapman solar-particle eclipse causing sudden changes in reflection heights from D to E region.

621.391.812.63:551.510.535 1988
On the Evaluation of the Group Refractive Index in Case of No Collisions—H. Unz. (*J. Atmos. Terr. Phys.*, vol. 20, pp. 189–194; March, 1961.) An alternative method of evaluating the group refractive index μ' in magneto-ionic theory is shown. Expressions are derived, simpler than those given, *e.g.*, by Shinn and Whale (1405 of 1951), and particularly suitable for calculating μ and μ' near the reflection point.

621.391.812.63:621.396.677 1989
Launching Over the Sea of Vertically Polarized Waves for Long-Distance Ionospheric Propagation—Willoughby. (See 1733.)

621.391.812.63.029.4 1990
Magneto-ionic Propagation Phenomena in Low- and Very-Low-Radiofrequency Waves Reflected by the Ionosphere—J. R. Johler. (*J. Res. NBS*, vol. 65D, pp. 53–65; January/February, 1961.) An analysis is given illustrating the dependence of the amplitude and phase of the reflected wave upon the direction of propagation relative to the direction of the earth's magnetic field. A plane sharply bounded ionosphere with plane-wave excitation is used. Tables applicable to VLF propagation are given.

621.391.812.63.029.45 1991
A New Approach to the Mode Theory of V.L.F. Propagation—J. R. Wait. (*J. Res. NBS*, vol. 65D, pp. 37–46; January/February, 1961.) Approximate forms of the wave functions appropriate to grazing incidence are introduced which lead to relatively concise results for the influence of the earth's curvature; influence of the earth's magnetic field is also discussed. Numerical results for the attenuation and phase velocity of the dominant mode are given.

621.391.812.63.029.45 1992
East-West Effect on V.L.F. Mode Transmission across the Earth's Magnetic Field—

D. Dobrott and A. Ishimaru. (*J. Res. NBS*, vol. 65D, pp. 47–52; January/February, 1961.) An analysis is given for modes propagating within a parallel-plate waveguide, the lower boundary being a perfect conductor and the upper a sharply defined semi-infinite plasma with a constant magnetic field applied. Some agreement with experimental results is found.

621.391.812.63.029.45 1993
Waveguide-Mode Propagation of Very-Low-Frequency Radio Waves—H. G. Martin. (*J. Atmos. Terr. Phys.*, vol. 20, pp. 206–209; March, 1961.) Theoretical calculations on the E-W asymmetry of VLF wave propagation are given.

621.391.812.63.029.45 1994
Random Fluctuations in Very-Low-Frequency Signals Reflected Obliquely from the Ionosphere—J. K. Hargreaves. (*J. Atmos. Terr. Phys.*, vol. 20, pp. 155–166; March, 1961.) The fluctuations of signals from VLF transmitters at distances of 800 and 6000 km were 0.15 and 1.02, respectively, of the mean amplitude. The results could be explained by a model with constant reflection coefficient but varying height.

621.391.812.63.029.45:523.5 1995
V.L.F. Phase Perturbation associated with Meteor Shower Activity—C. J. Chilton. (*J. Geophys. Res.*, vol. 66, pp. 379–383; February, 1961.) The diurnal phase variations of radio waves from Rugby, England, on 16 kc were measured at Boulder, Colorado. Anomalous phase changes were detected when the Lyrid, Aquarid and Perseid meteor showers occurred but the reasons have not been explained. The height of reflection was approximately 80 km.

621.391.812.631:551.510.535(98) 1996
Statistical Study in the Occurrence of Polar Blackouts—Kasuya. (See 1854.)

621.371:061.3 1997
Electromagnetic Wave Propagation [Book Review]—M. Desirant and J. L. Michiels, Eds., Academic Press, Inc., London, Eng., 730 pp., 1960, 157 s. (*J. Atmos. Terr. Phys.*, vol. 20, pp. 222–223; March, 1961.) The text is given of 54 papers presented at a conference associated with the International Exhibition in Brussels, Belgium, 1958.

RECEPTION

621.376.23 1998
Zeros of a Stationary Random Signal—H. Debart. [*Câbles & Trans.* (Paris), vol. 14, pp. 191–199; July, 1960.] An application is given of the Loeve-Karhunen expansion to the approximate calculation of the probability functions $P_0(t)\cdots P_n(t)$, probabilities for which, in the time interval t, there will be a prescribed number of zero crossings.

621.376.23:621.372.54 1999
Self-Adaptive Filter finds Unknown Signal in Noise—C. V. Jakowatz and G. M. White. (*Electronics*, vol. 34, pp. 117–119; February 17, 1961.) An automatic system forms a stored image of the signal after several occurrences. The system alters the stored image as the shape of the signal varies and forms an optimum filter.

621.376.23:621.391.822 2000
Likelihood Detection of Small Signals in Stationary Noise—P. Rudnick. (*J. Appl. Phys.*, vol. 32, pp. 140–143; February, 1961.) An approximation for the detection probability ratio is derived, applicable to any sufficiently long observation period.

621.391.812.624.029.63 2001
Variation in Received Signal Power with Narrow-Beam Antennas Rotated Horizontally in U.H.F. Beyond-the-Horizon Propagation—M. Hirai, R. Inoue, and Y. Kido. (*J. Radio Res. Labs., Japan*, vol. 7, pp. 487–507; September, 1960.) The received signal power depends on the mode of propagation, the geometry of the path and the speed of antenna rotation in addition to the antenna directivities. Assuming tropospheric scatter propagation, the antenna patterns are derived for different distributions of dielectric-constant irregularities and compared with experimental data.

621.396.62:523.164 2002
A 75-cm Receiver for Radio Astronomy and Some Observational Results—Seeger, Stumpers, and van Hurck. (See 1816.)

621.396.62:523.53 2003
Noise Suppression in Pulse Receivers—E. C. McLauchlan. (*Aust. J. Phys.*, vol. 13, pp. 750–752; December, 1960.) Modifications to a receiver system used for measuring meteor rates by radar methods are described. The gain of the video stage is a function of the steady background noise but is unaffected by the signal pulses. The reliability of echo rates during periods of high noise is increased.

STATIONS AND COMMUNICATION SYSTEMS

621.376.56:621.397 2004
Some Techniques of Pulse Code Modulation—W. Neu. (*Bull. schweiz. elektrotech. Ver.*, vol. 51, pp. 978–987; October 8, 1960. In English.) Various types of code and methods of code conversion are discussed, and a 54-level tube-type and an 81-level transistor-type coder for television are described.

621.391:621.376.56 2005
Design and Performance of Hyperbolic Binary Encoders—C. P. Villars. (*Bull. schweiz. elektrotech. Ver.*, vol. 51, pp. 987–990; October 8, 1960. In French.)

621.396.4:523.3 2006
Band-Pass Measurements of a Lunar Reflection Circuit—R. P. Ingalls, L. E. Bird, and J. W. B. Day. (PROC. IRE, vol. 49, pp. 631–632; March, 1961.) The correlation between signals at frequencies separated by up to 10 kc has been measured. In speech transmision tests SSB modulation was superior to FM.

621.396.65 2007
Intermediate-Frequency Section of a F.M. Radio-Link Installation with Small Number of Channels—A. Schellenberg. (*Bull. schweiz. elektrotech. Ver.*, vol. 51, pp. 971–977; October 8, 1960.) Design procedure and theoretical and measured characteristics are given for a 42-Mc IF stage in 7-channel R/T equipment.

621.396.72–519 2008
Remote Control Equipment for Unattended Telecommunication Stations—E. Baranowski. (*Telefunken Ztg.*, vol. 33, pp. 109–119; June, 1960. English summary, p. 157.) The equipment described comprises rack-mounted units for remote supervision and control of repeater and relay stations. The transmission of "reports" and "commands" is carried out by means of pulse trains which actuate stepping selector switches.

621.396.945 2009
Subsurface Communication for Survival—R. N. Ghose. (*Electronics*, vol. 34, pp. 43–45; February 3, 1961.) Theory of a system using underground transmitters and antennas is given.

SUBSIDIARY APPARATUS

621.311.62:537.54 2010
A 30-Kilowatt, 500-Microsecond Vacuum-Tube Pulser—R. A. Kawcyn. (*Rev. Sci. Instr.*, vol. 32, pp. 56–57; January, 1961.) A full description is given of a circuit designed for operation of gas-discharge tubes in plasma research.

621.311.69:621.383.5 2011
Distribution of Losses and the Efficiency of Different Processes in Photoelectric Solar Energy Converters—V. K. Subashiev. (*Fiz. Tverdogo Tela*, vol. 2, pp. 198–204; February, 1960.) An attempt at a quantitative analysis of essential processes is made.

621.352:541.135.6 2012
Theory of Electrochemical Diodes—I. Oshida. (*J. Phys. Soc. Japan*, vol. 15, pp. 2288–2294; December, 1960.) A theoretical analysis is given of the behavior of an electrochemical diode, based on the equation of diffusion of ions. The nonohmic characteristic, the shunting effect observed with a rapidly changing voltage, and the rectifying action are deduced.

TELEVISION AND PHOTOTELEGRAPHY

621.397.132(4):389.6 2013
Standardization of European Colour Television—W. Gerber. (*Bull. schweiz. elektrotech. Ver.*, vol. 51, pp. 994–999; October 8, 1960.) The development of existing monochrome standards is reviewed. The discussion deals mainly with the use of the 625-line standards for color television transmission by the NTSC method or its variants, and with related problems of program exchange, transmitter planning and receiver design.

621.397.2 2014
Storage and Frequency-Band Compression in Television—F. Schröter. (*Bull. schweiz. elektrotech. Ver.*, vol. 51, pp. 999–1004; October 8, 1960.) The possibilities of reducing television bandwidth by using storage-type picture tubes and taking advantage of the persistence of vision are discussed.

621.397.23:621.396.65 2015
Transmission of Slow Television Pictures over Telephone or Radiotelephone Links—A. Cazalas and B. Picot. (*Compt. rend. Acad. Sci., Paris*, vol. 250, pp. 3140–3141; May 9, 1960.) An outline is given of a narrow-band system using an isoscope camera tube developed by Barthélemy (445 of 1946), and a receiver having a display tube with a screen which turns violet-purple color under electron bombardment.

621.397.331.22 2016
A Plug-Type Image-Orthicon Target—S. A. Ochs. (*RCA Rev.*, vol. 21, pp. 558–569; December, 1960.) A new type of target consisting of an array of metal plugs embedded in Al oxide insulating film has been investigated. It has high resolution at low light levels and may be of use as a storage plate.

621.397.61–519 2017
San Salvatore—the First Remotely Controlled Television Relay Station in Switzerland—E. Schwarz. (*Tech. Mitt. PTT*, vol. 38, pp. 201–205; June 1, 1960. In German and Italian.) The remote control of the standard-type video and sound transmitters used is effected by means of pulse signals transmitted via telephone lines.

621.397.611:621.317(083.74) 2018
I.R.E. Standards on Video Techniques: Measurement of Resolution of Camera Systems, 1961—(PROC. IRE, vol. 49, pp. 599–602; March, 1961.) Standard 60 IRE 23.S2.

TRANSMISSION

621.396.61 2019
A Novel Type of High-Power Pulse Transmitter—K. Landecker and K. S. Imrie. (*Aust.*

J. Phys., vol. 13, pp. 638–654; December, 1960.) A symmetrical array of capacitors, charged and discharged as in the Marx impulse generator, is used to generate radio waves. The structure forms the tank circuit and the radiating magnetic dipole, and is capable of producing peak powers of the order of 10^4 mw.

621.396.61:621.395 2020
Transmission Characteristics of Anode-Modulated Telephony Transmitters with Highly Selective Aerials—M. Dick. (*Bull. schweiz. elektrotech. Ver.*, vol. 51, pp. 963–971; October 8, 1960.) Distortion, phase modulation and other problems arising from the use of antennas of less than optimum length for long-wave transmitters are investigated theoretically and methods of minimizing the adverse effects are given. Measurements to check the theoretical results were made on a 200-kc, 10-kw transmitter feeding an antenna whose electrical length is about 13 per cent of $\lambda/4$.

TUBES AND THERMIONICS

621.382+537.311.33]:061.3 2021
International Convention on Transistors and Associated Semiconductor Devices—(*Proc. IEE*, vol. 106, pt. B, suppl. nos. 15–18, pp. 265–570, 571–842, 843–1182, and 1183–1398; 1959.) The text is given of the papers presented and the session discussions at the IEE Convention held in London, England, May 27, 1959.

621.382.2/.3 2022
Effects of Electrons and Holes on the Transition-Layer Characteristics of Linearly Graded *p-n* Junctions—C. T. Sah. (Proc. IRE, vol. 49, pp. 603–618; March, 1961.) The dc theory of *p-n* junctions has been extended, taking into account the mobile carriers or electrons and holes in the transition region under forward-bias conditions both the transition-layer width and carrier capacitance increase exponentially with voltage.

621.382.22:621.318.57 2023
A 100-dB Microwave Semiconductor Switch—D. W. Feldman and B. R. McAvoy. (*Rev. Sci. Instr.*, vol. 32, pp. 74–76; January, 1961.) "A dual-diode microwave switch providing in excess of 100-dB switched attenuation with low insertion loss is described. Switching time of the device, limited by the diodes, is 3×10^{-7} sec. Application of the switch in a 9-Gc/s superheterodyne magnetic resonance spectrometer as a mixer crystal protector and as a microwave signal blanker is described."

621.382.23 2024
The Current Ratio I_{max}/I_{min} of Tunnel Diodes—M. Michelitsch. (*Naturwiss.*, vol. 47, p. 274; June, 1960.) The ratio is shown to be strongly dependent on the duration of the alloying time.

621.382.23 2025
Current/Voltage Characteristics of Alloyed and Diffused *p-n* Junction Diodes in InSb—H. J. Stocker. (*J. Appl. Phys.*, vol. 32, p. 322; February, 1961.) Measurements on sample diodes at liquid-nitrogen temperatures are described. The rectification ratios are two orders of magnitude higher than previously reported in the literature.

621.382.23:621.372.44 2026
High-Frequency Varactor Diodes—C. W. Mueller and R. D. Gold. (*RCA Rev.*, vol. 21, pp. 547–557; December, 1960.) Fabrication, impurity distribution, and the measurement of electrical characteristics at 2 Gc are described. These diodes have been used as phase-locked oscillators up to 17 Gc (pump frequency 34 Gc) and have also been used in microwave strip-line amplifiers.

621.382.233:621.318.57 2027
Theoretical Current Multiplication of a Cylindrical Hook Collector—D. P. Kennedy. (*IBM J. Res. & Dev.*, vol. 5, pp. 25–32; January, 1961.) A theoretical analysis of the "hook collector" which is an integral part of most four-layer, *p-n-p-n*, semiconductor switches. Design equations are presented in graphical form.

621.382.3 2028
Some Transconductance Measurements on Transistors—C. Milone. (*Note Recensioni Notiz.*, vol. 9, pp. 541–553; May/June, 1960.) Investigations are discussed of commercial-type transistors in earthed-emitter configuration under various operating conditions.

621.382.3 2029
Transistor Upper Noise Corner Frequency—H. F. Cooke. (Proc. IRE, vol. 49, p. 648; March, 1961.) Measured values of the upper noise corner frequency of four types of transistor have been compared with values calculated from a) the classical formula [757 of 1959 (Shea)], b) a more exact form of the expression derived by Nielsen (3337 of 1957) and c) the expression used in b), but substituting the transition frequency f_T in place of f_α. Over a range of cutoff frequencies from 40 to 600 Mc very good agreement was obtained between the measured values and those calculated by method b).

621.382.3–71 2030
Heat Dissipation of Transistors—W. Hilberg. (*Telefunken Ztg.*, vol. 32, pp. 200–207; September, 1959. English summary, pp. 211–212.) From a consideration of the heat conduction and dissipation processes in a transistor an equivalent circuit for the heat dissipation under static conditions is derived. Calculations regarding the thermal characteristics under dynamic conditions are based on this circuit and several simplifying assumptions. Methods are described for determining the barrier-layer temperature from measurements of transistor operating characteristics.

621.382.333 2031
A *p-n-p* High-Frequency Silicon Transistor—W. A. Little. (*J. Electrochem. Soc.*, vol. 107, pp. 789–791; September, 1960.) The construction and electrical characteristics of a double-diffused transistor are described.

621.382.333:621.318.57 2032
Properties and Applications of Junction Transistors as Switches—G. Meyer-Brötz. (*Telefunken Ztg.*, vol. 33, pp. 85–98; June, 1960. English Summary, p. 156.) The basic static and dynamic characteristics of junction transistors are examined for suitability in switching applications. The design of electronic switches with minimum residual voltage and current, and of transistor modulators for amplifier control is also considered. 44 references.

621.382.333.002.2 2033
Conditions for Obtaining Germanium Transistors by Double Diffusion—R. Deschamps. (*Compt. rend. Acad. Sci., Paris*, vol. 250, pp. 3137–3139; May 9, 1960.) A theoretical examination of conditions necessary for the production of an *n-p-n*-type transistor.

621.382.333.002.2 2034
Conditions for Applying Double Diffusion to Obtain Germanium Transistors—R. Deschamps. (*Compt. rend. Acad. Sci., Paris*, vol. 250, pp. 3290–3292; May 16, 1960.) Experimental results are described which confirm the theoretical conditions laid down in a previous paper (2033 above).

621.383.292.001.4 2035
Investigations of the Local Characteristics of Photomultipliers—P. Cachon. (*Ann. Telecommun.*, vol. 15, pp. 220–251; September/October, 1960.) A detailed report is given of work noted earlier (736 of February).

621.383.5 2036
Energy Diagram of a Real Silicon Photocell—V. K. Subashiev and É. M. Pedyash. (*Fiz. Tverdogo Tela*, vol. 2, pp. 213–220; February, 1960.) A description of a method for constructing the energy diagram of a photocell with its equilibrium carrier concentration is given. Two examples relating to photocells obtained by diffusion of Sb into *p*-type Si show the necessity for considering the field and potential drop in the diffusion layers when studying the operation of a cell.

621.383.5 2037
The Theory of Photocells with a *p-n* Junction—B. Ya. Moĭzhes. (*Fiz. Tverdogo Tela*, vol. 2, pp. 221–226; February, 1960.) An investigation is made of the effect of the distributed impedance of the current-removal layer on the characteristics of the photocell and of the movement of minority carriers in the diffusion layer taking account of the extended field and the changing mobility.

621.384.64 2038
Statistical Equilibrium of an Electron Space Charge with Cylindrical Symmetry in a Magnetron—J. Coste and L. Dagens. (*Compt. rend. Acad. Sci., Paris*, vol. 250, pp. 3009–3011; May 2, 1960.)

621.385.029.6 2039
Systematization and Technical State of Microwave Valves—L. Brück and W. Klein. (*Frequenz*, vol. 14, pp. 198–210; June, 1960.) Transit-time tubes and disk-seal triodes are reviewed with details of several commercial types.

621.385.032.21 2040
Potential Distribution above a Serrated Cathode—E. Weber. (*Bull. schweiz. elektrotech. Ver.*, vol. 51, pp. 1011–1014; October 8, 1960. In English.) The potential distribution is determined by means of the method of conformal mapping.

621.385.032.213 2041
Thermionic Emission Constants and their Interpretation—E. B. Hensley. (*J. Appl. Phys.*, vol. 32, pp. 301–308; February, 1961.) A critical review of the procedures used in the measurement and interpretation of thermionic emission with particular reference to nonmetallic cathodes.

621.385.2:621.391.822:621.372 2042
Nonlinear Thermal Fluctuations in a Diode—Van Kampen. (See 1742.)

621.385.3 2043
Nonlinear Distortion due to Transit Time Effects in Single-Grid Valves—H. Leysieffer. (*Arch. elekt. Übertragung*, vol. 14, pp. 269–282; June, 1960.) An investigation is made of the relation between transit phase angle and distortion dependent on transit time in amplifier triodes for use in SSB radio-link systems. Calculations deal with cubic distortion as only this alone can give rise to interference in the dm-λ range considered. Conditions in the cathode-grid and grid-anode spaces are treated separately. Measurements made for transit phase angles up to about 140° give results in closer agreement with theory for the grid-anode space than for the cathode-grid space.

621.385.6+621.382.23]:621.375.029.6 2044
Amplification—Modern Trends, Techniques and Problems—L. S. Nergaard. (*RCA Rev.*, vol. 21, pp. 485–507; December, 1960.) A review is given of the characteristics of traveling-wave tubes, tunnel diodes, parametric amplifiers and masers.

621.385.624 2045

The Amplification of Multiresonator Klystrons—H. Hagger. (*Bull. schweiz. elektrotech. Ver.*, vol. 51, pp. 1041–1046; October 8, 1960.) The gain of n-resonator klystrons is calculated using Derfler's theory of electron-beam interaction with a space-periodic structure (3438 of 1955). Results obtained are compared with theoretical and experimental data for various klystrons.

621.385.63:621.375.9:621.372.44 2046

Energy Balance in a Parametric Electron-Beam Amplifier—G. K. Grau. (*Arch. elekt. Übertragung*, pp. 247–255; June, 1960.) General energy relations are derived for the longitudinal parametric electron-beam amplifier. Using the principles adopted by Kogelnik (4245 of 1959), dc and ac energy flows can be separated. The energy relations obtained correspond to the Manley-Rowe relations and are discussed with reference to the analysis of Roe and Boyd (3420 of 1959).

621.385.63:621.375.9:621.372.44 2047

Coupled-Mode Theory of Electron-Beam Parametric Amplification—R. W. Gould and C. C. Johnson. (*J. Appl. Phys.*, vol. 32, pp. 248–258; February, 1961.) The theory is applied to amplification by transverse fields. Beam modes at a series of frequencies in addition to the signal frequency are coupled together. Quadrupole electric pump fields and the noise contribution from synchronous beam modes and higher cyclotron idler modes are discussed. Coupling by axially symmetric electric and magnetic fields, and lens effects on noise in the gun region are considered.

621.385.63:621.375.9:621.372.44 2048

A Cyclotron Wave Amplifier with Magnetic Pumping—P. N. Robson. (PROC. IRE, vol. 49, pp. 645–646; March, 1961.) A transverse twisting magnetic field is used to couple the fast and slow cyclotron waves.

621.385.63:621.391.822 2049

Reduction of Beam Noisiness by means of a Potential Minimum away from the Cathode—W. M. Mueller. (PROC. IRE, vol. 49, pp. 642–643; March, 1961.) A sudden discontinuous decrease in the noise figure of a traveling-wave tube was observed as the potential of the profile-shaping electrode was increased. This effect is discussed in relation to a simultaneous drop in the collector current. Explanations for the discontinuities are suggested. See also 1727 of 1959 (Currie and Forster).

621.385.632 2050

Bi-signal Amplification by a Forward-Wave Crossed-Field Amplifier—R. J. Collier. (PROC. IRE, vol. 49, p. 646; March, 1961.) Simultaneous amplification of two pulsed signals differing in frequency has been observed at X-band frequencies using a forward-wave crossed-field amplifier with emitting sole whose gain characteristics have been described earlier (*ibid.*, vol. 49, p. 372; January, 1961.). Results indicate that the system operates as a saturated amplifier rather than a locked oscillator.

621.385.69 2051

A Proposed Doppler-Helitron Oscillator—B. W. Hakki. (PROC. IRE, vol. 49, p. 626; March, 1961.) A method is proposed for magnifying the cyclotron frequency of a helical electron beam by 20–100 times through a Doppler shift.

621.385.832 2052

The Cathode Loading Limit in Circular-Beam Electron Devices—H. Moss. (*J. Brit. IRE*, vol. 21, pp. 35–39; January, 1961.) The analyses of Haine (2993 of 1957) and Schwartz (4054 of 1957) are extended and combined to develop a semi-universal curve which shows that low cathode loadings (0·1 a/cm²) are sufficient to cause severe beam-focus degradation, due to space-charge effects, for spot sizes common in normal CRT's.

621.385.832 2053

Selective Erasure and Nonstorage Writing in Direct-View Half-Tone Storage Tubes—N. H. Lehrer. (PROC. IRE, vol. 49, pp. 567–573; March, 1961.) A new type of storage tube that can erase selectively and display simultaneously stored and nonstored information has been developed. It incorporates a dual-effect target using secondary emission for writing and bombardment-induced conductivity for erasure.

621.385.832:621.396.963.3 2054

Practical Tubes for Bright Radar Displays—F.S. Veith. (*Bull. schweiz. elektrotech. Ver.*, vol. 51, pp. 1023–1030; October 8, 1960. In English.) Display and scan-conversion storage tubes are described.

621.387:621.318.57 2055

The Use of a Hot-Cathode Gas Diode for making a Short Sharp Interruption of Microwave Transmission—M. Laporte. (*Compt. rend. Acad. Sci., Paris*, vol. 250, pp. 3145–3146; May 9, 1960.) The relative performances of hot- and cold-cathode TR switches are considered and a helium-filled hot-cathode type is proposed having a permanently applied anode voltage which is slightly less than the ionizing potential of the gas.

621.387:621.318.57 2056

Study and Experimental Investigation of a Hot-Cathode Gas Diode for the Construction of a Microwave Switch—J. Godart. (*Compt. rend. Acad. Sci., Paris*, vol. 250, pp. 3299–3301; May 16, 1960.) Following the proposal of Laporte (2057 above), experimental results have been obtained using a hot-cathode TR switch. These show a more rapid response time and a greater sensitivity than can be obtained using a cold-cathode type of cell.

621.387:621.362 2057

A New Thermionic Generator—Gabor. (See 1969.)

621.387:621.362 2058

Low-Frequency Oscillations in a Filamentary-Cathode Cesium Diode Converter—Luke and Jamerson. (See 1970.)

621.387:621.374.32 2059

A Gas-Discharge Indicator Tube for Transistorized Decade Counting Circuits—T. P. J. Botden. (*Philips Tech. Rev.*, vol. 21, pp. 267–275; August 4, 1960.) A description of an indicator tube which responds to the small signals delivered by transistor circuits is given.

MISCELLANEOUS

061.3:[537.311.33:621.382 2060

International Semiconductor Symposium—(*Wireless World*, vol. 67, p. 191; April, 1961.) A brief report is given of the symposium organized by the S.F.E.R. and held in Paris, France, February 20–25, 1961.

061.4:621.3 2061

Physical Society Exhibition [1961]—(*Wireless World*, vol. 67, pp. 106–115; March, 1961.) Brief descriptions are given of selected exhibits.

001.891:621.396 2062

Radio Research 1959: The Report of the Radio Research Board and the Report of the Director of Radio Research [Book Review]—Her Majesty's Stationery Office, London, England, 34 pp., 1960, 3s. (*Nature*, vol. 189, pp. 539–540; February 18, 1961.)